I am writing to comment on the requirements for thermal storage outlined in the draft GUIDELINE ON BIOMASS, BIOGAS, AND BIOFUELS FOR ELIGIBLE RENEWABLE THERMAL GENERATION UNITS on Page 9 under section **9. Thermal Storage Requirements.** I am writing for myself as an individual and not as a representative of Clarkson University or our funding agency. However, we have extensive experience over the past 5 years in wood pellet boilers with thermal storage. Based on the research we have done on multiple units ranging in size from 25 kW (85303 BTU/h) to 500 kW (1.71 MMBTU/h), I would strongly suggest there are several problems with the minimum quantity of storage being required and the lack of a scaling of the storage capacity to the maximum fluid flow through the system.

First let me comment on the size of the system based on the attached PhD thesis of my student, Dr. Kui Wang, who performed a series of measurements on the two 25 kW systems. The thesis only contains partial data from the 2016-17 heating season. We have a manuscript under review at *Energy and Fuels* that includes more data, but is consistent with what is in the thesis. These data were then used to calibrate a dynamic system model of a boiler-thermal storage-load system based on a realistic load scenario. Details of the construction of this simulation model are presented in the thesis and further simulations are currently in progress. However, I wanted to bring to your attention the critical figure from this work in which we determine the optimum system performance as a function of thermal storage volume.

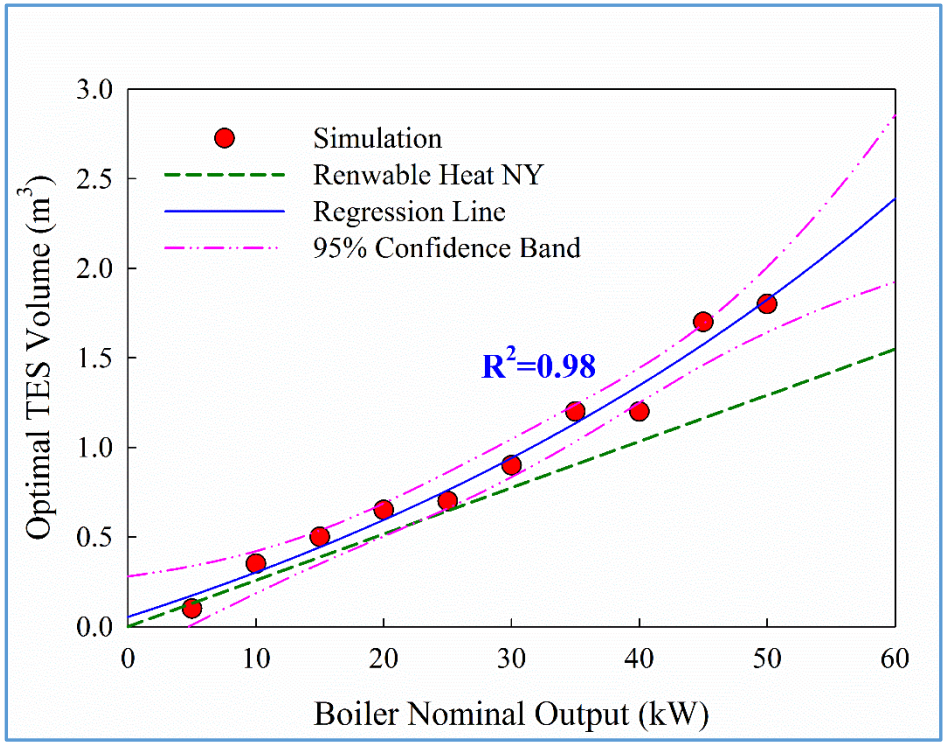

Figure **Error! No text of specified style in document.**-1. Optimum TES tank volume as a function of boiler nominal capacity compared with Renewable Heat NY recommendation line

It can be seen that for small systems, the NYSERDA guidance value of 2 gallons per 1000 BTU/h output are sufficient. However, as we move to larger systems, additional storage is required for optimum system performance. Our current in-progress work is extending these studies up to larger capacity systems and we would hope to have these results available by the end of 2017.

A second consideration is the system flows relative to the size of the thermal storage. We have worked on a 150 kW (500 MBTU/h) system that had a 500 gallon tank (1 gallon per 1000 BTU/h). However, the flow from the system to the building was 72 gal/m so the turnover time was so short, there could never be a thermocline developed in the system. Similarly on the 500 kW (1.71 MMBTU/h) system we have been evaluating, the tank size was 1800 gallons, but the flow was 60 gal/m and again only a weak thermocline developed. In both of these cases, the tanks really only represent a wider pipe and do not effectively function as thermal storage units. Thus, somewhere in the guidance document there needs to be a requirement that the tank size be compatible with the flow rates. Using variable speed circulators could solve the problem such that the high flow rates would only be required at maximum demand when the boiler would be running at full capacity to meet the demand. However, using fixed flow rate circulators that rapidly deplete the stored energy and stir the tank defeats the value of the thermal storage. Thus, there needs to be a recognition that just size of the tank relative to the output of the boiler is insufficient to ensure system performance. System flows also need to be accounted for in the overall design.

Philip K. Hopke, Ph.D.

CLARKSON UNIVERSITY

Wood Pellet Boiler Heating Systems Evaluation and Optimization

A Dissertation

By

Kui Wang

Department of Chemical and Biomolecular Engineering

Submitted in partial fulfillment of the requirements

for the degree of

Doctor of Philosophy, Chemical Engineering

April, 2017

Accepted by the Graduate School

_____ _____

Date Dean

The committee below have examined the thesis/dissertation entitled "**Wood Pellet Boiler Heating System Evaluation and Optimization**" presented by **Kui Wang**, a candidate for the degree of **Doctor of Philosophy**, and hereby certified that it is worthy of acceptance.

Date

Philip K. Hopke

Ross Taylor

Shunsuke Nakao

Yuncheng Du

Suresh Dhaniyala

Abstract

The use of wood pellet boilers for residential space heating has significantly increased over the past decade. Wood pellets are a biomass-based renewable energy made by pelletizing debarked wood fiber. Compared to log wood and wood chips, wood pellets have higher energy density, relatively uniform fuel quality, easier to automate their use, and therefore, are being more widely used.

A typical wood pellet heating system has three components: the boiler (energy generation unit), the thermal energy storage (TES) tank (energy storage unit), and the building (energy consumption unit). The three components form into two loops: the boiler to TES tank loop and the TES tank to building loop.

Three modern wood pellet boilers were installed and monitored in this research. Two 25 kW boilers (PB and WPB) were installed in the end of 2014 and a 50 kW boiler (LGB) was installed in March of 2016. PB is used only for radiant floor heating and WPB is used for traditional baseboard/cast iron radiators space heating as well as providing domestic hot water (DHW) supply. LGB boiler is used for concrete slab heating. The three boiler installations provide different methods of heating and different levels of building heat demand.

This research first evaluated the performance of residential scale wood pellet boilers (25 – 50 kW) in terms of boiler operation characteristics, thermal efficiency, boiler emissions, TES tank stratification and discharge efficiency, etc. Comparisons were also made among different boilers and suggestions for improvements were made.

A process dynamic simulation using VMGSim was built up based on the field monitoring data. Good agreement between the simulation and field data was found. The model was then used to size the TES tank with respect to different boiler capacities and heating demands. A system sizing algorithm was provided in the end. The results will be used to compose a guidance document for wood pellet boiler heating systems.

Key Words: *Wood Pellet Boiler Heating System, Performance Evaluation, Energy Efficiency, Thermal Energy Storage Tank, Process Dynamic Simulation, System Sizing*

Acknowledgements

First and foremost, I would like to express my sincere appreciation and gratitude to my academic advisor, Dr. Philip K. Hopke, who gave me a lot of opportunities and guided me all the way over the past 5 years. Without his wisdom and insights, this work cannot be fulfilled.

I would like to thank Dr. Marco Satyro for providing me a lot of help with the simulation. He was not only a great mentor but also a great friend. We will always remember his smile.

I would like to thank all my committee members, Dr. Ross Taylor, Dr. Shunsuke Nakao, Dr. Yuncheng Du, and Dr. Suresh Dhaniyala, for providing valuable feedback and suggestions to this work.

I want to thank my family. They offered me a dream and supported me all the way without any doubt.

I also thank all my friends and colleagues in CARES. They gave me a lot of good memories and help in the past 5 years. I want to tank Dr. Mauro Masiol for helping me with the emission data calculation, Dr. Mohammad A. Rahman for performing the wood pellet fuel property analysis, and Dr. Devraj Thimmaiah for helping to collect the emissions data.

Table of Contents

List of Tables

List of Figures

Chapter 1. Background

1.1 Renewable Energy

In order to address the impacts of global warming, it is necessary gradually to switch the world's primary energy supply from traditional fossil fuel energy to modern renewable energy. Unlike fossil fuel energy, which includes coal, oil, and natural gas, renewable energy is that produced from resources such as solar, wind, hydro, geothermal, biomass, etc.[1] Renewable resources have a wide geographical existence in contrast to fossil fuel. Solar, wind, and hydroelectricity are the three major expanding renewable resources of energy in the 21st century that might provide all global energy in the future.[2-3]

Solar energy comes from the sun's direct radiation that can either be captured by special photovoltaic (PV) panels and converted into electricity[4] or utilized directly for solar heating (solar thermal energy).[5] Wind energy is converted to electricity through wind turbines. Wind-powered turbines are one of the fastest growing sectors in renewable energy because they are pollution free and inexpensive to build.[6] Hydropower is one of the oldest power sources on earth.[7] Hydroelectricity is electricity generated from hydro energy through using the gravitational force of flowing and falling water to move turbines. A typical representation of hydropower is the Hoover Dam with an annual electricity generation of 4.2 billion kWh.[8] However, most hydro resources are already being exploited.

Apart from the three major renewable energy resources, other two renewable energy resources are geothermal and biomass. Geothermal energy refers to thermal energy generated from the earth. The geothermal gradient, which is the difference in

temperature between the earth core and the surface, is the driving force of geothermal energy (or heat) production from earth core to the surface.[9] A geothermal power plant can utilize the geothermal reservoir to produce electricity or simply to heat/cool buildings. Biomass refers to any source of energy produced from non-fossil biological materials.[10] Biomass has a wide range of application pathways including biomass to electricity,[11] biomass to biofuel,[12] and biomass to thermal energy.[13-14]

According to 2016 renewable energy global status report, renewable energy thrives in three major sectors: power sector (~ 23.7%), heating and cooling sector (~ 8%), and transport sector (~ 4%) with a total contribution about 19.2% to the total global energy consumption.[15]

Figure 1-1 shows (plotted based on data from IEA World Energy Outlook, 2001 – 2016; [16] IEA Key World Energy Statistics, 2001 – 200 [17]) the percentage of renewables in world total primary energy supply (TPES) changes over the past 16 years. A dramatic increase from 5% in 1999[18] to 13.8% in 2000 indicated the energy transformation in the 21st century from fossil fuel to clean and renewable energies. The average percentage of renewables in TPES after 2000 is around 13.3%.

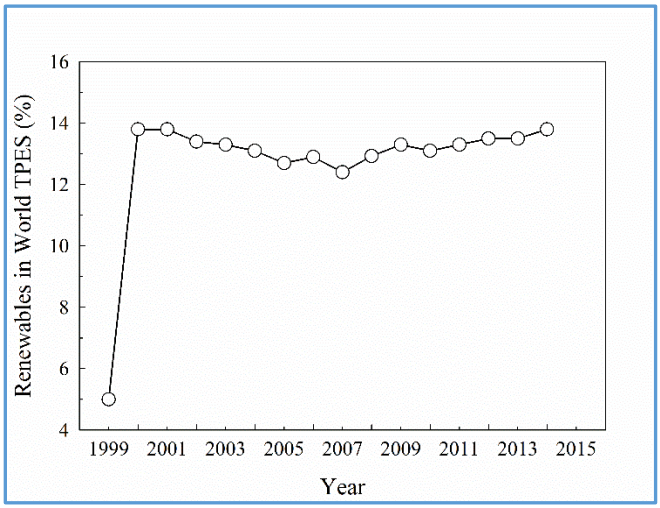

Figure 1-1. Change in the percentage of renewables in world total primary energy supply (TPES) from 1999 to 2014

Renewable energy has a significant role in environmental protection due to its potential for greenhouse gas emission mitigation[19-20] and thus reducing global warming. For example, Mann and Spath[21] showed that by mixing 15% biomass in a 360 MW capacity coal fired power plant would result in an 18.2% reduction in CO_2 emission as well as 12.4% diminution in energy consumption. A concentrating solar power plant can have CO_2 emission as low as 26 g of CO_{2eq} per kWh[22] which is 50 times less than a traditional coal fired power plant (as shown in Figure 1-2). Hence, renewable energy resources and their utilization are crucial for clean and sustainable development in the future.[23]

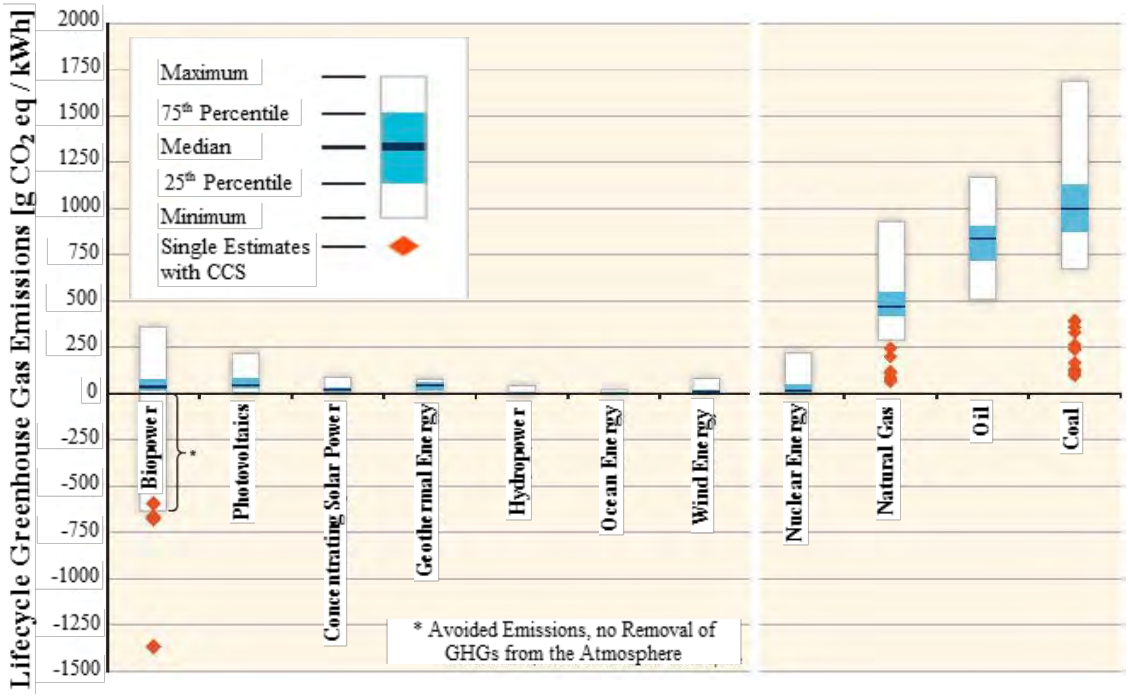

Figure 1-2. Lifecycle greenhouse gas emissions from electricity generation using renewable energy sources and non-renewable energy sources (excerpt from IPCC, 2011[24], CCS is short for carbon capture and storage)

In addition, the social-economic impact of renewable energy utilization is also noteworthy. For example, electricity generation from wind and solar energy rather than

traditional fossil fuels offer no associated pollution to the air and water[25], which can substantially decrease public health cost.[26] Machol and Rizk estimated that the economic value of health impacts from fossil fuel electricity use in the United States is $361.7 – 886.5 billion annually, representing 2.5 – 6.0% of the national GDP.[27] Traditional fossil fuel technologies are typically mechanized and capital intensive while modern renewable energy industry is more labor-intensive. For example, the German model reported a 55% increase in the total number of "green" jobs from 2004 to 2007.[28] O'Sullivan et al.[29] reported a total employment increase from 160,500 to 278,000 in renewable energy sector from 2004 to 2008 with over twofold employment rise in solar energy industry during the same period. Given the current global demand and policy on renewable energy, the increase will be continued in the future. Wei et al.[30] developed an analytical job creation model in the US power sector and estimated the total amount of jobs created by 2030 would be over 4 million. Hence, the social-economic benefits of renewable energy resources are also large.

In conclusion, the global transformation from fossil fuel energy to renewable energy has been gradually increasing over the past decade. The increasing use of renewable energy can substantially reduce greenhouse gas emissions and thus reducing global warming. Renewable energy industry also provides a significant number of jobs and becoming an indispensable part of global economy.

1.2 Biomass

Any organic material derived directly or indirectly from plants is considered as biomass.[31] Biomass energy is one of the oldest form of energy and has been used by humans since they began burning wood to make fires. In recent years, the use of biomass for energy is continuously increasing. According to 2016 renewable energy global status report, the share of biomass in global total final energy consumption was 14% in 2014 and 10.4% of the biomass energy was used for heating buildings.[15] In addition, for the final energy consumption by end-use sector in the same year, biomass accounted for 29.6% in heating buildings sector and 7.2% in heating industry sector.[15]

1.2.1 Basic Principle

Photosynthesis is the key process for biomass to store energy. Atmospheric CO_2 and H_2O are converted to carbohydrates through interaction with sunlight. Carbohydrates is the building block of biomass and stores solar energy in their chemical bonds. The stored solar energy in biomass can be extracted by breaking the chemical bonds through either high temperature chemical reactions, i.e. combustion, or biochemical reactions such as digestion, fermentation, hydrolysis, etc. with end products of CO_2 and H_2O. This cyclic way of energy storage-energy release is the basic principle of biomass energy utilization.

1.2.1.1 Sources of Biomass

Figure 1-3 shows the categories of biomass resources. In general, biomass resources include woody biomass, non-woody biomass, and other secondary/tertiary biomass resources.

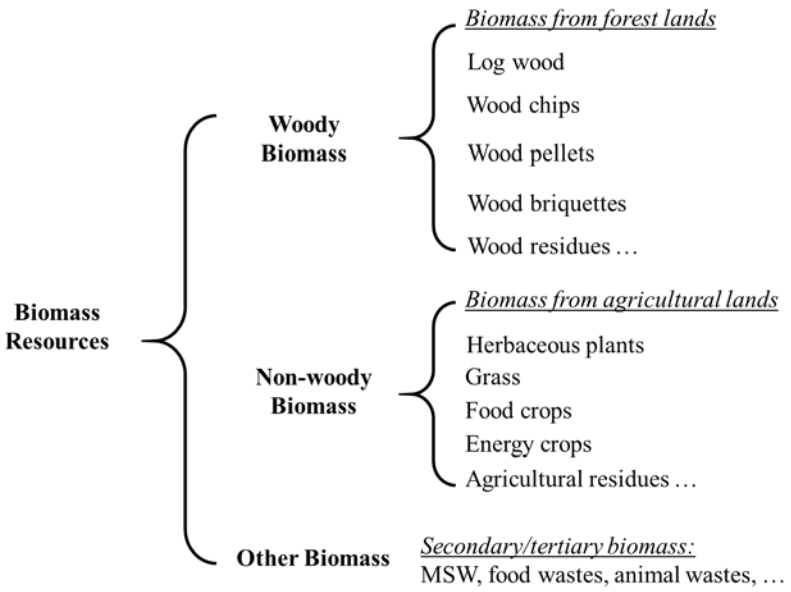

Figure 1-3. Biomass resources categorization (MSW: municipal solid waste)

1.2.1.2 Woody Biomass

Over the past three decades, due to the rise in the price of fossil fuels and government incentives, the use of woody biomass for energy has greatly increased.

Figure 1-4. Woody biomass examples (from left to right): wood logs (cord wood), wood chips, wood pellets and wood briquettes (source: Google Image)

Woody biomass is a product from forest lands (or trees) such as log wood, wood chips, wood pellets, wood briquettes, and wood residues (as shown in Figure 1-4). Woody biomass energy is the most widely used renewable energy source in the world.

Woody biomass can be utilized to generate electricity, produce biofuels, supply heat, and synthesis biochemicals, etc. There are 5 major types of woody biomass conversion:

(1) **Direct Combustion:** to burn woody biomass in a boiler, furnace, or stove system to supply heat either for space heating, hot water or both.

(2) **Cogeneration:** to produce both heat and electricity through a combined heat and power (CHP) system.[32]

(3) **Co-firing:** multiple fuels are combusted in the same system. The most common co-firing is to mix wood with coal in a power plant to reduce emission as well as increase system performance.[21]

(4) **Gasification:** to produce syngas (H_2 + CO). The difference between direct combustion and gasification is that gasification has very limited oxygen supply. Gasification is generally more efficient than direct combustion.

(5) **Liquid Biofuels:** including ethanol, methanol, bio-oil and biodiesel. Those liquid biofuels can be produced through woody biomass pyrolysis/gasification, fermentation, etc.[33]

Other types of woody biomass energy conversion includes biomass cooking,[34] anaerobic digestion to produce biogas,[35] biochar,[36] etc.

1.2.1.3 Non-woody Biomass

Generally speaking, non-woody biomass refers to biomass from agricultural lands such as herbaceous plants, grass, crops (especially energy crops), agricultural residues, etc. The differences between woody and non-woody biomass are that non-woody biomass have generally lower lignin contents, shorter growing cycles and higher yield of cellulose.[37] Typical representation of non-woody biomass is shown in Figure 1-5. Fast-growing plants including switchgrass and corn stalks have gained increasing interests in recent years in the United States.[38]

Figure 1-5. Non-woody biomass examples (from left to right): flax in the field, corn stalks, and dried straw (source: Google Image)

Non-woody biomass contains high fraction of cellulose than woody biomass, which contains high fraction of lignin. Cellulose is easier to convert into glucose through hydrolysis and subsequent fermentation to produce cellulosic ethanol than lignin.[31,39] Compared to grain ethanol such as corn ethanol, cellulosic ethanol is considered to be much more cost-effective, environmentally beneficial, and has a greater energy output to input ratio.[40]

Aside from biofuel, non-woody biomass can also be used as a substitute for woody biomass in direct combustion, co-firing, and gasification systems after

pelletization, but there are problems burning grass pellets as shown by Chandrasekaran et al.[41]

1.2.1.4 Other Biomass

There are also other secondary and tertiary biomass that are derived from woody or non-woody biomass such as food waste, MSW, animal manure, etc. This type of waste to energy utilization provides great environmental benefits. Those secondary and tertiary biomass contains high amount of moisture, which makes the pretreatment procedure is the key process for cost-effective utilization.

1.2.2 Environmental Implications

The impacts of using biomass energy on the environment include biomass production, land use, air pollution, water pollution, ecosystem and wildlife protection, deforestation, etc. Some work has been done to fully assess how different ways of using biomass can influence both local and global environment.[10,42]

1.2.2.1 Climate Change Mitigation

The biggest advantage of using biomass is that it has very low greenhouse gas emissions compared to fossil fuels (as shown in Figure 1-2) since biomass is made from atmospheric CO_2 and H_2O through photosynthesis. According to IPCC 2014, global greenhouse gas emissions by gas are: 65% CO_2 from fossil fuel and industrial processes, 16% CH_4, 11% CO_2 from forestry and other land use, 6% N_2O, and 2% fluorinated gases.[43] Global fossil fuel use is the primary source of CO_2. By replacing those fossil fuel energy with biomass, the corresponding net CO_2 emission can also be reduced. IEA bioenergy statistics reported that bioenergy is the single largest renewable energy source

today accounting for 10% of world primary energy supply and can provide up to 27% of world transportation fuel by 2050 and up to 60% in power generation by 2020.[44] IEA also encourages governments to ensure a biofuel supportive policies in response to current global climate change. For example, Farrell et al. estimates that bioethanol has a CO_2 reduction potential of 2% to 30% based on different processes.[45]

1.2.2.2 Air Pollution Consideration

One major issue of using biomass energy is the associated direct air pollution emissions including particulate matter (PM), volatile organic (VOC) matter, CO, NO_x and SO_x emission.

Unlike fossil fuels, biomass fuels have higher inorganic content and thus lead to higher PM emission than oil or gas. Fine PM emissions such as $PM_{2.5}$ (particle aerodynamic diameter less than 2.5 μm) and ultrafine PM emissions (particle aerodynamic diameter less than 0.1 μm) are produced during biomass combustion process. Those particles are harmful to human health and have been proven to be related to some respiratory[46] and cardiovascular diseases[47] and contribute to morbidity and mortality.[48]

Gaseous emissions (particularly CO emission) also have adverse effect on human health. Complete combustion of biomass converts carbohydrates into CO_2 and H_2O and release energy. Incomplete combustion of biomass fuels produces CO emission and VOC emission. CO is known to be toxic. Exposure to CO can lead to headache, nausea, brain damage, and even death. Most of the chemicals in VOC emission are related to

respiratory diseases such as asthma and long term exposure could lead to cancer.[49] NO_x and SO_x emissions are produced due to the release of fuel bound nitrogen and sulfur.

However, biomass PM and gaseous emissions are still much less than coal.[50,51] With proper control of fuel quality and combustion technology, the abovementioned emissions can be significantly reduced. Modern biomass burners are capable of having both high efficiency and low emissions, providing better opportunities for using biomass energy.

1.2.2.3 Other Environmental Issues

There are also other environmental issues associated with biomass energy utilization including deforestation, pressure on land/water resources, water/soil pollution, wildlife protection, etc. For example, Fargione et al.[52] reported that 1.5% annual rate of deforestation of tropical rainforests in Malaysia and Indonesia is due to the increasing production of palm diesel oil. In addition, the harvesting of biomass from land and water could increase potential soil and water degradation. Life cycle analysis (LCA) also indicates that biomass utilization can also generate CO_2 emission during harvesting, transportation, and pretreatment processes, which have been neglected for a long time.[53] Those issues may have not been recognized by many biomass energy utilization oriented project designers.

In conclusion, biomass energy utilization has both positive and negative environmental impacts. It is important to fully realize those impacts to ensure a sustainable and renewable biomass resource for energy utilization.

1.3 Properties of Biomass

The main properties of interest for biomass energy utilization including: moisture content, heating value, elemental composition, and ash content. Those properties determine the subsequent treatment and conversion pathways for different biomass resources. Two types of analysis are used to determine those properties: proximate analysis and ultimate analysis. In proximate analysis, biomass material is decomposed into four groups through thermogravimetric method: moisture, volatile, fixed carbon, and ash [54]. Ultimate analysis performs a quantitative element-based analysis on biomass materials including C, O, H, N, S, and (sometimes) Cl.[55]

1.3.1 Proximate Analysis

Table 1-1. Proximate analysis for some common biomass materials (selected from Vassilev et al.[56] Table 5)

Biomass Material	Moisture (%)	Volatile (%)	Fixed Carbon (%)	Ash (%)
Eucalyptus bark	12.0	68.7	15.1	4.2
Pine sawdust	15.3	70.4	14.2	0.1
Spruce wood	6.7	75.7	17.1	0.5
Willow	10.1	74.2	14.3	1.4
Wood	7.8	77.5	14.5	0.2
Wood residue	26.4	57.4	12.2	4.0
Switchgrass	11.9	70.8	12.8	4.5
Corn straw	7.4	67.7	17.8	7.1
Wheat straw	10.1	67.2	16.3	6.4
Almond hulls	6.5	69.0	18.8	5.7
Olive husks	6.8	73.7	17.4	2.1
Rice husks	10.6	56.1	17.2	16.1
Sugar cane bagasse	10.4	76.6	11.1	1.9
Chicken litter	9.3	43.3	13.1	34.3
Meat-bone meal	2.5	61.7	12.4	23.4
Wood agricultural residue	30.3	54.7	12.7	2.3
Wood straw residue	7.3	69.6	15.5	7.6
Furniture waste	12.1	72.9	11.8	3.2
Sewage sludge	6.4	45.0	5.3	43.3
Marine macroalgae	10.7	45.1	23.1	21.1

Table 1-1 lists the proximate analysis results for some common biomass materials based different biomass resources discussed in previous sections. A large variation is clearly observed among different biomass materials, which could be caused by the variation in moisture and ash content.

1.3.1.1 Moisture Content

Moisture evaporation is the first step of any biomass thermal conversion process. Moisture content (*MC*) of biomass refers to how much water is contained by the biomass material. It is highly depended on the different types of biomass resources. Wet basis ($MC_{\text{w.b.}}$) and dry basis ($MC_{\text{d.b.}}$) are two different ways to calculate moisture content as defined in equations (1-1) and (1-2). When not specified, moisture content is normally a wet basis value.

$$MC_{\text{w.b.}} = \frac{\text{H}_2\text{O}}{\text{Dry Biomass} + \text{H}_2\text{O}} \times 100\% \tag{1-1}$$

$$MC_{\text{d.b.}} = \frac{\text{H}_2\text{O}}{\text{Dry Biomass}} \times 100\% \tag{1-2}$$

Figure 1-6 shows the distribution of moisture content (as received) among different biomass resources categories (plotted based on data from Vassilev et al.[56]). An average of 14.4% moisture content was found for all biomass resources listed. Wood and woody biomass (WWB) has the highest moisture content and the largest variability of moisture distribution among different parts (such as bark, branch, trunk, etc.) and different sources (sawdust, fir mill residues, etc.). This wide distribution of moisture

content among different wood species indicates the significance of source identification when characterizing different biomass species.

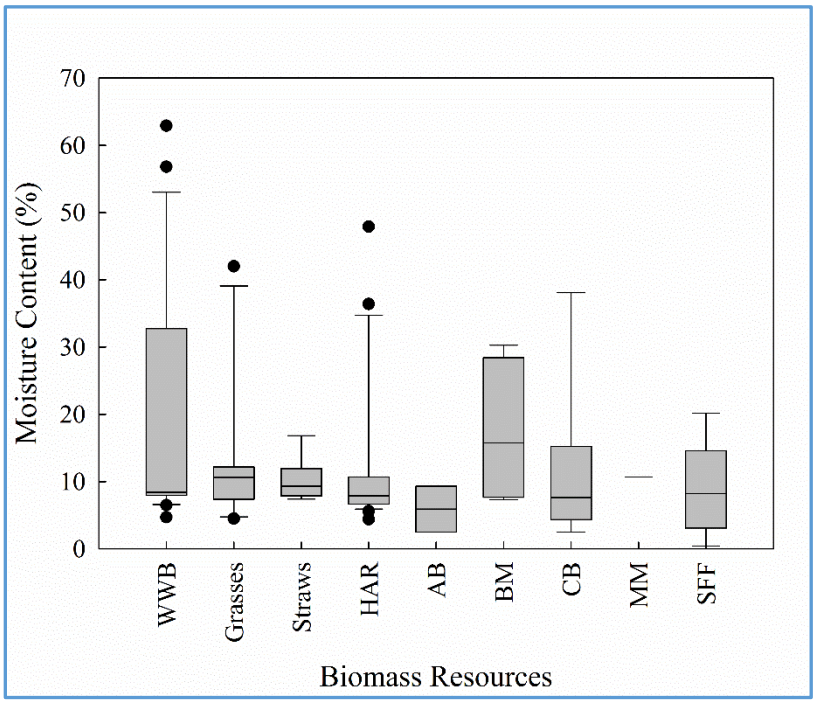

Figure 1-6. Distribution of moisture content for different biomass resources (Note: *WWB* – Wood and Woody Biomass; *HAR* – Herbaceous and Agricultural Residues; *AB* – Animal Biomass; *BM* – Biomass Mixture; *CB* – Contaminated Biomass; *MM* – Marine Macroalgae; *SFF* – Solid Fossil Fuels)

Moisture content can significantly affect biomass heating value that higher moisture content leads to lower gross heating value. In addition, moisture content is one of the determining factors on the appropriate conversion pathways for biomass resources in that thermal conversion requires relatively low feedstock moisture content while biochemical conversion (e.g. fermentation, anaerobic digestion) can tolerate high moisture content. Hence, low moisture content wood and woody biomass, herbaceous and agricultural biomass are suitable for thermal conversion while high moisture content biomass needs to use the bio-conversion pathway.

1.3.1.2 Volatile Content

After all the moisture have been completely evaporated, continuous heating leads to formation of volatile matter including light hydrocarbons, CO, CO_2, H_2, etc.[57] Dry basis volatile matter content in different biomass materials varies from 48 d.b. % to 86 d.b. %.[56] Herbaceous grass has slight higher volatile content (79 d.b. %) followed by wood and woody biomass (78 d.b. %) with animal biomass the least (55.5 d.b. %).[56]

1.3.1.3 Fixed Carbon Content

Fixed carbon refers to solid combustible residue after release of moisture and volatile matter. Volatile matter and fixed carbon content provide a measure of the combustibility of the biomass material. Biomass fixed carbon content can vary between 1 – 38%.[56] Herbaceous and agricultural biomass resources normally have higher fixed carbon content (19.1 d.b. %) than woody biomass resources (18.5 d.b. %), which could be related to the fact that herbaceous biomass have higher cellulose/hemicellulose fraction than woody biomass.[37]

1.3.1.4 Ash Content

Ash is the incombustible residue after biomass combustion. A large variation of 0.1 – 46% ash content among different biomass resources was observed by Vassilev et al.,[56] which indicates the importance of ash characterization when using biomass energy. Typically, wood and woody biomass have lower ash content (3.5 d.b. %) compared to herbaceous and agricultural biomass (5.7 d.b. %).[56] Debarked wood have less than 1% ash content. High ash content biomass fuels are easy to form sludge and clogs.

1.3.2 Ultimate Analysis

Table 1-2 lists the elemental composition of some common biomass materials. In order to eliminate the influence of moisture and ash content on the ultimate analysis results, C, O, H, N, and S are listed in dry ash free basis and Cl is listed in dry basis. The following discussion in this section with respect to each element is also based on this convention.

Table 1-2. Ultimate analysis for some common biomass materials (excerpted from Vassilev et al.[56] Table 5, daf means dry ash free basis and d.b. means dry basis)

Biomass Material	C (daf %)	O (daf %)	H (daf %)	N (daf %)	S (daf %)	Cl (d.b. %)
Eucalyptus bark	48.7	45.3	5.7	0.3	0.05	0.26
Pine sawdust	51.0	42.9	6.0	0.1	0.01	0.01
Spruce wood	52.3	41.2	6.1	0.3	0.10	0.01
Willow	49.8	43.4	6.1	0.6	0.06	0.01
Wood	49.6	44.1	6.1	0.1	0.06	0.01
Wood residue	51.4	41.9	6.1	0.5	0.08	0.05
Switchgrass	49.7	43.4	6.1	0.7	0.11	0.08
Corn straw	48.7	44.1	6.4	0.7	0.08	0.64
Wheat straw	49.4	43.6	6.1	0.7	0.17	0.61
Almond hulls	50.6	41.7	6.4	1.2	0.07	0.02
Olive husks	50.0	42.1	6.2	1.6	0.05	0.20
Rice husks	49.3	43.7	6.1	0.8	0.08	0.12
Sugar cane bagasse	49.8	43.9	6.0	0.2	0.06	0.03
Chicken litter	60.5	25.3	6.8	6.2	1.20	0.5
Meat-bone meal	57.3	20.8	8.0	12.2	1.69	0.87
Wood agricultural residue	52.4	41.2	6.0	0.4	0.04	0.03
Wood straw residue	51.7	41.5	6.3	0.4	0.13	0.13
Furniture waste	51.8	41.8	6.1	0.3	0.04	0.01
Sewage sludge	50.9	33.4	7.3	6.1	2.33	0.04
Marine macroalgae	43.2	45.8	6.2	2.2	2.60	3.34

Carbon (C): Woody biomass (52.1%) normally have higher carbon content than herbaceous biomass (49.9%). Biomass material generally have lower carbon content than coal.

Oxygen (O): Herbaceous biomass (42.6%) generally have higher oxygen content than woody biomass (41.2%). Some biomass materials have extremely high oxygen content (e.g. pepper plant: 49%, coffee husks: 48.3%).[56]

Hydrogen (H): Biomass hydrogen content varies from 3% to 11%. Hydrogen in biomass materials is usually bond with carbon to form carbon hydrocarbons or carbohydrates. Comparing to coal, biomass has higher atomic H:C ratio and atomic O:C ratio.[60] Wood, cellulose, and lignin biomass are oxygen rich solid fuels, resulting in lower heating value compared to coal.

Nitrogen (N): In general, nitrogen content is lowest in woody biomass and highest in grass biomass.[58] Biomass nitrogen content varies between 0.1% and 12% and woody biomass nitrogen content is around 0.4%.[56]

Sulfur (S): Like nitrogen, sulfur content is also the lowest in woody biomass, which indicates the association of nitrogen and sulfur in biomass materials. Sulfur content in biomass varies between 0.01% and 2.3%. Compare to solid fossil fuels, biomass has much lower sulfur content.

Chlorine (Cl): Cl content in biomass ranges from 0.01% to 0.9%. Similar to N and S, Cl also has the lowest content in woody biomass, also suggesting possible association between N, S, and Cl in biomass materials.

1.3.3 Ash Properties

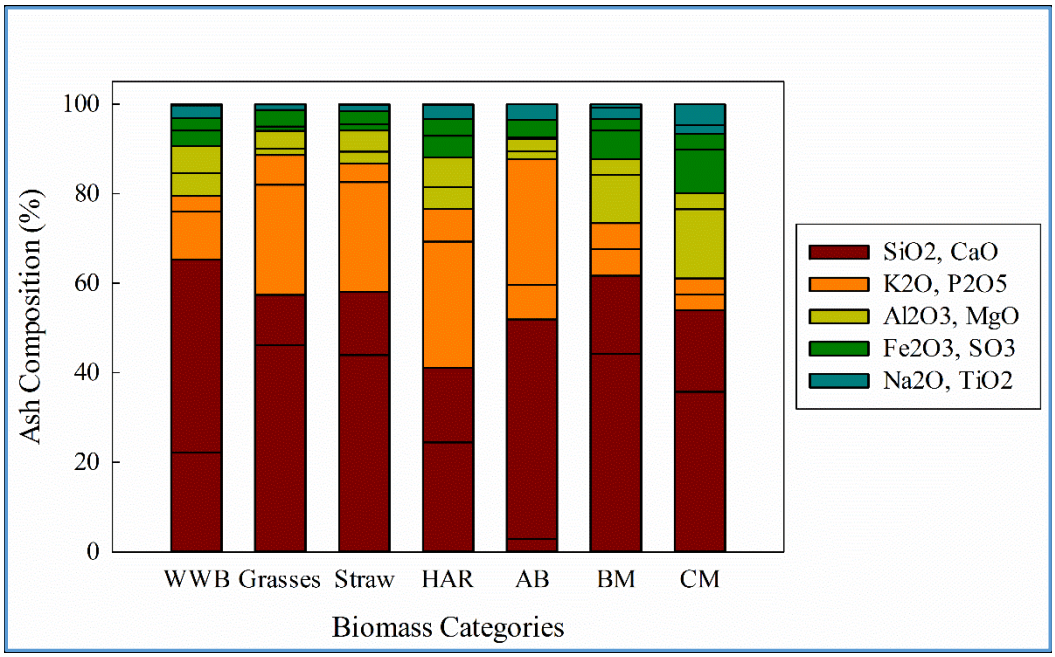

Figure 1-7. Biomass ash composition for different categories (Note: abbreviations are shown in Figure 1-6, replotted from Vassilev et al.[56])

Studies have identified that Ca, Si, K, Mg, Al, Na, Fe, and P are major ash forming elements for all different types of biomass resources.[56] These elements can form many inorganic compounds during combustion, mostly metal oxides such as CaO, SiO_2, K_2O, MgO, Al_2O_3, P_2O_5, etc. Figure 1-7 shows the ash composition for different groups of biomass resources (replotted from Vassilev et al.[56]). It is clear that SiO_2 and CaO are two major compounds having over 50% of the total ash weight, especially in wood and woody biomass (WWB). Herbaceous biomass ashes are rich in K_2O and P_2O_5. Wood chips and wood pellets chemical composition study by Chandrasekaran et al.[59] showed major ash forming elements as Ca (45%), K (37%), and Mg (8%). The difference could be caused by the bark of WWB.

Study on high temperature ash-melting behaviors for biomass fuels[60] showed that low concentrations of Ca and high concentrations of K biomass fuels, such as straw, cereals, and grass, have a significantly lower sintering temperatures than woody biomass fuels. This observation indicates that wood and woody biomass (WWB) are better used for thermal energy conversion than herbaceous biomass.

Aside from major ash-forming elements, there are also some minor ash-forming elements such as: Fe, Al, Mn and other heavy metals. In addition, there are also trace amount of heavy metals (Cd, Zn, Hg, etc.) in biomass fuel, and they will either bound to fly-ash or remain gaseous or as aerosols in the flue gas after combustion. In this case, emissions from this type of fuel should be strictly controlled because they are factors contributing to a series of public health problems.

1.3.4 Heating Value

Two types of heating values are commonly used: gross calorific value (GCV) and net calorific heating value (NCV). The difference between GCV and NCV lies in the energy restoration from flue gas water condensation, GCV includes the evaporation energy of the water presented in flue gas while NCV does not. Biomass solid fuels usually have GCV values vary between 18 and 22 MJ/kg (d.b.) and can be calculated based on fuel ultimate analysis as shown in (1-3).[61]

$$\mathrm{GCV} = 0.3491X_{\mathrm{C}} + 1.1783X_{\mathrm{H}} + 0.1005X_{\mathrm{S}} - 0.0151X_{\mathrm{N}} - 0.1034X_{\mathrm{O}} - 0.0211X_{\mathrm{ash}} \quad (1\text{-}3)$$

where X_i is the content of carbon (C), hydrogen (H), sulfur (S), nitrogen (N), oxygen (O) and ash in wt% (d.b.). If an accurate value of GCV is needed, a bomb calorimeter shall be

used. It can be seen from (1-3) that C, H, and S contribute positively to the GCV while N, O, and ash content contribute negatively. NCV can be calculated from GCV based on fuel moisture content (MC) as[60]

$$\mathrm{NCV} = \mathrm{GCV}\left(1 - \frac{MC_{\mathrm{w.b.}}}{100}\right) - 2.444\left(\frac{MC_{\mathrm{w.b.}}}{100}\right) - 2.444\left(\frac{X_{\mathrm{H}}}{100}\right)8.936\left(1 - \frac{MC_{\mathrm{w.b.}}}{100}\right) \tag{1-4}$$

where $MC_{\mathrm{w.b.}}$ is the fuel moisture content in wet weight basis and X_{H} is the fuel hydrogen content in dry basis percentage. From (1-4), fuel heating value drops linearly with fuel moisture content. Therefore, proper fuel treatment shall be applied for high moisture content fuels before thermal conversion is necessary.

1.4 Biomass Energy Utilization

A series of different conversion types and conversion processes exist for different biomass resources. Many factors influence the final conversion process such as biomass feedstock type, desired energy form, environmental regulations, etc. In most cases, the final desired energy form determines the biomass conversion route. In general, thermo-chemical conversion and bio-chemical conversion are two major pathways currently for biomass energy utilization around the world in three major forms: power, heat, and transportation fuels.

1.4.1 Thermo-chemical Conversion

In thermo-chemical conversion pathway, there are three main processes: combustion, pyrolysis, and gasification.

1.4.1.1 Combustion

Biomass feedstock can release energy through burning with excess air (oxygen). The released energy can provide heat, mechanical power, or electricity through subsequent processes. The released energy is in the form of hot flue gas at temperature around 800°C to 1000°C. In general, biomass feedstock with moisture content <50% is suitable for combustion, otherwise, pretreatment process to dry the feedstock is required before combustion.

Biomass for heat is usually in the form of stoves (radiation energy), furnaces or boilers (thermal energy). Biomass is either the primary fuel or supplied as a co-

combustion fuel. Biomass for heat energy conversion efficiency typically ranges from 60% to 85%.

Biomass for electricity is usually achieved through steam turbines and turbo generators. High pressure steam is produced by steam boilers through combustion of biomass feedstock. The overall process efficiency usually ranges from 20% to 40%.[62] Higher efficiencies are usually achieved through co-combustion with coal.

Biomass cogeneration is the production of heat and power simultaneously (combined heat and power system or CHP, typically a Stirling engine). Cogeneration through integration of biomass and solar energy have also been studied.[63]

1.4.1.2 Pyrolysis

Biomass feedstock can produce liquid oil, solid char, and volatile gases through pyrolysis, a direct thermal decomposition process. The difference between pyrolysis and combustion is that there is no air supply in pyrolysis process and the temperature is controlled around 500°C.[62]

Pyrolysis products can be controlled through different conversion technologies. Traditional slow pyrolysis (heat rate up to 100°C/s) is used to produce charcoal with up to 35% yield[62] when biomass feedstock is heated to around 500°C. Residence time of the vapor products varies from 5 min to 30 min.[57] Recently, the application of short-residence time pyrolysis (or fast pyrolysis) has shown promising application. The heating rate in fast pyrolysis (up to 1000°C/s) is much higher than slow pyrolysis, resulting in a much shorter gas residence time (typically < 2 s).[57] Fast pyrolysis at lower temperature (400 – 500°C) can produce bio-oil and fuel gas with up to 80% yield.[62] Higher yield of

bio-oil up to 95% can be obtained from specific biomass feedstock such as wood, paper, etc. Pyrolysis oil has the potential as a fuel oil substitute after subsequent treatment to remove water and corrosive compounds. A common process for bio-oil application is fast pyrolysis followed by catalytic steam reforming and shift conversion of specific fractions to obtain H_2.[64] Table 1-3 shows typical properties of bio-oil from wood pyrolysis in comparison with heavy fuel oil.[57]

Table 1-3. Typical properties of wood pyrolysis bio-oil in comparison with heavy fuel

Physical Property	Bio-oil	Heavy Fuel Oil
Moisture (wt %)	15 – 30	0.1
pH	2.5	–
Specific Gravity	1.2	0.94
Elemental Composition (wt %)		
C	54 – 58	85
H	5.5 – 7.0	11
O	35 – 40	1.0
N	0 – 0.2	0.3
Ash	0 – 0.2	0.1
HHV (MJ/kg)	16 – 19	40
Viscosity (at 500 °C, cP)	40 – 100	180
Solids (wt %)	0.2 – 1.0	1
Distillation Residue (wt %)	Up to 50	1

1.4.1.3 Gasification

At high combustion temperature (> 800°C) with insufficient air (oxygen) supply (and/or steam), biomass combustion is incomplete (partial oxidation) resulting in a mixture of gaseous products (CO, H_2, CH_4, and CO_2) called producer gas. The producer gas can further be used as feedstock to produce other chemicals such as methanol, or be used directly for electricity generation in gas turbines.

About 2.5 – 3.0 Nm^3 of gas product can be obtained by gasifying 1 kg of air-dried biomass.[65] Several types of biomass gasifiers are used in the process: updraft (or counter-current) gasifier, downdraft (or co-current) gasifier, cross-draft gasifier, and fluidized bed gasifier. Product gas generation occurs in two steps inside a biomass gasifier. Firstly, fuel rich exothermic reaction between pyrolysis gas and insufficient air supply to significantly increase gasifier temperature resulting in gaseous products of mainly CO_2 and H_2O; secondly, endothermic reaction of CO_2 and H_2O with high temperature char to form CO, H_2, and CH_4.[66]

1.4.2 Bio-chemical Conversion

Fermentation and anaerobic digestion are two main processes for bio-chemical conversion of biomass.

1.4.2.1 Fermentation

Sugar crops (e.g. sugar cane) and starch crops (e.g. maize, wheat) are commonly used to produce ethanol through fermentation process. During fermentation, yeast or some bacterial are added. Product ethanol is then distilled to obtain higher purity and concentration and used as gasoline additive. Taking corn fermentation as an example, the yield of ethanol is about 450 liter per ton of dry corn (35% yield).[62]

1.4.2.2 Anaerobic Digestion

Anaerobic digestion is the process to convert biomass to biogas, which is a mixture of CH_4 and CO_2. Anaerobic digestion is widely used and commercially proven technology to convert high moisture content biomass (i.e. 80 – 90%) to biogas. The

product biogas can be further purified and upgraded to natural gas quality for production of electricity. The overall biomass to electricity efficiency based on this process is about 10 – 16%.[62]

1.5 Biomass Burners

Thermo-chemical conversion of biomass has a higher efficiency of energy utilization compared to bio-chemical conversion. Biomass combustion systems are the only bioenergy utilization systems with a variety of energy output capabilities ranging from small residential scale to large industrial scale. Biomass burners can be categorized based on their configurations and heat carriers as biomass stoves and biomass boilers.

1.5.1 Biomass Stoves

Cooking and heating stoves are two main types of biomass stoves widely used.

1.5.1.1 Biomass Cooking Stoves

Biomass cooking stoves are mainly used in developing countries for household cooking purpose. The biomass resources are mainly wood and agricultural residues (i.e. rice straw).

Traditional cooking stoves usually have low efficiency and high emissions of CO and particulate matter. Modern advanced cooking stoves, on the other hand, are able to reduce emissions and increase energy efficiency with proper design and combustion optimization through gasification, forced draft, and better insulation.[67]

1.5.1.2 Biomass Space Heating Stoves

In developed countries, biomass heating stoves are usually used for residential space heating purpose. This type of stoves has high combustion efficiency and low emissions. The fuels are usually wood and densified woody biomass such as wood pellets.

Wood chips and wood logs are also used. Air is used as the heat carrier. Figure 1-8 shows a typical representation of modern space heating stoves using wood pellet as fuel.[68]

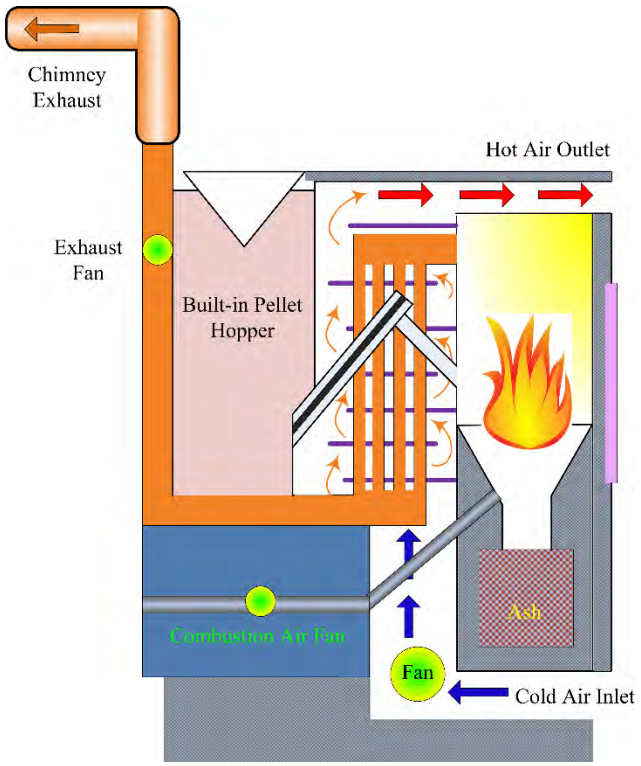

Figure 1-8. Cutaway diagram of a typical wood pellet stove for residential space heating

In recent years, catalytic wood stoves have been developed to achieve higher combustion efficiency, longer burn times, and lower emissions. Compared to non-catalytic wood stoves, catalytic wood stoves are usually equipped with a ceramic honeycomb brick coated with catalysts (precious metal) that allows hot combustion gas to pass through and undergo secondary combustion.[69] Catalytic wood stoves can have an average of 14% increase in energy efficiency than traditional non-catalytic wood stoves.[69]

1.5.2 Biomass Boilers

Unlike biomass stoves, biomass boilers use water (or steam) as the heat carrier. Biomass is combusted in the boiler combustion chamber. Hot flue gas transfers heat to water through a fire-tube heat exchanger to produce either hot water or steam. Biomass boilers can be categorized based on the biomass fuel used.

1.5.2.1 Wood Boilers

Wood boilers are the main type of biomass boilers. Wood log, wood chip, and wood pellets are the three commonly used wood fuels. Figure 1-9 shows typical schematics of the three different wood fuel boilers.[70]

Figure 1-9. From left to right: wood log, wood chip, and wood pellet boilers (source: euroheat.co.uk, ecoheat.co.uk, and woodboilers.com)

Wood log boilers burn wood logs directly. Wood logs are usually seasoned to achieve moisture content of 20% or less. Unseasoned wood logs have moisture content up to 50%. Based on the combustion techniques, updraft (direct combustion) and down draft (gasification combustion) wood log boilers are commonly seen. Gasification combustion wood log boilers have higher efficiency and lower emissions than direct

combustion wood log boilers. Wood log boilers usually have thermal efficiency around 75%.

Wood chip boilers use chipped, debarked wood as fuel. Wood chips usually have moisture content around 30 – 40%.[59] Compared to wood logs, wood chips are easier to burn and thus wood chip boilers have higher combustion efficiency than wood log boilers. Wood chips are usually stored in an external storage silo and transported into boiler combustion chamber through auger delivery system. The best wood chip boilers usually have thermal efficiency around 80%.

Wood pellet boilers use densified wood pellets as fuel, which has higher energy density than wood chips and much lower fuel moisture content (around 6%[59]) than wood logs and wood chips. The use of wood pellets enables efficient transportation, delivery and feeding can be more easily automated. Wood pellet boilers have the lowest emissions among the three aforementioned wood boilers and are widely used in European countries for residential space heating. The best wood pellet boilers usually have thermal efficiency around 85 – 90%.

1.5.2.2 Other Biomass Fueled Boilers

Aside from wood boilers, there are also other types of biomass boilers fueled with non-woody biomass resources. Herbaceous biomass are also pelletized to achieve higher energy density and transportation efficiency. For example, grass pellet boilers have shown great potential in many herbaceous biomass rich areas such as Vermont.[71] Comparing to wood and woody biomass, herbaceous biomass have much shorter growing cycle. However, they do have higher ash content than wood pellets resulting in higher

PM emissions[41] and potential higher ash slagging tendency.[72] Further research on utilization of herbaceous biomass pellets fueled boilers is needed to fully understand ash formation and emission mechanisms.

1.6 Emission Standards and Regulations

1.6.1 National Ambient Air Quality Standards

Main emissions from biomass burning are CO, NO_x (NO and NO_2), SO_2 and PM, as well as trace amount of organic carbonaceous materials (OGC). Table 1-4 lists the national ambient air quality standards (NAAQS) from US Environmental Protection Agency (EPA) for the major pollutants related to biomass combustion.[73]

Table 1-4. US NAAQS table for major pollutants

Pollutant		Primary/Secondary	Averaging Time	Level
CO		Primary	8 hours	9 ppm (10 mg/m^3)
			1 hour	35 ppm (40 mg/m^3)
NO_2		Primary	1 hour	100 ppb (188 μg/m^3)
		Primary and Secondary	1 year	53 ppb (100 μg/m^3)
SO_2		Primary	1 hour	75 ppb (197 μg/m^3)
		Secondary	3 hour	0.5 ppm (1310 μg/m^3)
PM	$PM_{2.5}$	Primary	1 year	12.0 μg/m^3
		Secondary	1 year	15.0 μg/m^3
		Primary and Secondary	24 hours	35 μg/m^3
	PM_{10}	Primary and Secondary	24 hours	150 μg/m^3

According to EPA data, a total of roughly 2.9 million homes in US use wood heat, and mostly are pellet and wood stoves with growing market. On February 2015, EPA announced a 5-year phase plan to meet the controlled final emission limits by 2020 for residential small scale biomass burners. The first step-down will set PM emission limit for new wood and pellet stoves at 4.5 g/h. The next phase will take effect in 2020 with the PM emission limit at 2 – 2.5 g/h, depending on different wood types.[74]

1.6.2 European Emission Regulations for Small-Scale Units

For gaseous emissions, there are no pertinent regulations and standards available in the US. In 2015, the US EPA announced the New Source Performance Standards (NSPS) which was a compliance requirements for residential wood heaters including (1) wood stoves and pellet stoves, (2) wood-fired hydronic heaters, and (3) wood-fired forced air furnaces.[75] The NSPS set the PM limit at 0.32 pounds per million Btu heat output (or 0.14 g/MJ heat input) with a cap of 18 grams per hour for individual test runs.

A lot of official regulations for emissions from small scale wood combustion system in some European countries, as listed in Table 1-5.[76]

Table 1-5. Official regulations for emissions from small scale wood combustion systems

Regulation	Mode	Nominal Output (kW)	mg/m^3 dry base flue gas, 10% O_2, 0 °C, and 1 atm		
			CO	OGC	Dust
EN 303-5	M	<50	5000	150	150
	A	<50	3000	100	-
Swedish Boverket	M/A	<50	2000	150[a]/250[b,c]	100
German Federal Ministry of Economics and Labor[c,d]	M/A	<15	250[e]/500[f]	-	50
Bundes-Immissions Schutzgesetz-BimSchV[c,g]	M/A	15 – 50	4000	-	150

Mode: M – Manual, A – Automatic;
a – for pellet boiler;
b – for pellet heating stoves;
c – limit values are defined for 13% O_2 in the dry flue gas;
d – boiler efficiency has to be minimal of 85%;
e – nominal load;
f – low load;
g – no regulation for boiler/stoves smaller than 15 kW.

For small-scale biomass combustion systems, the main emission control method is to apply quality marks for individual combustion unit. Table 1-6 lists some quality labelling for pellet boilers in EU.[13]

Table 1-6. Quality requirements of pellet boilers as per relevant quality labels in EU

Quality Label	Efficiency (%)	Power (kW)	Operation Mode	CO_2 ($\%_{min}$)	mg/m^3 at 10% dry O_2, 0 °C, 1 atm			
					CO	OGC	NO_x	Dust
P-mark	≥80[a]/≥86[b]	≤25[c]/100[d]	Auto	ND	2000	75	-	-
Swan mark[g]	≥79	≤100	Nominal	ND	2000	70	340	70
			Low	ND	2000	70	-	-
Blue Angel[e]	≥90	≤15	Nominal	ND	100	5	150	SV
	≥88		Low	ND	300	5	150	30
	≥90	15 – 50	Nominal	ND	100	5	150	SV
	≥88		Low	ND	250	5	150	15
UZ-37-Austria[f]	≥90	≤400	Nominal	ND	60	3	100	15
			Low	ND	135	3	-	-/SV
Flamme Verte[g]	≥70	≤50	Manual	ND	6500	225	-	165
			Auto	ND	4000	150	-	165
	≥70	50 – 70	Manual	ND	3750	150	-	165
			Auto	ND	3500	115	-	165
SEI-Ireland[g]	≥80	≤10	Auto	ND	2500	80	-	150
Optimaz[g]	≥89	≤70	Nominal	12.5	110	-	120	NYD
	≥89		Low					
Optimaz-el[g]	≥91	≤70	Nominal	12.5	110	-	120	NYD
	≥97		Low					
EU-ecolabel	NYD	NYD	NYD	NYD	NYD	NYD	NYD	NYD

SV – specify the value; NYD – Not yet defined;
Optimaz and Optimaz-el values in mg/kWh and fueled with liquid fuels
a – when tested according to sections 5.2 and 5.3 of SP-METHOD 2502;
b – when tested according to sections 5.2 and 5.3 of SP-METHOD 2503;
c – burners only;
d – boilers with or without hot water tank;
e – values measured in the dry exhaust gases at 0 °C and 1 atm with oxygen of 13%;
f – values are given in mg/MJ;
g – permissible efficiency based on the heat output.

Based on Table 1-6, Optimaz-el quality label has the highest efficiency requirement for pellet boilers while Blue Angel quality label has the strictest emission requirement for CO, OGC, NO_x and dust. There is no SO_2 emission in that wood has very low sulfur content and hence negligible SO_2 emission.

Chapter 2. Introduction and Literature Review

2.1 Wood Pellet and Combustion

Wood pellets are pelletized wood that have lower moisture content, higher energy density and packing density than log wood, which enables easier transportation and quality control for wood as a fuel. Wood pellets also makes modern automated combustion systems easier to design and build. The basic combustion mechanics, on the other hand, is similar to raw wood combustion.

2.1.1 Wood Pellet Production

Raw wood are harvested from the field (or from other sources) and usually debarked to remove high ash content barks and branches. The wood are then chopped into small chips and transported for grinding, drying, pelletizing, and cooling processes to obtain final product of wood pellet. The schematic and a typical representation of the final product are shown in Figure 2-1.[77]

Wood Resource: The wood resource comes from several sectors: forest log wood, wood chip, sawdust, wood shavings, etc. Recycled wood can sometimes also be used.

Coarse Grinding: The raw wood is milled into coarse sawdust for efficient subsequent drying process.

Drying: Most raw wood materials have high moisture content up to 50%. Drying is critical to produce the final product since high moisture content material is hard to pelletize. Drying is an energy intensive process in the overall procedure. Moisture content less than 10% is suitable for pelletizing.[78]

Fine Grinding: The dried, coarse ground raw material is then fine ground into flour like material for pelletizing.

Pelletizing: Fine ground wood raw material is the separated for final pelletizing. A combination of hot water and steam (1 – 2%) are used to heat the fine ground wood to around 70 °C. The heating ensures the release of lignin and hence softened the raw material for pressing. Binding additives (usually starch and lignin based chemicals[79]) are added for more efficient binding during pelletizing. Typical pellets are 6 – 12 mm in diameter and 10 – 30 mm in length with green-brown in color, as shown in Figure 2-1.

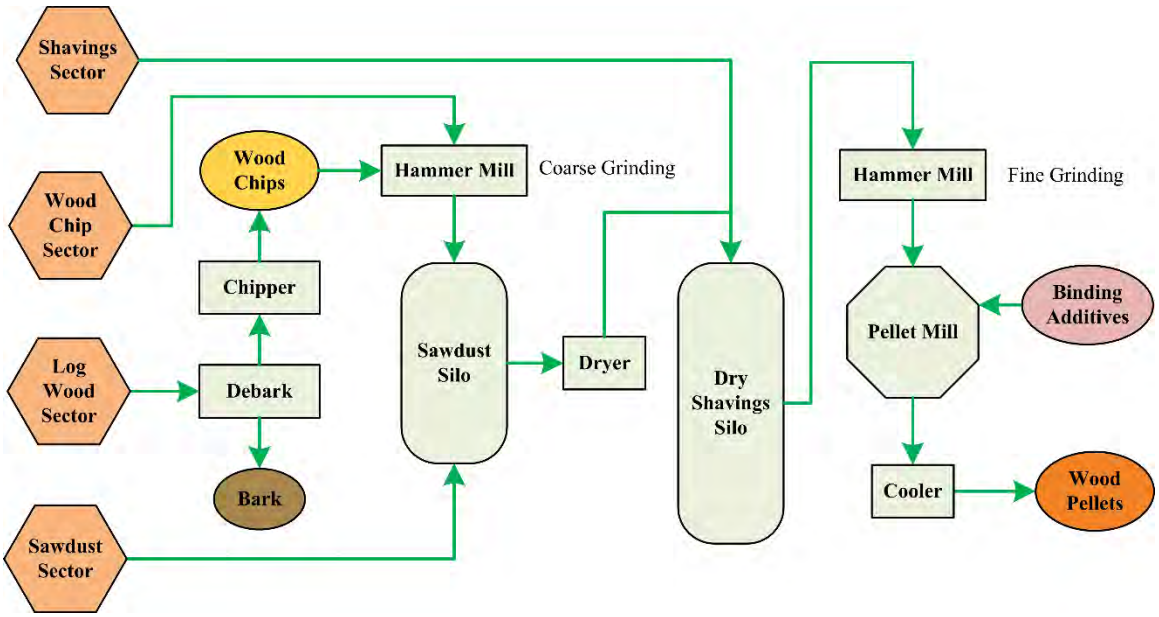

Figure 2-1. Schematics of wood pellet production procedures and final product

Cooling: The product wood pellets are cooled and stored in pellet silos ready for delivery to customers. Cooling process increases the durability of the pellets and hence decreases the formation of dust during transportation.

Packaging and Delivery: Bulk pellets are truck-delivered to customers. Pneumatic tube delivery of wood pellets from delivery truck to customer pellet storage silo is the most common method. Small volume delivery usually comes in 40 lb bags.

2.1.2 Quality Control

Many factors influence the final product quality. Quality control of wood pellets ensures relatively uniform pellet fuel quality. The European countries have developed related standards and guidelines for wood pellet market.

2.1.2.1 United States Wood Pellet Standards

Pellet Fuel Institute (PFI) developed voluntary standards for residential/commercial densified fuel standards, as listed in Table 2-1.[80]

Table 2-1. Residential/commercial densified wood pellet fuel standards (Pellet Fuel Institute Standards Program)

Fuel Property	PFI Premium	PFI Standard	PFI Utility
Bulk Density, kg/m^3	640.7 – 736.8	608.7 – 736.8	608.7 – 736.8
Diameter, cm	0.584 – 0.724	0.584 – 0.724	0.584 – 0.724
Pellet Durability Index	≥ 96.5	≥ 95.0	≥ 95.0
Fines, %	≤ 0.50	≤ 1.0	≤ 1.0
Inorganic Ash, %	≤ 1.0	≤ 2.0	≤ 6.0
Length, % greater than 1.5 inches	≤ 1.0	≤ 1.0	≤ 1.0
Moisture, %	≤ 8.0	≤ 10.0	≤ 10.0
Chlorine, ppm	≤ 300	≤ 300	≤ 300

2.1.2.2 European Wood Pellet Standards

European countries have developed a series of pellet fuel standards for both testing and specifications for pellet fuels, as listed in Table 2-2.[81] Those standards set limit values for physical, mechanical, and chemical properties of wood pellets. Physical

properties are pellet size, bulk density, moisture content, and fines content. Mechanical property is pellet durability. Chemical properties are heating value, ash content, and trace elements of N, S, and Cl.

Table 2-2. Wood pellet quality control standards in European countries

Countries	Standards	Note
Austria	ÖNORM M 7135	For wood pellets and briquettes.
Sweden	SS 187120	Defined three categories of wood pellets.
Germany	DIN 51731	For wood pellets and briquettes.
	DIN EN 15270	For high-quality pellets.
Italian	CTI-R04/05	For biomass pellets including wood pellets and herbaceous pellets.
French	ITEBE	Government recommendation for wood pellets.
European Union	CEN/TC 335	For all forms of solid biofuel in Europe, including wood chips, wood pellets, wood briquettes, wood logs, sawdust, and straw bales.

Table 2-3 lists the solid biofuel standard published by the European Standard Committee as CEN/TC 335.[82] Although the general CEN/TC 335 standard exists, individual standards are still being applied in different EU countries. Hence, it is of great significance to establish a globally accepted standard that will benefit both pellet trade and solid fuel combustion technology transfer.

Table 2-3. Solid biofuel specifications and set limits in CEN/TC 14588: 2004, published by the European Standard Committee CEN/TC 335 including analytical techniques

Solid Fuel Property	Fuel Specification and Limits
Size (mm): D – Diameter L – Length	D06: D ≤ 6 ± 0.5 and L ≤ 5D D08: D ≤ 8 ± 0.5 and L ≤ 4D D10: D ≤ 10 ± 0.5 and L ≤ 4D D12: D ≤ 12 ± 1.0 and L ≤ 4D D25: D ≤ 25 ± 1.0 and L ≤ 4D
Moisture (%)	M10: ≤ 10%; M15: ≤ 15%; M20: ≤ 20%
Ash (%)	A0.7: ≤ 0.7%; A1.5: ≤ 1.5%; A3.0: ≤ 3.0%; A6.0: ≤ 6.0%; A6.0+: > 6.0%
Elemental Content (%)	
N	N0.3: ≤ 0.3%; N0.5: ≤ 0.5%; N1.0: ≤ 1%; N3.0: ≤ 3.0%; N3.0+: > 3.0%
S	S0.05: ≤ 0.05%; S0.08: ≤ 0.08%; S0.1: ≤ 0.1%; S0.2: ≤ 0.2%; S0.2+: > 0.2%
Cl	CL0.03: ≤ 0.03%; CL0.07: ≤ 0.07%; CL0.1: ≤ 0.1%; CL0.1+: > 0.1%
Durability[a] (%)	DU97.5 ≥ 97.5% DU95 ≥ 95%; DU90 ≥ 90%
Fines Content (%, < 3.15 mm)	F1.0: ≤ 1%; F2.0 ≤ 2%; F2.0+: > 2%
Bulk Density (kg/m^3)	Recommended values included by manufacturer
Heating Value (kcal/kg)	Recommended values included by manufacturer
Additives	Binding materials and ash inhibitory included

a – durability is defined as the percentage of whole pellets left after testing.

2.1.3 Wood Pellet Combustion

Wood pellet combustion process can be divided into four steps based on thermogravimetric analysis (TGA) method: drying, pyrolysis, gasification, and combustion based on the temperature range as shown in Figure 2-2.[60,88] Certain degree of overlap and temperature shift can occur among different phases for different biomass materials.

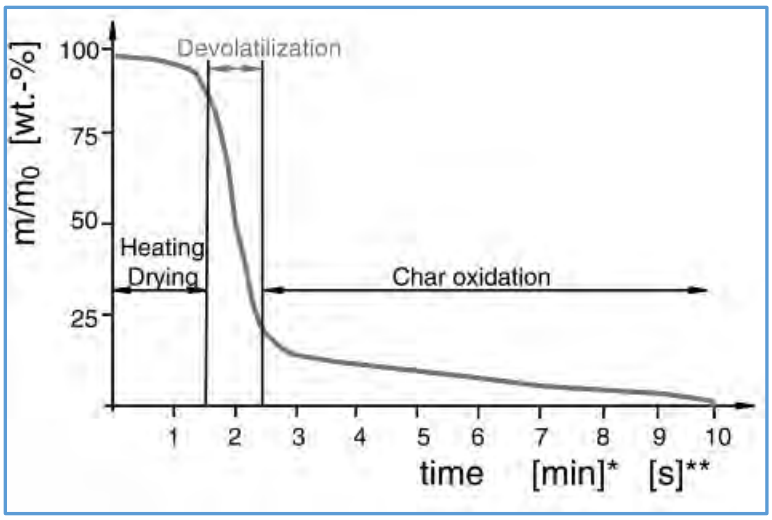

Figure 2-2. Beech wood particle mass loss as a function of time (*[min]: TGA of beech wood, m_0 = 100 mg, dT/dt = 100 °C/min; **[s]: particle combustion with m_0 = 1 mg) (source: Nussbaumer, T. 2003,[88] with permission to use)

2.1.3.1 Step 1: Drying

Drying is the first step of solid fuels combustion since moisture evaporates when temperature increases. Drying is completed when temperature reaches approximately 150°C. High moisture content fuels such as green wood (up to 60% of moisture) need to be pretreated to lower its moisture content for efficient combustion because significant energy is absorbed to evaporate the moisture instead of maintaining the optimum

combustion temperature inside the combustion chamber. Hence, low moisture content wood pellets are better than other types of solid fuels for efficient combustion.

2.1.3.2 Step 2: Pyrolysis/Devolatilization

As mentioned in section 1.4.1.2, pyrolysis is the thermal degradation (or devolatilization) of wood pellets in the absence of oxygen. According to Figure 2-2, devolatilization starts simultaneously when the drying step ends at temperature from 150 °C to 300 °C. The devolatilization rate increases with increasing temperature. The wide range of temperatures for devolatilization indicates different decomposition temperature ranges for cellulose, hemicellulose, and lignin, the three main compositions of any woody material. At lower temperatures, cellulose starts to decompose followed by hemicellulose. Lignin mainly decomposes at higher temperatures around 400 – 500°C. The main products from wood pellet pyrolysis/devolatilization include low molecular weight hydrocarbons, solid char, and tar, and small amounts of CO, CO_2, H_2, CH_4, etc., which are similar to the volatile product in the proximate analysis process. Cellulose, hemicellulose, and lignin are responsible for CO, CO_2, and H_2/CH_4 yields, respectively.[83]

2.1.3.3 Step 3: Gasification

Gasification is different from pyrolysis/devolatilization in that a small amount of oxygen is supplied. Gasification can also refer to the high temperature (800 – 1100°C) char reaction with CO_2 or H_2O. Gasification products are mainly CO, CO_2, H_2O, H_2, CH_4, and other gaseous hydrocarbons. Gasification can be achieved with air to produces low calorific value gases (GCV = 4 – 7 MJ/Nm^3 dry, comparing to natural gas with a GCV of

36 MJ/Nm^3) or H_2O to produce medium calorific value gases (GCV = 12 – 20 MJ/Nm^3 dry).[60] The gasification step can be described with the following chemical reactions:[84]

Oxidation:

$$C + O_2 \rightarrow CO_2 \quad (2\text{-}1)$$

$$C + \frac{1}{2}O_2 \rightarrow CO \quad (2\text{-}2)$$

Boudouard:

$$C + CO_2 \rightarrow 2CO \quad (2\text{-}3)$$

Water-gas:

$$C + H_2O \rightarrow CO + H_2 \quad (2\text{-}4)$$

$$C + 2H_2O \rightarrow CO_2 + 2H_2 \quad (2\text{-}5)$$

Methanation:

$$C + 2H_2 \rightarrow CH_4 \quad (2\text{-}6)$$

Water-gas Shift:

$$CO + H_2O \rightarrow CO_2 + H_2 \quad (2\text{-}7)$$

Steam Reforming:

$$CH_4 + H_2O \rightarrow CO + 3H_2 \quad (2\text{-}8)$$

2.1.3.4 Flame Combustion

All the gaseous products from devolatilization and gasification will be oxidized into CO_2 and H_2O during complete combustion. Hot combustion gas with a temperature around 1200°C transfers heat into boiler jacket water through a fire tube heat exchanger for the production of heat (used for space heating) or steam (used for electricity generation).

Complete combustion requires three T's: temperature, turbulence, and time. The combustion chamber should maintain high temperature with sufficient turbulence to mix the combustible gases with oxygen and hold the process long enough to achieve all the combustion reactions. Incomplete combustion produces CO, soot, and unburnt fuel residues. Hence, oxygen supply and degree of mixing play significant role in determining the combustion efficiency. Air fuel ratio (*AFR*) is defined as the ratio of the mass of air to the mass of fuel presented in a combustion process.). If exactly enough air is provided to completely burn all of the fuel, the ratio is known as the stoichiometric *AFR*, or AFR_{Stoich}.

The excess air ratio (denoted as λ) is defined below as the actual *AFR* to AFR_{Stoich}.

$$\lambda = \frac{AFR}{AFR_{stoich}} \tag{2-9}$$

In real wood pellet combustion systems, air supply is always a little higher than the stoichiometric need since the mixing between fuel and oxygen is not perfect. The quantity of air supplied in excess of stoichiometric air is called excess air (*EA*), expressed in percentage as:

$$EA = (\lambda - 1) \times 100\% \tag{2-10}$$

EA or λ plays a significant role in the combustion process. Low values of *EA* or λ create incomplete combustion resulting emissions of CO, OGC, etc. High values of *EA* or λ can lead to low combustion temperature and high stack loss. Table 2-4 shows the recommended values for boilers burning different fuels at full load.[85]

In general, drying, pyrolysis/devolatilization, gasification, and flame combustion are the four main steps during combustion process. There are no physical boundaries between each step, and hence, it is not possible to separate each step individually. The real combustion process such as the combustion of wood pellets inside a wood pellet boiler is a complex mixture of the four processes.

Table 2-4. Recommended excess air levels for boilers using different fuels at full load

Boiler Fuel Type	Recommended *EA* (%)
Natural Gas	10 – 20
Fuel Oil	10 – 20
Pulverized Coal	20 – 25
Stoker Coal	35 – 40

2.2 Wood Pellet Stoves and Boilers

In residential space heating, wood pellet stoves and boilers are the two main types of wood pellet technology. Wood pellet stoves are usually used for a single room space heating, while wood pellet boilers can heat an entire building or even can be a central district heating unit.

2.2.1 Wood Pellet Stoves

Modern wood pellet stoves have high combustion efficiency and low emissions. They are controlled thermostatically and can be programmed to burn at different rates. A typical wood pellet stove with built in pellet hopper is shown in Figure 2-3.[86]

Figure 2-3. Typical wood pellet stove (source: Rika pellet stove)

Wood pellets are stored in the built-in hopper (storage capacity: 10 – 25 kg) for 1 – 2 days' fuel use. When there is a call for heat, the pellets are delivered into the combustion pot through the screw-auger delivery system from the bottom of the pellet hopper. The pellets are usually fed into the combustion pot from the top. The burner pot varies in size for different output stoves with air blowing in from the bottom by the primary air blower. The pellets are usually ignited electrically with a hot air gun. The combustion chamber is located above the burner pot with proper design to optimize combustion from three aspects: turbulence (air-fuel mixing), temperature, and residence time. A rising yellow

flame can be seen through the window of the stove. Typical temperatures are between 800°C and 1000°C. A hot air circulating fan blows in room air (usually from the bottom) and exchange heat with the hot combustion gas (convective heat transfer) to blow out the heated air (from the top). Most modern pellet stoves have a heat-resistant glass window that the flame is visible. It also helps through radiative heating. The ash is removed from the bottom of the stove.

2.2.2 Wood Pellet Boilers

Unlike wood pellet stoves, wood pellet boilers use water as the heat carrier. A typical wood pellet boiler is shown in Figure 2-4.[87]

Figure 2-4. Cut away diagram of a typical wood pellet boiler (source: pellergy alpha pellet boiler)

The basic operation of wood pellet boilers are similar to that of a wood pellet stove. However, there are some differences. First, the heat carrier is water, which means a wood pellet boiler is a pressure vessel and external heat storage (e.g. water tank) and heat dissipation units (e.g. baseboard heaters) are required. Second, most wood pellet boilers have an external wood pellet storage silo. Hence, another auger is needed to deliver pellets from the external silo into the wood pellet boiler. Third, wood pellet boilers can have a wide range of output capacity ranging from less than 10 kW up to more than 100 MW.[88] Last, modern wood pellet boilers have

very sophisticated control systems to ensure high boiler efficiency. For example, lambda control allows the boiler to monitor exhaust gas oxygen concentration to change suction fan speed for optimal combustion; negative pressure control allows the boiler to monitor the draft continuously; flame sensor allows the boiler to monitor the light intensity of the combustion flame; self-cleaning turbulators allow the boiler to clean its fire tube heat exchangers at the beginning of each boiler cycle, etc.

Based on the different positions of the pellets delivered into boiler combustion chamber, wood pellet boilers can be categorized as top-fed, horizontal-fed and bottom-fed types. The screw auger feeding types are shown in Figure 2-5.[76]

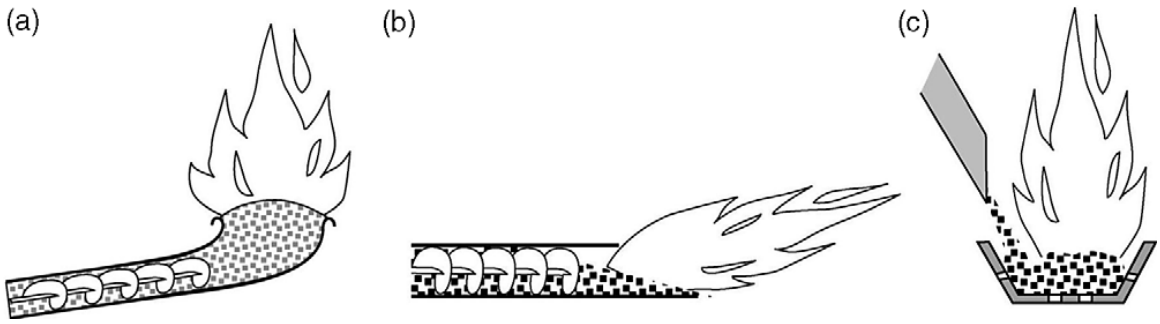

Figure 2-5. Types of pellet boilers by the feed screw auger position: (a) bottom fed; (b) horizontal fed; (c) top-fed (source: Fiedler 2004[76]).

2.2.2.1 Top-Fed Wood Pellet Boiler

Most European market small scale residential wood pellet boilers (and stoves) use top-fed burners. The advantage of this type of burner is that the fuel storage is separated from the combustion flame eliminating the risk of back burning as well as long term after glow when the boiler is turned off.[89] Another advantage is that the output capacity of the boiler can be precisely controlled by changing the amount of pellets fed into the boiler.

However, there also exist disadvantages of the top-fed type boiler. The main issue is that the fresh pellets fed into the combustion chamber can disturb the existing combustion conditions and increase the emissions of dust and unburnt fuel particles.

2.2.2.2 Horizontal-Fed Wood Pellet Boiler

Horizontal-fed wood pellet boilers have similar construction as top-fed wood pellet boilers. The only difference is the burner pot design and the need of an additional ash removal mechanism.[76] In addition, regular maintenance such as cleaning of the heating surface and the burner pot must be performed.[90]

2.2.2.3 Bottom-Fed Wood Pellet Boiler

The bottom-fed boiler design is typical for wood chip boilers (also suitable for wood pellet boiler).[76] Pellets are fed into the burner pot from the bottom and push the fuel upward into the combustion chamber where the primary air is supplied. Secondary air is usually supplied through the burner rings on top of the burner pot or provided through additional air tubes above the burner pot. Ash is displaced by bottom-fed pellets and falls over the edge of the burner. Bottom-fed boiler design has very consistent combustion behavior but also has very long burn-out time due to the supply principle of the fuel. Additional stop mechanism is needed for prevention of back-fire.

2.2.3 Wood Pellet Boiler Performance Study

The performance of a wood pellet boiler includes the boiler's efficiency (combustion efficiency, thermal efficiency, and heat transfer efficiency), and the boiler's

emissions. A good wood pellet boiler design achieves both high efficiency and low emissions.

2.2.3.1 Wood Pellet Boiler Efficiency

Table 2-5 lists related studies on wood pellet boiler efficiency. Most of the studies focus on small scale residential wood pellet boilers.

Table 2-5. List of studies related on wood pellet boiler studies

Reference	Capacity (kW)	Fuel	Method	Efficiency (%)
91	150/500	Wood pellets	ASHRAE 155p	70 – 86/75 – 91
92	15	Agro-pellets	Indirect	80 – 94
93	15 – 35	Wood pellets	Siegert method[a]	70 – 90
94	35, 40	Multi	Siegert method[a]	88 – 91
95	12	Agro-blended	Indirect	88 – 90[b]
			Direct	76 – 89[c]
96	25	Wood pellets	Indirect	82 – 94[b]
			Direct	76 – 89[c]
97	6 – 26	Wood pellets	Direct	67 – 85[d]

a: Siegert method is used for calculating combustion efficiency.
b: boiler combustion efficiency.
c: boiler thermal efficiency.
d: annual boiler thermal efficiency.

Carvalho et al.[92] studied the performance of a 15 kW wood pellet boiler fired with different agricultural pellets and found that improved boiler control was needed to use their high ash content agricultural pellets. Frequent cleaning of the heat exchangers was also essential. Verma et al.[93] studied five wood pellet boilers with capacities ranging from 15 kW to 35 kW and three different burner pot designs at both full and reduced load conditions. They found that to achieve high efficiency, the boilers should always fire at high load output rather than reduced load conditions. Comparing to nominal load, top-fed boilers had higher CO emission at reduced loads. Horizontal-fed boilers had higher NO_x at reduced loads. Bottom-fed boilers had the higher combustion efficiencies at reduced

load. Verma et al.[94] also compared boiler performance in both a standard lab test and under field conditions. They found that combustion efficiencies were 2% lower in real use conditions. Žandeckis et al.[96] studied the combustion and thermal performance of a 25 kW wood pellet boiler in a standard laboratory test and applied the optimized parameters to a 100 kW wood pellet boiler's control algorithm. Better performance was achieved through adjusting the flue gas O_2 content, and the location of air intake point. They found exponential decrease of boiler efficiency and increase in CO emission with increasing flue gas O_2 content. Carlon et al.[97] studied the performance for five residential systems with boiler capacity ranging from 6 kW to 26 kW in terms of annual fuel conversion efficiency. They found a strong relationship between boiler thermal efficiency and boiler output load following a first-order response.

There are two methods for calculating wood pellet boiler efficiency: the direct method and the indirect method. Boiler thermal efficiency is usually calculated using the direct method while boiler combustion efficiency is usually assessed with indirect method. The direct method[98] is based on the heat input and heat output of the boiler, as shown below.

$$\eta_{\text{th}} = \frac{E_{\text{out}}}{E_{\text{in}}} \times 100\% \tag{2-11}$$

where η_{th} is the boiler thermal efficiency, E_{out} and E_{in} are boiler energy output and heat input, respectively.

The indirect method[99] is based on the heat loss of the boiler combustion including thermal loss, chemical loss, and other heat losses, as shown below.

$$\eta_{\mathrm{com}} = 100\% - L_{\mathrm{g}} - L_{\mathrm{h}} - L_{\mathrm{m}} - L_{\mathrm{CO}} - L_{\mathrm{in}} - L_{\mathrm{un}} \quad (2\text{-}12)$$

where L_{g} is heat loss due to dry flue gas (thermal heat loss); L_{h} is heat loss due to burning of fuel hydrogen (latent heat loss); L_{m} is heat loss due to fuel moisture content (latent heat loss); L_{CO} is heat loss due to the formation of CO; L_{in} is heat loss due to heat exchange with the environment; and L_{un} is the heat loss due to unburnt fuel. Compared to the direct method, indirect method can itemize heat losses and is more useful in determining the efficiency loss in the boiler. A widely recognized relationship between boiler combustion efficiency and excess air ratio is that combustion efficiency drops linearly with increasing excess air.[100]

2.2.3.2 Wood Pellet Boiler Emissions

Compared to fossil fuels, wood pellet combustion produces greater emissions, which makes the application of wood-burning appliances and wood-burning systems even harder. Table 2-6 lists the possible emissions from a common wood pellet boiler.

Table 2-6. List of possible emission pollutants from wood pellet combustion.

Emission Categories	Pollutants
Particulate	Ultrafine particles, $PM_{2.5}$, PM_{10}, Black Carbon, Soot, etc.
Gaseous	CO, SO_x, NO_x, etc.
Liquid	Tar, Creosote, Bio-oil, etc.

Many studies have been made on the emissions characterization of wood pellet boilers. In general, emission studies can be divided into four categories: (I) emissions from different pellet fuels for the same boiler; (II) emissions from different boilers using the same pellet fuel; (III) emissions from the same boiler under different operation conditions; (IV) combination of previous categories. In general, category IV is the most

common in published literature as this category offers the most complexity for research. Table 2-7 summarizes related studies in this area.

Table 2-7. Summary of wood pellet boiler emission studies

Burner	Fuel	Category	Reference	Notes
10 – 30 kW (old and modern)	Wood log, pellets, oil	IV	101	(1). Old burners have highest emissions; (2). TOC, Semivolatiles, PAH emissions follow well with CO emission; (3). It is urgent to replace old burners.
11 kW, 22 kW, burner; 6 kW, stove	Wood pellets & briquettes	IV	102	(1). Particle emissions only: 34 – 240 mg/Nm^3, 10^7 -10^8 #/Ncm^3, submicron particles dominate; (2). K, S, Cl, O are main inorganic components; (3). Excess air affects particle number-size distribution.
8 kW, stove	5 pellets from stem/bark, 1 wood pellets	I	103	(1). Top-fed stove; (2). 5 bark/stem pellets all have emissions of NO_x, CO, and PM1.0 higher than wood pellets; (3). PM1.0 is the major fine particle emissions, independent of fuel type.
22 kW, boiler	3 types of pellets	IV	109	(1). Different operation conditions (half load to full load) significantly affect CO and HC emissions, but not for NO_x emissions; (2). At reduced load, CO: 400 – 600 ppm, NO_x: 50 – 500 ppm; HC: 50 – 100 ppm. At high load, CO: 200 – 1000 ppm; NO_x: 50 – 500 ppm; HC: 10 -200 ppm. (3). Industrial wood wastes and peach stones are great alternative fuels for wood pellets.
Burner: 10 kW, 20 kW; stove: 4 kW, 7 kW; boiler: 8 kW, 25 kW	Softwood pellets from different suppliers	IV	104	(1). Two combustion conditions – flaming and glowing lab test for HC emissions; (2). Field test of stove and boiler, CO: 10 - 500 ppm (40 ppm for 25 kW boiler); (3). Stove has the highest emissions for CO, CH_4, Benzene emissions.
13 kW, boiler	4 types of pellets	IV	105	(1). Flue O_2 decreases linearly with boiler input; (2). CO: 500 – 1700 mg/Nm^3 for all pellets; (3). NO_x: 100, 200, 350 mg/Nm^3 for three pellets but increased linearly with flue O_2 for the first type pellet; (4). Maximum CO at boiler start, up to 1.5%.
20 kW, boiler (with DHW); 12 kW, stove (with solar); three other 20 kW boiler (all with solar)	3 batch of wood pellets	IV	106	(1). CO: increase dramatically when start and stop stages are included; (2). NO: pretty constant around 60 – 95 mg/MJ; (3). TOC: less than 10 mg/MJ when not including start and stop stages; (4). PM2.5: 55 – 83 mg/MJ without start and stop; PM2.5 #: 1.8 – 4.0 × 10^{13} per MJ.
25 kW boiler	Wood pellets	III	107	(1). Load and air staging affect particle and gaseous emission factors; (2). Primary air reduction decreases emission factors, PM1 from 12.2 to 5.9 and 3.0 mg/MJ; (3). Lowest emission of K and SO4 from reduced

	primary air supplies; (4). Reduction in secondary air supply increases OC and particle emissions and larger particle size. Ratio of $\lambda_{prim}/\lambda_{sec}$ is the most important.

Particle emissions are dominated by submicron particles.[102] Particle number emission factors are of the order of 10^{13} #/MJ.[101,106,108] $PM_{2.5}$ mass emission factors are typically less than 100 mg/MJ, ranging from 10 – 80 mg/MJ.[101,103,106,108] The inorganic components of the submicron particles are mainly K, S, Cl, and O, leading to the formation of K_2SO_4, KCl, etc. For example, Johansson et al.[102] found a typical alkali compounds composition of a submicron particle from wood pellet combustion was 69% K_2SO_4, 24% KCl, 2% NaCl, Na_2CO_3, Na_2SO_4, and 1% Na_2CO_3.

CO emission factors for different systems using different fuels and operating at different stages vary significantly from less than 100 mg/MJ to over 1000 mg/MJ.[101,103,106,108] Due to the relatively low combustion temperature of wood pellets, NO_x emissions are mainly from fuel contained nitrogen.[88, 109 , 110] Rabaçal et al.[109] measured the emissions from a 22 kW wood pellet boiler using several different pellet fuels and obtained a high linear correlation between NO_x emissions and pellet fuel nitrogen content. Nussbaumer[88] demonstrated the formation of NO_x during wood pellet combustion from fuel nitrogen to intermediate components such as HCN and NH_i (i = 0, 1, 2, 3), as shown in Figure 2-6.

Other gaseous emissions such as PAHs,[111] PCBs,[112] SO_2,[91] etc. were also studied. However, due to the extremely low content of fuel-bound sulfur and chlorine and advanced combustion in modern wood pellet boilers, those emissions are negligible in most cases.

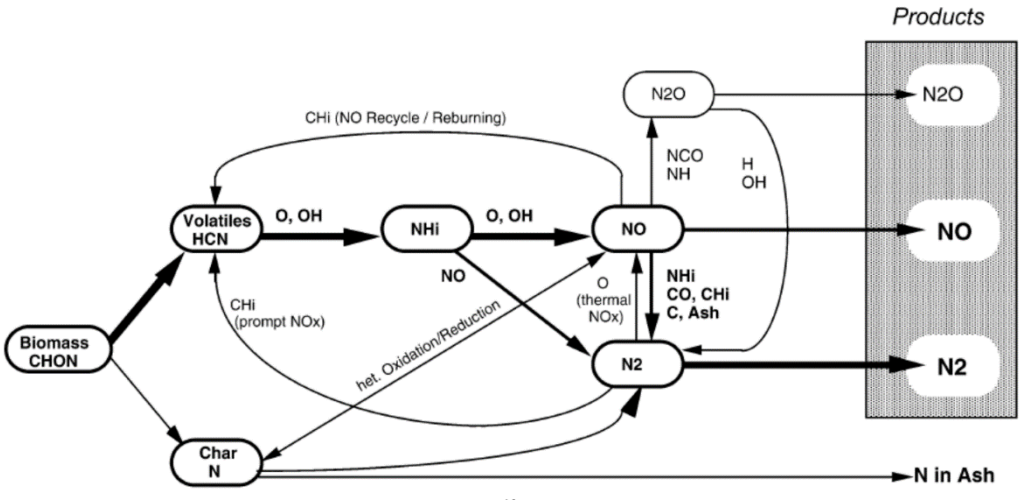

Figure 2-6. NO_x emissions formation from biomass fuel-bound nitrogen (source: Nussbaumer 2003,[88] with permission to use)

2.3 Stratified Hot Water Storage Tank

Stratified water tanks were initially utilized in solar heating systems as thermal storage tanks. Researchers discovered that by maintaining the stratification inside the thermal energy storage (TES) tanks, the energy delivered by a solar system can be increased substantially.[113] This stratification can also be utilized to improve the TES tanks in modern wood pellet heating systems.

2.3.1 Thermal Stratification

Thermal stratification inside a water storage tank is caused by the difference in water density arising from the supply and return water temperature difference. A typical fully stratified water storage tank is shown in Figure 2-7.

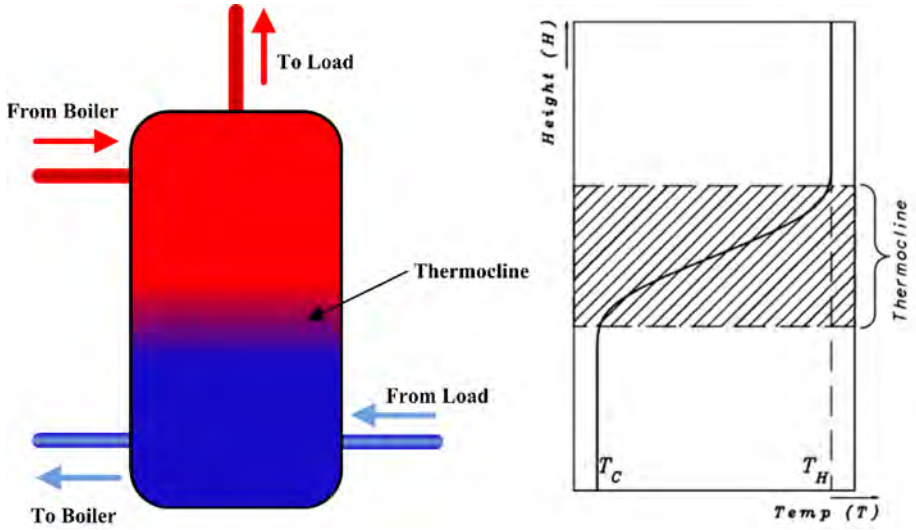

Figure 2-7. Schematic of a typical stratified hot water storage tank (left) and its temperature profile (right)

Lower density, hot boiler supply water is present at the top of the tank due to its buoyance while higher density, cold building return water stays at the bottom of the tank.

The differentiation between hot and cold water inside the tank is called the thermocline. There is no thermocline in a fully mixed water tank. The presence of stratification enhances storage tank performance compared to a fully mixed storage tank.

2.3.2 Analysis of Thermal Stratification

The governing equations to describe the fluid dynamics inside a stratified hot water storage tank (as shown in Figure 2-7) include the continuity equation, the momentum equation, and the energy equation, as listed below (in cylindrical coordinates).

Continuity Equation:

$$\frac{1}{r}\frac{\partial(rv_r)}{\partial r}+\frac{1}{r}\frac{\partial v_\theta}{\partial \theta}+\frac{\partial v_z}{\partial z}=0 \tag{2-13}$$

Momentum Equation:

$$\rho\left(\frac{\partial v_r}{\partial t}+v_r\frac{\partial v_r}{\partial r}+\frac{v_\theta}{r}\frac{\partial v_r}{\partial \theta}+v_z\frac{\partial v_r}{\partial z}-\frac{v_\theta^2}{r}\right)$$
$$=-\frac{\partial p}{\partial r}+\mu\left[\frac{\partial}{\partial r}\left(\frac{1}{r}\frac{\partial(rv_r)}{\partial r}\right)+\frac{1}{r^2}\frac{\partial^2 v_r}{\partial \theta^2}+\frac{\partial^2 v_r}{\partial z^2}-\frac{2}{r^2}\frac{\partial v_\theta}{\partial \theta}\right] \tag{2-14}$$
$$+\rho g_r\beta\Delta T$$

$$\rho\left(\frac{\partial v_\theta}{\partial t}+v_r\frac{\partial v_\theta}{\partial r}+\frac{v_\theta}{r}\frac{\partial v_\theta}{\partial \theta}+v_z\frac{\partial v_\theta}{\partial z}+\frac{v_r v_\theta}{r}\right)$$
$$=-\frac{1}{r}\frac{\partial p}{\partial \theta}+\mu\left[\frac{\partial}{\partial r}\left(\frac{1}{r}\frac{\partial(rv_\theta)}{\partial r}\right)+\frac{1}{r^2}\frac{\partial^2 v_\theta}{\partial \theta^2}+\frac{\partial^2 v_\theta}{\partial z^2}+\frac{2}{r^2}\frac{\partial v_r}{\partial \theta}\right] \tag{2-15}$$
$$+\rho g_\theta\beta\Delta T$$

$$\rho\left(\frac{\partial v_z}{\partial t}+v_r\frac{\partial v_z}{\partial r}+\frac{v_\theta}{r}\frac{\partial v_z}{\partial \theta}+v_z\frac{\partial v_z}{\partial z}\right) = -\frac{\partial p}{\partial z}+\mu\left[\frac{1}{r}\frac{\partial}{\partial r}\left(r\frac{\partial v_z}{\partial r}\right)+\frac{1}{r^2}\frac{\partial^2 v_z}{\partial \theta^2}+\frac{\partial^2 v_z}{\partial z^2}\right]+\rho g_z\beta\Delta T \quad (2\text{-}16)$$

Energy Equation:

$$\rho c_p\left(\frac{\partial T}{\partial t}+v_r\frac{\partial T}{\partial r}+\frac{v_\theta}{r}\frac{\partial T}{\partial \theta}+v_z\frac{\partial T}{\partial z}\right)=k\left[\frac{1}{r}\frac{\partial}{\partial r}\left(r\frac{\partial T}{\partial r}\right)+\frac{1}{r^2}\frac{\partial^2 T}{\partial \theta^2}+\frac{\partial^2 T}{\partial z^2}\right]+\mu\boldsymbol{\Phi}_v \quad (2\text{-}17)$$

Where v_r, v_θ, and v_z are velocities in r, θ, and z directions, respectively (m/s); T is temperature (K); μ is dynamic viscosity (Pa·s); ρ is density, β is thermal expansion coefficient (K^{-1}); c_p is specific heat ($J\cdot kg^{-1}\cdot K^{-1}$); k is thermal conductivity ($W\cdot m^{-1}\cdot K^{-1}$); $\boldsymbol{\Phi}_v$ is viscous dissipation; g_r, g_θ, and g_z are gravitational acceleration in r, θ, and z directions, respectively, (m/s^2); p is fluid pressure (Pa). Equations (2-13) to (2-17) are valid only for incompressible fluids with constant k. In addition, the viscous dissipation term, $\boldsymbol{\Phi}_v$ is often neglected in hot water storage tanks as the velocity gradients inside the tank are usually negligible.

2.3.2.1 One-Dimensional Model

Many models have been developed based on the governing equations for real problems.[114] A simplified one-dimensional model analysis is shown in Figure 2-8.[115] The cylindrical tank is divided into N equal elements along its height. With the initial temperature known, an energy balance performed on each element gives the governing equation for the one-dimensional transient conduction problem, considering heat conduction along the tank wall. Equations (2-18) and (2-19) are the governing equations for this model.

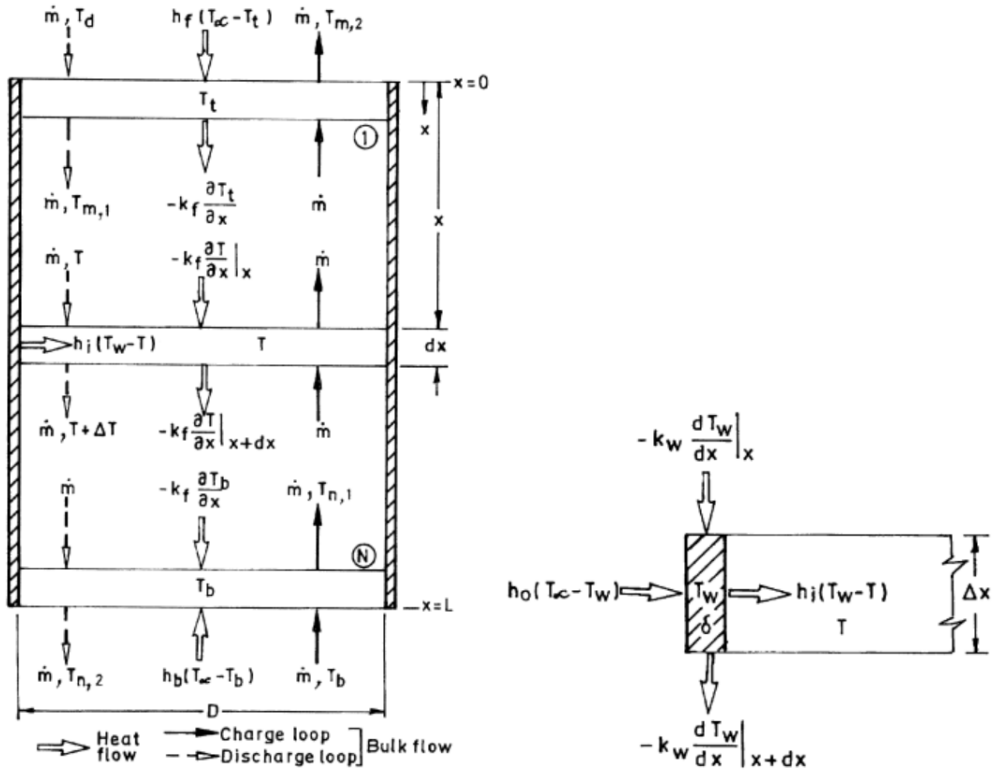

Figure 2-8. Schematics of the elemental volume analysis of stratified tank (left) and the wall heat transfer analysis (right) (source: Nelson et al., 1999[115])

$$\frac{\partial T}{\partial t} = \frac{k_f}{\rho_f c_f}\frac{\partial^2 T}{\partial x^2} - \frac{\dot{m}}{A_f \rho_f}\frac{\partial T}{\partial x} + \frac{h_i P}{A_f \rho_f c_f}(T_w - T) \tag{2-18}$$

$$\frac{\partial T_w}{\partial t} = \alpha_w \frac{\partial^2 T_w}{\partial x^2} + \frac{h_o P}{A_w \rho_w c_w}(T_\infty - T_w) - \frac{h_i P}{A_w \rho_w c_w}(T_w - T) \tag{2-19}$$

where $\dot{m}$ is the tank charge or discharge rate (kg/s), P is perimeter of the tank (m), and α_w is thermal diffusivity of the wall. Subscript *f* stands for fluid, and subscript *w* stands for wall; subscript *i* stands for internal, and subscript *o* stands for external.

2.3.2.2 Two-Dimensional Model

One dimensional model can approximate the temperature profile in a stratified water tank. However, a one-dimensional model cannot describe detailed flows. Hence,

two dimensional models are developed based on the governing equations from equations (2-13) to (2-17) (in Cartesian coordinates). For simplicity, the governing equations are transformed into dimensionless equations.[114] For different cases, the final form of the model may vary.

Continuity Equation:

$$\frac{\partial(\rho^* u^*)}{\partial x^*} + \frac{\partial(\rho^* v^*)}{\partial y^*} = 0 \tag{2-20}$$

Momentum Equation:

$$\frac{\partial u^*}{\partial t} + \frac{\partial(\rho^* u^*)}{\partial x^*} = \frac{\partial p^*}{\partial x^*} + \frac{1}{\mathrm{Re}}\left(\frac{\partial^2 u^*}{\partial x^{*2}}\right) \tag{2-21}$$

$$\frac{\partial v^*}{\partial t} + \frac{\partial(\rho^* v^*)}{\partial y^*} = \frac{\partial p^*}{\partial y^*} + \frac{1}{\mathrm{Re}}\left(\frac{\partial^2 v^*}{\partial y^{*2}}\right) + \mathrm{Ri}\theta \tag{2-22}$$

Energy Equation:

$$\frac{\partial \theta}{\partial t} + \nabla \cdot (u^* \theta) = \frac{1}{\mathrm{RePr}} \nabla^2 \theta \tag{2-23}$$

where $x^* = 2x/D$, $y^* = y/H$ (D is tank diameter, H is tank height; $u^* = u/u_0$, $v^* = v/v_0$, (u_0 and v_0 are initial flow speed at x and y directions); $p^* = p/P$ (P is the pressure at the inlet position); $\theta=(T - T_\infty)/(T_\mathrm{i} - T_\infty)$ (θ is dimensionless temperature); Re, Pr, and Ri are Reynolds number, Prandtl number, and Richardson number, respectively.

$$\mathrm{Re} = \frac{\rho u D}{\mu} \tag{2-24}$$

$$\mathrm{Pr} = \frac{c_p \mu}{k} \tag{2-25}$$

$$\mathrm{Ri} = \frac{\mathrm{g}}{\rho}\frac{\nabla\rho}{(\nabla u)^2} = \frac{\mathrm{g}\beta\Delta TH}{u^2} \tag{2-26}$$

2.3.2.3 Other Models

Three dimensional models are also often used in computational fluid dynamics (CFD) simulation.[116-117] CFD is a powerful tool to formulate complex tank geometries and flow conditions to simulate real case scenario.

2.3.3 Factors Affecting Thermal Stratification

Three factors affect the stratification inside a water tank: tank geometry, flow conditions, and operation conditions.

2.3.3.1 Tank Geometry

Tank geometry such as tank aspect ratio (*AR*), tank size, tank inlet/outlet positions, tank diffuser types, etc. Table 2-8 lists related study on the effect of tank structure on stratification performance.

Table 2-8. List of related studies on tank geometry effect on thermal stratification

Tank Geometry	Note
Inlet location and port size,[118,119,120] inlet diffuser,[121]	(1). Inlet location shall be as close to the bottom as possible; (2). Large inlet port is better than small port (same flow rate); (3). Inlet diffuser reduces flow mixing and enhances stratification.
Baffle/obstacles,[122,123] plates[124]	(1). Baffles improve tank stratification and enhance tank performance; (2). Plate diameter and distance from the bottom have significant effect on stratification.

Tank aspect ratio[118, 125,	(1). Stratification increases with AR, optimal AR: 3 – 4; (2). Long tank is preferable for small storage volumes, optimal AR is suggested to be 3 as no significant improvement for larger AR.
Tank wall thickness,[126] material selection[125,127]	(1). Thicker tank wall has larger heat conduction rate; (2). Low thermal conductivity wall material can reduce de-stratification (stainless steel is better than copper).

Altuntop et al.[122] studied 12 different baffles (as shown in Figure 2-13) placed inside a water tank both numerically and experimentally. They found two most effective baffle configurations for thermal stratification are number 7 and number 11. The effect of obstacles types and positions from the tank bottom were studied by Erdemir and Altuntop[123] and they found that by placing obstacles between 0.2 m and 0.3 m from the tank bottom the best thermal stratification can be achieved.

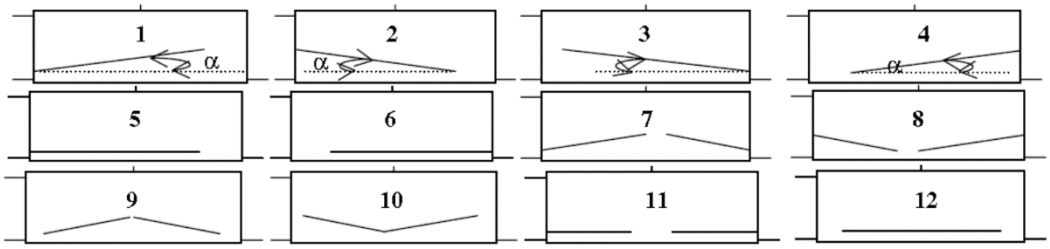

Figure 2-9. Twelve baffle assembly within water tank and their geometries (source: Altuntop et al., 2005[122])

2.3.3.2 Flow Conditions

Flow conditions significantly affect the stratification level inside a water tank. Flow conditions include inlet/outlet flow rate and flow temperature. Lavan and Thompson[118] found that tank performance decreases with increasing flow rate due to increase in turbulent mixing caused by high flow rates. In addition, tank performance increases with increasing outlet/inlet temperature difference as large temperature difference between the stored hot water and incoming cold water into the bottom

produces a stabilizing effect.[118] Other researchers have also found similar results.[119, 125,128]

2.3.3.3 Operation Conditions

A hot water storage tank has two operation stages: charge and discharge. Charge is the process of external heating device heats the tank to a set value of temperature and discharge is the tank provides energy to heat consumption units. Hence, the charge mode will destroy the stratification to achieve an uniform water temperature while the discharge mode establishes thermal stratification. Nelson et al.[125] studied a stratified chilled water storage system with respect to storage tank charging, discharging, and stagnation modes and developed mathematical expressions for each mode.

2.3.4 Thermal Stratification Performance

Several methods can be used to quantify thermal stratification performance such as stratification index, energy efficiency, and exergy efficiency.[114] Those different methods can be categorized as coefficients/numbers index and efficiency index. Efficiency index is more commonly used.

2.3.4.1 Coefficients and Numbers

Wu and Banerot [129] defined stratification coefficient (St_c) as a mean square deviation of temperatures in the storage from the mean storage temperature by dividing the tank into several segments.

$$\mathrm{St}_c = \frac{1}{m_{\mathrm{store}}} \sum_i m_i \left(T_i - T_{\mathrm{avg}}\right)^2 \tag{2-27}$$

where m represents mass of storage fluid, T_i is temperature of the i^{th} segment, and T_{avg} is the average temperature of the tank.

Adams et al.[130] introduced "moment of energy" (M_{E}). For a storage tank, M_{E} is an integration of the sensible energy content (E) along its vertical axis (y) weighted with local height of each segment (total of N segments) of height y_i.

$$M_E = \sum_{i=1}^{N} y_i E_i \tag{2-28}$$

The mix number (MIX) is then defined as the difference of moment of energy between a perfectly stratified storage tank ($M_{\mathrm{E,str}}$) and the measured tank ($M_{\mathrm{E,Exp}}$) divided by the difference of moment of energy between a perfectly stratified storage tank and a fully mixed storage tank ($M_{\mathrm{E,Mix}}$), as shown below.

$$\mathrm{MIX} = \frac{M_{\mathrm{E,Str}} - M_{\mathrm{E,Exp}}}{M_{\mathrm{E,Str}} - M_{\mathrm{E,Mix}}} \tag{2-29}$$

Stratification number (Str) is defined as the ratio of mean temperature gradients at each time to the temperature gradient at the beginning (or maximum gradient), as shown in equation (2-30).[131] Equations (2-31) and (2-32) are the expressions of mean and maximum temperature gradients.

$$\mathrm{Str} = \frac{\overline{(\partial T/\partial z)_t}}{(\partial T/\partial z)_{max}} \tag{2-30}$$

$$\overline{\left(\frac{\partial T}{\partial z}\right)_t} = \frac{1}{J-1}\left[\sum_{j=1}^{J-1}\left(\frac{T_{j+1}-T_j}{\Delta z}\right)\right] \tag{2-31}$$

$$\overline{\left(\frac{\partial T}{\partial z}\right)_{max}} = \frac{T_{max}}{J-1}\frac{T_{in}}{\Delta z} \tag{2-32}$$

2.3.4.2 Efficiency Index

Efficiency index for quantifying stratification includes extraction efficiency[118], and energy/exergy efficiency.[114,131]

Extraction efficiency (η_{extr}) was defined by Lavan and Thompson[118] as

$$\eta_{\text{extr}} = \frac{\dot{Q}t^*}{V} \tag{2-33}$$

where $\dot{Q}$ is the volumetric flow rate of the outlet flow, V is the volume of the tank, and t^* is defined as the time when initial inlet/outlet temperature difference has dropped to a pre-assigned value (in this case, 0.9). Based on this definition, they obtained the following correlation between extraction efficiency and several influencing factors such as flow conditions (Re), tank geometry (L/D), and temperature difference (Gr).

$$\eta_{\text{extr}} = 1 - \left\{\exp\left[-0.067\text{Re}_d^{-0.55} Gr_D^{0.35}(L/D)^{0.58}\right]\right\} \tag{2-34}$$

Energy efficiency is usually defined as the ratio of delivered energy and stored energy.[132] For a stratified tank, it is usually referred to as discharge efficiency (φ_{Dis}).

$$\varphi_{\text{Dis}} = \frac{E_{\text{out}}}{E_{\text{in}} + E_{\text{st}}} \tag{2-35}$$

where E_{out}, E_{in}, and E_{st} are energy output, energy input, and energy stored in the tank, respectively.

Comparing to energy evaluation, exergy analysis not only accounts for energy stored in a stratified storage tank, but also includes the temperature at which the energy is stored.[133] The definition of exergy efficiency (ψ_{Dis}) is similar to that of energy efficiency described in equation (2-35).

$$\psi_{\mathrm{Dis}} = \frac{\mathrm{Ex_{out}}}{\mathrm{Ex_{in}} + \mathrm{Ex_{st}}} \tag{2-36}$$

where $\mathrm{Ex_{out}}$, $\mathrm{Ex_{in}}$, and $\mathrm{Ex_{st}}$ are exergy output, exergy input, and exergy stored in the tank, respectively.

2.3.5 Modern Thermal Energy Storage (TES) Tanks

Modern wood pellet boilers are usually connected with external TES tanks to ensure high boiler performance. The use of TES tanks in wood pellet heating systems has many benefits. According to Siegenthaler,[134] TES tanks in wood pellet heating systems can: (1) store excess heat; (2) meet intermittent loads without firing the boiler; (3) prevent boiler shot cycling due to partial load; (4) prevent thermal shock to the boiler; (5) supplement boiler output at high load; (6) act as a heat sink of residual heat during power outage; (7) catch residual heat after boiler shutdown; (8) stabilize domestic hot water (DHW) production; (9) act as hydraulic separator in multiple circulator systems; (10) provide thermal storage for additional heating system such as solar, etc. Figure 2-10 shows the comparison of burner ignition numbers per year between conventional pellet boilers without TES tank and a commercial pellet boiler with a 45 gallon built-in TES tank.[135] The reduction of boiler ignition is significant, especially when the boiler is at partial load. In addition, the existence of thermal stratification also enhances the performance of TES tanks.

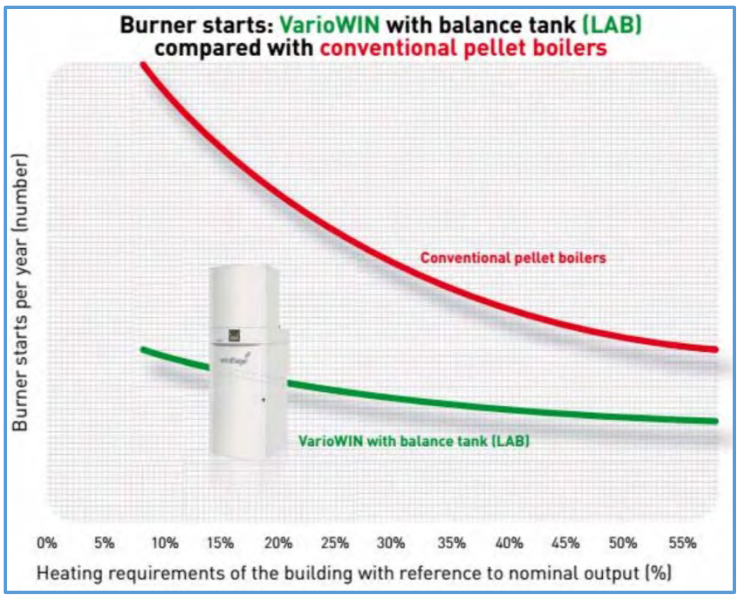

Figure 2-10. Comparison between modern pellet boiler with TES tank (built-in, 45 gallons) and conventional pellet boiler without TES tank in terms of boiler starts per year (source: VarioWin[135])

In general, two types of TES tanks used in modern residential heating systems: unpressurized and pressurized tanks.[134] Unpressurized TES tanks are also called open buffer tanks and typically cost less than pressurized TES tanks. However, they do need one or more internal heat exchangers to interface with boiler distribution system. A typical unpressurized TES tank is shown in Figure 2-11. External insulation, regular water treatment and level monitoring, and biological slime control are important for the efficient use of this type of TES tanks. Check valves are needed to prevent thermo-siphoning.

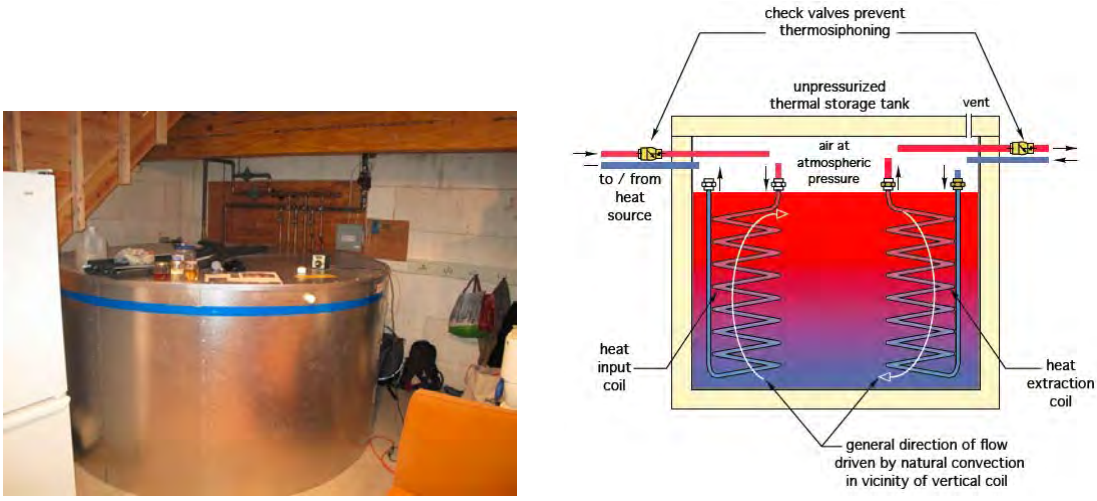

Figure 2-11. Photo of on-site installation (left) and schematic (right) of a typical unpressurized (or open) TES tank flow direction (source: NYSERDA renewable heat NY hydronics training)

Pressurized TES tanks are often called closed TES tanks. For residential use, TES tanks are often 119 gallons (0.45 m^3) because tanks greater than 120 gallons must be ASME certified.[134] Pressurized TES tanks do not need internal heat exchangers, but they do require external expansion tanks. A typical installation is shown in Figure 2-16.

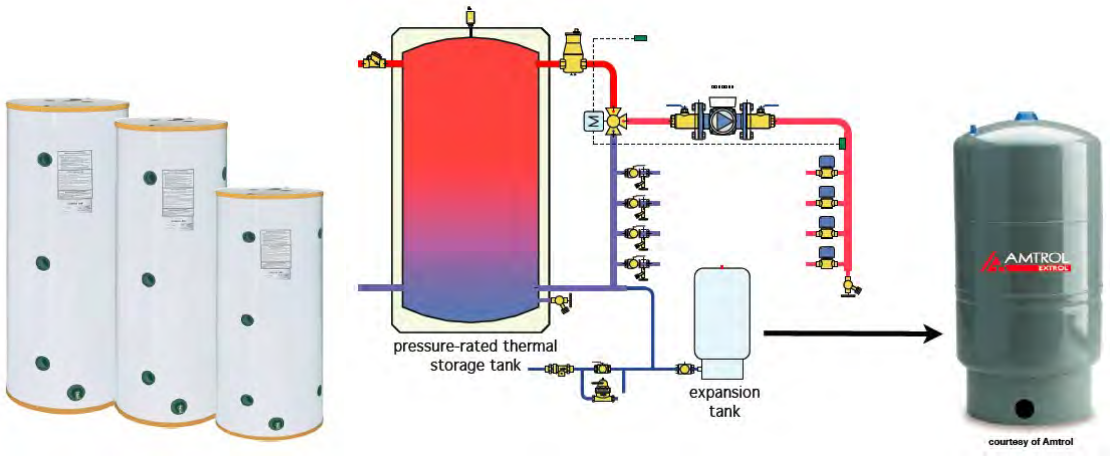

Figure 2-12. Commercially available pressurized TES tanks (left) and schematic of installation with expansion tank (source: NYSERDA renewable heat NY hydronics training)

Proper design of TES tanks is critical for maintaining a high level of stratification during operation. The return water to the tank should not be in the bottom of the tank due to the increase in induced mixing. A better design is to separate boiler loop and building loop on both sides of the tank, as shown in Figure 2-13.

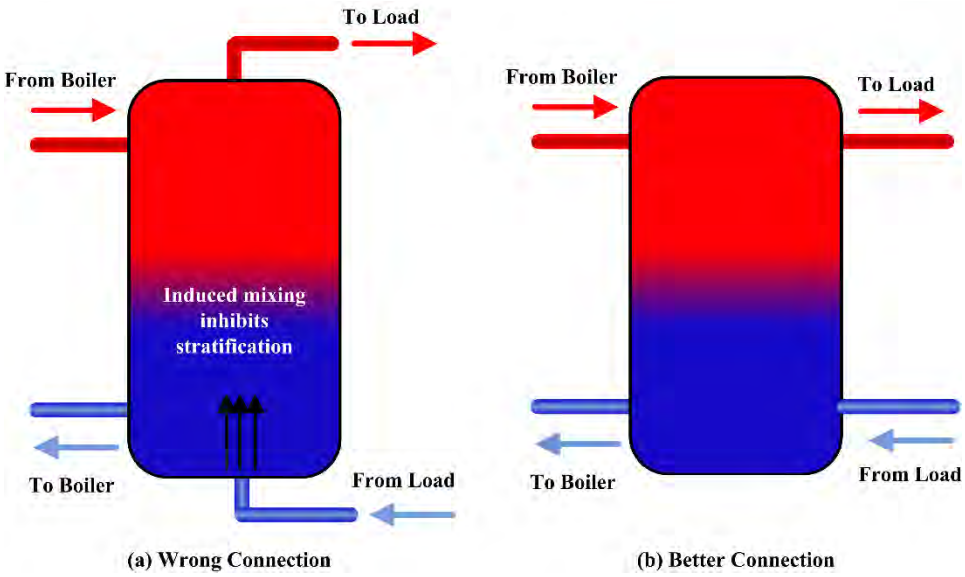

Figure 2-13. Comparison between two common TES tank designs: (a) avoided design; (b) preferred design

2.4 Wood Pellet Heating System

Modern wood pellet heating system has three components: wood pellet boiler (heat generation), thermal energy storage (TES) tank (heat storage) and building heat demand units (heat consumption). A typical configuration is shown in Figure 2-14.

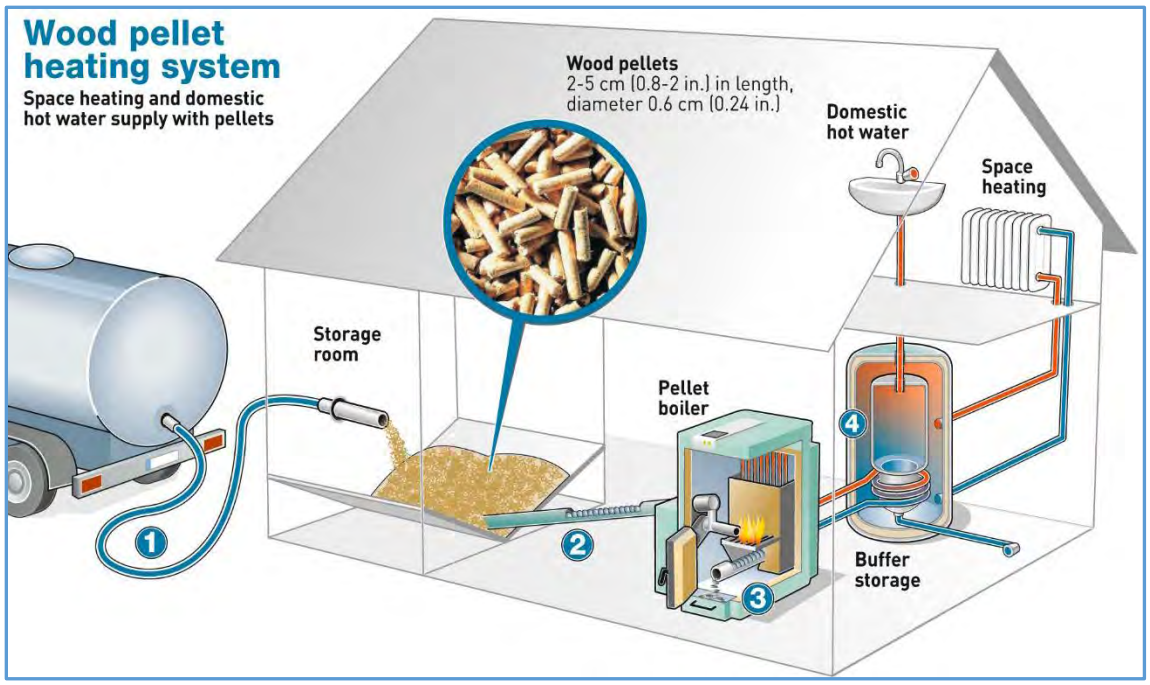

Figure 2-14. A typical wood pellet heating system from pellet delivery to heat consumption (credit: biomass magazine)

Wood pellets from the manufacturer are delivered to the customer by truck as needed. Pellets are pneumatically transported into wood pellet silo with an inclined ramp built in the bottom. The pellets in the silo are delivered into the boiler's pellet box through the first stage auger delivery system. The pellets are then delivered into boiler combustion box through the second stage auger delivery system. A level sensor monitors the level of the pellets inside the pellet box. Once the level drops below to a set point (usually 60 – 80% of the total), the first stage auger delivery system operates to refill the

pellet box with fresh pellets. Wood pellets are burned in the pellet boiler to produce hot water. The TES tank stores hot water as a heat reservoir and delivers heat to the building. When the TES tank temperature increases to the high set value (thermocouple placed at the bottom of the tank), the boiler stops firing. When the TES tank temperature decreases to the low set value (thermocouple placed at the top of the tank), the boiler fires again to heat the tank. The process is called TES tank charge and discharge. During TES tank discharge, hot water supplied to the building heat consumption units from the top of the TES tank and cold water returned to the bottom of the tank, which creates stratification inside the tank. The existence of stratification enhances the overall performance of the system.

2.4.1 Types of Space Heating

There are different types of space heating such as radiant floor heating, baseboard heating, ceiling heating, slab heating, etc. Different heating types require different water temperatures. For example, radiant floor heating, slab heating, and ceiling heating can be categorized as low temperature space heating (down to 40 °C), while baseboard heating (especially older heat emitters) requires high temperature water (>70 °C). Modern residential space heating is gradually moving from high temperature heating to more efficient and sustainable low temperature heating.

2.4.2 System Sizing

The heat load from the building depends on the size of the building (heating area), the ambient temperature, the use of domestic hot water, the type of heating, the building

temperature setting, the level of house insulation, etc. Hence, it is important to correctly size the boiler and TES tank to ensure sufficient heating at a moderate cost.

Boiler sizing is mainly based on the heat load calculations. Based on previous discussions, a good boiler sizing should allow the boiler to fire at its high output range for relatively long cycle time (typically > 1 h). In general, for systems where the pellet boiler is the only heat source, the boiler is typically sized to the design load; for systems where there are auxiliary heat supply such as a gas or oil boiler, the pellet boiler is often sized for 60% (at most 75%) of the design load.[134]

TES tank sizing is also critical for the overall system performance. Currently there are no standards available to scientifically size the TES tank with respect to pellet boiler size and space heating types. Hence, in real case scenarios, the size of a TES tank is usually a recommended value based on the contractor's experience.

2.5 Research Description

Three wood pellet boiler heating systems (two residential units and one commercial unit) were installed and monitored since the beginning of 2015. Data have been collected and the systems have been modified and retrofitted for several times over the past two years to improve their performance.

A process dynamic simulation was also built based on field data to simulate the dynamic behavior of each system. The simulation permits a parametric study to be performed to find the parameter values that optimize the system operation.

There are two main objectives of this research:

(1) to systematically evaluate the performance of wood pellet boiler heating systems in terms of boiler (efficiency, emissions), TES tank (stratification performance), and heat demand characteristics (building heat demand profiles at different scenarios);

(2) to scientifically size the system, especially TES tank with respect to boiler capacity, heat demand profiles, etc.

This work will establish a performance-based sizing methodology for modern wood pellet heating systems to achieve higher system efficiency.

Chapter 3. Boiler On-site Monitoring

3.1 Boiler sites Details and Installation

Three wood pellet boilers were installed and monitored in the field to supply the data for this study. The boiler details are given in Table 3-1. The two 25 kW boilers were installed in local family houses in November 2014. The 50 kW boiler, which was later modified to 35 kW, was installed in NYS Department of Environmental Conservation's boat maintenance facility at Lake George. Weather information at the three sites was accessed through Weather Underground[136].

Table 3-1. Boiler installation details

Boiler Capacity (kW)	Boiler Make	Site	Installation Date
25	EvoWorld	Parishville	November, 2014
25	EvoWorld	West Potsdam	November, 2014
50 (modified to 35)	EvoWorld	Lake George Boat Garage	November, 2015

3.1.1 Parishville Boiler

The 25 kW Parishville boiler (PB) was installed to provide radiant floor heating for the basement and main floor of a house with a total calculated heating area of 407 m^2. The maximum design heating load is 27 kW, given an inside temperature of 20°C and minimum outdoor temperature of -23°C. The floor heating in the basement uses traditional slab heating with plastic tubing buried inside the

Figure 3-1. Radiant floor heating piping and insulation for the main floor at PB site

slab. The main floor heating utilizes “tube and plate” piping, as shown in Figure 3-1, that increases the heat transfer area.

The PB was placed inside an insulated shipping container outside the building, as shown in Figure 3-2. About 1/3 of the container is used as wood pellet storage (sloped bottom, total capacity: 2300 kg) and the rest is used for the wood pellet boiler, thermal energy storage (TES) tanks, and piping. The numbered items in Figure 3-2 are: (1) pellet storage access door; (2) pellet refill inlet; (3) pellet storage venting outlet; (4) pellet boiler chimney; (5) outside lamp; (6) pellet boiler room entrance. Because the piping between the house and the boiler in underground, a constant circulation is required to avoid water freezing under cold weather. The initial installation had this circulation loop connected to the TES tanks.

Figure 3-2. Parishville boiler (PB) heating system inside an insulated shipping container.

Figure 3-3 shows the current piping schematics of PB heating system along with data acquisition devices after the recent modifications in October 2016. The old

installation did not include the building loop 3-way actuator that separates the TES tank from the constant circulation.

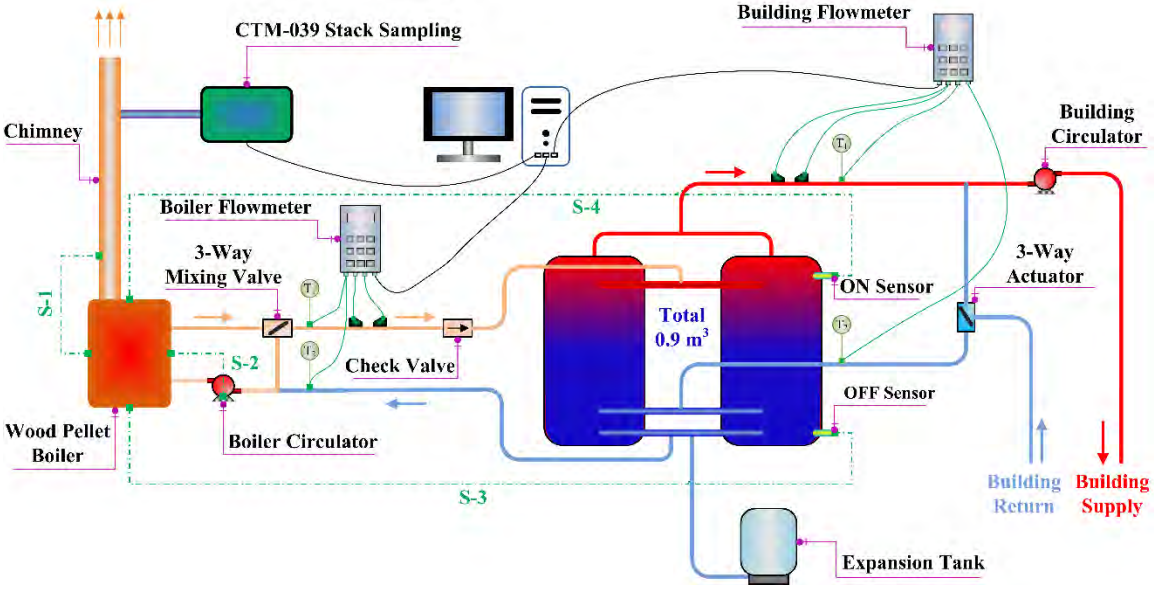

Figure 3-3. PB piping schematics and data acquisition devices. Note: S-1: flue gas oxygen control signal; S-2: boiler circulator control signal; S-3: boiler OFF temperature signal; S-4: boiler ON temperature signal.

The two TES water tanks connected in parallel provide a total storage volume of 0.9 m^3 (238 gallons). The top and bottom temperature sensors control the boiler ON and OFF in the way that when the top sensor reaches the set temperature, the boiler fires and when the bottom sensor reaches the set temperature, the boiler shuts down.

There are two loops in the system: the boiler to TES tank loop (boiler loop) and the TES tank to building loop (building loop). A 3-way mixing valve acts as anti-condensation protection for the boiler that the valve maintains fully closed until the return water temperature exceeds 60 °C. The check valve is installed to stop any thermal siphoning that causes reverse flow in the system. In the TES tank loop, the building circulator ran constantly due to concerns for freezing in the underground piping. When

there is a call for heat, the 3-way actuator in the building loop is energized and the TES tanks supply heat to the building. However, when there is no call for heat, the 3-way actuator is de-energized and the TES tanks are removed from the circulation loop to avoid additional heat loss and loss of stratification. Compared to the original installation, adding building loop 3-way actuator is a key system update.

The system was monitored for flow and temperature data for both loops to calculate boiler efficiency and tank efficiency. The flowmeters used are clamp-on ultrasonic flowmeters (EnduroFlow^{TM} Series, EF10 Wall-Mount Ultrasonic Flowmeter) with temperature sensors that can be attached to the pipe surface. Both flowmeters were calibrated by the company before installation. Flow rates and supply/return temperature data were recorded every 10 seconds and stored in the on-site computer.

Boiler emissions were studied with 3 sets of stack sampling using EPA CTM-039 sampling method[137] at the end of the 2014 – 2015 heating season (April, 2015). CTM-039 is a dilution based stack sampling method that quickly mixes hot flue gas with ambient air to simulate the emissions in the real world. Figure 3-4 shows the schematics of the stack sampling system used in this study.

Hot flue gas is pulled into the sampling probe through a $PM_{2.5}$ cyclone, heated by the hot box, and then mixed with HEPA (high-efficiency particulate air) filtered ambient air in the residence chamber. At the end of the residence chamber there are 6 sampling ports to be used for individual emission analysis including particle mass (TEOM), particle number concentration (FMPS), gaseous products (CO, NO_x and SO_2) and filter based analysis (Teflon and Quartz filters). Semi-volatile organic compounds (SVOC) are collected using polyurethane foam (PUF) filters. Table 3-2 and

Table 3-3 list all the instrument and filter based analysis in this study.

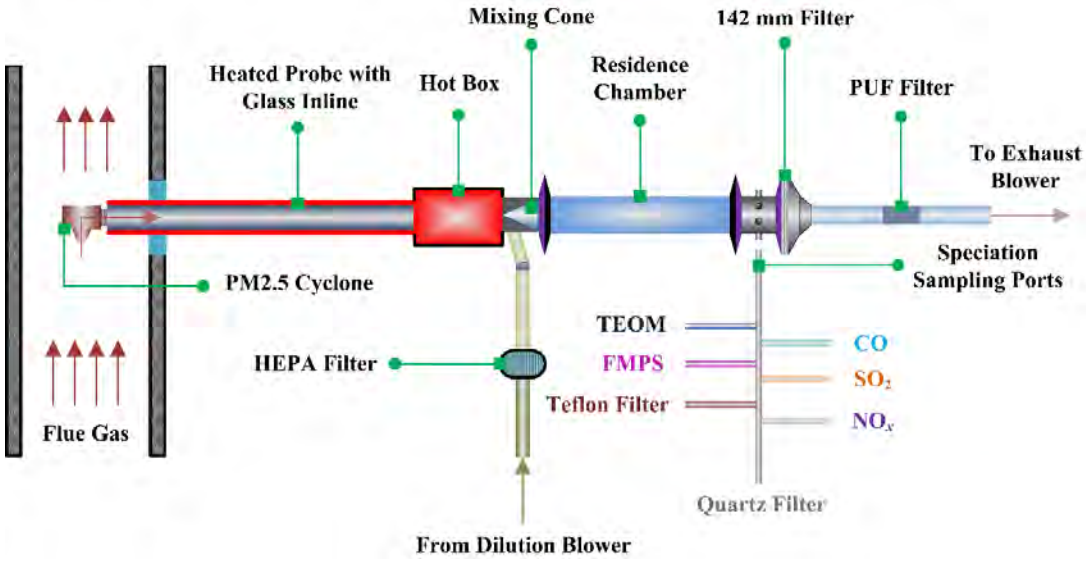

Figure 3-4. EPA CTM-039 stack sampling train for wood pellet boiler emissions measurement (PM, CO, SO_2, NO_x, and SVOC)

Table 3-2. Wood pellet boiler emissions measurement and instrumentation

Emissions	Instrument	Measurement Principles
NO_x	Model 42i, Thermo Scientific	Chemiluminescence
SO_2	Model 43i, Thermo Scientific	Photometric Ultraviolet
CO	Model 48i, Thermo Scientific	Non-dispersive Infrared
$PM_{2.5}$	TEOM 1400a (with FDMS, model 8500b), R&P Co. Inc.	Oscillation Frequency
	FMPS, model 3091, TSI Inc.	Electrostatic Classification

Table 3-3. Filter based analysis and instrumentation

Filter Types	Size (mm)	Analytical Purpose	Instrument
Teflon	47	Particle compositions	Spectro XEPOS XRF
Quartz	47	Filter particle loadings	Sartorius, MC5 Micro Balance
Quartz	142	Particulate phase organics	DSQ II GC-MS, Thermo Scientific
PUF	-	Gaseous phase organics	

3.1.2 West Potsdam Boiler

The 25 kW West Potsdam boiler (WPB) was installed as a part of a traditional heating system including cast iron baseboard, fin-tube baseboard, and cast iron radiators, as shown in Figure 3-5. The total space heating area is estimated to be 142 m^2 and the design maximum heating load is 23 kW based on minimum outdoor temperature of -23°C and indoor temperature of 20°C.

Figure 3-5. Heat emitters used in WPB residential building: (a) cast iron baseboard (~ 9 m long); (b) fin-tube baseboard (~ 7 m long); (c) cast iron radiators

There are several other differences between WPB and PB aside from the type of heating: (1) WPB heating system has an auxiliary boiler (oil boiler); (2) there is a domestic hot water (DHW) tank connected to provide domestic hot water; and (3) the TES tank is piped differently.

There has been two major modifications for WPB system. The original installation from November 2014 to May 2015 is shown in Figure 3-6. There was only one 0.45 m^3 (119 gallon) tank installed, which was causing boiler short-cycling due to insufficient heat storage volume. The oil boiler was not isolated from the system resulting in constant energy loss when hot supply water passed through it.

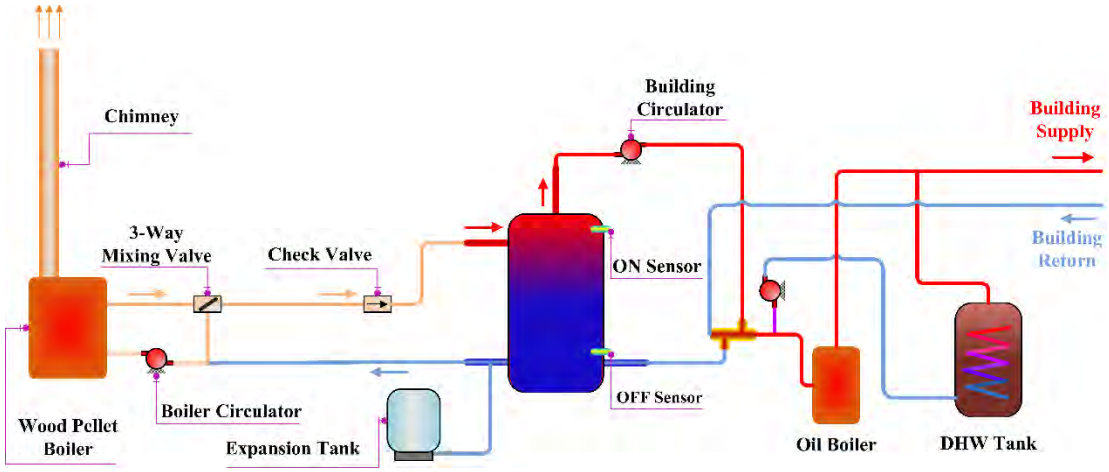

Figure 3-6. WPB piping schematic during 2014 – 2015 heating season

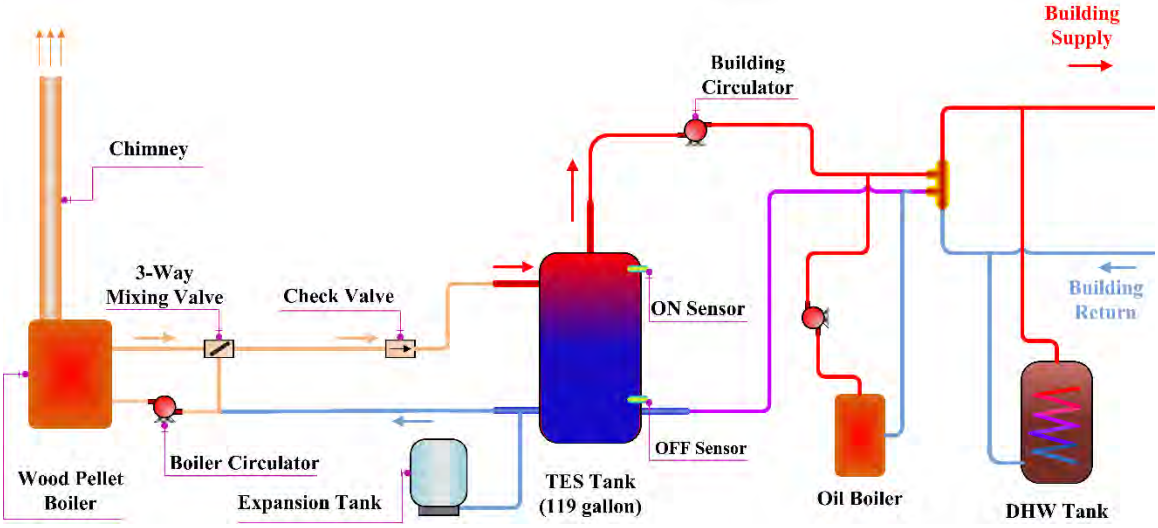

Figure 3-7. WPB schematic during 2015 – 2016 heating season

In the summer of 2015, the system was reconstructed to isolate the oil boiler and divided the building heat demand into independent zones as shown in Figure 3-7. The TES tank was not changed until the summer of 2016 that the original 119 gallon tank was replaced with a 210 gallon tank. The piping of the tank was also changed from 4-pipe configuration into 2-pipe configuration. The current WPB heating system is shown in Figure 3-8 after the most recent change on December 2016.

The existence of an auxiliary oil boiler and DHW tank make the system control critical for overall system performance. The current system is controlled in a way that the wood pellet boiler is the main boiler that supplies heat to the TES tank for space heating and the oil boiler is secondary boiler only acts as a backup when the wood pellet boiler fails (or has no pellets).

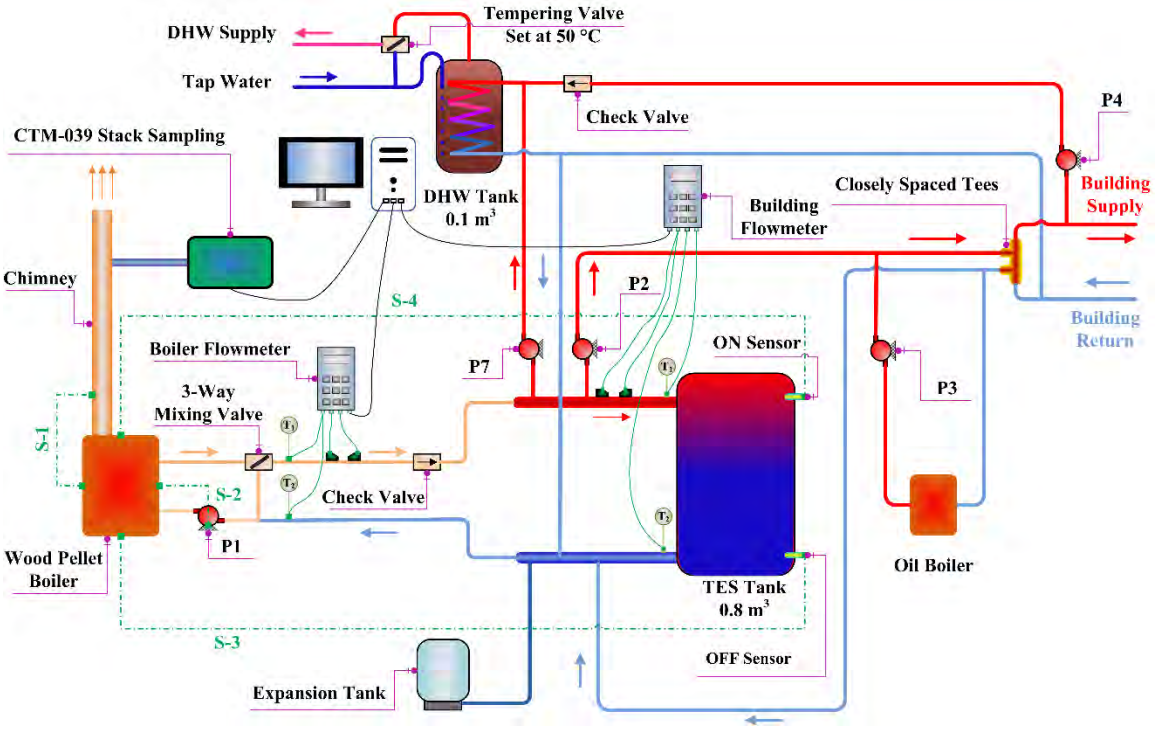

Figure 3-8. WPB 2016 – 2017 piping schematics and data acquisition devices. Note: S-1: flue gas oxygen control signal; S-2: boiler circulator control signal; S-3: boiler OFF temperature signal; S-4: boiler ON temperature signal; P1: boiler circulator; P2: main circulator; P3: oil boiler circulator; P4 and P7: DHW tank circulators.

In addition, the 0.8 m^3 (210 gallons) TES tank has only 1 inlet and 1 outlet. This TES tank piping is often called a 2-pipe configuration while the traditional type of piping is a 4-pipe configuration (as shown in Figure 3-3). One of the advantages of using 2-pipe configuration is that it can reduce hot water flow rate (and hence flow velocity) into the

top of the TES tank and hence minimize disruption of thermal stratification inside the tank. There is no constant circulation between the building and TES tank because all the pipes are located inside the basement and circulator P2 will only run when there is a call for heat from the building. Hence, the heat demand profile will also be different from that in PB boiler heating system.

The data acquisition system is the same as described in PB boiler. Three sets of stack sampling were also performed on April 2015 to evaluate the combustion emissions from the boiler using the same method as described in PB boiler.

3.1.3 Lake George Boiler

The Lake George boiler (LGB) is used for slab heating of the boat garage with a total output capacity of 50 kW. Like the WPB system, a propane boiler was also installed as a secondary heat source with a total output capacity of 29 kW. The piping schematic is shown in Figure 3-9.

There are two TES tanks connected to the boiler with a total volume of 1.6 m^3 (420 gallons). The piping is different from both PB and WPB in that it is 2-pipe reverse return piping configuration. This type of piping can ensure flow balance between the two tanks. In addition, multiple temperature sensors were also installed vertically along each tank to record the vertical temperature profile.

In order to monitor the temperature distribution in the slab, several temperature sensors were also placed at different depths inside the slab, namely, 0, 2, 4, 6, 8, 10, 12 and 32 inches depth. The deepest temperature is the subsoil temperature beneath the insulation of the slab.

No stack sampling was performed for this boiler site. Flow and temperature data monitoring is also the same as PB and WPB sites using the same type of ultrasonic flowmeters.

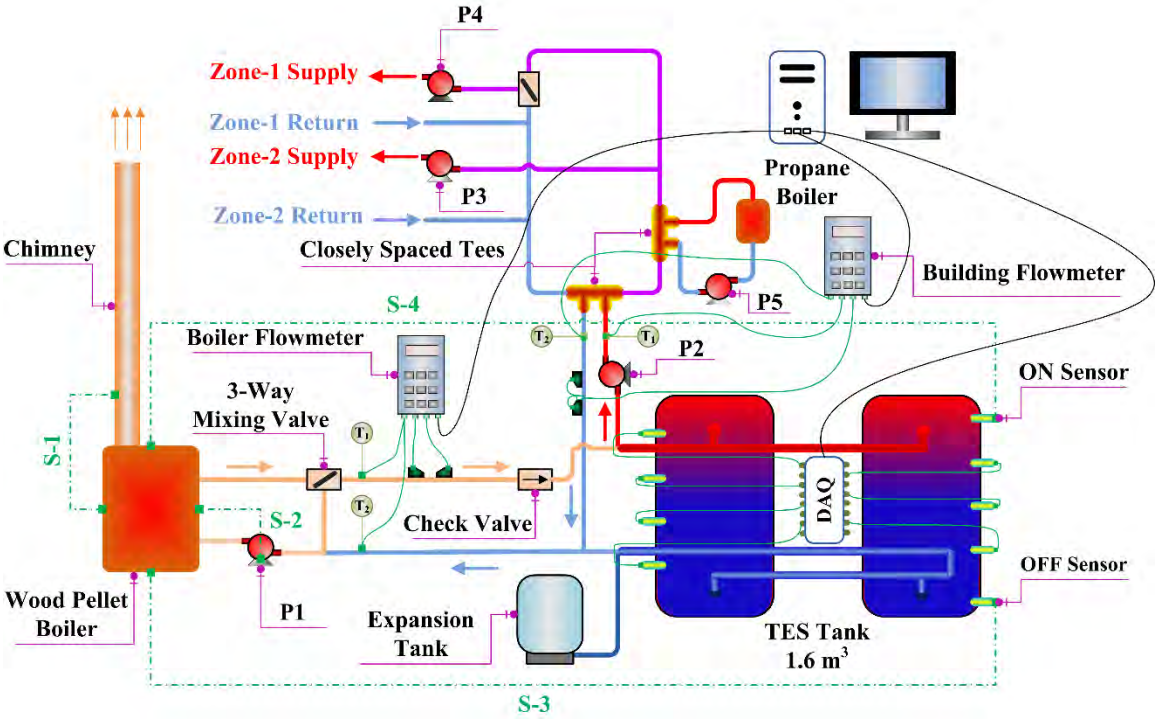

Figure 3-9. LGB heating system piping schematics with data acquisition devices. Note: S-1: flue gas oxygen control signal; S-2: boiler circulator control signal; S-3: boiler OFF temperature signal; S-4: boiler ON temperature signal; P1: boiler circulator; P2: main circulator; P3 and P4: zone circulators; P5: propane boiler circulator.

3.2 Summary of Available Data and Notations

This section presents the results from the three boiler systems collected through January 31, 2017. Because of the major modifications discussed previously to PB and WPB systems, the amount of usable data is limited.

Table 3-4 lists all the useable data for the three systems available as of the end of January 2017. The LGB system has been more different due to several issues: (1) the long distance from Potsdam makes routine checks and maintenance of the boiler unrealistic; (2) lack of reliable internet connection adds more trouble; and (3) local construction work causes frequent power outages. Hence, the usable data from LGB site is even less. The LGB was downgraded from 50 kW to 35 kW in October 2016.

Table 3-4. List of usable data for three boiler sites

Boiler Sites	Usable Data Period	Total Days	Total Boiler Cycles	Notation
PB	February 1, 2015 – April 11, 2015	70	493	PB-1
	December 1, 2015 – April 1, 2016	123	392	PB-2
	January 5, 2017 – January 31, 2017	27	122	PB-3
WPB	December 28, 2016 – January 31, 2017	35	223	WPB-3
LGB	March 9, 2016 – March 31, 2016	23	32	LGB-2
	January 25, 2017 – January 31, 2017	7	14	LGB-3

3.3 Wood Pellet Fuel Characterization

The pellet characterization is critical for boiler heat input calculation and understanding combustion emissions. For the three boiler sites, wood pellet samples were collected at the beginning of each heating season and analyzed from 2014 to 2017. Both proximate and ultimate analysis were performed. Table 3-5 lists all the parameters and corresponding analytical methods being used.

Table 3-5. List of parameters and analytical methods used to characterize wood pellet fuel at the three boiler sites

Parameters	Analytical Methods
GHV	ASTM E 711-87 (2004)
Moisture	ASTM E 871-82 (2006)
Ash	ASTM D 1102-84 (2007)
C	ASTM E 777-87 (2004)
H	ASTM E 777-87 (2004)
N	ASTM E 778-87 (1996)
O	By difference
Cl	ASTME 776-87 (2009)
S	ASTM E 775-87 (2004)
Heavy Metals	ICP-MS

3.3.1 Basic Properties

Basic properties for wood pellets includes gross calorific value (GCV), moisture content and ash content. During the past heating seasons, wood pellets were sampled four times at PB and WPB while only one time at LGB. Figure 3-10 shows the distribution of wood pellets basic properties at the three boiler sites.

The average values of GCV are 19.10 ± 0.25 MJ/kg, 18.81 ± 0.19 MJ/kg, and 18.35 ± 0.08 MJ/kg for PB, WPB and LGB, respectively. GCV at PB and WPB are very similar because they share the same local wood pellet manufacturer. GCV varies between

different wood species made into pellets. Softwoods have GCV between 19.66 MJ/kg and 20.36 MJ/kg, while hard woods have GCV between 17.63 MJ/kg and 20.81 MJ/kg.[138] The wood pellets for the three sites are probably made from hardwood or a blend of hardwood and softwood. The relatively high variance at PB and WPB suggests different sources of wood being used among different batches for the past years.

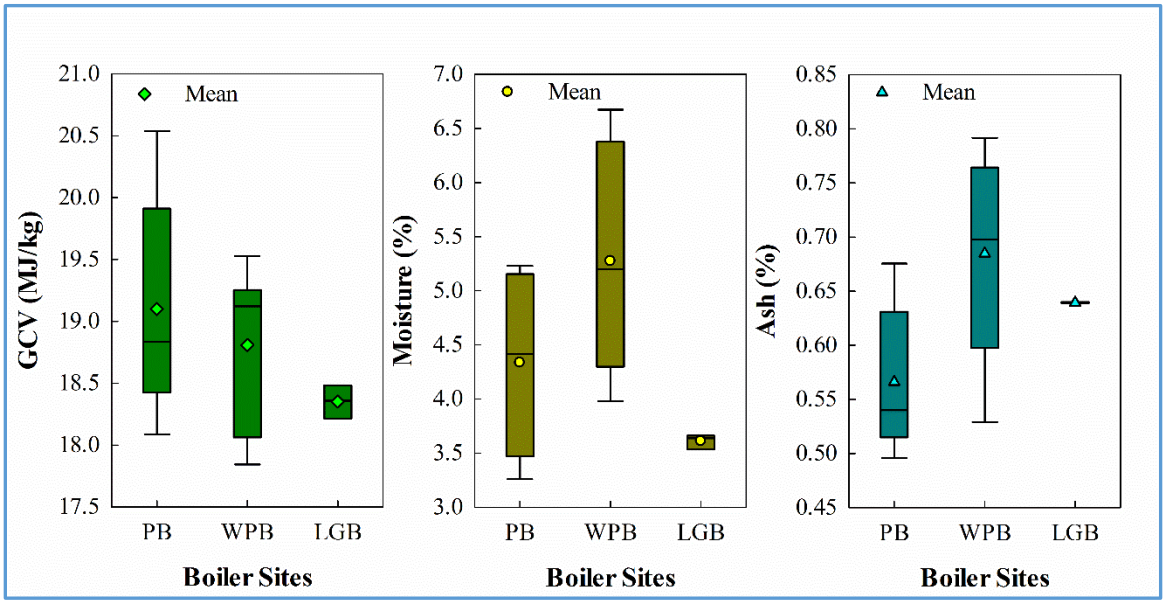

Figure 3-10. Characterization of GCV, moisture content and ash content for wood pellets at the three boiler sites

Average moisture content are 4.33 ± 0.25%, 5.27 ± 0.29% and 3.61 ± 0.04%, for PB, WPB, and LGB, respectively. The moisture content values are lower compared to other related studies[59] that showed an average of 6% moisture content for most wood pellets. Average ash content are 0.57 ± 0.02%, 0.68 ± 0.03% and 0.64 ± 0.0003%, for PB, WPB, and LGB, respectively. Chandrasekaran et al. showed that similar wood pellets have ash content ranged from 0.29% to 1.53%.[59] Hence, wood pellets in this study are also in the lower range of the distribution.

3.3.2 Elemental Composition

Because both PB and WPB have the same wood pellets supplier, the elemental and some heavy metal (ash digestion) compositions were only analyzed for one sample from PB. The elemental compositions are listed in Table 3-6.

Table 3-6. Elemental compositions of wood pellets from PB

Elemental Compositions	Dry-base Weight (d.b.%)
C	46.64
H	6.40
N	0.14
O	46.23
Cl	0.00388
S	0.00689

Sheng and Azevedo[139] derived a simple method of predicting GCV of wood pellets based on elemental compositions with high accuracy based on the following correlations:

$$\mathrm{GCV} = -1.3675 + 0.3137\,\mathrm{C} + 0.7009\,\mathrm{H} + 0.0318\,\mathrm{O} \quad (3\text{-}1)$$

Substituting the values in Table 3-6, the estimated GCV for PB is 19.22 MJ/kg. Compared to the actual value of 19.10 MJ/kg, the absolute error is only 0.6%.

From Figure 3-10 and Table 3-6, the pellets used in this research meet the U.S. PFI premium standards listed in Table 2-1.

3.3.3 Heavy Metals

Ash from the wood pellet samples was acid digested and analyzed for some heavy metals including As, Cd, Co, Cr, Cu, Mn, Mo, Ni, Pb, Sb, V, and Zn. Hg was analyzed from direct digestion of wood pellets because most of the Hg will be released during

combustion.[140] The results from both PB and WPB are shown in Figure 3-11. The similarity indicates pellets were made from the same tree species for PB and WPB.

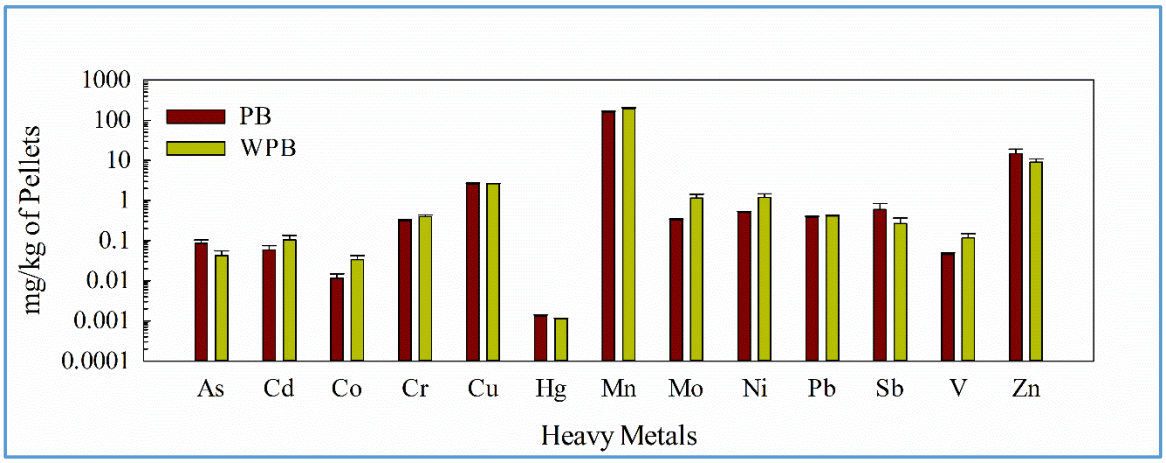

Figure 3-11. Some typical heavy metals in wood pellets used in PB and WPB sites

Heavy metals in wood pellets exist in the following decreasing order as: Mn, Zn, Cu, Sb, Ni, Pb, Mo, Cr, As, Cd, V, Co, and Hg. The weight of all those heavy metals accounts for only 0.02% of dried pellets. The analysis is helpful to understand the elemental compositions of particles emitted from wood pellet combustion.

3.4 Wood Pellet Boiler Operation Characteristics

3.4.1 Boiler Cycle Stages

The general operation procedures for modern wood pellet boilers have been introduced in section 2.2. Typical modern residential scale wood pellet boilers have different operation stages represented by boiler state indexes, as shown in Figure 3-12.

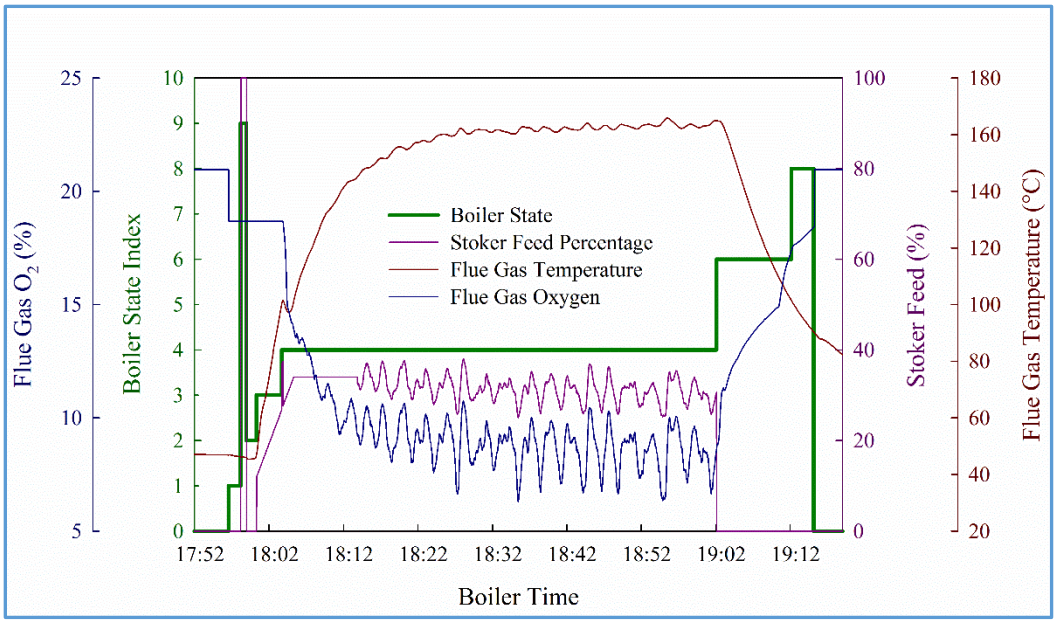

Figure 3-12. Boiler operation characteristics: boiler stages (represented by boiler state index numbers), stoker feed percentage, flue gas O_2 and temperature change.

A complete boiler cycle includes the following stages as indicated by their state indexes: 0 – standby, 1 – flush, 9 – filling, 2 – ignition, 3 – stabilization, 4 – automatic combustion, 6 – burnout, 8 – post-ventilation.

0 – Standby: The boiler is OFF.

1 – Flush: The ON sensor in the top of the TES tank calls the boiler for heat. The boiler first removes all the residual ash accumulated in the combustion chamber from last

boiler cycle into the ash bins by opening the bottom grate. This step is also called a pre-combustion cleaning process as the fire tube heat exchanger is also being cleaned by the turbulators. Figure 3-13 shows a photo of the fire tube heat exchanger with turbulators. The hanger will move the turbulators up and down when the bottom grate opens and closes to clean the inside surface of the fire tube heat exchanger. This process is repeated three times.

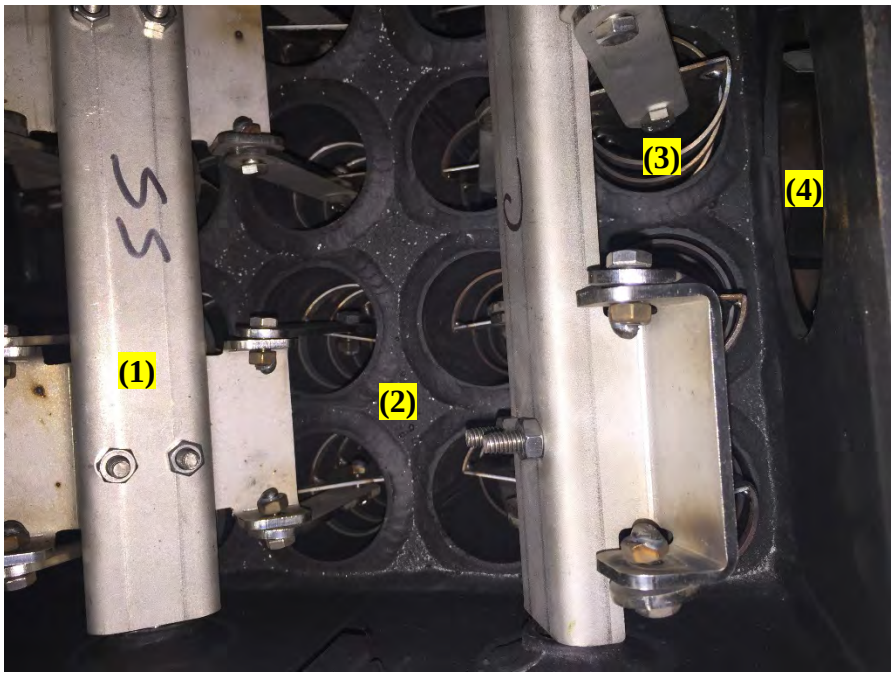

Figure 3-13. Photo of the fire tube heat exchanger of the boiler: (1) turbulator hanger, (2) fire tube heat exchanger, (3) turbulators, (4) exhaust fan blades.

At the end of the cleaning cycle, the exhaust fan starts running to bring fresh air inside the combustion chamber as well as blow out any residual CO from last burn cycle. The exhaust fan only runs for a couple of seconds before the next stage. The oxygen content drops to around 18%, indicating possible residual burning in the combustion chamber from last boiler cycle after the boiler went off.

For small scale wood pellet boilers less than 50 kW, the exhaust fan is the only fan for air intake as well as vacuum control in the combustion chamber. Hence, proper sizing and material selection is critical for the boiler operation.

9 – Filling: The stoker starts to run at 100% for a short time to quickly fill the combustion chamber with fresh wood pellets ready for ignition.

2 – Ignition: At the end of filling process, the hot air gun starts to run and blows hot air into the combustion chamber to ignite the pellets. The exhaust fan controls the air intake. A light detector is attached to the top of the combustion chamber through a side glass, as shown in Figure 3-12. Once the illuminance reached the set value of 1600 lx, the hot air gun stops and ignition has been completed.

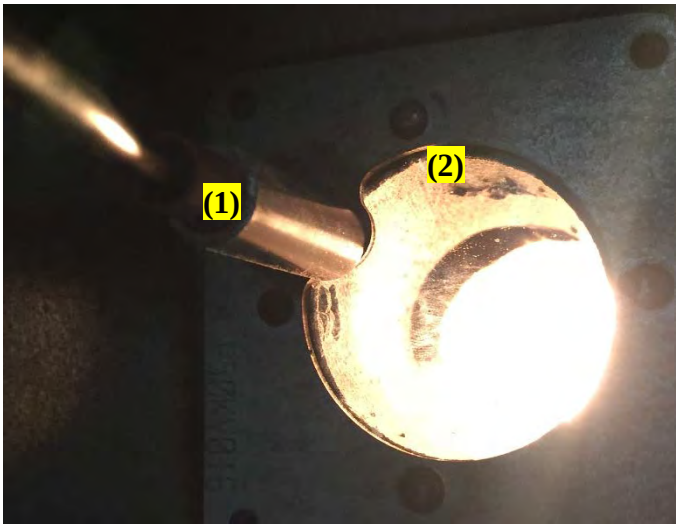

Figure 3-14. Light detector (1) attached to the circular side window (2) above the combustion chamber of the boiler

Since the ignition process is controlled by the illuminance read by the light detector, it is important to clean the circular glass window frequently to avoid soot accumulation resulting in false reading of the actual illuminance. Fast soot accumulation

on the glass window is also an indicator that the boiler vacuum control is not working properly.

3 – Stabilization: At the end of ignition, the boiler stoker starts to run and add pellets into the combustion chamber, as shown in Figure 3-12. During stabilization, the stoker feed percentage gradually increases to the maximum set value. Flue gas O_2 drops to around 15% and flue gas temperature increases sharply. As indicated by the name, stabilization stage is to stabilize the boiler combustion conditions. Once the flue gas temperature reaches 100 °C, the stabilization stage is ended.

4 – Automatic Combustion: This stage of a boiler cycle should be the longest. In this stage, the flue gas temperature reaches a steady maximum around 160 °C and flue gas O_2 changes with respect to the stoker feed rate but maintains an average value around 10% (boiler set value). Figure 3-12 shows the flue gas oxygen content changes simultaneously with stoker feed rate, which is driven by the boiler's oxygen control algorithm, as shown in Figure 3-15. A perfect correlation between the stoker feed fraction and the flue gas O_2 content is observed at PB and LGB boilers. For WPB boiler there is no clear correlation, which is probably due to a slight boiler output upgrade at the beginning of the installation that changed the manufacturer's settings for fan and stoker control. The regression equations at PB and LGB are:

$$[O_2]_{PB} = 18.92 + 5.69 \ln(|\varepsilon - 0.14|) \tag{3-2}$$

$$[O_2]_{LGB} = 5.03 + 35.06\varepsilon \tag{3-3}$$

where [O_2] is flue gas oxygen content in %, and ε is stoker feed fraction. Note that equations (3-2) and (3-3) are only used for flue gas O_2 control during automatic combustion stage.

The OFF sensor in the bottom of the TES tank stops the stoker feeding when the bottom of the TES tank reaches the set temperature.

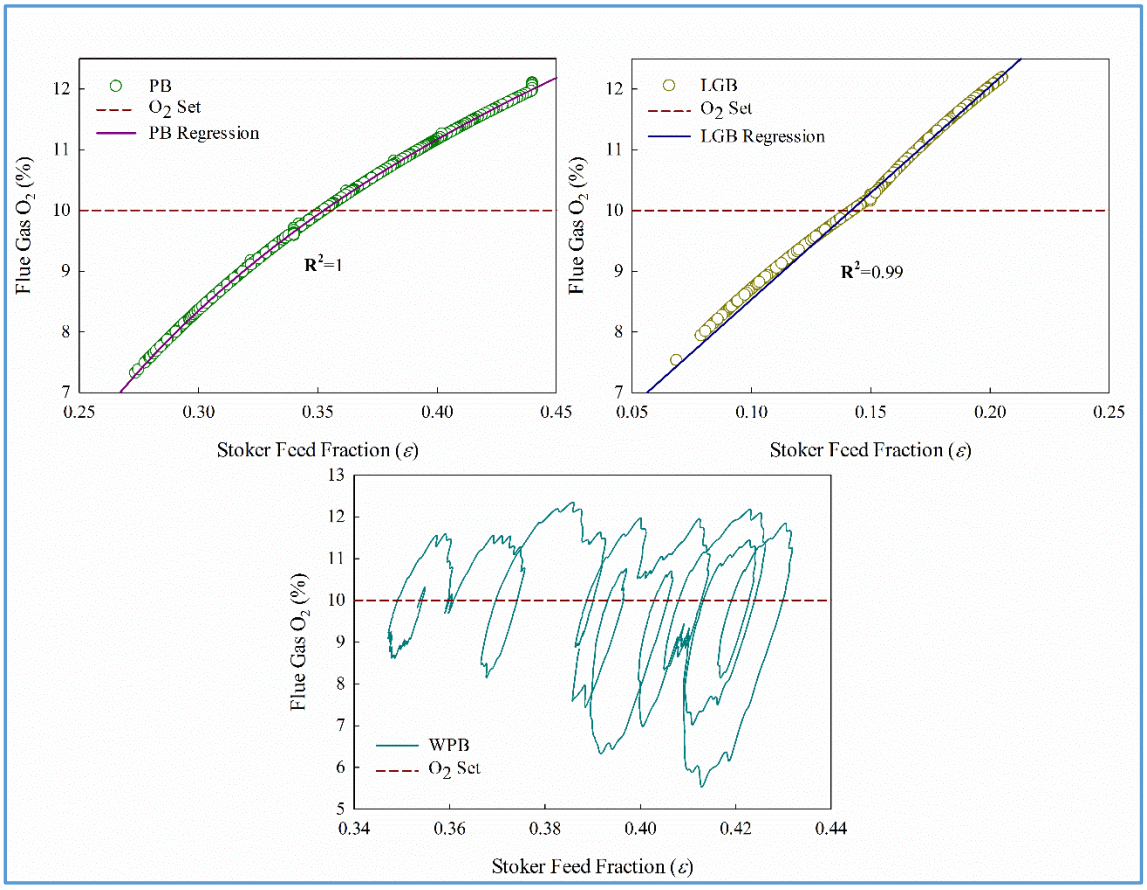

Figure 3-15. Wood pellet boiler flue gas O_2 control during automatic combustion stage for the three boiler sites

In addition, the automatic combustion stage flue gas temperature also correlates with flue gas O_2 content. Higher O_2 content suggests lower flue gas temperature and vice

versa, as shown in Figure 3-16. Significant correlations were observed over several heating seasons.

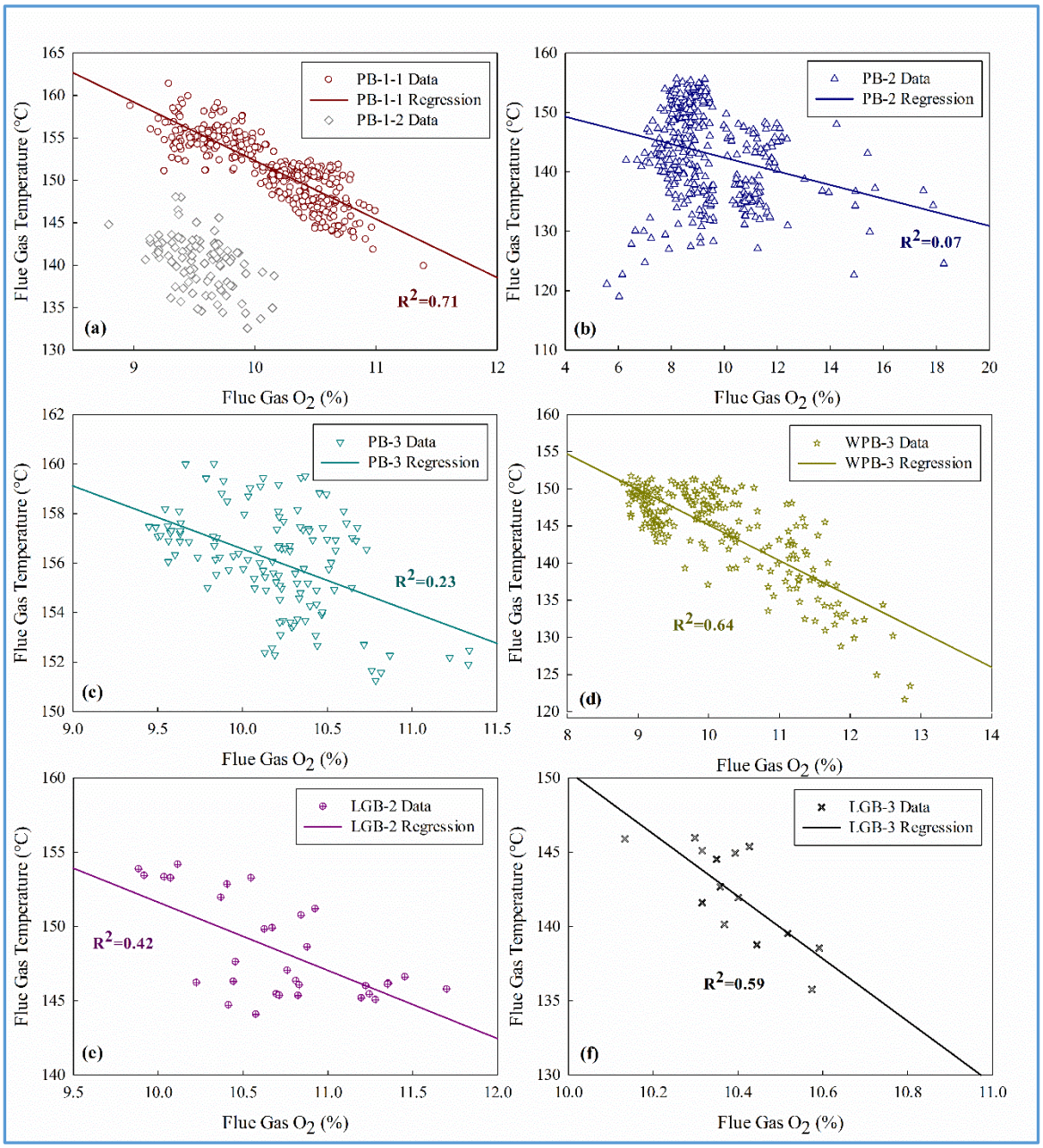

Figure 3-16. Flue gas temperature as a function of flue gas O_2 content for all the three boiler sites in different heating seasons (PB-1-1: before boiler update, PB-1-2: after boiler update)

6/8 – Burnout/Post-ventilation: The residual pellets will be combusted in the burnout stage after the stoker stops feeding. At the same time, residual heat from the combustion chamber is also being moved into the TES tank during burn out and post-ventilation stages. The post-ventilation stage ends when the flue gas temperature is less than 85 °C. Hence, the boiler completes one burn cycle and goes into standby stage, waiting for next call for heat.

3.4.2 Time Analysis of Boiler Stages

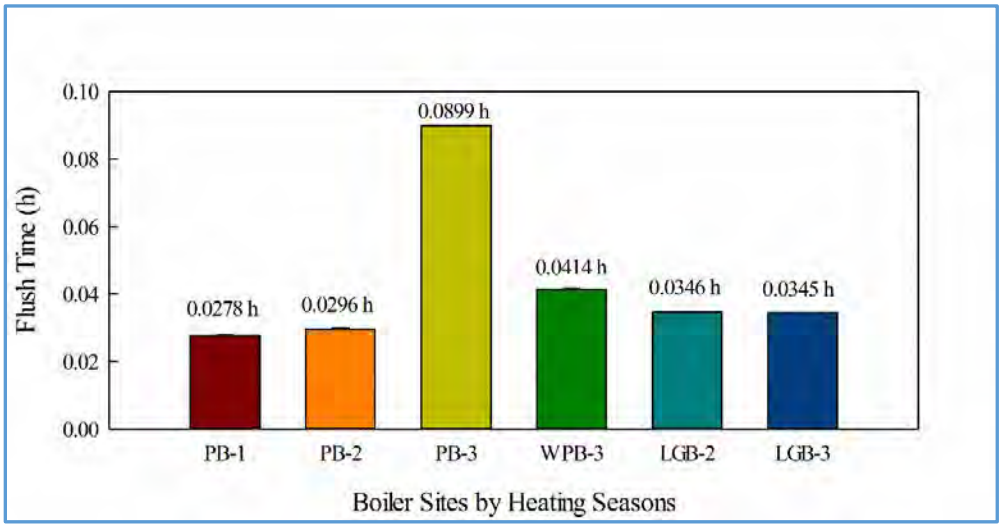

Figure 3-17. Flush time distribution for the three boiler sites by heating seasons

Figure 3-17 shows the average flush time distribution for the three boiler sites. The notations for each heating season is listed in Table 3-4. It can be seen that PB-1 and PB-2, LGB-2 and LGB-3, have almost identical flush time in each boiler cycle. The highest value occurs at PB-3, which is 0.0899 h or 324 s. Flush time in PB-3 is over 3 times higher than PB-1 and PB-2, which could be caused by the recent modification that

changed the relative position of the cleaning side rod due to a constant failure of cleaning in this heating season. WPB-3 also has a higher flush time than PB-1 and PB-2.

Figure 3-18 shows the distribution of fill times for the three boilers. The highest fill time occurred for PB-2 and the lowest for PB-1. The difference is 39 seconds or 0.14 kg of pellets. LGB has a relatively higher fill time because the boiler has larger output capacity. Fill time is a preprogrammed parameter by the boiler software. There was a software upgrade in each heating season.

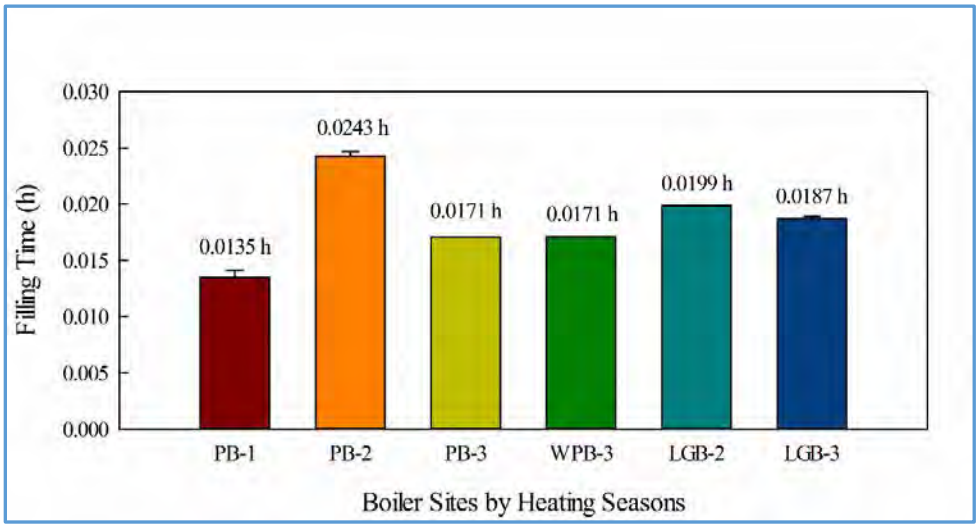

Figure 3-18. Filling time distribution for the three boiler sites by heating seasons

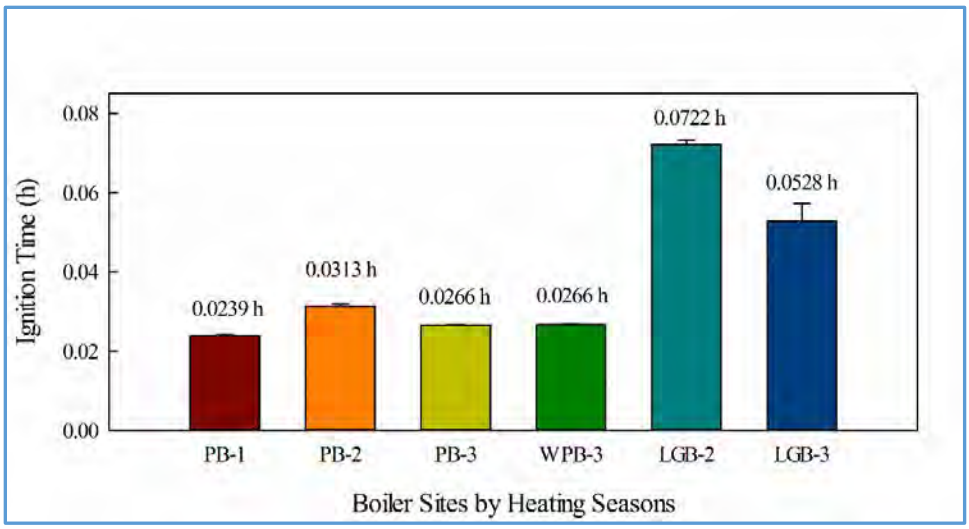

Figure 3-19. Ignition time distribution for the three boiler sites by heating seasons

Figure 3-19 shows the ignition time distribution. As expected, the ignition time follows the fill time because longer fill time means more pellets to be ignited. The highest two ignition times for LGB-2 and LGB-3 suggest possible fouling of the hot air passage in the combustion chamber, as ignition failure is the most common failure of LGB according to the boiler logs.

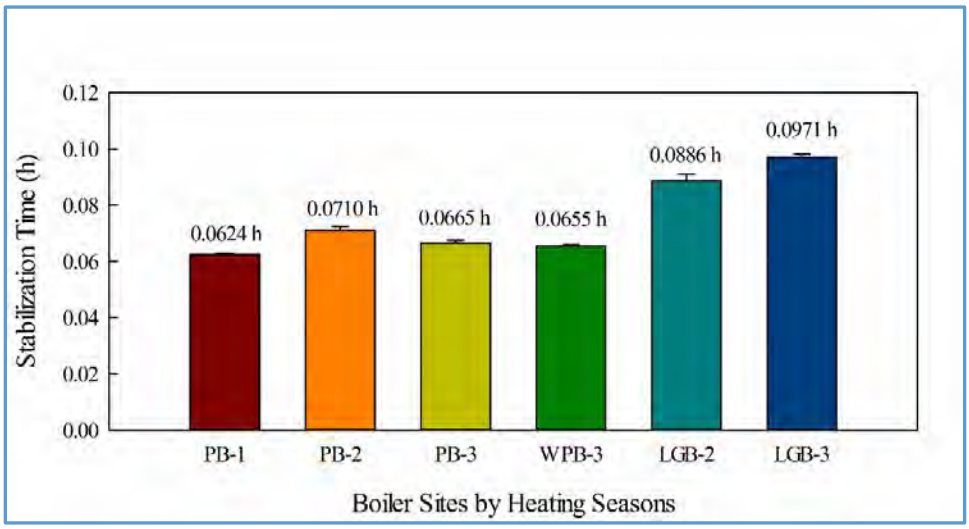

Figure 3-20. Stabilization time distribution for the three boiler sites by heating seasons

Figure 3-20 shows the stabilization time distribution. The criteria of end of stabilization is flue gas temperature reaching 100°C. Several key factors will determine how fast the boiler can achieve this goal: (1) the water volume of the fire tube heat exchanger; (2) return water temperature; (3) heat transfer efficiency of the fire tube heat exchanger; and so on. The LGB has a higher water volume and much lower boiler return temperature (high thermal mass of concrete slab) than PB and WPB. Thus, the LGB has a higher stabilization time than PB and WPB. In addition, recent information shows severe fouling of the fire tube heat exchanger that further deteriorated the heat transfer.

Figure 3-21 shows the automatic combustion time distribution. The length of automatic combustion time is mostly determined by the ON and OFF temperature settings in the TES tank and sometimes by extremely high heat demand from the building such that the TES tank cannot meet the demand. For example, at PB-1 and WPB-3, constant ON/OFF temperature settings of 56°C/64°C and 67°C/75.6°C were maintained and hence there were less variance and very similar automatic combustion times were observed. The extremely short time at LGB-2 was caused by very narrow ON/OFF settings of 75.6°C/77.6°C. The real automatic combustion time for LGB is represented by LGB-3 with ON/OFF settings of 40.6 C/76.7°C.

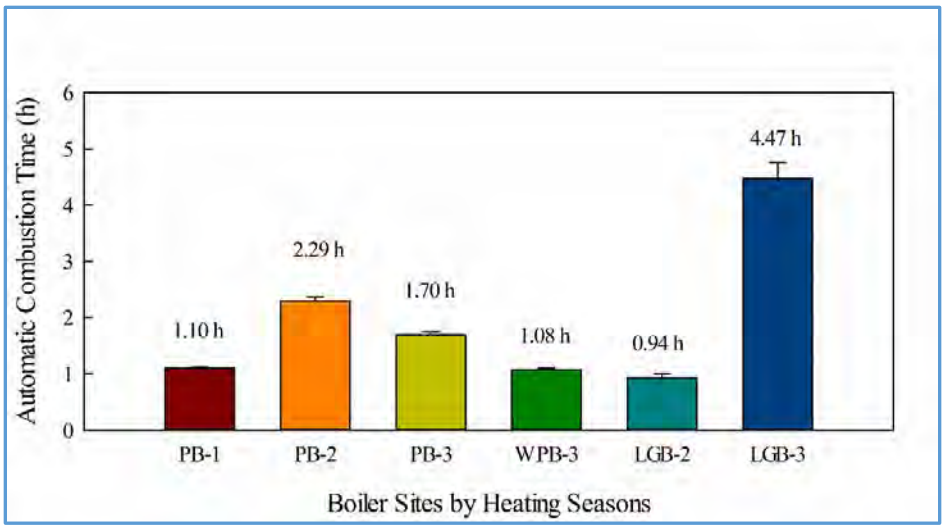

Figure 3-21. Automatic combustion time distribution for the three boiler sites by heating seasons

Figure 3-22 shows burnout and post-ventilation time distribution. This stage is controlled by boiler output capacity. Small boilers have shorter burnout/post-ventilation time and vice versa (note: LGB-2 is 50 kW and LGB-3 is 35 kW).

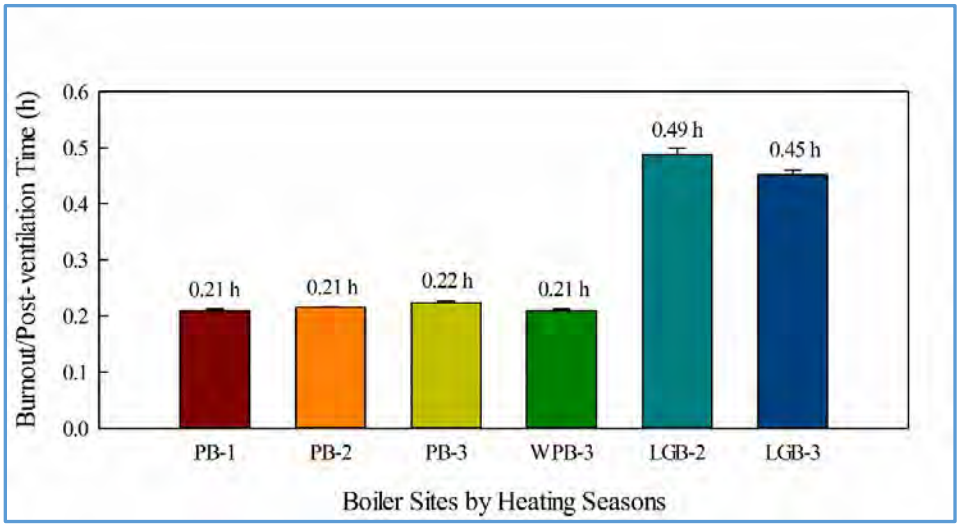

Figure 3-22. Burnout/post-ventilation time distribution for the three boiler sites by heating seasons

3.4.3 Boiler Cycling Characteristics

Since the boiler operation is based on cycles and each cycle has flush, fill, ignition, stabilization, automatic combustion, and burnout/post ventilation stage, it is important to evaluate the boiler based on a complete cycle rather than a given time interval, e.g. 15 minutes. The time interval based method is useful when there is no TES tank in the system such that the boiler operates continuously through load modulation.

The theoretical length of a boiler cycle time t_c can be calculated based on the TES tank volume and ON/OFF temperature settings as

$$t_c = \frac{V \rho_w c_{p,w} (T_{OFF} - T_{ON})}{N} \tag{3-4}$$

where V is the total volume of the TES tank (m^3), ρ_w is water density (kg/m^3), $c_{p,w}$ is water heat capacity (kJ/kg/K), T_{OFF} and T_{ON} are boiler OFF and ON temperature settings (°C), and N is boiler nominal output capacity (kW). For example, PB-1 was operating at a constant ON/OFF temperature difference of 8°C with a total volume of 0.9 m^3, the theoretical t_c is calculated as 0.33 h. However, in reality, boiler output is always less than its nominal output and the TES tank constantly supplies heat to the building. The actual boiler cycle time is always higher than the theoretical value.

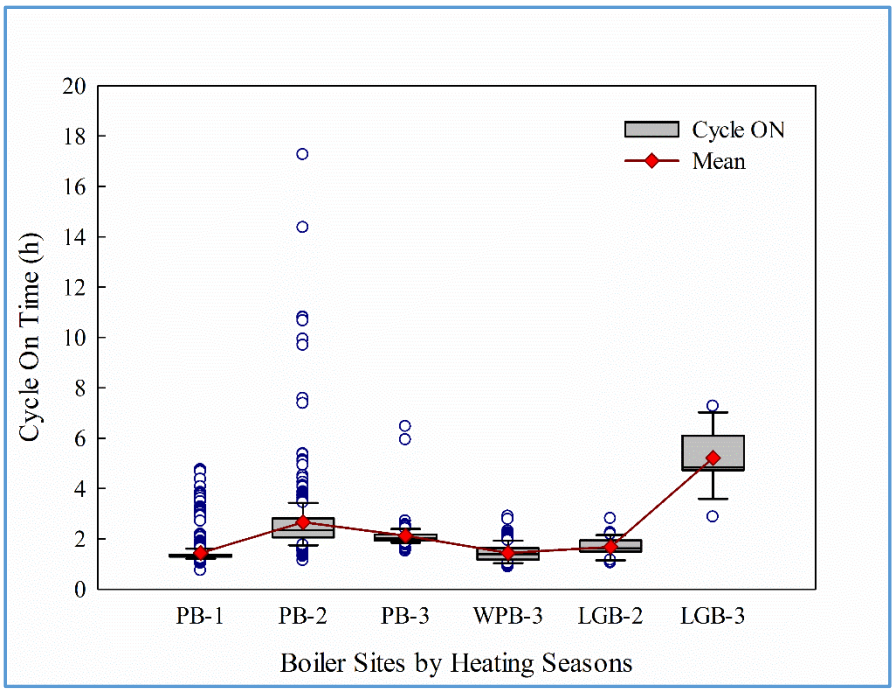

Figure 3-23. Boiler cycle ON time distribution at each boiler sites by different heating seasons with mean value and outliers

Figure 3-23 shows the boiler cycle ON time distribution. PB-1 has a constant TES ON/OFF temperature setting (8 °C) and thus the ON time distribution is very consistent with an average of 1.44 h. However, when there is an increase in heating demand from the building while the boiler is ON, the boiler cycle time is extended and appears as outliers. For PB-2, five different ON/OFF temperature differences were tried, ranging from 11 °C to 31 °C. Therefore, PB-2 has higher average cycle ON time (2.66 h). PB-3 and WPB-3 both have constant difference of ON/OFF settings (12 °C and 8.6 °C), but WPB has a smaller TES tank volume and smaller temperature difference than PB, resulting in an average cycle ON times for PB-3 and WPB of 2.12 h and 1.44 h, respectively. LGB-2 (average 1.67 h) has much shorter cycle ON time than LGB-3 (average 5.21 h) because the ON/OFF temperature difference for LGB-2 was only 2 °C

while LGB-3 was kept at 36.1 °C. The high variability in LGB-3 was also inflicted by the heat demand profile.

Figure 3-24 shows the boiler OFF time and the distribution of the OFF/ON ratios. The OFF time varies between PB and WPB, but the ratio for the two boiler sites are very similar (PB-1: 1.51, PB-2: 1.35, PB-3: 1.57 and WPB-3: 1.7). High ratio was observed at LGB-2, which was caused by very short boiler cycle ON time.

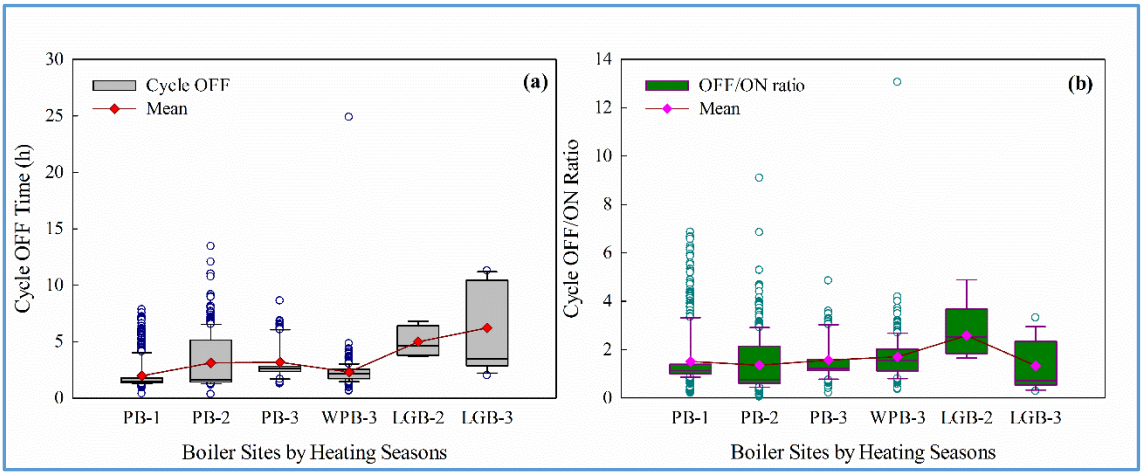

Figure 3-24. Boiler cycle OFF time distribution (a) and OFF/ON ratio distribution (b) at each boiler sites by different heating seasons with mean value and outliers

In general, the boiler cycle OFF time has no relationship with boiler cycle ON time. However, given a constant TES tank ON/OFF setting, the effect of heating demand can strongly affect boiler cycles, as shown in Figure 3-25.

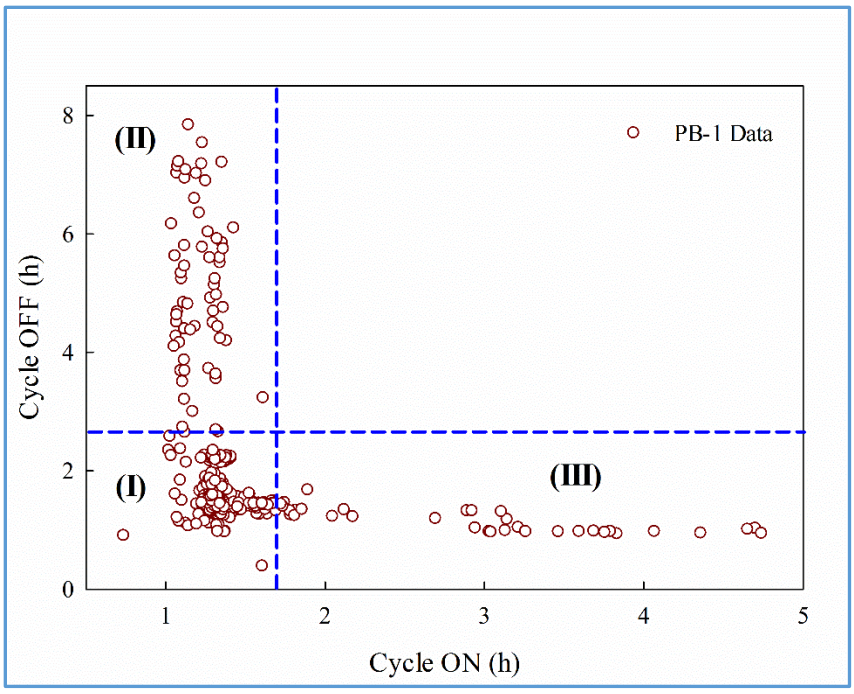

Figure 3-25. Zoning of boiler cycle ON and cycle OFF chart

There are three zones that can be clearly identified. Zone I is when the outdoor temperature is mild and the boiler has a cycle OFF/ON ratio around 1. Zone II is when the outdoor temperature is approaching the set temperature of the thermostat in the building, the heating demand from the building is very low, and therefore the boiler has a cycle OFF/ON ratio much larger than 1. Zone III is when outdoor temperature is extremely low and a constant high level of heat demand from the building keeps the boiler running for very long cycles with very short OFF times, leading to very small OFF/ON ratios. For successful wood pellet heating system sizing, zone II should be maximized and zone III should be minimized. It should also be noted that both zone I and Zone II have cycle ON times less than 2.0 h.

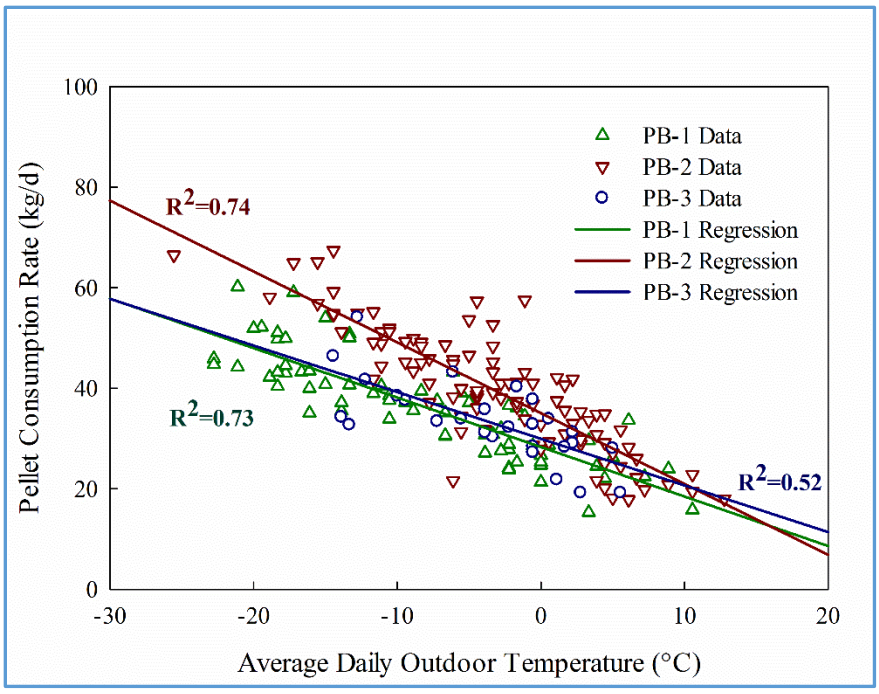

Figure 3-26. Daily wood pellet consumption as a function of outdoor temperature at PB

When the wood pellet boiler is used for space heating, the pellet consumption is then a function of outdoor temperature as shown in Figure 3-26. The slope increase from PB-1 to PB-2 indicates an energy efficiency drop for the boiler since the homeowner did not change the thermostat settings over the two heating seasons. In addition, the boiler repair and manual cleaning after PB-2 did improve the boiler performance since the PB-3 regression line is very close to PB-1. The overall correlation for PB-1, PB-2 and PB-3 is ($\mathbf{R^2}$ = 0.57):

$$P = 32.33 - 1.04\bar{T}_{\text{Outdoor}} \tag{3-5}$$

where P is daily pellet consumption (kg/d) and $\bar{T}_{\text{Outdoor}}$ is average outdoor temperature (range: -30°C < $\bar{T}_{\text{Outdoor}}$ < 20°C). Hence, based on equation (3-5), pellet requirement for the heating season can be estimated.

3.4.4 Potential Improvement

Based on previous time analysis, several suggestions can be made to further improve boiler operation:

(1) PB site has the historical issue of cleaning failure in flush stage because the boiler uses a single motion sensor to track the movement of the cleaning rod. It would be better to use two sensors at different positions in case one fails.

(2) The programing of filling and ignition stages should consider combustion chamber fouling and the circular glass window fouling. After each boiler cleaning, the fouling can be reset. A hearth temperature probe could be used to record boiler combustion chamber temperature.

(3) More stringent flue gas O_2 control is needed as [O_2] deviates a lot from the set value, as shown in Figure 3-15.

3.5 Wood Pellet Boiler Efficiency Analysis

3.5.1 Thermal Efficiency

The direct method in equation (2-11) is used to calculate the boiler thermal efficiency (or overall cycle efficiency) and is written as:

$$\eta_{\text{th}} = \frac{\sum Q \rho_w c_{p,w} (T_1 - T_2) \Delta t}{\text{GCV} \cdot \kappa \cdot \varepsilon \cdot t_c} \times 100\% \tag{3-6}$$

where Q is boiler flow rate (m^3/h), T_1 and T_2 are boiler supply and return water temperature (°C), Δt is the data sampling rate of the ultrasonic flow meter (Δt = 10 s), GCV is gross calorific value of the wood pellets (kJ/kg), κ is the 100% stoker feed rate (kg/h), and ε is stoker feed fraction. ρ_w is calculated based on the log mean temperature of boiler return and supply water temperatures T_{LN},[141] neglecting the effect of pressure change, as:

$$T_{\text{LN}} = \frac{T_1 - T_2}{\ln \frac{T_1}{T_2}} \tag{3-7}$$

$$\rho_w = 1000 \left[1 - \frac{(T_{\text{LN}} + 288.9414)(T_{\text{LN}} - 3.9863)^2}{508929.2(T_{\text{LN}} + 68.12963)} \right] \tag{3-8}$$

The 100% stoker feed rate was calibrated at the beginning and the end of each heating season. The boiler has a constant speed stoker auger and the most recent calibration was used for the calculations. The calibration results are shown in Figure 3-27.

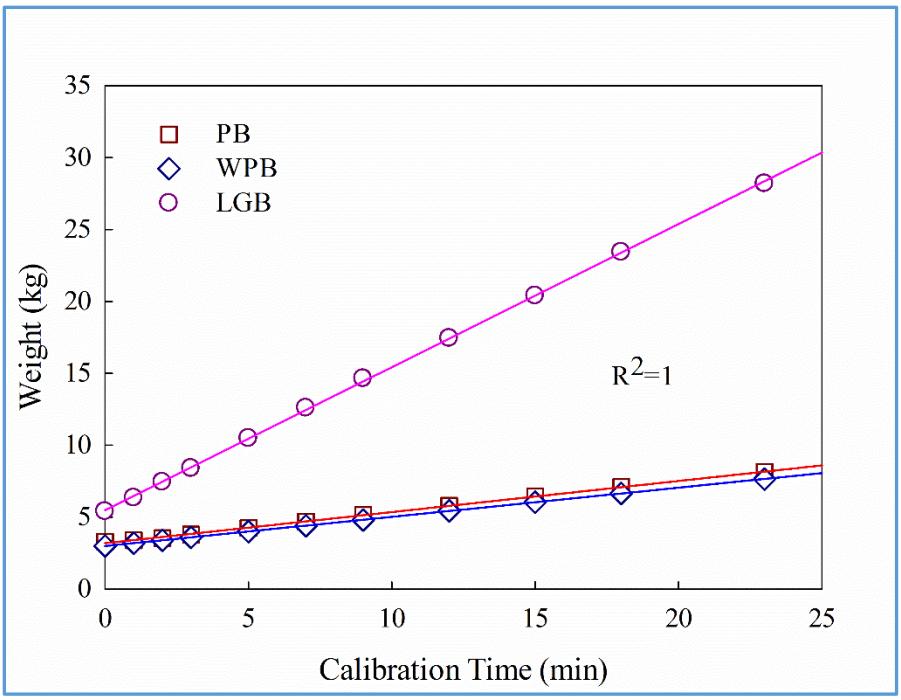

Figure 3-27. Stoker auger calibration for the three boiler sites

The results are: κ_{PB} = 12.978 kg/h, κ_{WPB} = 12.174 kg/h and κ_{LGB} = 59.706 kg/h. The fact that κ_{PB} and κ_{WPB} are so close also indicates that the stoker auger is a constant speed auger because PB and WPB are both 25 kW boilers. Boiler output load χ is calculated as the ratio of actual output to nominal output based each boiler cycle time, as

$$\chi = \frac{\sum Q \rho_w c_{p,w} (T_1 - T_2) \Delta t}{3600 \cdot N t_c} \times 100\% \tag{3-9}$$

where N is boiler nominal output capacity. Divide equation (3-6) by (3-9), the following relationship can be derived

$$\frac{\eta_{th}}{\chi} = \frac{3600N}{GCV \cdot \kappa} \left(\frac{1}{\varepsilon}\right) \tag{3-10}$$

Thus, if the boiler was running at a constant stoker feed fraction, the boiler thermal efficiency will change linearly with boiler output load. Equation (3-10) indicates that in order to obtain high thermal efficiency, the boiler should fire at high output load.

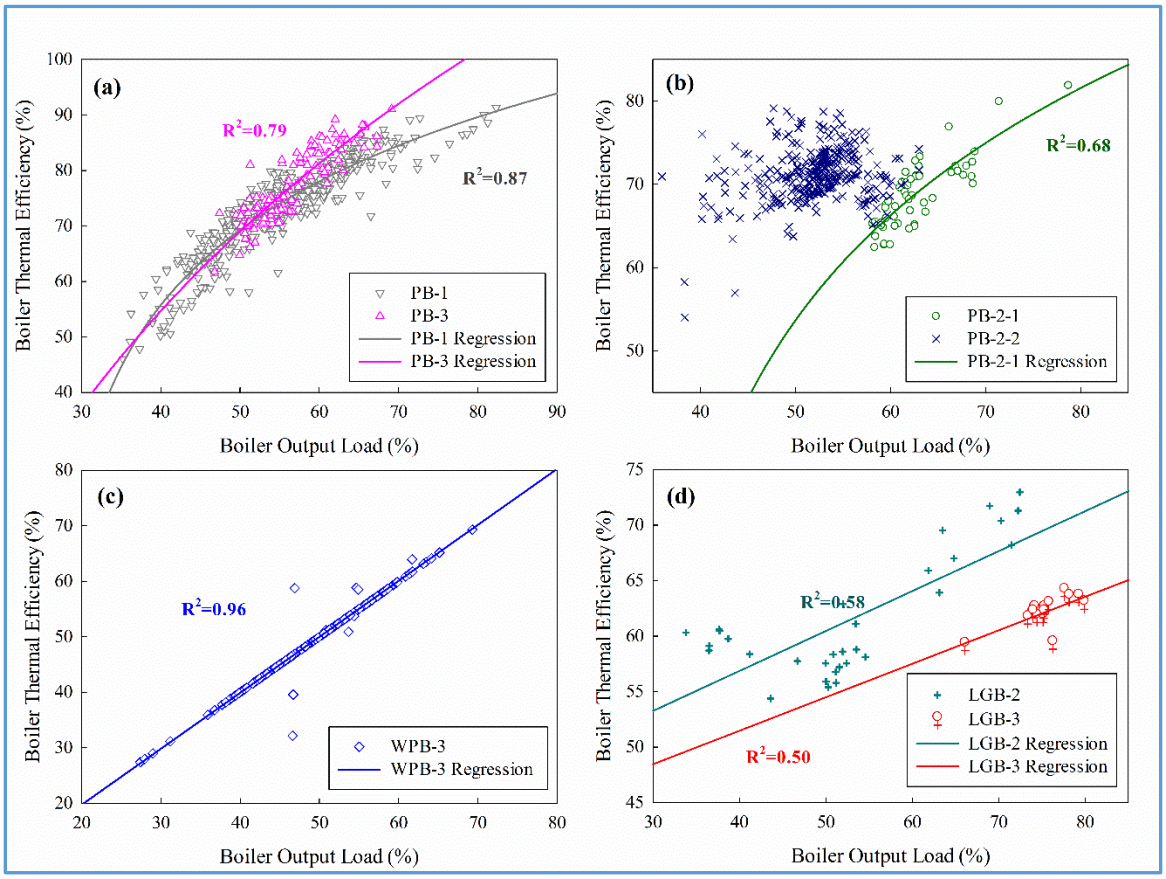

Figure 3-28. Boiler thermal efficiency as a function of boiler output load for the three boilers in different heating seasons (Note: a boiler software update was carried out on January 6, 2016 and PB-2-1 represents data before update and PB-2-2 represents data after update)

Figure 3-28 shows boiler thermal efficiency as a function of boiler output load for the three boilers in different heating seasons. It can be clearly seen that the stoker feed rate at PB has much more variability than WPB and LGB. The correlation equations for PB-1, PB-2-1 (before software update) and PB-3 are:

$$\eta_{\text{th}}|_{\text{PB}-1} = -10.09 + 25\ln(\chi_{\text{PB}-1} - 26.08) \quad (3\text{-}11)$$

$$\eta_{\text{th}}|_{\text{PB}-2-1} = -26.32 + 27.95\ln(\chi_{\text{PB}-2-1} - 32.51) \quad (3\text{-}12)$$

$$\eta_{\text{th}}|_{\text{PB}-3} = -286.3 + 85.24\ln(\chi_{\text{PB}-3} + 14.61) \quad (3\text{-}13)$$

The above correlations are similar to the boiler flue gas O_2 control at PB using stoker feed shown in equation (3-2). For WPB-3, a linear correlation was observed as

$$\eta_{\text{th}}|_{\text{WPB}-3} = -4.23 + 1.01\chi_{\text{WPB}-3} \quad (3\text{-}14)$$

The linear correlation of thermal efficiency and load at WPB-3 is because boiler cycle efficiency at WPB was generally lower than PB. Efficiency bins for each of the pellet sites by heating seasons is shown in Figure 3-29.

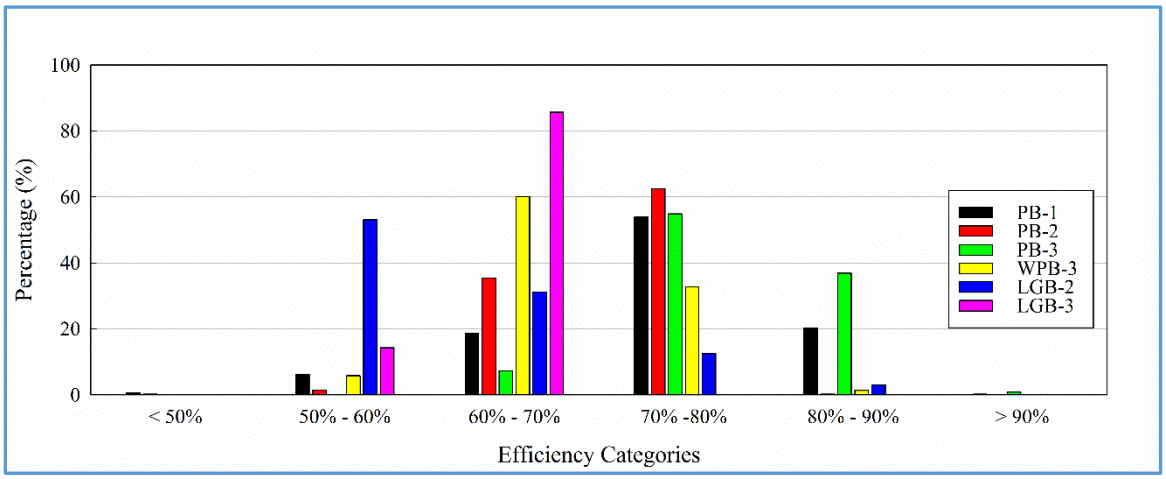

Figure 3-29. Efficiency bins for the three boiler sites in different heating seasons

Generally speaking, PB-1 and PB-3 have the highest cycle efficiencies while LGB-2 and LGB-3 have the lowest cycle efficiencies. WPB-3 lies in the middle. PB-1 had 495 total boiler cycles with 368 of them (or 74.3% of the total) operating at thermal efficiencies above 70%. PB-2 has more low efficiency cycles and almost no cycle

efficiency above 80%. This decrease was caused by a lack of fire tube heat exchanger cleaning. After cleaning and some cleaning, the boiler was operating at higher efficiency ranges, as shown by PB-3. For most of the time (over 60% of boiler cycles), WPB was operating in the low efficiency ranges. It was found to be caused by the boiler output load modulation driven by high return temperatures exceeded boiler safety temperature limit (STL = 85 °C). The load modulation in WPB system is related to the 2-pipe configuration of TES tank shown in Figure 3-8. Compared to PB system, which is a 4-pipe configuration, 2-pipe configuration cannot isolate the boiler loop and tank loop when the boiler is firing and the building is call for heat. Although 2-pipe configuration does have some benefits as described in Chapter 3, it does not always perform better than 4-pipe configuration. For example, WPB system has a low thermal mass unit (DHW tank) that the simultaneous operation of the boiler and the heat demand will lead to high boiler return temperatures and cause boiler modulation and sometimes short-cycling.

LGB-2 and LGB-3 have the lowest efficiency ranges with most of the boiler cycles were below 70%. These low values were caused by the lack of cleaning for the boiler as no maintenance was performed since the installation of the boiler in 2015.

Aside from boiler load effect on cycle efficiency, the cycle time also affects cycle efficiency. Longer cycle time results in higher thermal efficiency since the fraction of low efficiency stages in each cycle is reduced. Figure 3-30 shows an example based on data from PB-1.

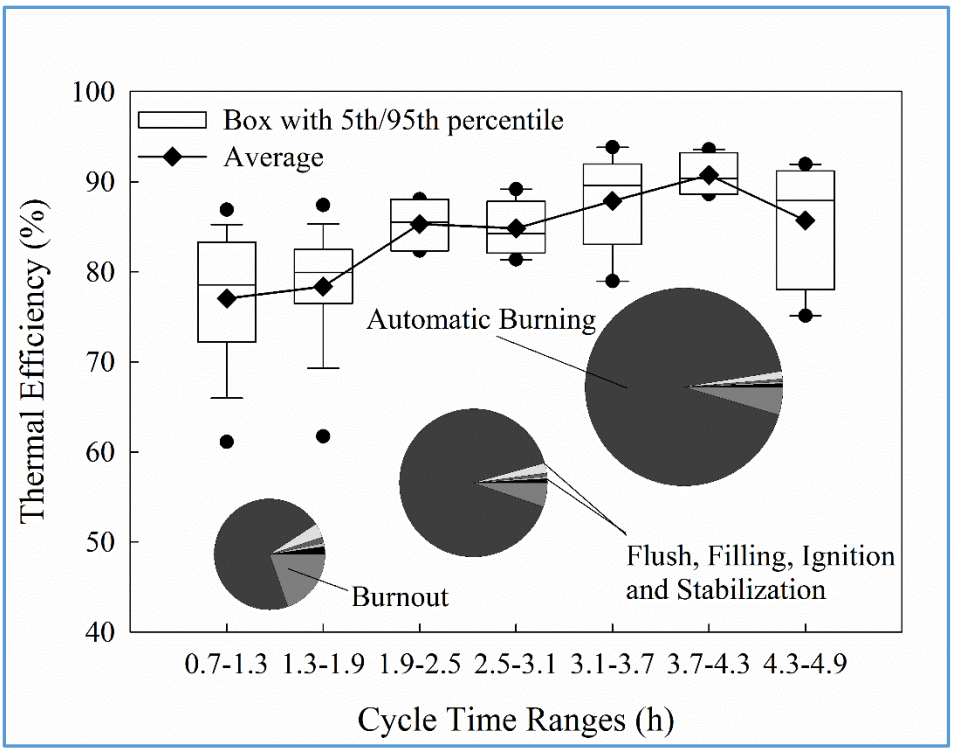

Figure 3-30. Boiler cycle efficiency as a function of cycle time for PB-1

3.5.2 Combustion Efficiency

Instead of the indirect method using equation (2-12), boiler combustion efficiency was calculated using Siegert method[94] by subtracting flue gas losses qA from 100% as described below:

$$\eta_{\text{com}} = 100\% - qA \tag{3-15}$$

$$qA = f\frac{T_{\text{g}} - T_a}{[\text{CO}_2]} \tag{3-16}$$

where f is a fuel specific factor (0.68 for wood pellets[94]), T_{g} and T_a are average flue gas temperature and average boiler room temperature, respectively. $[CO_2]$ is flue gas CO_2 content in percentage. $[CO_2]$ can be calculated using $[CO_2]_{max}$ and $[O_2]$ as

$$[CO_2] = [CO_2]_{max} \frac{20.9\% - [O_2]}{20.9\%} \quad (3\text{-}17)$$

where $[CO_2]_{max}$ = 20.4%, calculated based on composition analysis of wood pellets. It should be noted that T_g and $[O_2]$ are both average values for the automatic combustion stage of a boiler cycle. They are measured and recorded by the boiler software that can be retrieved for analysis. Based on the boiler room temperature measurements at each of the three boiler sites, the following boiler room temperatures are used in the combustion efficiency calculations: $T_a|_{PB}$ = 20 °C, $T_a|_{WPB}$ = 15 °C and $T_a|_{LGB}$ = 20 °C.

Figure 3-31 shows boiler combustion efficiency as a function of excess air λ, defined as

$$\lambda = 1 + \frac{[O_2]}{20.9\% - [O_2]} \quad (3\text{-}18)$$

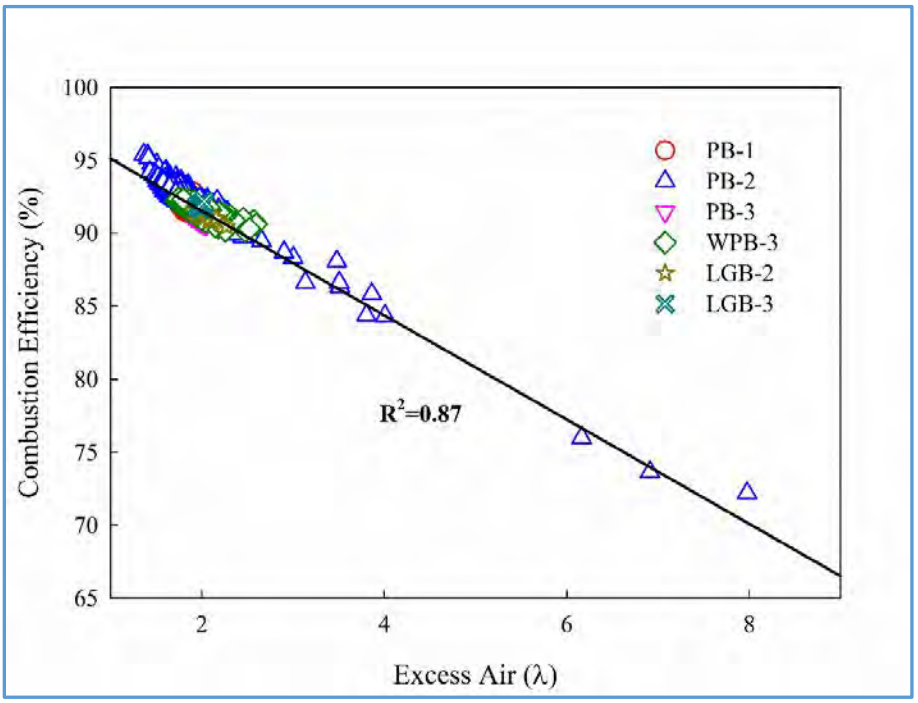

Figure 3-31. Boiler combustion efficiency as a function of excess air

The overall regression equation for all the data at three boiler sites is

$$\eta_{\mathrm{com}} = 98.68 - 3.57\lambda \tag{3-19}$$

Thus, by monitoring flue gas O_2, the boiler combustion efficiency can be calculated. Equation (3-19) also indicates that the theoretical maximum combustion efficiency for the wood pellet boilers studied in this research is $\eta_{\mathrm{com}}|_{\mathrm{max}} = 95.11\%$ when $\lambda = 1$.

Figure 3-31 shows that PB-2 data has a wide spread of λ from 1.3 to 8 while all the rest of the data are clustered around 2. This phenomenon indicates O_2 control at PB-2 was not working properly, as indicated by Figure 3-16 (b).

Boiler combustion efficiency can also influenced by outdoor temperature as shown in Figure 3-32. Low outdoor temperature results in high heat loss from the boiler room, which will decrease the combustion air temperature causing lower combustion efficiency.

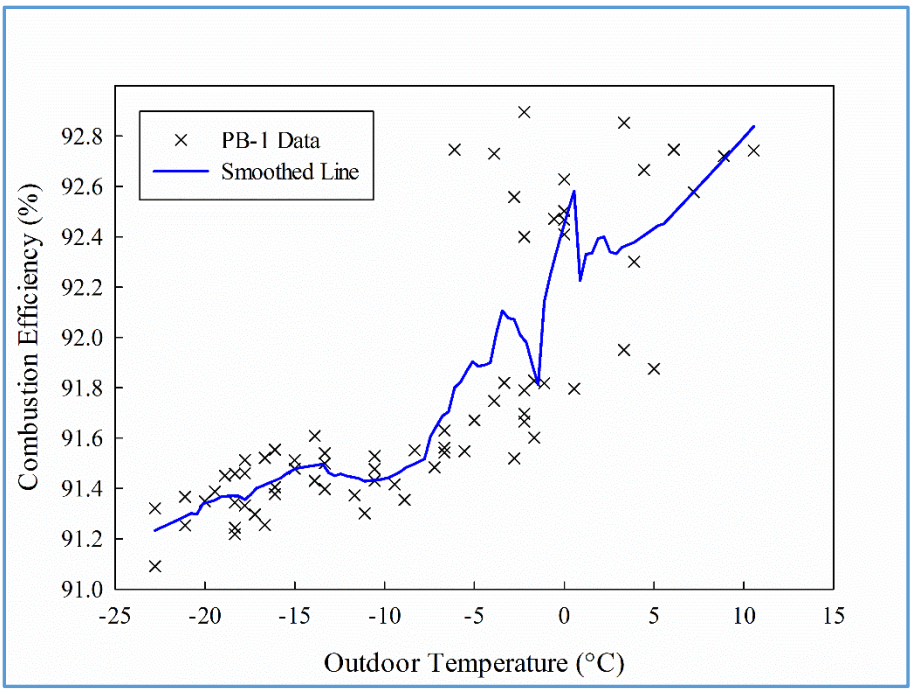

Figure 3-32. Outdoor temperature effect on combustion efficiency

3.5.3 Heat Transfer Efficiency

Heat transfer between the hot flue gas and water in the fire tube heat exchanger is one of the controlling factor that determines the overall performance of the boiler. Heat transfer efficiency (η_{HT}) is defined as the ratio of thermal efficiency and combustion efficiency:

$$\eta_{HT} = \frac{\eta_{th}}{\eta_{com}} \times 100\% \tag{3-20}$$

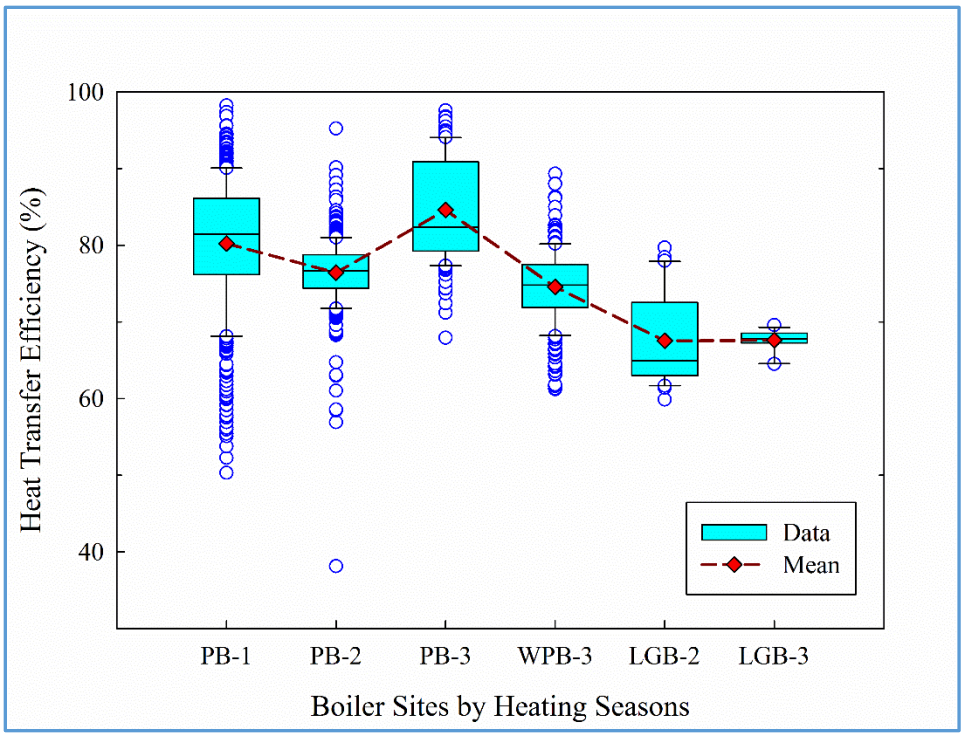

Figure 3-33. Heat transfer efficiency distribution for all boilers by heating seasons

Heat transfer efficiency is a good indicator of the heat transfer resistance inside the fire tube heat exchanger. It is a key factor determining boiler thermal efficiency and overall performance. Figure 3-33 compares heat transfer efficiency among the different boilers over the different heating seasons. The average heat transfer efficiencies are 80.2%, 76.4%, 84.6%, 74.6%, 67.5% and 67.6 for PB-1, PB-2, PB-3, WPB-3, LGB-2 and LGB-3, respectively. The highest average heat transfer efficiency is at PB-3, which could be caused by frequent manual cleaning of the boiler and that only a short period of data available. PB-1 showed a stable, uninterrupted distribution of heat transfer efficiency in the first year of operation with an average value of 80.2%. The LGB has a very low heat transfer efficiency, which is one of the key reasons why the boiler has very low thermal efficiencies.

By examining η_{HT} of each boiler cycle, the fouling rate of the fire tube heat exchanger can be determined, and therefore, the frequency of manual cleaning of the fire tube heat exchanger can be recommended.

The method used is called Mann-Kendall trend test (MK test).[142 - 143] The hypotheses are that the analyzed data have a monotonic trend. MK test is based on the test statistic *S* defined as

$$S = \sum_{i=1}^{n-1} \sum_{j=i+1}^{n} \text{sgn}(x_j - x_i) \tag{3-21}$$

where x_j and x_i are data values ($j > i$), n is the number of total data points, and sgn(x_j - x_i) is the sign function defined as

$$\text{sgn}(x_j - x_i) = \begin{cases} +1, & x_j - x_i > 0 \\ 0, & x_j - x_i = 0 \\ -1, & x_j - x_i < 0 \end{cases} \tag{3-22}$$

Mann[142] and Kendall[143] have shown that when $n \geq 18$, S is approximately a normal distribution with expectation of 0 and variance as

$$\sigma^2(S) = \frac{n(n-1)(2n+5) - \sum_{i=1}^{m} t_i(t_i-1)(2t_i+5)}{18} \tag{3-23}$$

where m is the number of tied groups and t_i denotes the number of ties of extent i. A tied group is defined as a set of sample with the same value. The standard normal test (or Z-test) statistic Z_S is computed as

$$Z_S = \begin{cases} \dfrac{S-1}{\sqrt{\sigma^2(S)}}, & \text{if } S > 0 \\ 0, & \text{if } S = 0 \\ \dfrac{S+1}{\sqrt{\sigma^2(S)}}, & \text{if } S < 0 \end{cases} \tag{3-24}$$

$Z_S > 0$ means increasing trends while $Z_S < 0$ means decreasing trends. A Theil-Sen's line is usually used to estimate the slope of the trend.

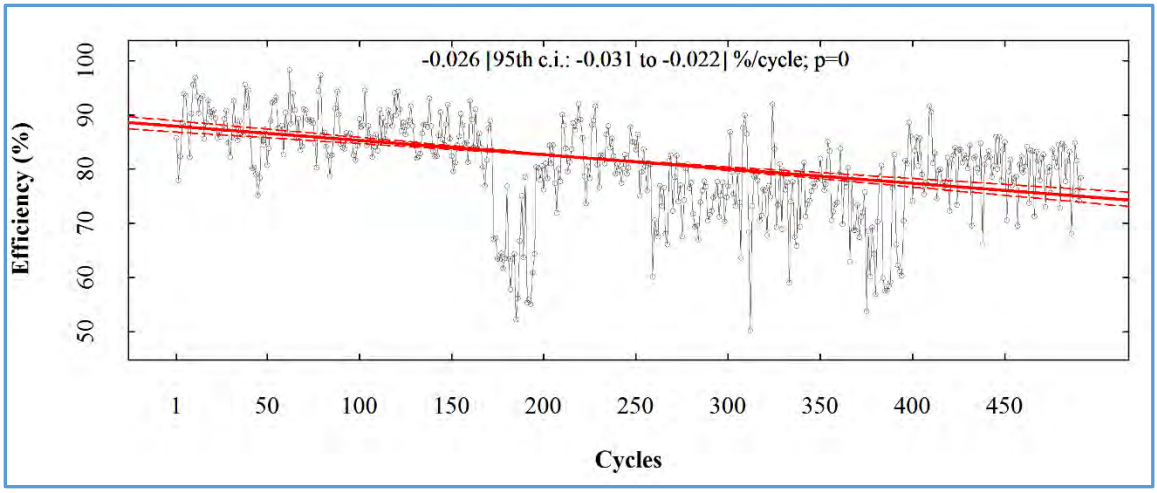

Figure 3-34. Sen's slope of heat transfer efficiency for PB-1 (c.i. – confidence interval)

During PB-1, there were a total of 493 boiler cycles in 70 days, or an average of 7 boiler cycles per day. Figure 3-34 shows the decreasing trends of heat transfer efficiency for PB-1 with an averaged decreasing rate of 0.026 % per boiler cycle. Suppose the boiler has to be cleaned manually when the heat transfer efficiency has dropped by 10%, then the boiler has to be cleaned after 385 boiler cycles, or 55 days of continuous operation.

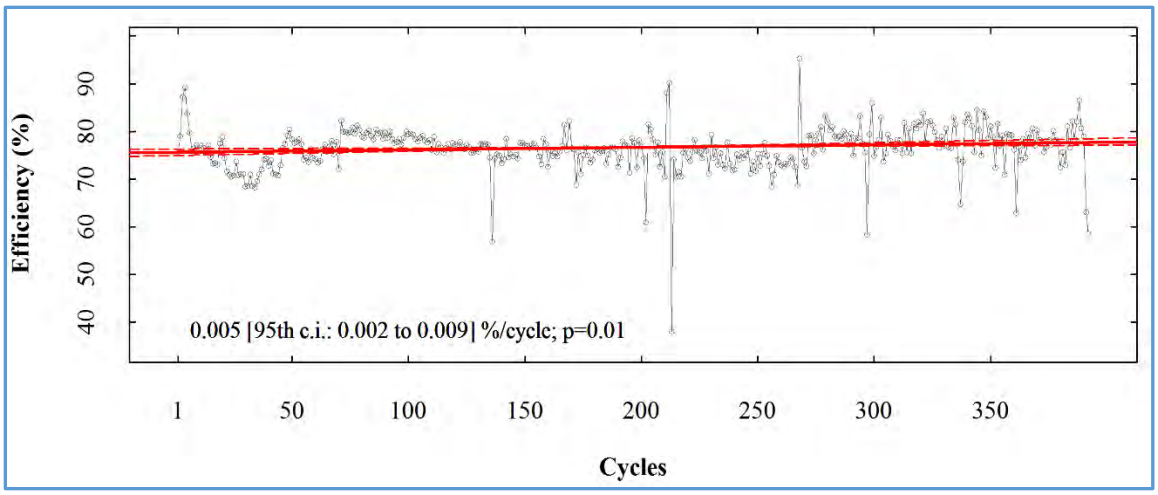

Figure 3-35. Sen's slope of heat transfer efficiency for PB-2 (c.i. – confidence interval)

No similar trend was observed for the other boiler. PB-2 had a relatively constant heat transfer efficiency (as shown in Figure 3-35) with the trend line flat at around 75%. The lower heat transfer efficiency suggests the boiler needed to be cleaned manually. In fact, PB was not cleaned during either of the PB-1 and PB-2 periods. The distribution of PB-2 data indicates the boiler can only maintain an average of 75% heat transfer efficiency after firing for two heating seasons (PB-1 and PB-2), if no manual cleaning is performed.

For PB-3, the effect of boiler cleaning can be clearly seen as an increasing heat transfer efficiency from 75% to 90% (Figure 3-36).

Comparing the starting cycles of PB-1 from Figure 3-34 with the ending cycles of PB-3 from Figure 3-36, the boiler was able to maintain its heat transfer efficiency through over multiple heating seasons, if sufficient cleaning was performed.

For WPB-3, the drop of heat transfer efficiency is not statistically significant.

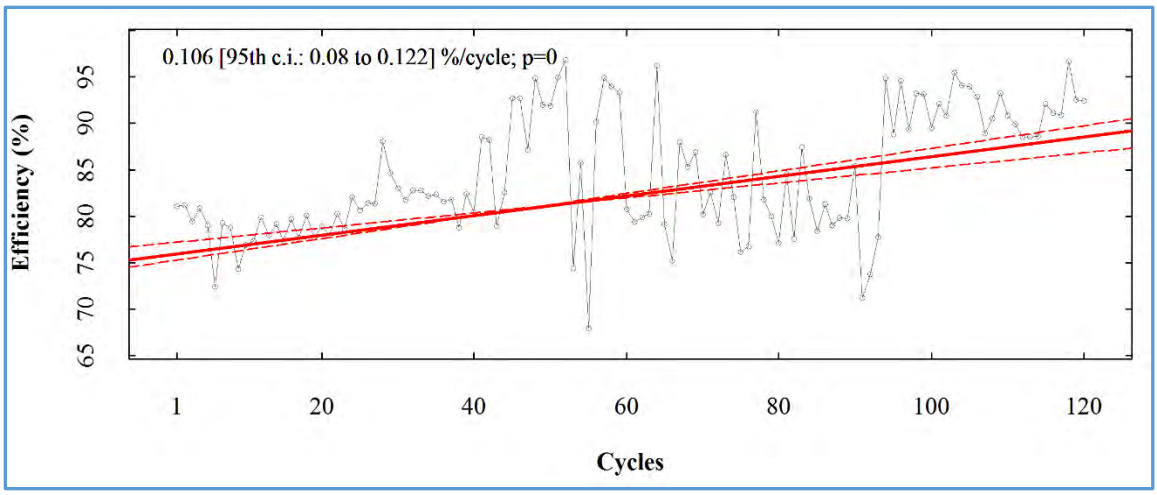

Figure 3-36. Sen's slope of heat transfer efficiency for PB-3 (c.i. – confidence interval)

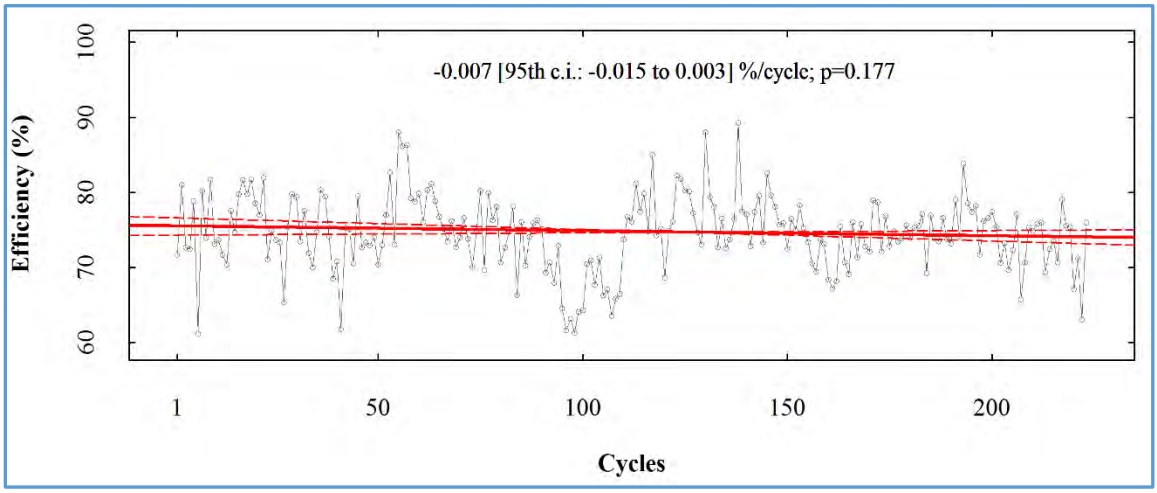

Figure 3-37. Sen's slope of heat transfer efficiency for WPB-3 (c.i. – confidence interval)

3.6 Emissions Characterization

Emissions from the WPB and PB systems were measured in February and April of 2015. No emission measurements were performed for LGB system. Three groups of measurements were performed with two runs for each group, given a total of 12 experiment runs. The emissions from PB and WPB will be discussed and analyzed.

3.6.1 Time Lag

Due to the length of the sampling train, a time lag of 4 minutes was determined and applied to the data analysis for two boilers by correlating flue gas CO and O_2 concentrations based on the fact that flue gas O_2 is measured by the boiler directly and should have a strong correlation with flue gas CO emission. The cross correlation is shown in Figure 3-38. Hence, it will take 4 minutes for the change in boiler flue gas to be reflected in the gas monitors used for emission measurement.

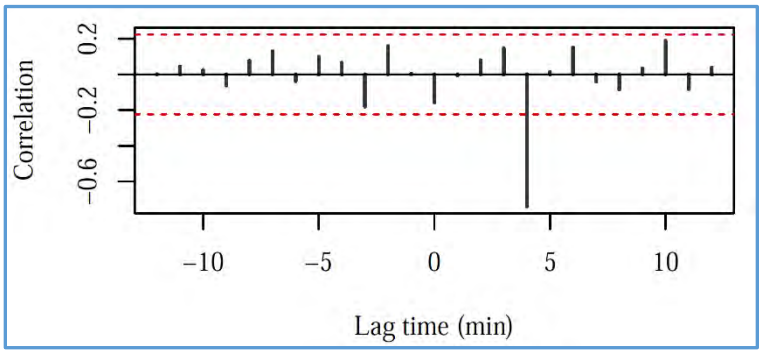

Figure 3-38. Cross correlation factor (CCF) for flue gas O_2 and CO concentrations as a function of lag time

3.6.2 Gaseous Emissions

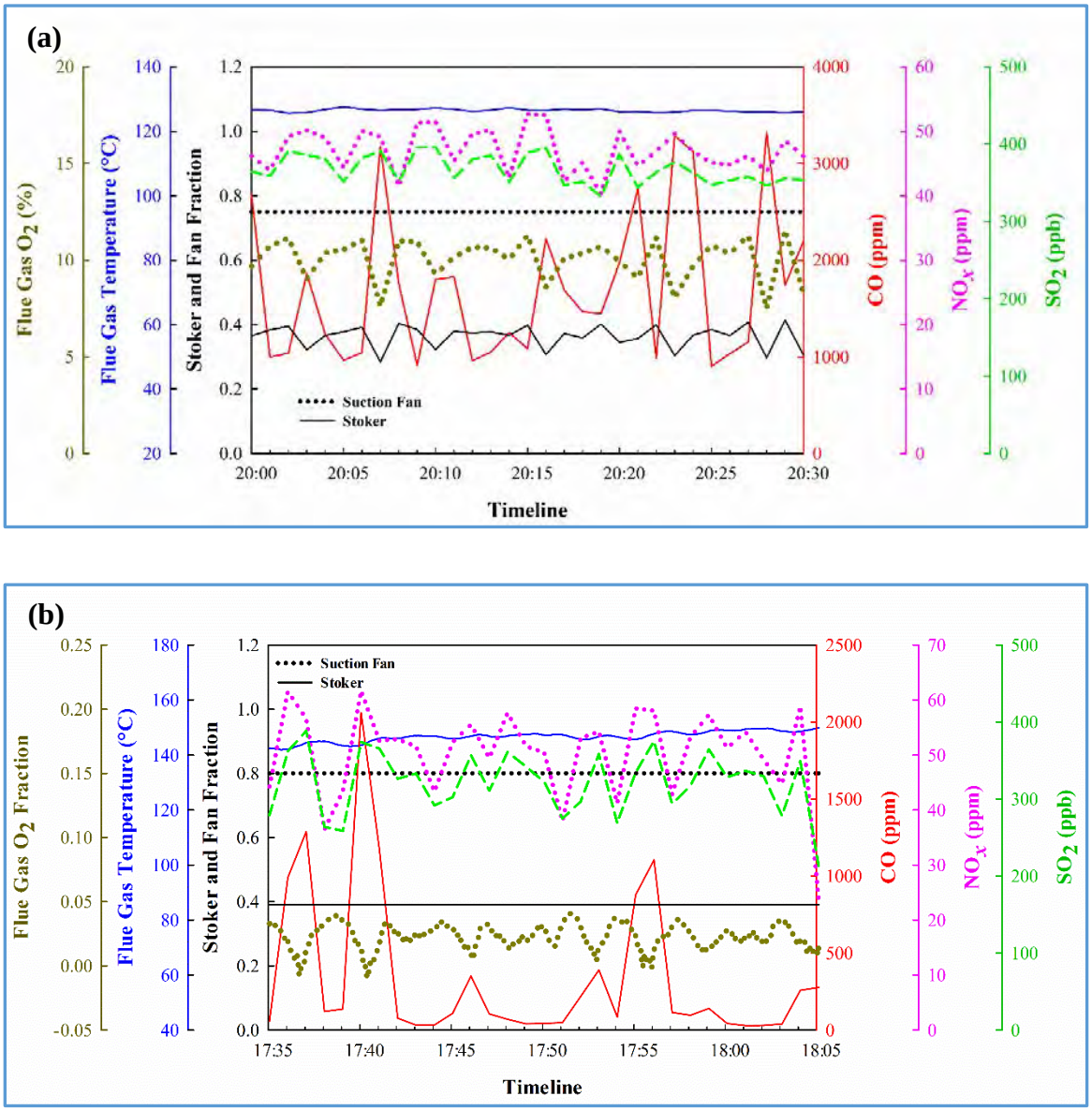

Figure 3-39. Gaseous emissions from PB (a) and WPB (b) in comparison with boiler operation parameters (Run 1-1 of each boiler)

Figure 3-39 shows a typical emission profile of CO, NO_x and SO_2 for both boilers. The boiler operational parameters are listed for comparison in Table 3-7. The two boilers have almost identical stoker feed and suction fan speed. However, PB had flue gas O_2 at 10.3% while WPB was at 2.3% (boiler O_2 set point is 10%). WPB should have much

higher CO concentration than PB, which is not the case as indicated by Figure 3-39. Several explanations can be hypothesized: (1) the lambda sensor was not properly calibrated; (2) the boiler cannot utilize proper O_2 control based on stoker feed, as indicated by Figure 3-15 that PB and LGB have O_2 control through stoker feed fraction while no clear relationship between the two parameters were found in WPB.

Table 3-7. List of boiler operation parameters of PB and WPB during stack sampling

Boiler	T_g (°C)	O_2 (%)	ε	Suction Fan (%)
PB	126	10.3	0.37	75
WPB	147	2.3	0.39	80

Figure 3-39 shows high concentration of CO concentrations corresponding with O_2 content minima, suggesting that low flue gas O_2 content means insufficient combustion and thus, high emission of CO.

Table 3-8. Pearson correlation among different variables (correlations significant at $p <$ 0.05 are in bold)

	$\boldsymbol{\varepsilon}$	T_g	[O_2]	[CO]	[NO_x]	[SO_2]
$\boldsymbol{\varepsilon}$	1	-	-	-	-	-
T_g	**-0.17**	1	-	-	-	-
[O_2]	**0.97**	**-0.16**	1	-	-	-
[CO]	**-0.59**	0.05	**-0.70**	1	-	-
[NO_x]	-0.11	**0.16**	-0.07	**0.23**	1	-
[SO_2]	-0.10	**-0.28**	-0.03	0.04	**0.63**	1

By utilizing the Pearson correlation among all pairs of variables discussed above, correlations of several variables was observed: CO and flue gas O_2 content; flue gas O_2

content and stoker feed fraction; NO_x and SO_2. The correlation results are listed in Table 3-8. The correlation between flue gas O_2 and CO emission is shown in Figure 3-40.

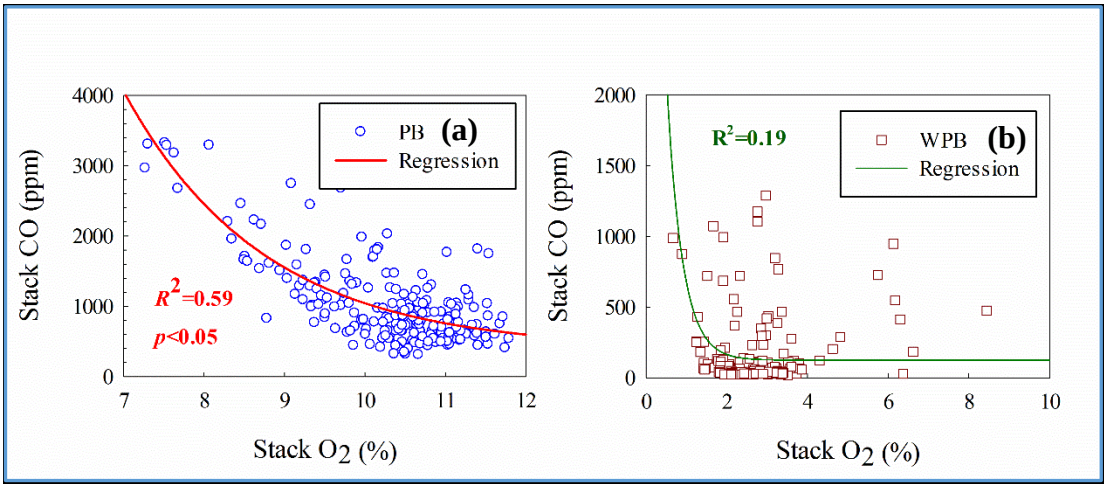

Figure 3-40. CO emission as a function of flue gas O_2 content for all emission data at PB (a) and WPB (b)

A good correlation was found for PB but not for WPB, which was possibly related to the lambda sensor issue and the internal oxygen control mechanism of the boiler. However, WPB did have lower CO emission than PB, which means higher combustion efficiency of WPB during stack sampling. The regression equation for PB is

$$[\mathrm{CO}]_{\mathrm{ppm}} = 391.8 + 20400\exp(-0.575[\mathrm{O_2}]) \tag{3-25}$$

Similar correlation has also been seen in other studies.[92,96,105] Low flue gas O_2 content leads to high CO emissions and vice versa.[144] Based on equation (3-25), a minimum of CO emission of 412 ppm can be achieved by setting flue gas O_2 control to 12% for PB. Consequently, λ = 2.35 and the corresponding combustion efficiency η_{com} = 90.3% from equation (3-19). The stoker feed fraction ε can also be determined equation (3-2) as ε = 0.44. Those provides a set of optimized parameters for PB boiler operation and emission control based on minimum CO emission.

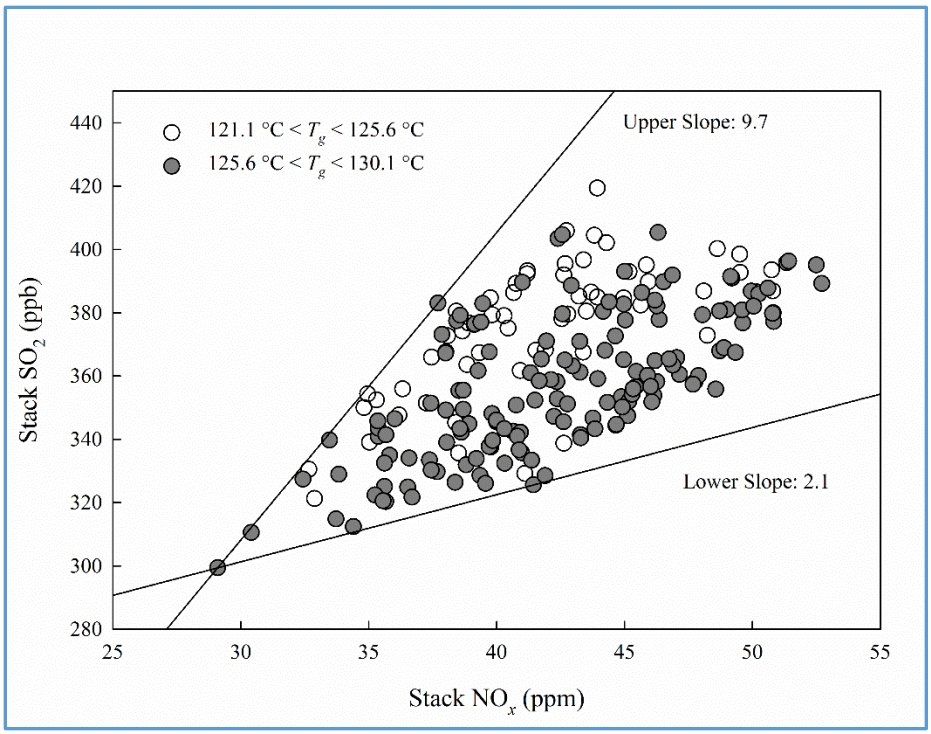

Figure 3-41. SO_2 and NO_x emission band at different flue gas temperature ranges for PB

Figure 3-41 shows the upper and lower bounds of SO_2 and NO_x emissions. For a specific type of wood pellets, the ratio of [SO_2] and [NO_x] should be roughly constant because studies have shown that fuel-bound nitrogen and sulfur are the major source of SO_2 and NO_x emissions.[76,101,109] However, Figure 3-41 shows a wide range of slope from 2.1 to 9.7. This result is a good indicator of the formation of other forms of N-bonded emissions such as NH_3, N_2, HCN, etc.[145] aside from NO_x. Figure 3-41 also indicates that when the flue gas temperature increases, the formation of thermal NO_x increases leading to a lower slope and vice versa.

For WPB, a good correlation between SO_2 and NO_x emissions was found, as shown in Figure 3-42. There was less variation of the data that suggests less formation of other nitrogen containing species.

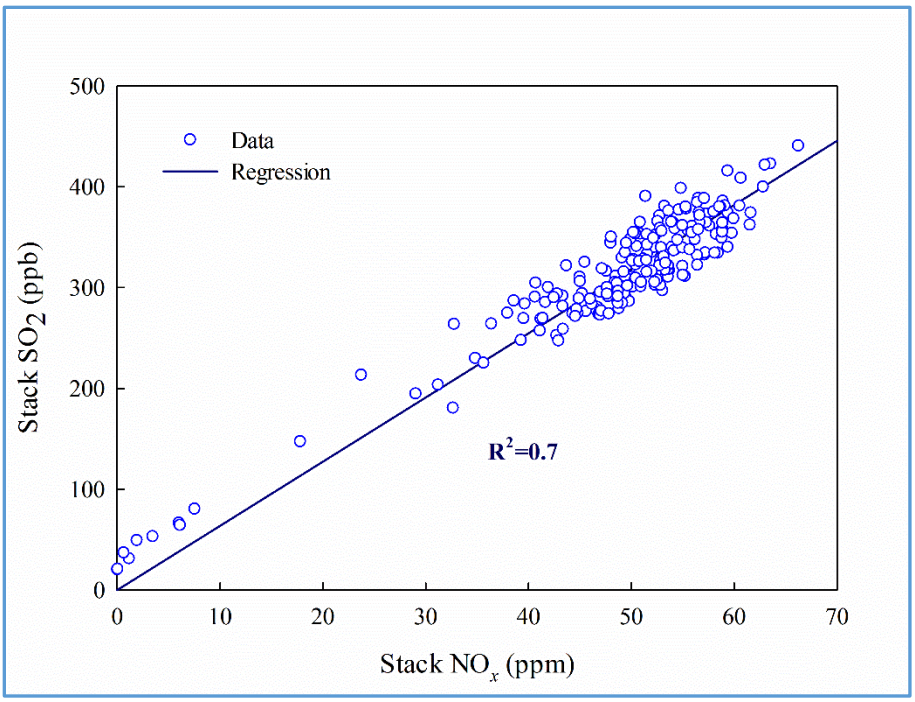

Figure 3-42. SO_2 and NO_x emissions correlation for WPB (regression line passes through origin)

The correlation equation is

$$[SO_2] = 6.37[NO_x] \tag{3-26}$$

where $[SO_2]$ and $[NO_x]$ are SO_2 and NO_x emissions in ppb and ppm, respectively.

Experiment set 3 for WPB stack sampling studied the emissions during boiler start-up and boiler shut down operations, as shown in Figure 3-43. The stoker line in Figure 3-43 (a) indicates the boiler transitioning from stabilization stage into automatic combustions stage. During this time, emissions of CO, SO_2 and NO_x were increasing from 0 to the highest values. SO_2 and NO_x emissions were following each other up and down during the sampling time while CO emission dropped to about half after the boiler went into steady state combustion.

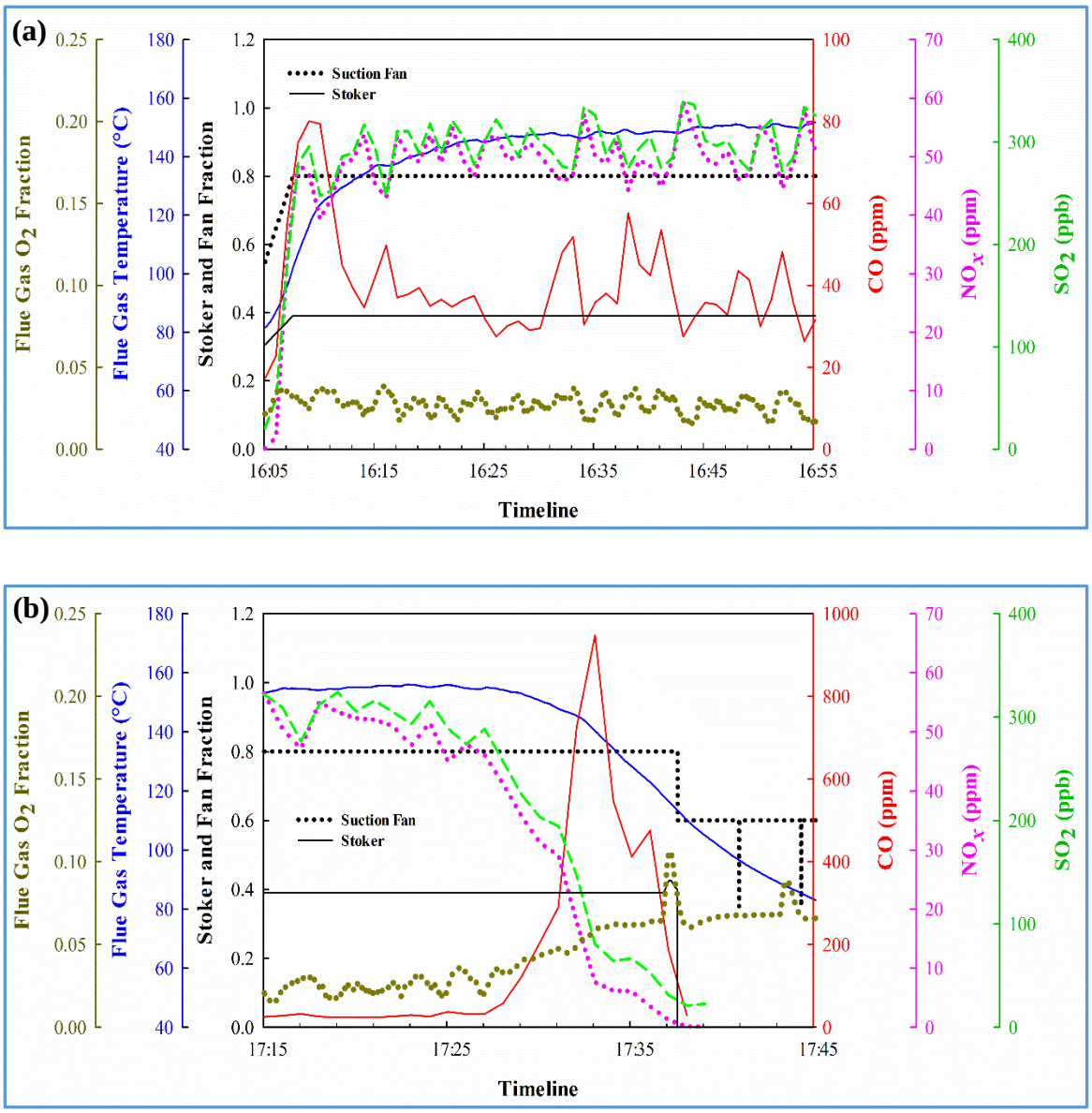

Figure 3-43. Emissions from boiler start-up and boiler shut down operations in WPB (stack sampling set 3)

During boiler shut down, as shown in Figure 3-43 (b), SO_2 and NO_x emissions decreased exponentially. CO emission increased dramatically due to the insufficient combustion of the remaining wood pellets (smoldering). The highest CO emission reached 950 ppm, which is over 10 times higher than the highest CO during boiler start-up operation. Thus, boiler shut down can produce much higher CO emission than start-

up. A summary of the average gaseous emissions during the sampling period are listed in Table 3-9 with units of mg/m^3 and mg/MJ.

Table 3-9. Stack sampling results for gaseous emissions expressed in different units (mg/m^3 is normalized to 25 °C and 1 atm with 10% O2 correction)

Experiment Sets	[CO]		[NO_x]		[SO_2]	
	mg/m^3	mg/MJ	mg/m^3	mg/MJ	$\mu g/m^3$	μg/MJ
PB Run 1-1	1979	930	89	42	975	458
PB Run 1-2	1395	654	88	41	943	442
PB Run 2-1	1101	530	80	39	1009	486
PB Run 2-2	795	383	84	40	983	473
PB Run 3-1	1078	520	70	34	927	447
PB Run 3-2	826	392	74	35	895	425
WPB Run 1-1	224	106	54	26	478	227
WPB Run 1-2	185	88	54	26	492	233
WPB Run 2-1	99	47	60	28	555	263
WPB Run 2-2	76	36	59	28	553	262
WPB Run 3-1	28	13	53	25	447	212
WPB Run 3-2	153	73	40	19	356	169

The conversion from ppm to mg/MJ is based on the calculation of the flue gas mass per unit mass of pellets burned[146] using the following equation

$$W_{\mathrm{g}} = \left(C_{\mathrm{b}} + \frac{12C_{\mathrm{s}}}{32}\right) \times \left(\frac{44[\mathrm{CO_2}] + 32[\mathrm{O_2}] + 28[\mathrm{N_2}] + 28[\mathrm{CO}]}{[12([\mathrm{CO_2}] + [\mathrm{CO}])]}\right) \quad (3\text{-}27)$$

where W_{g} is the flue gas mass in kg/kg pellets burned; C_{b} and C_{s} are fuel carbon and sulfur content in fractions, respectively; [CO_2], [O_2], [N_2] and [CO] are gas concentrations expressed in %. [N_2] is determined by subtracting [CO_2], [O_2], and [CO] from 100%.

Based on Table 3-9, CO emissions ranged from 383 to 930 mg/MJ and from 28 to 224 mg/MJ for PB and WPB, respectively. The relatively high CO emission indicates high efficiency loss during pellet combustion.[147] CO emission ranged from 192 to 547 mg/MJ was reported by Win et al.[148] for a 20 kW residential wood pellet boiler. A

relatively constant CO concentration of 200 mg/m^3 (about 160 ppm) was observed by Olsson and Kjällstrand[147] when a 30 kW ecolabelled residential boiler was at full flaming combustion condition. The WPB showed relatively low emissions while the combustion conditions in PB needs to be optimized for minimum CO emission. NO_x and SO_2 emissions have an average of 39 ± 1 mg/MJ and 455 ± 9 μg/MJ for PB and 25 ± 1 mg/MJ and 228 ± 14 μg/MJ for WPB, respectively. The relatively low emissions of NO_x and SO_2 from WPB suggests that pellets used in WPB had lower fuel bound nitrogen and sulfur contents. Compared to most other studies[101,108,148,149], NO_x and SO_2 emissions from this boiler operation are low, indicating lower combustion temperature of the boiler minimizing the formation of NO_x, as wood as a fuel has roughly constant fuel bound nitrogen and sulfur content.[150]

3.6.3 $PM_{2.5}$ Emission

Studies have shown that wood pellet combustion particulate matter (PM) emissions are dominated by particles with aerodynamic diameter of less than 2.5 μm ($PM_{2.5}$).[102,151,152] The SEM (scanning electron microscope) picture of the filter loading is shown in Figure 3-44. The morphology and size distribution of the particles can be clearly observed. The white dots can be clearly seen and EDS (energy dispersive spectroscopy) analysis indicates they are mostly K and Na.

The average $PM_{2.5}$ emission determined is 40 ± 2 mg/m^3 (at 25 °C, 1 atm and 10% O_2) (or 19 ± 1.3 mg/MJ, or 0.044 ± 0.003 lb/MMBtu) which is lower than most similar studies.[91,101,153,154] This result reflects the nature of the pellets used in this study that have very low ash content.[103,155] A typical particle size distribution during the experiment is shown in Figure 3-45.

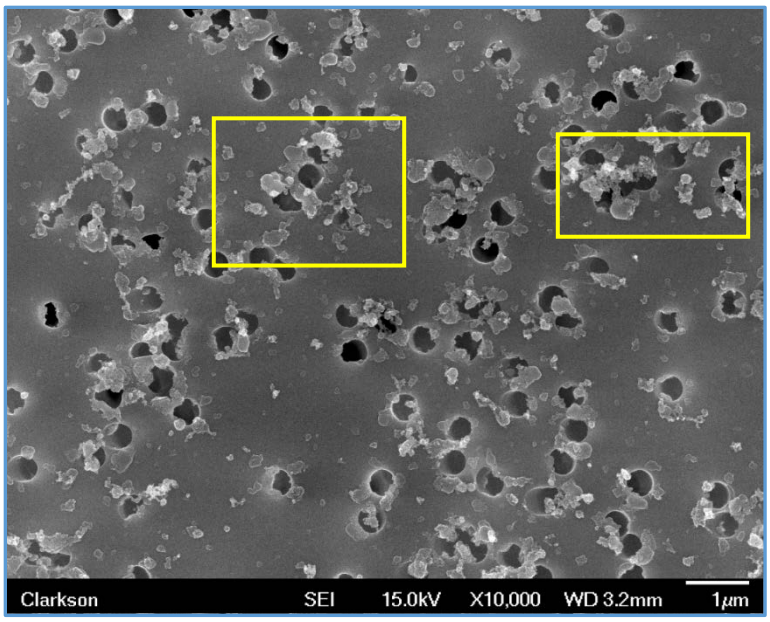

Figure 3-44. SEM image of fine particle emissions from wood pellet combustion with particle clusters marked

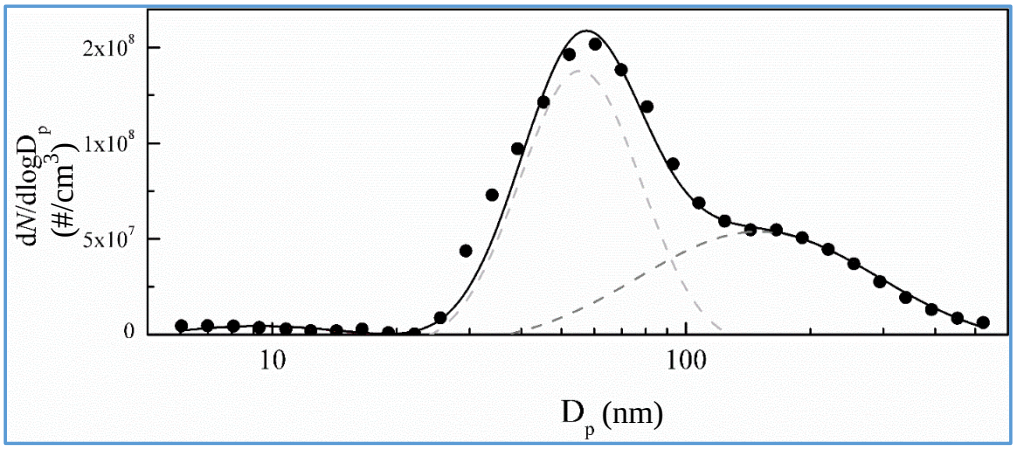

Figure 3-45. A typical particle size distribution of stack sampling with log-normal fitting to the data at PB

Two distinct modes can be observed: the major peak is at 50 to 60 nm and the minor peak is at 120 to 150 nm. Those peaks are fitted using log-normal distributions. Other studies have reported similar results for the major peak [91, 156] and the minor peak.[107,157] Figure 3-45 indicates that $PM_{2.5}$ emission from wood pellet combustion are

dominated by ultrafine particles (particle size less than 100 nm). Particle number concentrations are also in the range reported by other studies.[91,102,151,152]

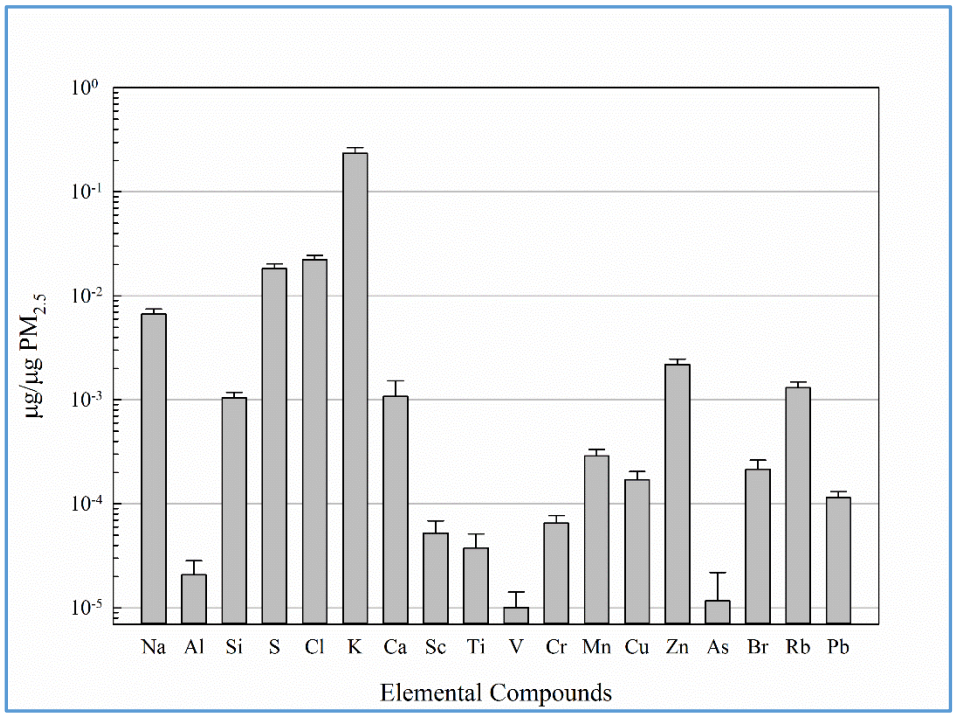

Figure 3-46. Inorganic elemental components in $PM_{2.5}$ emission from wood pellet boiler

Figure 3-46 shows the inorganic elemental compositions of $PM_{2.5}$ emissions. All of the analyzed elements account for 31.5 ± 3.8 % of the total $PM_{2.5}$ mass. Hedberg et al. [158] reported that the elemental composition of $PM_{2.5}$ emissions from birch wood combustion in a wood stove that the sum of all of the elements accounts for only 5% of total $PM_{2.5}$ mass with emissions of 60 mg/kg wood burned. The high fraction of inorganic components in the $PM_{2.5}$ emissions in the present study indicating higher combustion efficiency of this wood pellet boiler compared to wood stoves. Other studies have shown that complete combustion of wood pellets produce inorganic ash particles with sphere-

like shape of diameter between 50 and 125 nm,[159] which is in consistent with the size distribution shown in Figure 3-46.

As expected, high concentrations of Na, Si, K, and Ca are observed because they are major ash-forming elements.[160] K alone accounts for 80% of the total elements. K is the major element to form alkali compounds such as K_2O, K_2SO_4, KCl, and K_2CO_3 in the emitted $PM_{2.5}$ particles,[102] and this is the reason why K is often used as a marker for wood smoke.[161] Mg and P were found below detection limit, although they were reported by other studies.[91, 162] Fe was also found below detection limit (high blank levels) although it is most commonly found in wood combustion emissions.[91,158,160] Zn and Rb were found as the most abundant metals with atomic number larger than 20, which is in consistent with previous study showing fairly high levels of Zn and Rb found in northeastern United States tree species.[163]

The sum of the atomic number >20 elements account for 0.85% of total $PM_{2.5}$ mass and Zn accounts for 45% of the total heavy metals. The heavy metals tend to concentrate in the fly ash rather than the bottom ash.[164] Studies have shown that due to the high fraction of inorganic compounds in the PM emissions from complete combustion of wood, the toxicity level of those PM emissions are significantly higher.[165] Thus, proper control should be applied to reduce the $PM_{2.5}$ emissions.

3.6.4 Organics Emissions

A total of 71 organic compounds (from both particulate and gaseous phases) were analyzed. Categorized organics emissions are shown in Figure 3-47 with similar categorizations have been reported by other researchers.[91,166]

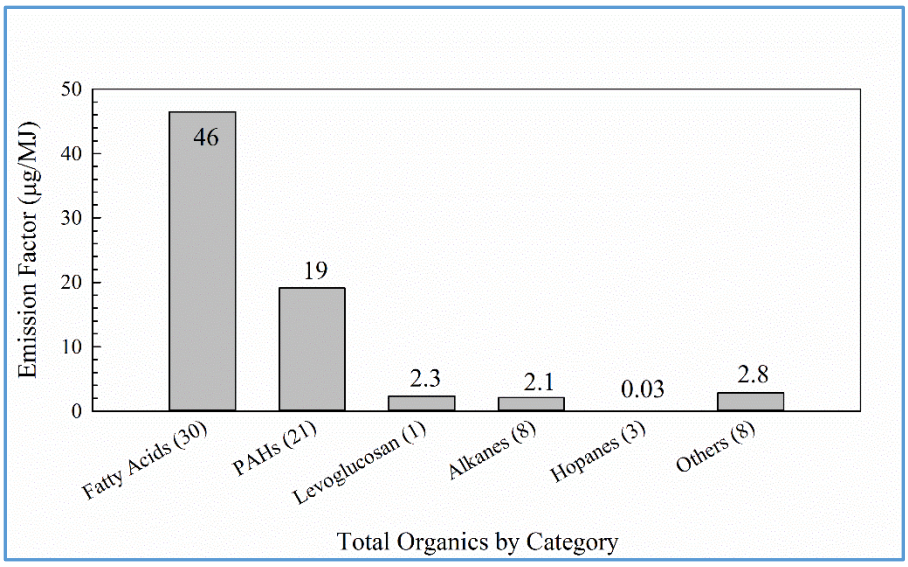

Figure 3-47. Total organic emissions by different categories

High concentrations of fatty acids (such as octadecenoic acid, octadecanoic acid, and hexadecanoic acid) were observed, consistent with reported emissions from wood stove combustion of prevalent United States tree species[167] and similar research.[162,166] Figure 3-47 shows that the total emission rate of fatty acids was 46.5 µg/MJ and the total emission rate of PAHs was 19.1 µg/MJ. PAHs are likely to bound into particles, which increases the toxicity of particle emissions because some PAHs are carcinogens.[168,169]

The alkane emission rate was 2.1 µg/MJ. Levoglucosan is commonly used as a tracer for biomass burning[170,171,172] and the emission rate was 2.3 µg/MJ. Hopanes have a low emission rate, determined to be 33 ng/MJ. Studies have shown that hopanes are ubiquitously present in crude oil[173] and are often used as petroleum biomarker.[174]

3.7 TES Tank Analysis

The existence of TES tanks in a wood pellet heating system isolates the heat source, – the boiler, from the heat sink, – the building so that the boiler heats the TES tank and the TES tank stores and heats the building. This separation improves system efficiency by allowing the boiler to run at maximum load for a cycle rather than continuously running at a reduced load.

3.7.1 TES Tank Operation

As discussed before, the boiler is controlled by two temperature sensors inserted into the top (ON) and bottom (OFF) of the tank. There are two distinctive stages for the operation of a TES tank, the charge and discharge stages, as shown in Figure 3-48.

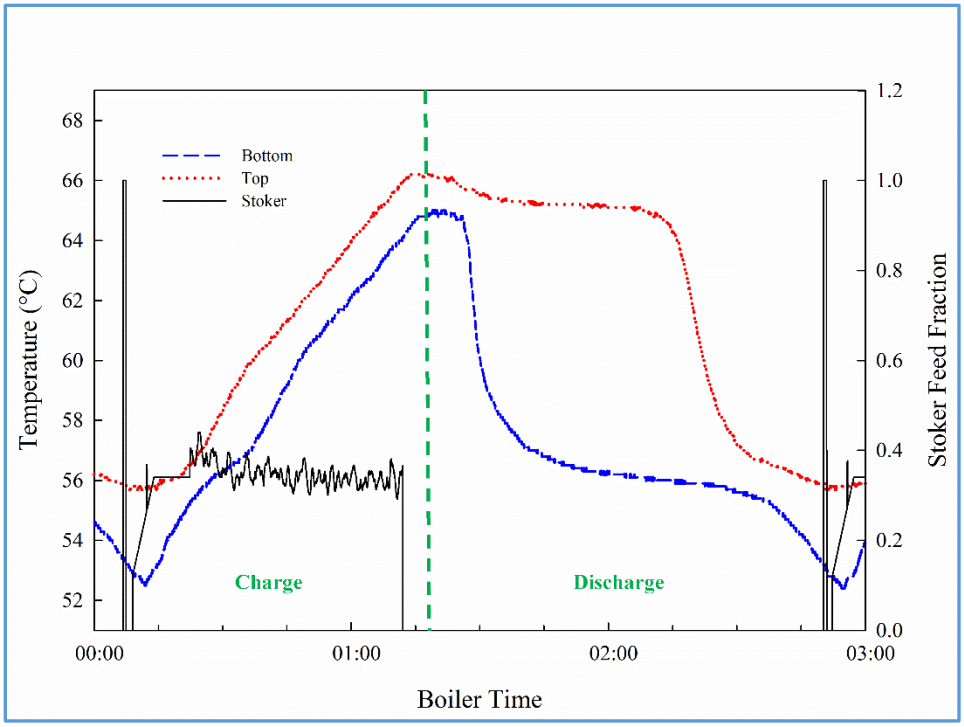

Figure 3-48. TES tank charge and discharge operation with temperature distribution (data from PB-1)

The stoker line represents the status of the boiler. The red and blue lines are the temperatures at the top and bottom of the boiler. In Figure 3-48, the ON/OFF set temperatures were 56 ℃/64 ℃. In the charge stage, the boiler heats the tank to a uniform temperature of 64 ℃ and then shuts down. The top and bottom temperature difference is at minimum at the end of boiler cycle, as indicated by the green dash line in Figure 3-48. Because the TES tank continuously supplies heat to the building even when the boiler is running, a temperature difference of 0 cannot always be achieved. In the discharge stage, the TES tank alone supplies heat to the building to satisfy the demand. Hot water flows into the building from the top of the tank and colder water returns into the tank from the bottom. The bottom of the tank temperature drops and a thermal stratification develops. As the thermocline moves up and the top temperature drops below 56 ℃, the boiler starts a new cycle.

The heat delivered can be used directly for space heating or used as the heat source for a domestic hot water (DHW) tank, as shown in Figure 3-8 for the WPB heating system.

3.7.2 TES Tank Stratification

Thermal stratification is induced by the temperature difference between TES tank supply and return water temperatures since the colder water will remain in the bottom of the tank due to its higher density. Two temperature differences exist: the TES tank supply and return water temperature difference $\Delta T_{S/R}$ and the temperature difference between the top and bottom of the TES tank ΔT_{TES}. Figure 3-49 shows ΔT_{TES} distribution for PB heating system during two normal operational days in comparison with stoker feed.

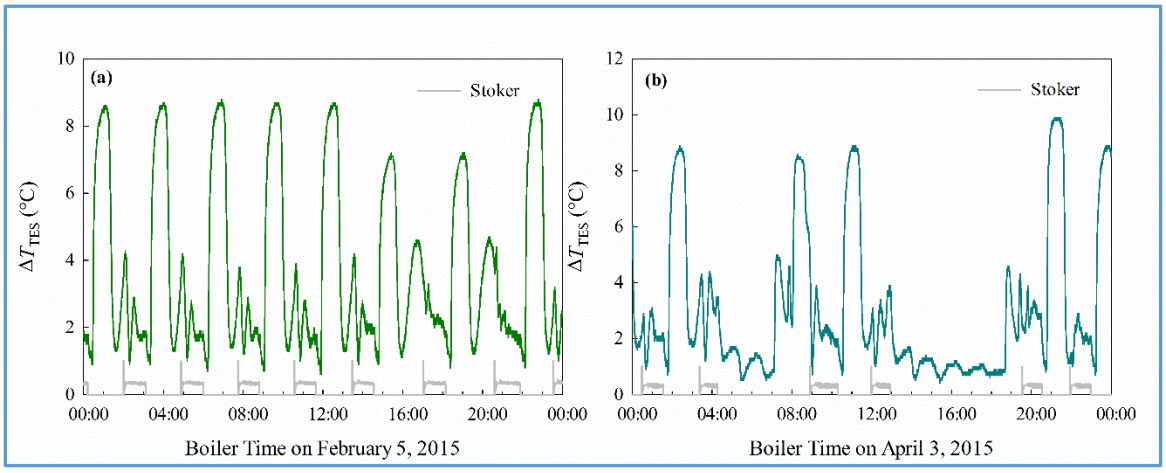

Figure 3-49. Temperature difference inside the TES tank during a normal day operation (data from PB-1)

High ΔT_{TES} occurs when there is a high heat demand from the building resulting in high $\Delta T_{S/R}$. In Figure 3-49 (a), when outdoor temperature is low and the heat demand from the building is constantly at a high level, the highest ΔT_{TES} will occur at the end of each boiler cycle. However, when the outdoor temperature increases, the heat demand from the building decreases, low ΔT_{TES} values will occur, as shown in Figure 3-49 (b).

Figure 3-50 shows the distribution of ΔT_{TES} for the different systems by heating season. In general, there was a low level of stratification for the PB system. The WPB shows improved stratification with a higher ΔT_{TES} while the LGB system has the highest level of stratification because the LGB system has the highest thermal mass relative to the heat demand producing very large $\Delta T_{S/R}$.

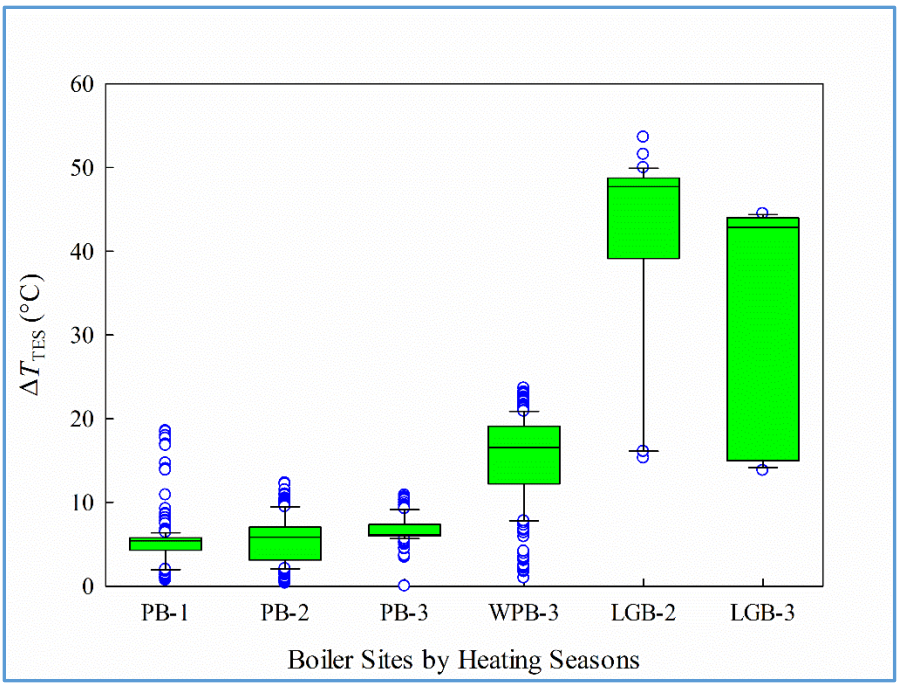

Figure 3-50. Comparison of ΔT_{TES} at different boiler sites among different heating seasons

Compared to the PB system, the WPB system has a higher because unlike PB, where the main circulator is running constantly (except for PB-3), the WPB system calls for heat in a short time period with high heat demands (also for the LGB system). A comparison of the two different types of heat demand is shown in Figure 3-51. The PB system heat demand is a constant low demand while the WPB system is a short time spike demand capable of creating large $\Delta T_{S/R}$. Thus, the WPB system is better for creating high stratification inside TES tank. The spike in Figure 3-51 for PB-3 could be caused by door opening when the home owner returned back home from work, as the average outdoor temperature was -10 °C on that day.

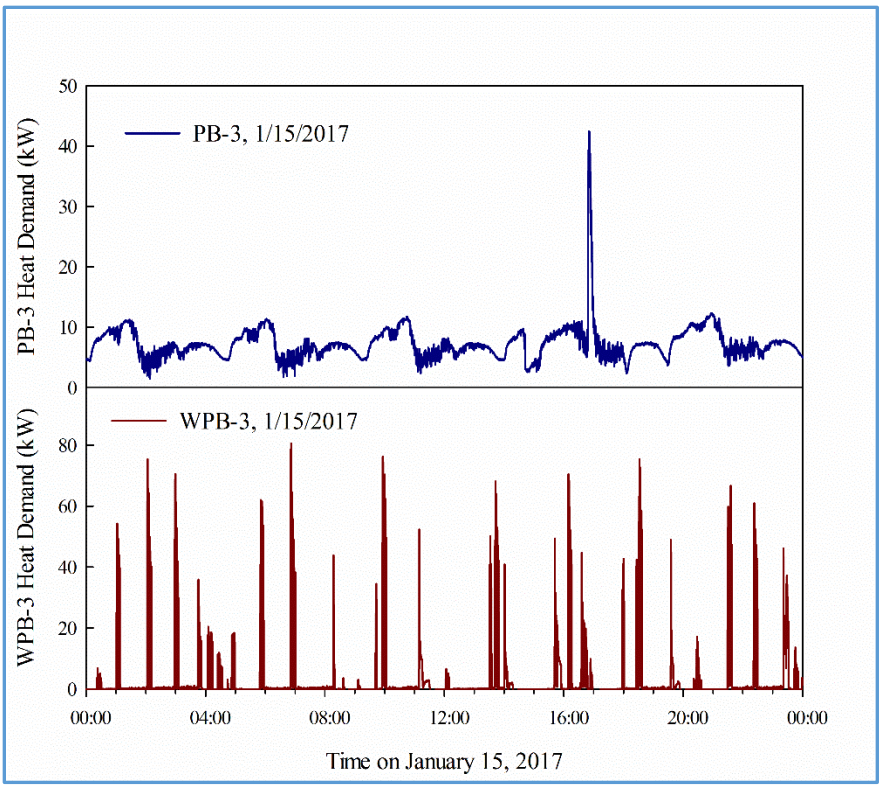

Figure 3-51. Comparison of two different types of building heating demand profile

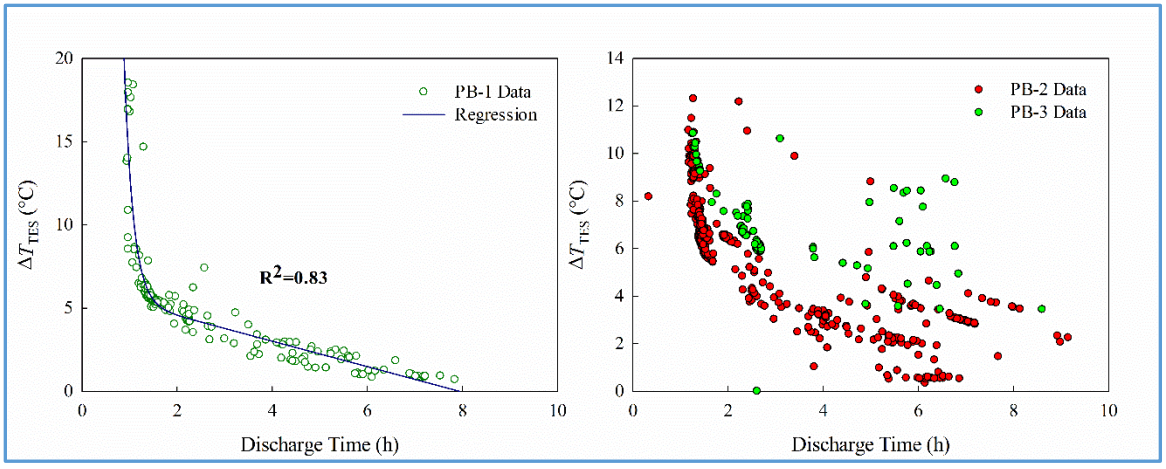

Figure 3-52. TES tank stratification as a function of discharge time

Figure 3-52 shows ΔT_{TES} as a function of discharge time (or cycle OFF time) for the PB system. No such relationship was observed at WPB, which is probably due to the

operation of DHW that interrupts with TES tank stratification. It can be seen that longer discharge times lead to smaller ΔT_{TES}. This result is because lower building heat demand resulting in longer discharge times and vice versa. A high correlation was observed for PB-1 but not for PB-2 and PB-3. This result is because a constant TES tank ON/OFF temperature setting was used over the heating season but in PB-2 and PB-3, a variety of TES tank ON/OFF temperature settings were tried that destroyed the correlation. PB-2 and PB-3 still follow the same trend as PB-1. The correlation equation for PB-1 data is

$$\Delta T_{\mathrm{TES}} = 6.07 + 1472\exp(-5.23t_d) - 0.77t_d \tag{3-28}$$

where t_{d} is TES tank discharge time (or cycle OFF time) in h. Therefore, no stratification will form when t_{d} = 8 h.

3.7.3 Thermocline Analysis

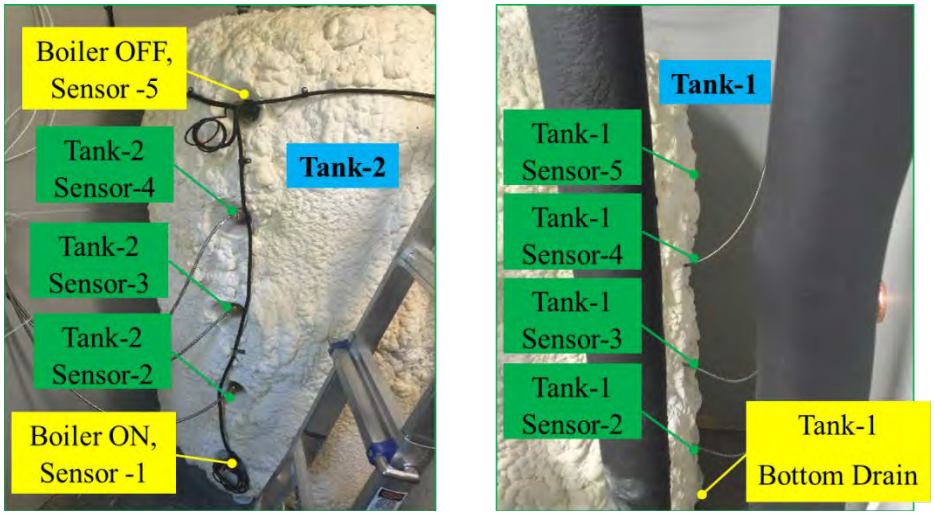

Figure 3-53. Vertical temperature sensor positioning in TES tanks at LGB site

In order to know the detailed temperature distribution in the TES tank, a total of 9 temperature sensors were installed vertically in the two TES tanks in the LGB system, as

shown in Figure 3-53. The 5 temperatures from tank-2 will be used for analysis with ON/OFF setting at 40.6/76.7 °C.

This TES tank has a total volume of 210 gallons (0.79 m^3) with diameter of 81.3 cm (32 inch) and height of 152.4 cm (60 inch). The 5 temperature sensors are located at 6 inch (T-1), 18 inch (T-2), 30 inch (T-3), 42 inch (T-4) and 54 inch (T-5) from the bottom of the tank. The supply and return ports are located at 6 inch away from top and bottom of the tank with diameter of 7.78 cm (or 3.063 inch) (same height as T-5 and T-1).

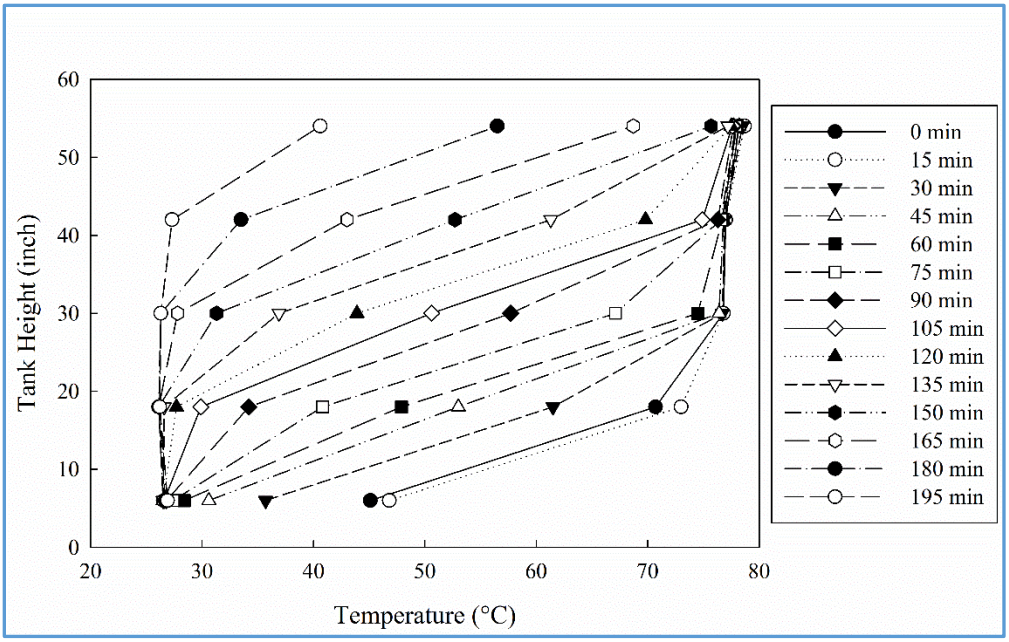

Figure 3-54. Temperature distribution along vertical height of the tank with evolving time

Figure 3-54 shows the temperature distribution inside tank-2 of the LGB system over a typical discharge time. At the end of previous boiler cycle (0 min), a thermocline has already built up within the tank due to heat demand from the building when the boiler is firing. The thermocline moves to about 18 inch from the bottom (T-2 position) with the top half of the tank at a relatively uniform temperature around 77 °C for T-3, T-4 and T-5.

After 60 minutes, the top of the thermocline reaches 30 inches high and T-3 drops to 74.5 °C. After 105 minutes, T-4 drops by 1 °C to 74.9 °C. T-5 starts to drop at 150 minutes from 77 °C to 76 °C. After 165 minutes, the bottom half of the tank reaches a uniform temperature around 27 °C.

At 105 minute mark, the tank is divided into three zones: bottom cold zone, middle thermocline zone and top hot zone. T-2 and T-4 are located at the bottom and top of the thermocline indicating the thermocline has grown to at least 24 inch (or 60.96 cm) thick, which is over 1/3 of the total tank height. The large portion of thermocline with respect to tank height indicates high level of mixing during tank operation. Therefore, proper measures such as adding inlet diffuser or baffles shall be considered to minimize the mixing and hence decrease the thickness of the thermocline.

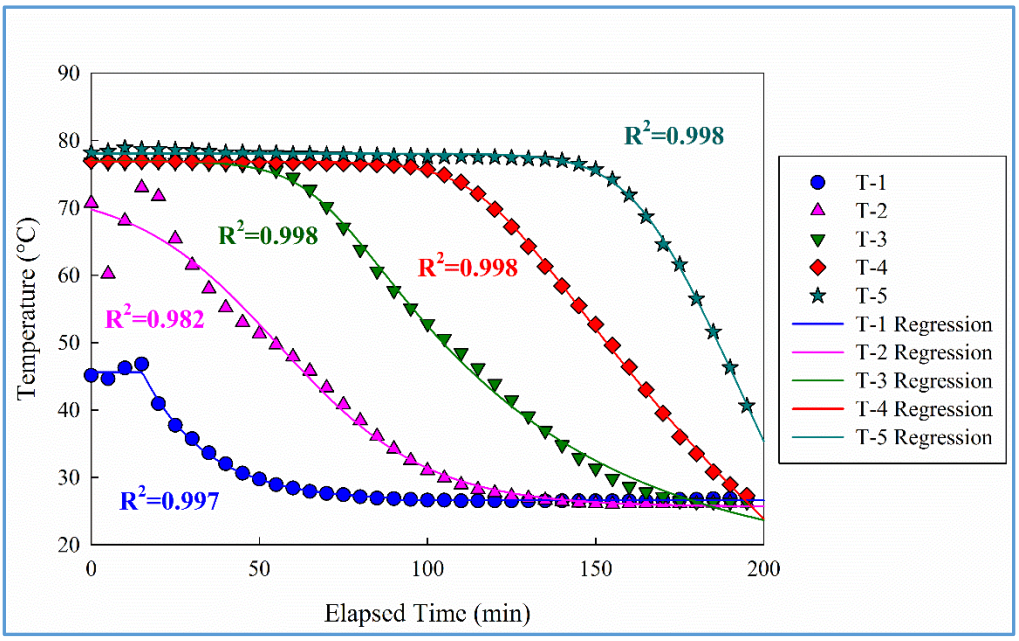

Figure 3-55. Temperature change at 5 vertical positions of the tank during discharge

Figure 3-55 shows the temperature change at the five sensor locations with discharge time. Perfect sigmoid shape of correlation were found for all five temperature curves. The sigmoid correlation is a 5 parameter equation with the general formulation as shown below and detailed results listed in Table 3-10.

$$y = y_0 + \frac{a}{\left[1 + e^{-\left(\frac{x-x_0}{b}\right)}\right]^c} \tag{3-29}$$

Table 3-10. Sigmoid function correlation for the temperatures change with time during TES tank discharge for each sensor location

y	a	b	c	x_0	y_0	R^2
T-1	19.04	-0.1055	0.0055	15.13	26.57	0.9973
T-2	47.46	21.59	0.9605	55.00	25.61	0.9817
T-3	60.16	-9.533	0.1580	68.86	16.80	0.9982
T-4	124.6	-10.24	0.0686	117.3	-47.77	0.9995
T-5	355.5	-10.10	0.0360	164.4	-277.4	0.9985

From Figure 3-55, it takes about 130 minutes (from x = 15minutes to x = 145minutes) for the thermocline to move from T-1 to T-5 (a total of 48 inches). Therefore, an average speed of 0.37 inch/minute (or 0.94 cm/min) can be calculated based on current heat demand and pump speed in the LGB system. Thermocline movement speed is an indicator of TES tank flow rate and the degree of mixing inside the tank.

3.7.4 TES Tank Efficiency

TES tank efficiency is calculated based on energy input and energy output and therefore two types of tank efficiency can be defined: the overall efficiency (φ_{Ove}) and discharge efficiency (φ_{Dis}).

$$\varphi_{\mathrm{Ove}} = \frac{E_{\mathrm{Cha}} + E_{\mathrm{Dis}}}{B_{\mathrm{Tot}}} \times 100\% \tag{3-30}$$

$$\varphi_{\mathrm{Dis}} = \frac{E_{\mathrm{Dis}}}{B_{\mathrm{Tot}} - E_{\mathrm{Cha}}} \times 100\% \tag{3-31}$$

where B_{Tot} is the total energy output from the boiler into the TES tank; E_{Cha} and E_{Dis} are energy delivered to the building during boiler charge and discharge stages, respectively. Due to the existence of TES tank stratification, both φ_{Ove} and φ_{Dis} are possible to have values larger than 100% because the stored energy of the TES tank is not considered in the above definitions.

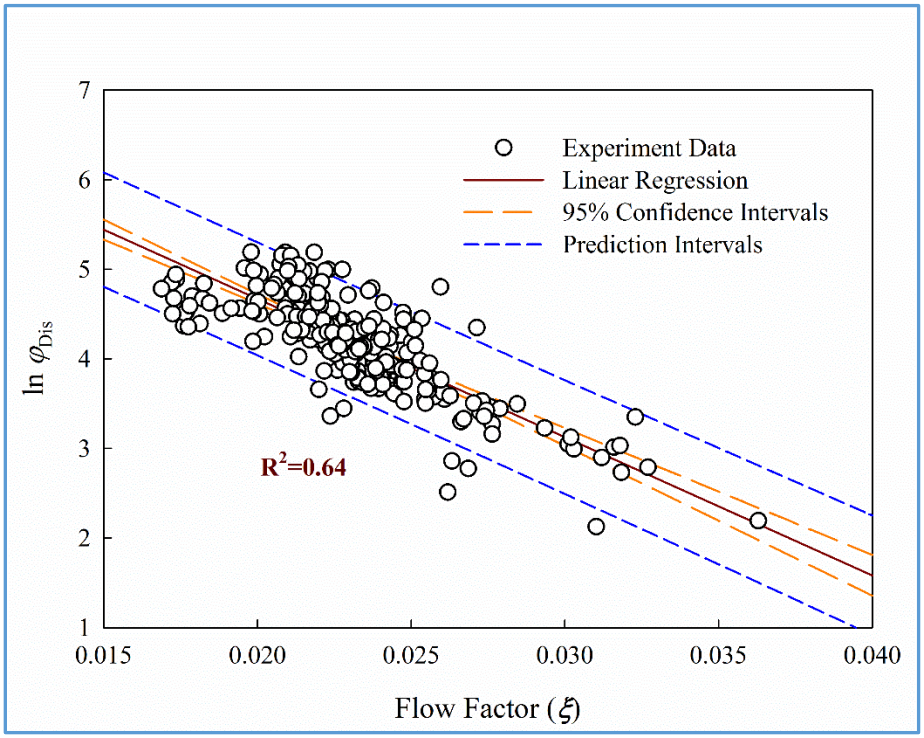

Figure 3-56. TES tank discharge efficiency correlated with dimensionless flow factor at PB-1

φ_{Dis} is a good indicator of the stratification inside the tank when the boiler is OFF. Previous discussions (section 2.3.3) have shown that a lot of factors contribute to the stratification of the tank. The present evaluation will focus on the operation conditions as

a fixed geometrical tank was installed at each site. Figure 3-56 shows the correlation of φ_{Dis} with a dimensionless number ξ in the following equation

$$\ln \varphi_{\mathrm{Dis}} = 7.76 - 154.41\xi \tag{3-32}$$

where φ_{Dis} is in % and ξ is expressed in pipe Reynolds number ($\mathrm{Re_d}$) and temperature differences as

$$\xi = \left(\frac{\Delta T_{\mathrm{TES}}}{\Delta T_{\mathrm{S/R}}}\right)^{0.35} (\mathrm{Re_d})^{-0.41} \tag{3-33}$$

where ΔT_{TES} is the average TES tank top and bottom temperature difference during discharge period and $\Delta T_{\mathrm{S/R}}$ is the average TES tank supply and return temperature difference during the same discharge period. Figure 3-56 indicates that increases in $\mathrm{Re_d}$ and decrease in the ratio of $\Delta T_{\mathrm{TES}}/\Delta T_{\mathrm{S/R}}$ will lead to exponential increase in tank discharge efficiency. For a specific TES tank, increase of $\mathrm{Re_d}$ means an increase of the flow rate, which corresponds with previous studies that the TES tank discharge efficiency (or extraction efficiency) increases with increasing flow rate.[118175,176] Thus, inlet flow diffusers and baffles[122,175,177] are used to minimize flow mixing and maintain a high level of stratification. The ratio of $\Delta T_{\mathrm{TES}}/\Delta T_{\mathrm{S/R}}$ is an indicator of the amount of heat delivered to the building. The maximum value of $\Delta T_{\mathrm{TES}}/\Delta T_{\mathrm{S/R}}$ is 1 when there is no heat delivered to the building. Small ratios of $\Delta T_{\mathrm{TES}}/\Delta T_{\mathrm{S/R}}$ suggest large TES tank supply and return temperature differences, which further indicates large amount of heat consumed by the building.

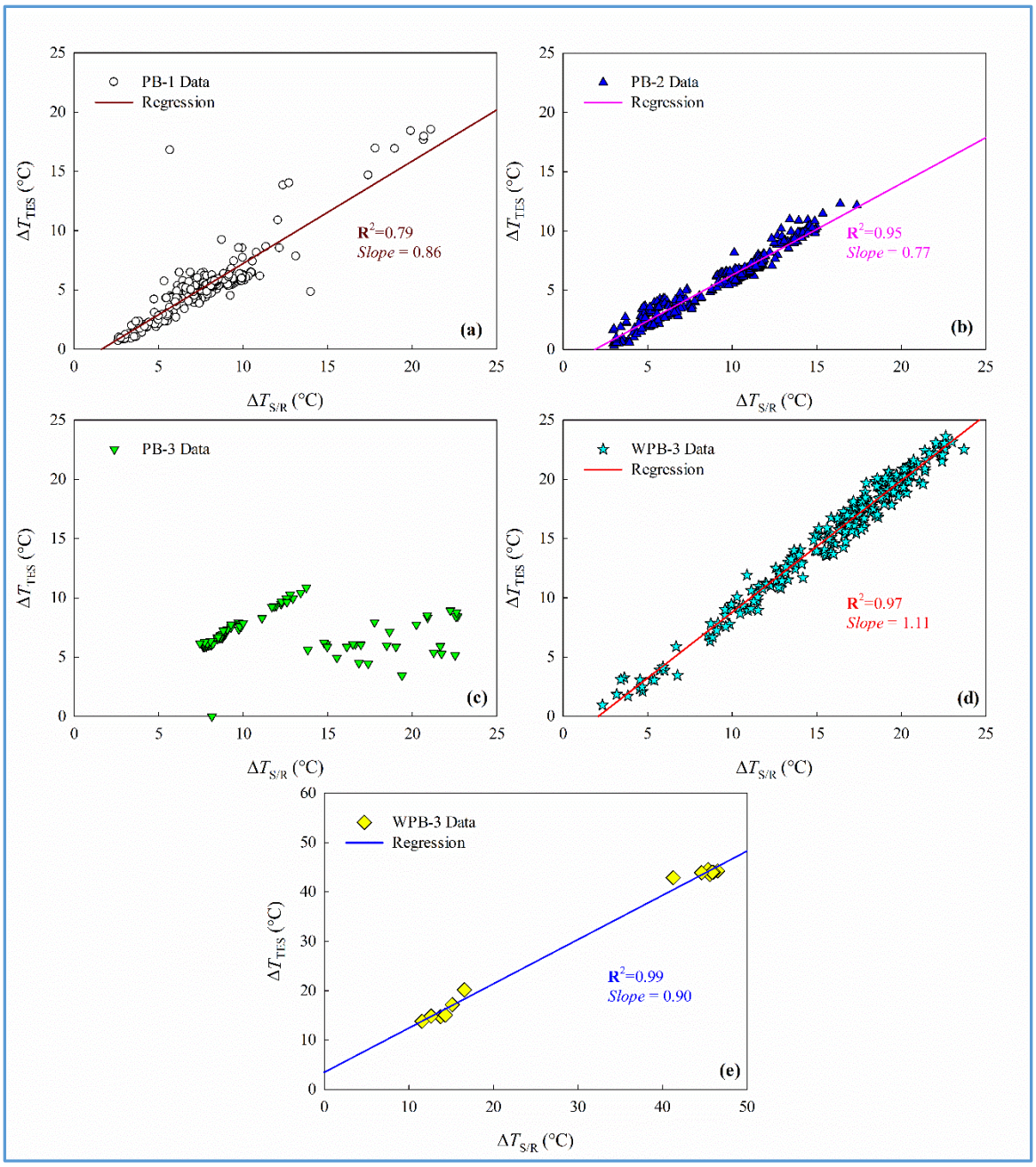

Figure 3-57. ΔT_{TES} correlates with $\Delta T_{S/R}$ for PB, WPB and LGB systems by heating seasons

. Figure 3-57 shows the correlation between ΔT_{TES} and $\Delta T_{S/R}$ for the three boilers in different heating seasons. For PB and LGB, regression slopes are all less than 1, which means the average return water temperature from the building is lower than the TES tank

bottom temperature for most of the time. For WPB, the regression slope is higher than 1, which means the average return water temperature is higher than the TES tank bottom temperature. This phenomenon could be caused by the simultaneous operation of boiler and building heat demand, as indicated by Figure 3-8, that the low thermal mass of WPB heating system cannot dissipate all the heat from the boiler, resulting higher return temperature into the bottom of the tank.

Therefore, low slope values indicate that the TES tank return water temperature is lower than the TES tank bottom temperature, which is helpful for maintaining the stratification.

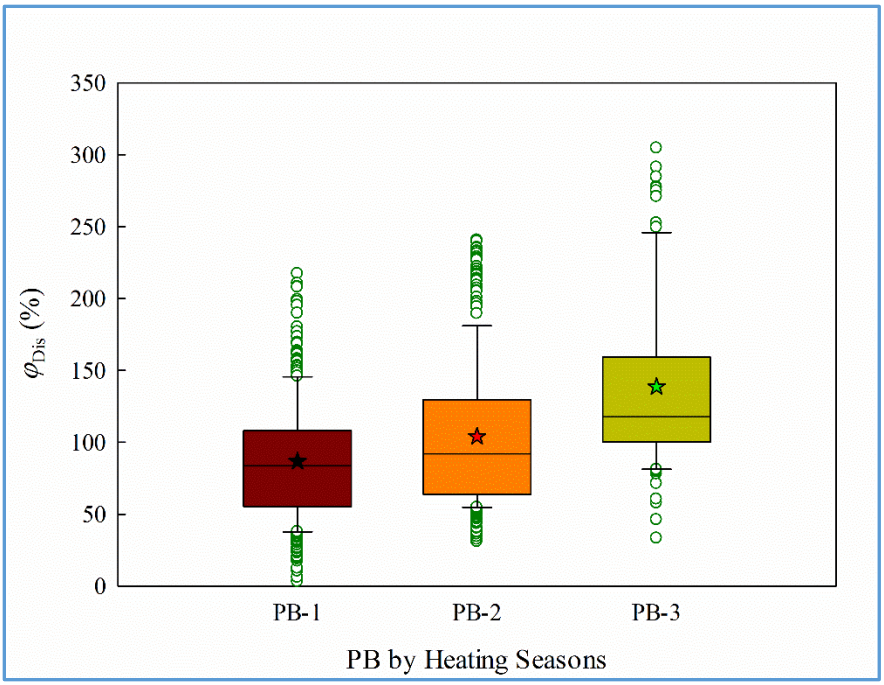

Figure 3-58. TES tank discharge efficiency distribution for the three boilers in different heating seasons (average values are marked by the star)

Figure 3-58 shows the TES tank discharge efficiency for PB by heating seasons. Due to different pipings, TES tank discharge efficiency at WPB and LGB are not able to

be calculated based on current data monitoring plan because the amount of heat delivered into the TES tank cannot be isolated.

Due to the low level of stratification in TES tank, PB-1 has the lowest average TES tank efficiency of 86.6%. The situation improved in PB-2 when a wide range of boiler ON/OFF settings were applied, which increased the stratification of TES tank. In PB-3, the addition of a 3-way actuator (as shown in Figure 3-3) that separates the TES tank from the constant circulation loop when there is no call for heat significantly improved the TES tank performance by allowing the TES tank to develop a high level of stratification.

3.8 System Efficiency

System efficiency (η_{sys}) was calculated as the total heat delivered to the building divided by the total heat input to the boiler (pellet consumption) on a daily basis.

$$\eta_{sys} = \frac{\sum_{i=1}^{n}(E_{Dis}|_i + E_{Cha}|_i)}{P \cdot GCV} \times 100\% \quad (3\text{-}34)$$

where P is pellet consumption rate (kg/d), $E_{Dis}|_{©}$ and $E_{Cha}|_{©}$ are heat delivered to the building during boiler OFF and ON time, n is total number of boiler cycles per day. System efficiency looks at the heating system from the beginning and the end. In ideal situation without heat loss, η_{sys} can be expressed as

$$\eta_{sys} = \eta_{com} \cdot \eta_{th} \cdot \varphi_{Ove} \quad (3\text{-}35)$$

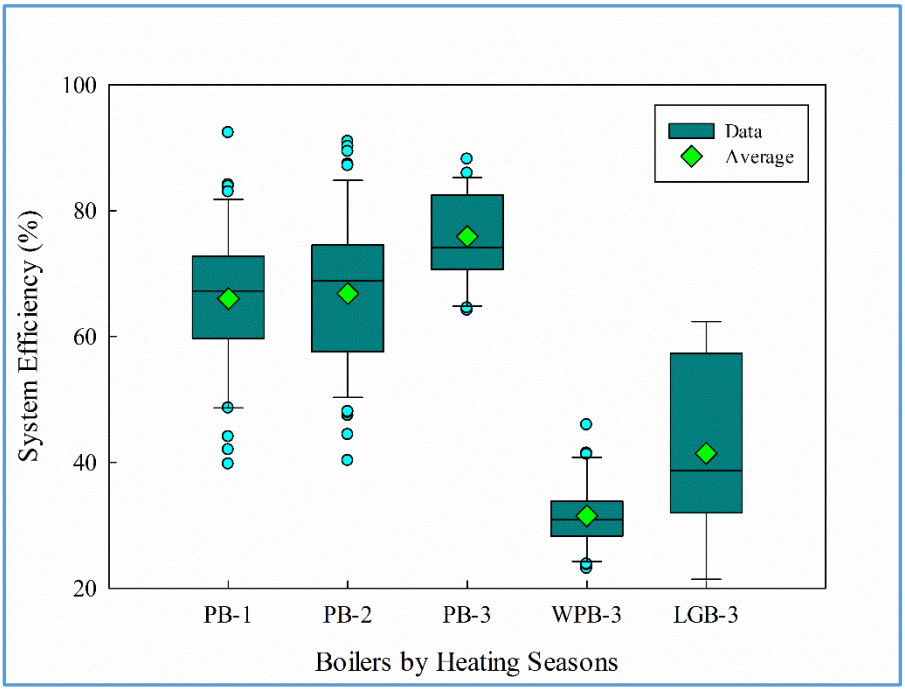

Figure 3-59. System efficiency for three boilers in different heating seasons

Figure 3-59 shows the system efficiency distribution of the three boilers in different heating seasons (no LGB-2 data available for TES tank output calculation). PB-1 and PB-2 were very close with average system efficiency of 66% and 67%. However, PB-3 was improved with average system efficiency of 76%. The improvement was due to the adding of 3-way actuator that allows the TES tank to be isolated from the constant circulation loop when there is no call for heat from the building, as shown in Figure 3-3. Both WPB and LGB showed low system efficiencies, which was probably due to the fact that 2-pipe configuration cannot form two isolated loops like 4-pipe configuration when the boiler is firing and the building is call for heat at the same time. Thus, the delivered heat in 2-pipe configuration system is actually larger than measured. The rational for the 2-pipe configuration is that it is a combination of two types of heating: when the boiler is ON and the building is calling for heat, the boiler heats the building; when the boiler is OFF and the TES tank heats the building.

Chapter 4. Process Dynamic Simulation and Optimization

4.1 TES Tank Sizing

TES tanks are needed in modern residential space heating systems to provide the benefits discussed in previous sections. An undersized TES tank will only behave like a large pipe that will cause boiler short-cycling because of the complete mixing of the tank. An oversized TES tank can significantly increase the initial capital cost as well as increasing heat loss from the tank. Therefore, sizing of TES tanks is very important for optimal system performance.

Currently, no scientifically based sizing techniques exist either in the United States or the European Union to correctly size TES tanks with respect to boiler output capacity and different types of building heat demands. The United Kingdom Corporation Homemicro made a concise summary on some of the current TES tank sizing information.[178] Two typical TES tank sizing methods are:

(1). *Boiler output load based sizing*: utilizes a recommended value of TES tank volume per kW of boiler output load. For example, a typical value for biomass heating system is 10 L/kW (in many cases, 20 L/kW).[178] Renewable Heat NY recommends 2 gallons per 1000 Btu/h storage,[179] which is 25.8 L/kW. Large differences exist between recommendations made by different organizations.

(2). *Boiler cycle time based sizing*: by giving a minimum boiler cycling time, the total volume of TES tank can be determined through equation (3-4).

Different systems vary a lot. Therefore, a systematic sizing technique should be built to improve TES tank sizing as part of the overall system design.

4.2 Process Simulation

Virtual Materials Group (VMG) developed a process simulator, VMGSim, which is capable of real time dynamic process simulation. The most recent version, VMGSim v9.5, was used in this research to simulate wood pellet heating systems. The objective of the simulation was to size the TES tank with respect to different boiler nominal output capacities and different thermal mass of the heat demand units.

4.2.1 Model Construction

Figure 4-1 shows the flow sheet of the wood pellet heating system process simulation. A detailed step-by-step simulation is provided in the Appendix.

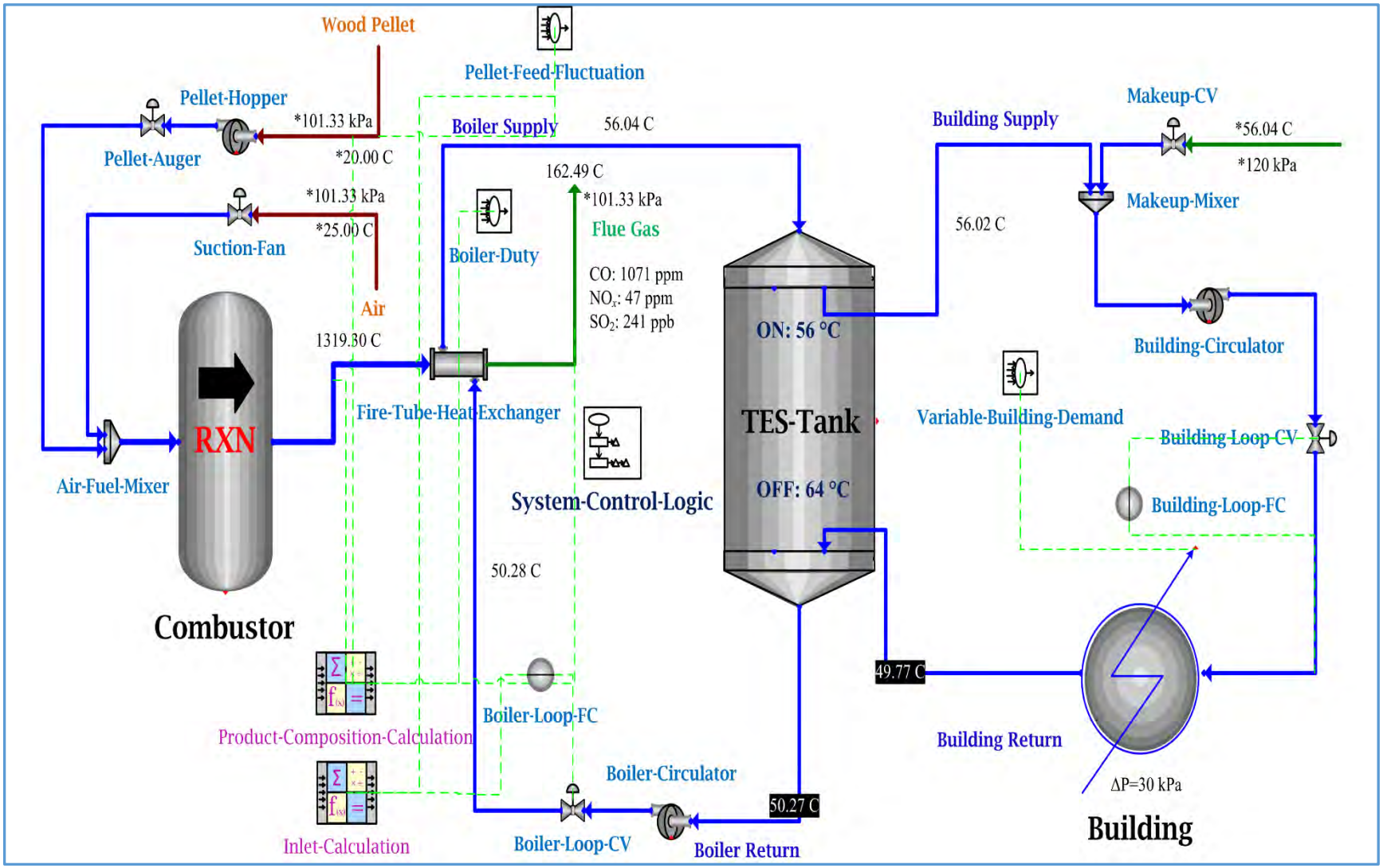

Figure 4-1. Flow sheet of wood pellet heating system process simulation

There are three components in this model: the boiler, the TES tank, and the building heat demand. The following sections will discuss each stage of the model in detail. The thermodynamic model selected is the gasification model with a simple solid phase model included. Model and property package selection details are shown in Figure 4-2.

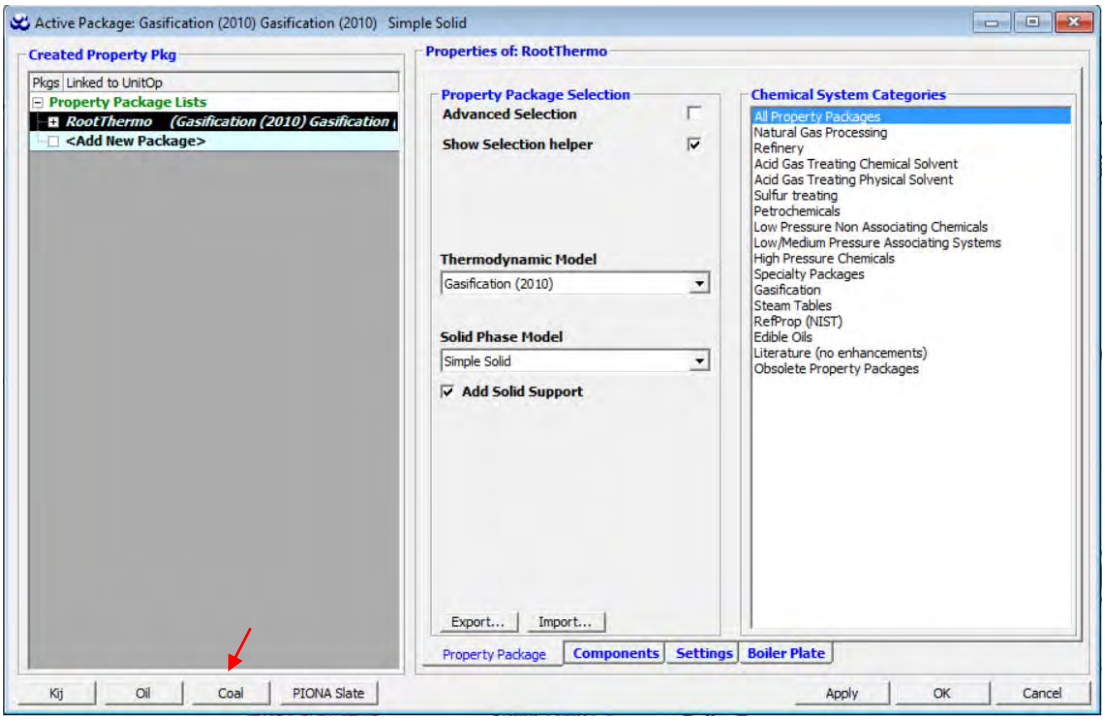

Figure 4-2. Thermodynamic model and property package selection

4.2.1.1 Components Specification

Wood pellet fuel was defined by treating the fuel as coal (as marked by the arrow in Figure 4-2) and characterizing the elemental compositions based on existing wood pellet fuel characterization data including elemental composition, moisture content, and ash content. The ash composition was characterized by adding oxides of major ash-forming elements as discussed in the $PM_{2.5}$ composition analysis in Chapter 3. Specifically, four oxides are included: CaO, K_2O, Na_2O, and SiO_2. An estimated

molecular weight of 10,000 was used. Table 4-1 lists the elemental compositions of wood pellets defined in this model. The estimated GCV using the listed compositions was 19.26 MJ/kg, which is 0.7% higher than the measured GCV listed in Table 3-6. After defining all the elements, the wood pellet fuel is characterized and installed.

Table 4-1. List of components in wood pellet fuel characterization (total: 100%)

Component	Mass Fraction (%)	Component	Mass Fraction (%)
C	46.64	N	0.14
CaO	0.018	Na_2O	0.08
Cl	0.004	O	46.23
H	6.4	S	0.007
K_2O	0.464	SiO_2	0.018

Other pure components such as H_2O, O_2, N_2, CO, CO_2 etc. were added through the software database. A hypothetical compound called "Volatile", an intermediate gasification product, was defined using molecular formula $C_{1.9316}H_{5.7546}O_{2.3751}$ based on Chaney et al.[180] and Zhang et al.[181] Benzene (C_6H_6) was also added to represent liquid tar emissions from wood pellet combustion.

4.2.1.2 Wood Pellet Combustion Simulation

Wood pellet combustion details have been discussed in section 2.3.1. In the simulation, a conversion reactor was chosen to represent the wood pellet combustion process. A total of 14 reactions occurred in the reactor, representing each stage of the combustion process.

Drying: In this stage, wet wood pellets loose water and become dried pellets through the following reaction:

$$\text{Wet Pellets} \xrightarrow{100\%} \text{Dried Pellets} + H_2O \uparrow \quad (4\text{-}1)$$

The conversion is 100%. The reaction is an endothermic reaction with product temperature set at 105 °C.

Pyrolysis: In this stage, dried pellets are decomposed into solid, gaseous, and liquid products. Solid products are char, sulfur and ash; gaseous products are volatile, methane, and ammonia; and liquid product is benzene. The following reactions represent the formation process of those products.

$$0.8\ \text{Dried Pellets} \xrightarrow{80\%} 119.07\ \text{Volatile} + 0.16\ CH_4 + 1.14\ NH_3 \quad (4\text{-}2)$$

$$0.18\ \text{Dried Pellets} \xrightarrow{90\%} 140.87\ C \quad (4\text{-}3)$$

$$0.02\ \text{Dried Pellets} \xrightarrow{51\%} 2.56\ C_6H_6 \quad (4\text{-}4)$$

$$0.098\ \text{Dried Pellets} \xrightarrow{100\%} 1.07\ CaO + 0.1486\ K_2O + 0.0968\ Na_2O + 0.1247\ S \quad (4\text{-}5)$$

where volatile is represented by $C_{1.9316}H_{5.7546}O_{2.3751}$. The stoichiometry of the above four reactions are determined through general assumption of wood pyrolysis products containing 80% volatile, 18% char, 1.36% tar, 0.6% ash, and 0.04% sulfur.

Char and Volatiles Oxidation: Char and volatiles are further oxidized in this stage. Volatiles are assumed to be fully converted into CO and H_2O through the following reaction[180,182]

$$C_{1.9316}H_{5.7546}O_{2.3751} + 1.2169\ O_1 \xrightarrow{100\%} 1.9316\ CO + 2.8773\ H_2O \quad (4\text{-}6)$$

Char oxidation is a strong temperature dependent reaction with products of CO and CO_2. The following reaction has been used by most researchers in modeling[181,183,184]

$$\theta\ \mathrm{C} + \mathrm{O_2} \xrightarrow{99.9\%} 2(\theta - 1)\ \mathrm{CO} + (2 - \theta)\ \mathrm{CO_2} \tag{4-7}$$

where θ is a temperature dependent parameter, calculated as

$$\theta = \frac{2\left[1 + 4.3\ e^{(-3390)/T}\right]}{2 + 4.3\ e^{(-3390)/T}} \tag{4-8}$$

where T is the reaction temperature in K. The 0.1% unburnt carbon are considered as fly ash or PM emissions, based on data from on-site emission characterization.

Flame Combustion: All the combustible products are then quickly oxidized during this stage of combustion with final products of CO_2, H_2O, and emissions (both gaseous and particulate matter). Many reactions take place during this stage and the most important reaction is the oxidation the most abundant product, CO

$$\mathrm{CO} + \frac{1}{2}\mathrm{O_2} \xrightarrow{99.88\%} \mathrm{CO_2} \tag{4-9}$$

where the unburnt 0.02% is considered as CO emission based on field stack sampling data. Methane is assumed to be fully converted into CO through the following reaction

$$\mathrm{CH_4} + \frac{3}{2}\mathrm{O_2} \xrightarrow{100\%} \mathrm{CO} + 2\mathrm{H_2O} \tag{4-10}$$

The liquid product benzene is assumed to be converted into CO_2 through

$$\mathrm{C_6H_6} + \frac{15}{2}\mathrm{O_2} \xrightarrow{99.9\%} 6\mathrm{CO_2} + 3\mathrm{H_2O} \tag{4-11}$$

Ammonia oxidation is the source of NO_x emissions from wood pellet combustion. The reaction consists of the following two steps[185]

$$NH_3 + O_2 \xrightarrow{50.9\%} NO + H_2O + \frac{1}{2}H_2 \quad (4\text{-}12)$$

$$NH_3 + NO \xrightarrow{100\%} N_2 + H_2O + \frac{1}{2}H_2 \quad (4\text{-}13)$$

The byproduct H_2 is completely oxidized into H_2O through the following reaction

$$H_2 + \frac{1}{2}O_2 \xrightarrow{100\%} H_2O \quad (4\text{-}14)$$

Finally, the oxidation of sulfur is produces SO_2 emissions. The reaction is

$$S + O_2 \xrightarrow{100\%} SO_2 \quad (4\text{-}15)$$

The final output temperature is calculated from energy balance, and was typically around 1200 °C for the simulation based on PB-1 field data. Therefore, by using reactions (4-1) to (4-15), the wood pellet combustion can be modeled. This component is shown in Figure 4-3 (combustion chamber volume is set at 0.019 m^3, or 5 gallons).

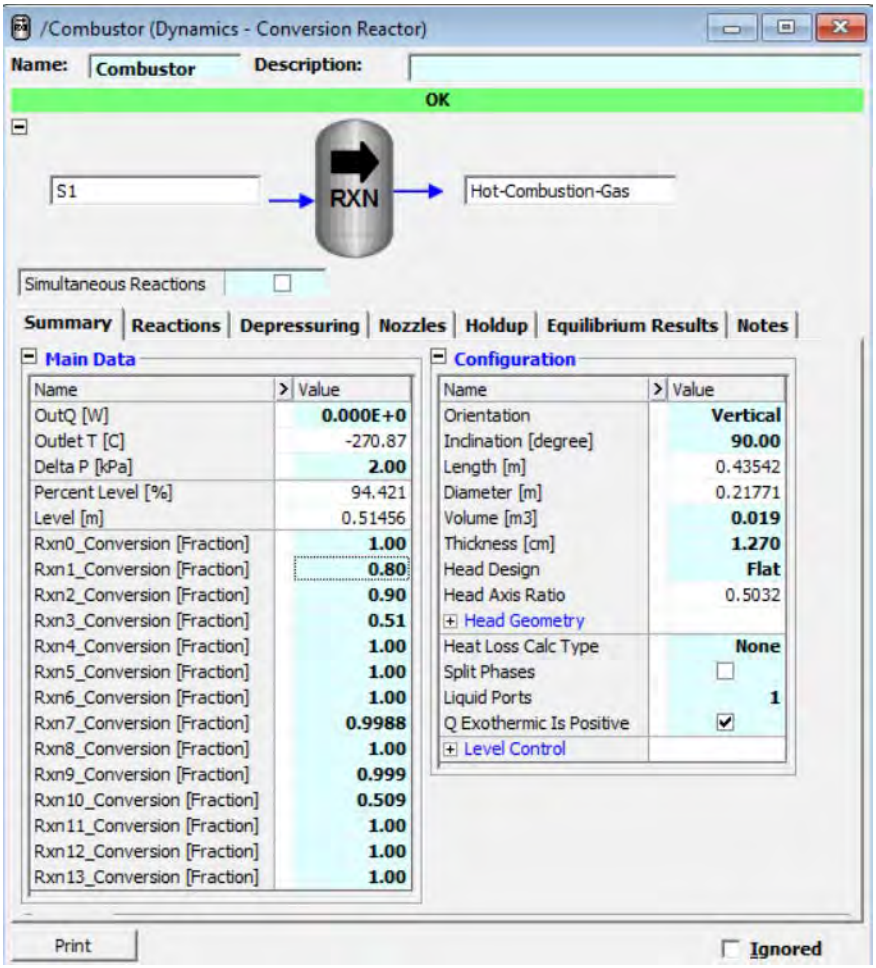

Figure 4-3. Simulation of wood pellet combustion in a conversion reactor

4.2.1.3 Fire-Tube Heat Exchanger Simulation

The hot flue gas, produced from the flame combustion stage, transfers heat to water through the fire-tube heat exchanger built inside the boiler. The jacket water volume is 37.9 L (10 gallons) for 25 kW boiler and 55 L (14.5 gallons) for 50 kW boiler, respectively. The heat transfer process simulation is done by setting the pressure drop, water volume, and heat transfer coefficient. Based on PB-1 data, the average output load is 17.65 kW, given an average thermal efficiency of 73.6%. The component is shown in Figure 4-4.

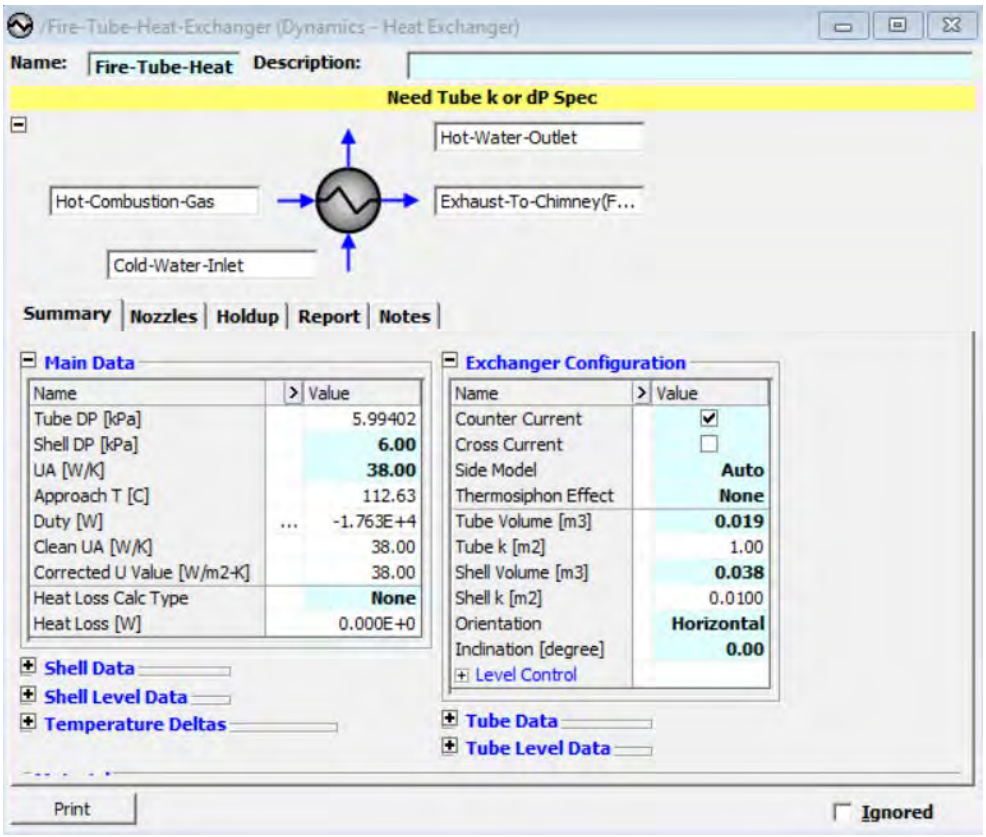

Figure 4-4. Simulation of flue gas heat transfer process using a shell and tube heat transfer exchanger

The resulting exhaust temperature is around 160°C with gaseous and particulate emissions match the stack sampling data.

4.2.1.4 TES Tank Simulation

The TES tank was represented using a pipe segment, as there is no available hot water storage tank component in the software. The pipe segment was set to a total volume of 0.9 m^3 (or 238 gallons) with diameter and height of the tank same as the manufacturer's schematics. The pipe was divided into 20 segments so that the profile of each segment can be plotted. A single phase, low Re calculation method was used. Heat

loss from the tank was calculated using a simple method by setting the heat transfer coefficient value at 4.5×10^{-5} W/m^2/K. The component is shown in Figure 4-5.

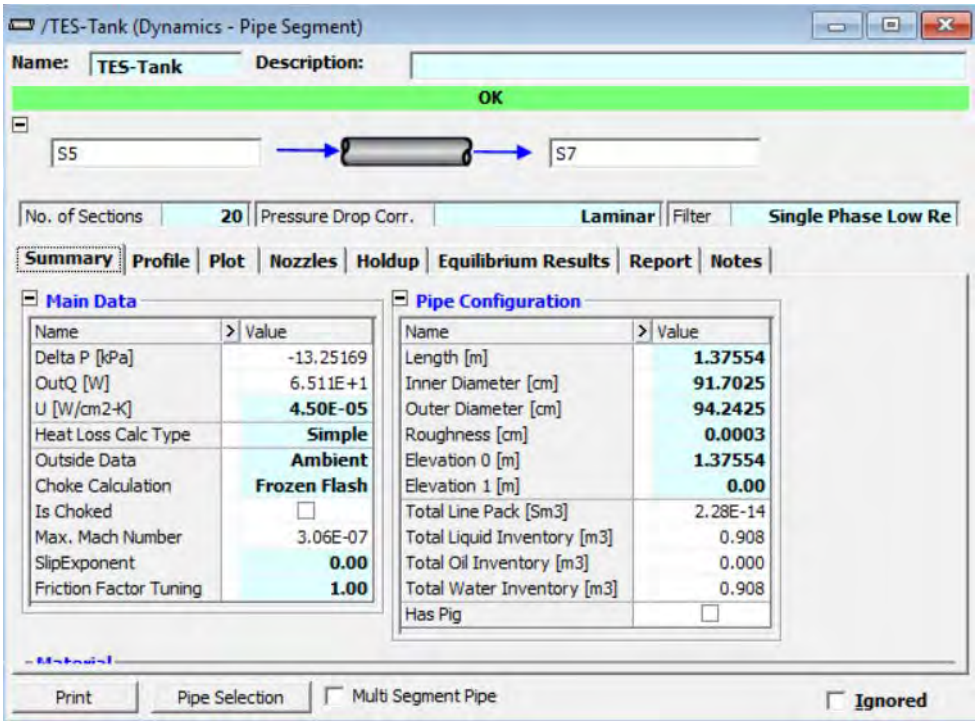

Figure 4-5. TES tank simulation using pipe segment

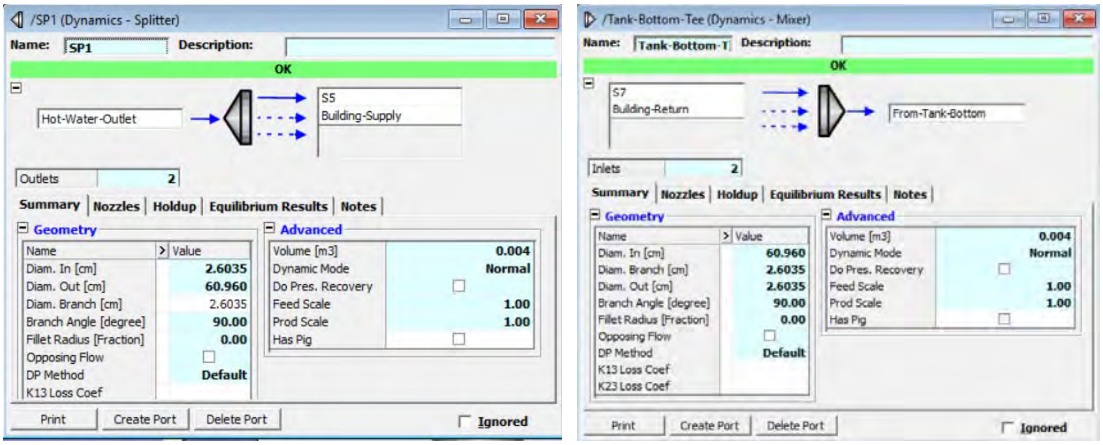

Figure 4-6. TES tank top splitter (left) and bottom mixer (right) specification

The top of the pipe was connected through a splitter and the bottom of the tank was connected using a mixer, which forms a 4-pipe configuration. The volume of the

splitter and mixer were also calculated based on the inlet and outlet port positions from the manufacturer's schematics. The two components are shown in Figure 4-6.

4.2.1.5 Building Simulation

Building is the heat consumption unit in a wood pellet heating system. The building was represented by a chiller. By specify the duty of the chiller, the thermal mass of the building can be changed. A large pressure drop was specified. The component is shown in Figure 4-7.

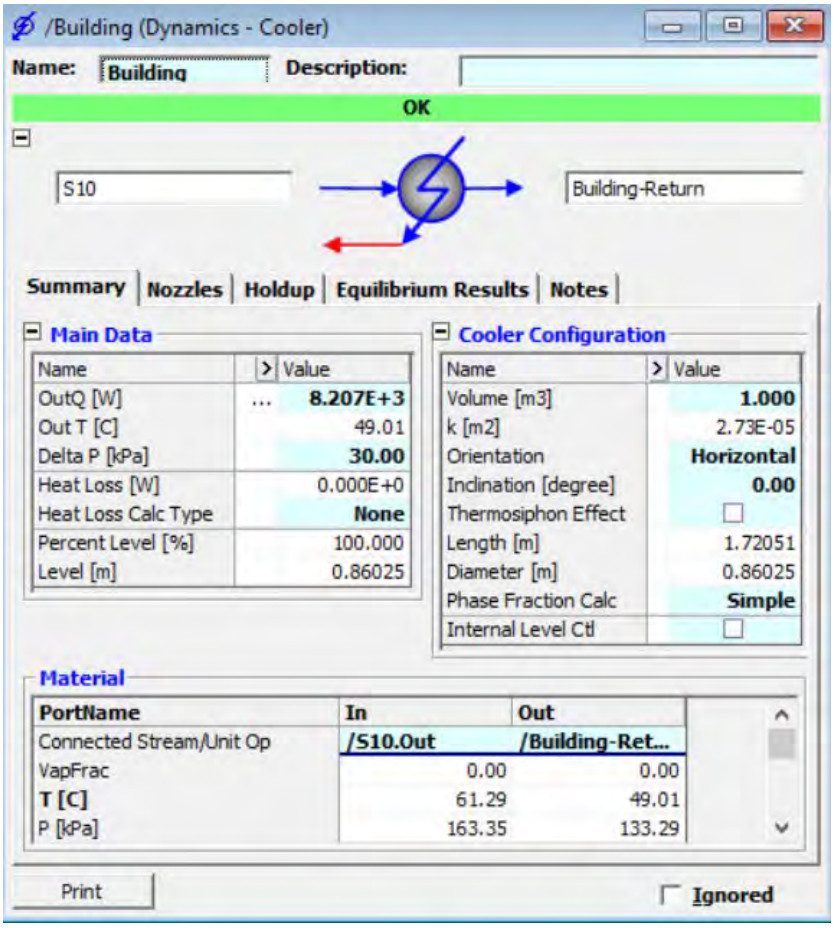

Figure 4-7. Simulation of building heat demand using a cooler

Figure 4-1 shows the simulation flow sheet of wood pellet heating system. The three components (boiler, tank, and building) and two loops (boiler to tank loop and tank to building loop) can be seen.

The system control logic is that when the top of the TES tank temperature drops below 56°C, the boiler fires up and when the bottom of the TES tank temperature rises to 64°C, the boiler shuts down. Boiler loop and building loop flow rates are controlled by the opening of the control valves. The amount of air supply is adjusted to keep the flue gas O_2 at 10%.

4.2.2 Dynamic Simulation of the System

The dynamic simulation was tested using data from PB-1. Although PB-1 does not represent the optimum configuration because of the constant circulation loop, it does provide the data needed to test the model. The average pellet fuel mass flow rate was determined to be 3.72 kg/h and corresponding air flow rate was 28.2 m^3/h. To simulate the start-up stages of the boiler operation, a pellet-fuel inlet ramping was used. Figure 4-8 shows the comparison of stoker feed between simulation and experiment data. The simulation data oscillated at a lower frequency than the experiment data but the error in the stoker feed values between simulation and experiment is less than 5%.

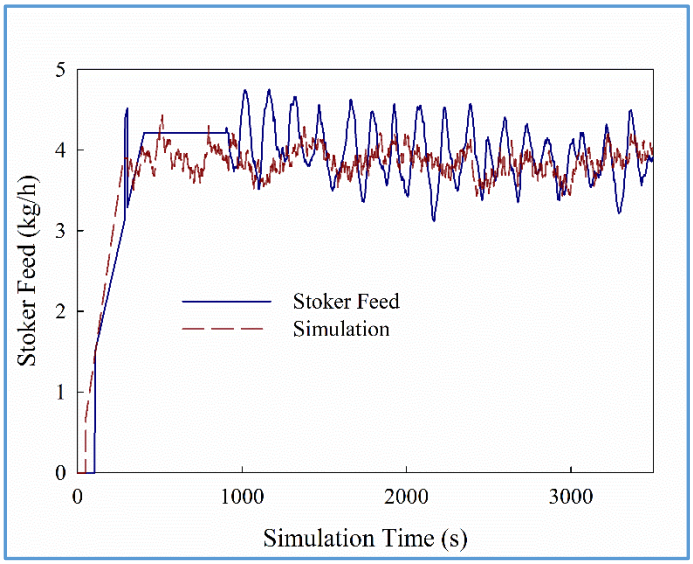

Figure 4-8. Boiler stoker feed compared between simulation and field data

Figure 4-9 shows flue gas O_2 content in comparison with simulation data. Field data varies around an average of 9% with frequent oscillations while simulation data showing quite stable average around 10%.

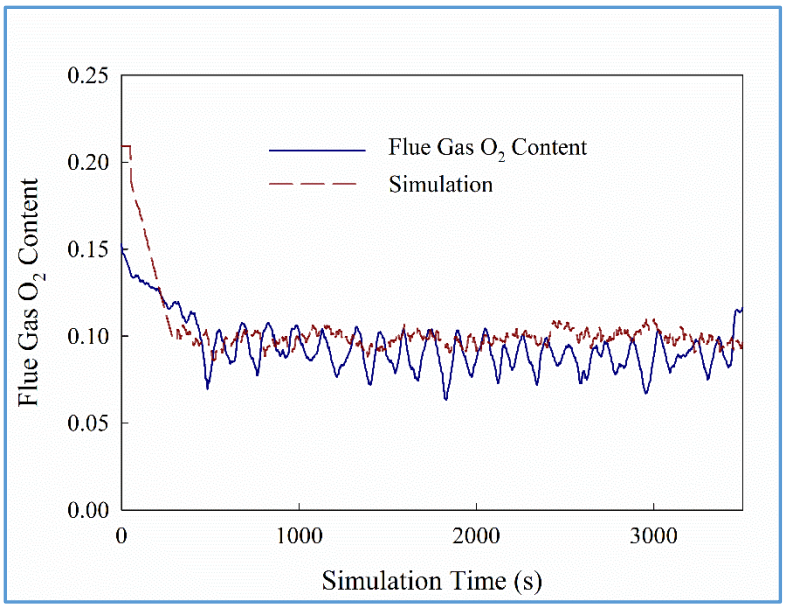

Figure 4-9. Flue gas O_2 content compared between simulation and field data

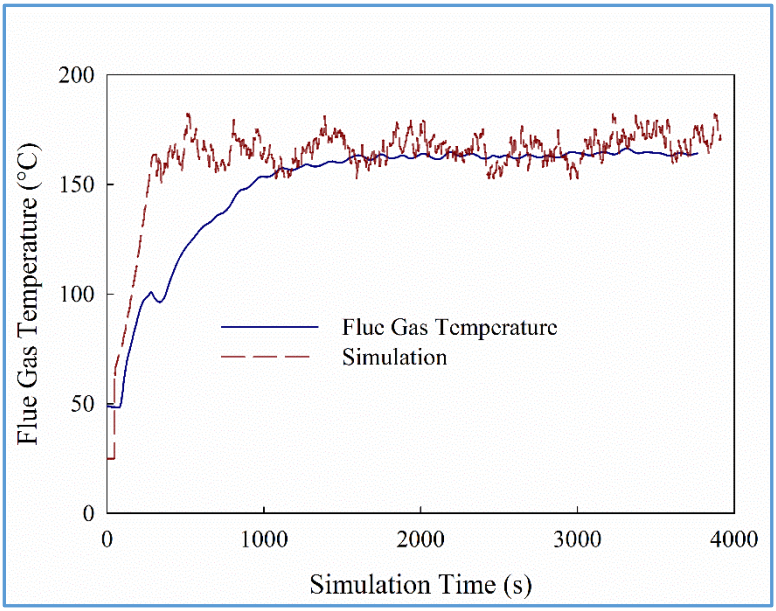

Figure 4-10. Flue gas temperature compared between simulation and field data

Figure 4-10 shows the comparison of flue gas temperature between simulation and field data. A good match between simulation and field data was observed when combustion stabilized. However, high deviations occurred during boiler start-up and

stabilization stages. The deviation is caused by the instant combustion and heat transfer inside the boiler when the boiler is ON, which clearly is not the case in real operational conditions. Therefore, the simulation data can only be used to simulate conditions when the boiler is stabilized.

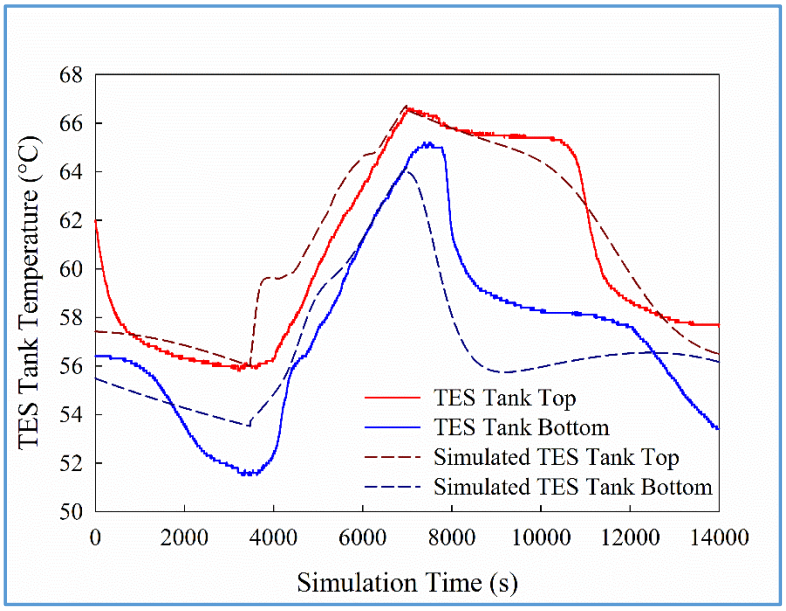

Figure 4-11. TES tank stratification between simulation and field data

Figure 4-11 shows the comparison of TES tank stratification between simulation and field experiment. Generally, the simulation can represent real operational conditions. The error could be caused by the difference in TES tank geometries since the simulation utilized only 1 TES tank rather than 2 identical, smaller TES tanks connected in parallel (but the aspect ratio and total volume were kept the same).

To summarize, the dynamic wood pellet heating system model can represent real operational conditions within the error.

4.3 System Optimization through Dynamic Simulation

The dynamic simulation is built and ready to use to properly size the TES tank to optimize system efficiency. The system has two loops: boiler loop and TES tank loop. The dynamic process simulation enables analysis for a wide range of a wide range of boiler systems based on the validation from field experiment.

For the boiler loop simulation, key factors include stoker data, fire-tube heat exchanger data, and boiler flow rate data. For the TES tank loop simulation, several key parameters are discussed and evaluated including tank aspect ratio (*AR*), TES tank top and bottom temperature difference ΔT_{TES}, discharge efficiency φ_{Dis}, TES tank flow rate, etc.

4.3.1 Boiler Loop Simulation

Most modern wood pellet boiler heating systems utilize the 4-pipe configuration. The boiler loop flow and tank loop flow are separated. In the boiler loop, the boiler circulator pumps cold water from the bottom of the TES tank and hot water flows back into the TES tank from the top. This process is called TES tank charge. During charge, the TES tank has almost no thermal stratification because the purpose of TES tank charge is to heat the tank to a uniform temperature.

A linear relationship between boiler's nominal capacity and boiler flow rate was found. Figure 4-12 shows the correlation of boiler flow rate with boiler nominal capacity through the following equation:

$$Q_{\mathrm{B}} = 0.086\,N \tag{4-16}$$

where Q_B is boiler flow rate in m^3/h and N is boiler nominal output capacity in kW. Using equation (4-16), Q_B for any output capacity boiler can be estimated. For example, a small residential house has a residential boiler with N = 15 kW, and the boiler flow rate can be estimated as 1.2 m^3/h (or 5.3 gpm).

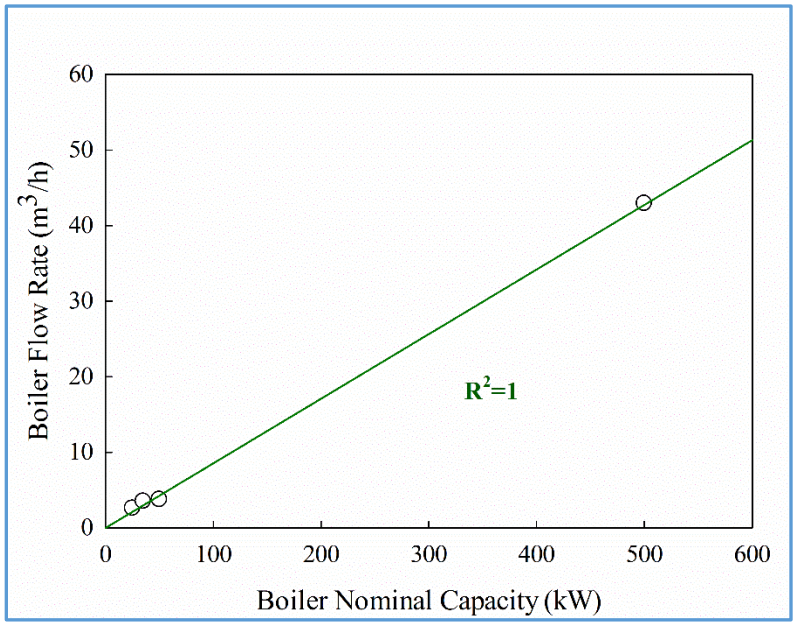

Figure 4-12. Boiler flow rate and nominal capacity correlation (500 kW boiler flow rate was measured at another site)

The boiler flow rate also determines the temperature increase (TI_B) over the boiler fire-tube heat exchanger. Based on the definition of boiler output load in equation *(3-4)*, TI_B can be rewritten as following:

$$TI_B = \frac{3600 \cdot \chi N}{Q_B \rho_w c_{p,w}} \tag{4-17}$$

Substitute equation (4-16) into the above equation and use ρ_w = 990 kg/m^3, $c_{p,w}$ = 4.18 kJ/(kg·K) at an average of 50 °C water temperature:

$$TI_{\mathrm{B}} = 10.87\chi \tag{4-18}$$

Equation (4-18) is an easy way to estimate TI_{B}. For example, PB-1 had an average χ = 56%, which resulted in an average TI_{B} = 6.1°C. For most wood pellet boilers, TI_{B} = 6.5 °C is an average estimation.

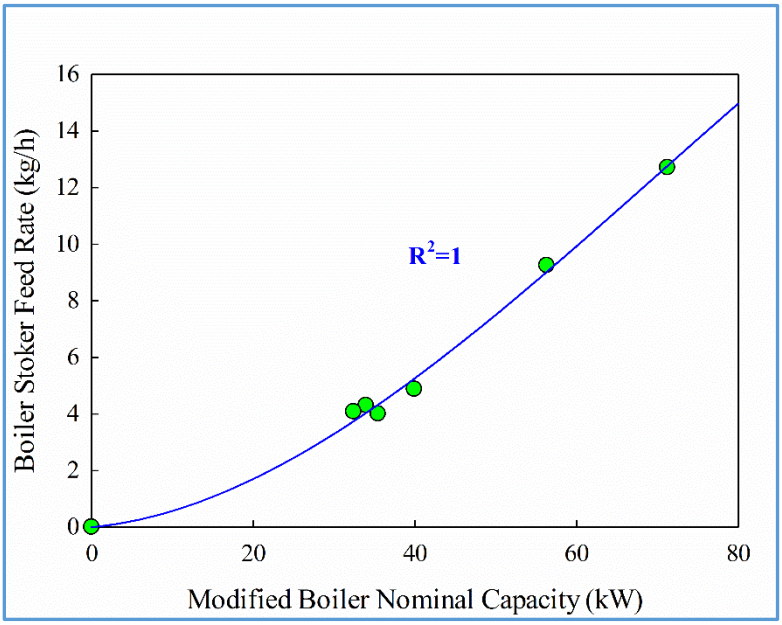

Figure 4-13. Stoker feed rate as a function of modified boiler nominal capacity

Figure 4-13 shows stoker feed rate (wood pellet mass flow rate into the combustion chamber) correlates with modified boiler capacity as

$$\dot{m} = 0.0672N_{\mathrm{Mod}} + 0.00159N_{\mathrm{Mod}}^2 \tag{4-19}$$

where $\dot{m}$ is stoker feed rate in kg/h, N_{Mod} is modified boiler nominal capacity expressed as

$$N_{\mathrm{Mod}} = \frac{N}{\eta_{\mathrm{th}}} \tag{4-20}$$

For example, for a nominal output N = 25 kW boiler with boiler thermal efficiency η_{th} = 77%, N_{Mod} = 25/0.75 = 33.33 kW. Substitute into equation (4-19), $\dot{m}$ = 4.01 kg/h, which is exactly the wood pellet mass flow rate in the simulation for 25 kW boiler.

To maintain a 10% flue gas O_2 content, the air flow rate was calculated to be 8.59 m^3/kg pellets, given air temperature at 20 °C and pressure at 1 atm. Therefore:

$$\dot{Q}_{Air} = 8.59\dot{m} \tag{4-21}$$

where $\dot{Q}_{Air}$ is the volumetric flow rate of supplied air in m^3/h.

Based on the above discussion, the boiler loop simulation can be performed for any given nominal capacity wood pellet boilers with thermal efficiency data, as shown below:

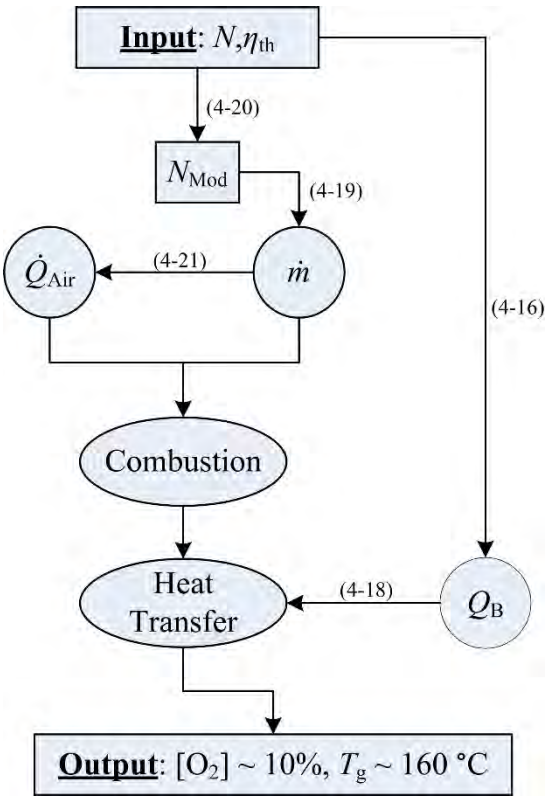

Figure 4-14. General simulation procedure for boilers with different nominal capacities

4.3.2 TES Tank Loop Simulation

The performance of the TES tank is determined by both its geometrical parameters and operational conditions. By fixing the operational conditions, the optimized geometrical parameters can be determined; and consequently, by fixing the geometrical parameters, the best operational conditions can be found. The criterion is to achieve the maximum TES tank discharge efficiency.

4.3.2.1 TES Tank Aspect Ratio

The TES tank aspect ratio is defined as the ratio of tank height (*H*) to tank inner diameter (*D*):

$$AR = \frac{H}{D} \tag{4-22}$$

When the total volume (*V*) is a constant (for example, V = 0.9 m^3), TES tank inner diameter can be expressed in terms of AR as

$$D = \sqrt[3]{\frac{4V}{AR \cdot \pi}} \tag{4-23}$$

A set of *AR* values ranging from 1 to 5 with an interval of 0.5 were used to run the simulation with constant building demand of 8.3 kW at 0.54 m^3/h water flow rate determined through field data monitoring in PB-1. The discharge efficiency φ_{Dis} of tanks with the different AR values were compared as shown in Figure 4-15. When the flow rate is constant, *AR* affects φ_{Dis} through the degree of stratification that TES tanks with higher *AR* are easier to build up stratification than the same TES tanks with lower *AR*.

For each value of *AR*, a total simulation time of 86400 seconds (1 day) were used, producing an average of 7 boiler cycles per day. The discharge efficiency φ_{Dis} was calculated based on (3-31). Figure 4-15 shows that *AR* = 3 generates the highest average φ_{Dis}. Computational fluid dynamics (CFD) study by Ievers and Lin[186] showed that *AR* = 3.5 was an idea value for TES tanks used in most cases (close to the value found here).

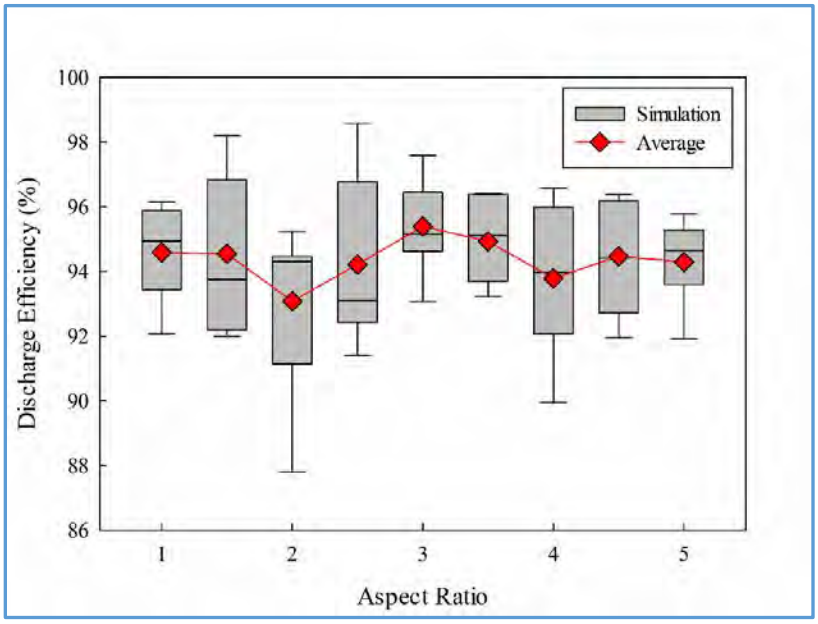

Figure 4-15. TES tank aspect ratio effect on discharge efficiency

Figure 4-16 shows TES tank surface area increases linearly with increasing *AR*. Therefore, better TES tank insulation must be performed for high *AR* TES tanks to minimize heat loss and prevent the destruction of thermal stratification caused by natural convection currents. Figure 4-17 shows the effect of insulation level on the TES tank top and bottom temperature difference ΔT_{TES} (or simply, thermal stratification). Insufficient insulation can lead to a low level of stratification while sufficient insulation can help maintain high level of stratification. In addition, sufficient insulation prevents less heat loss from the tank and therefore increases overall energy efficiency of the system.

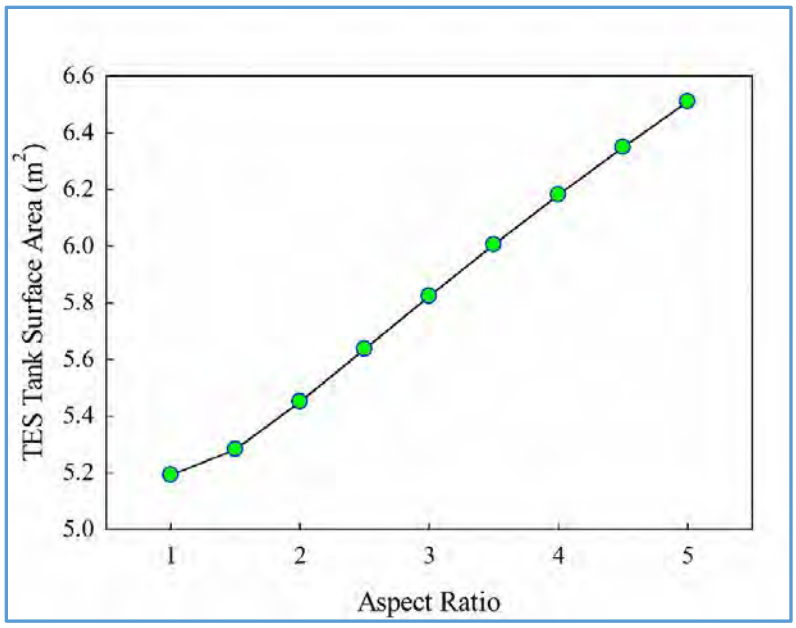

Figure 4-16. TES tank surface area as a function of aspect ratio (V = 0.9 m^3)

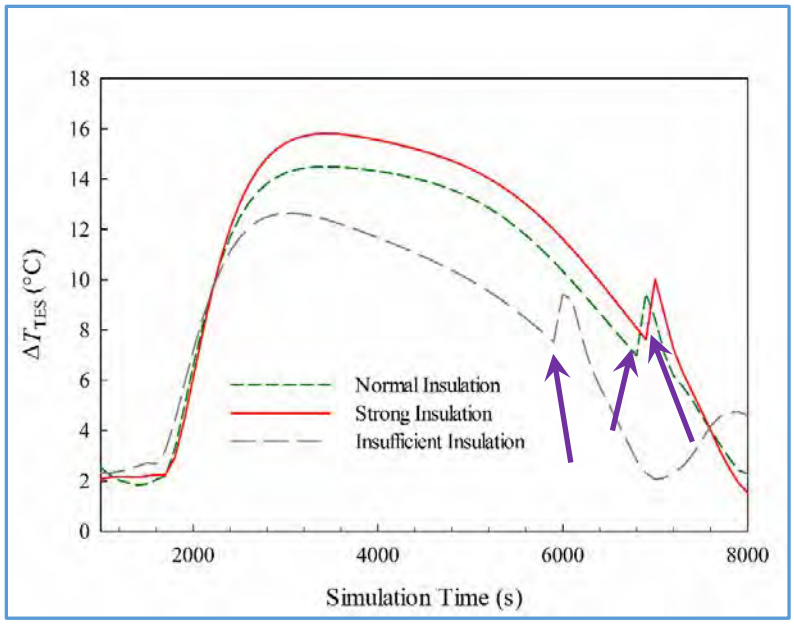

Figure 4-17. TES tank top and bottom temperature difference ΔT_{TES} changes with different levels of insulation (the arrows point out the time at when the boiler is ON)

4.3.2.2 Building Flow Rate and TES Tank Volume

By fixing AR = 3 and a constant heat demand from the building, the proper volume of the TES tank can be determined by achieving the maximum discharge efficiency.

After the volume of the TES tank has been determined, a range of building flow rates will be used to run the simulation. The optimum flow conditions are determined when maximum discharge efficiency is achieved.

Building loop flow rate is mainly determined by the level of heat demand P_{Bld} from the building, which is calculated as

$$P_{\mathrm{Bld}} = \frac{Q_{\mathrm{Bld}} \rho_{\mathrm{w}} c_{\mathrm{p,w}} T_{\mathrm{S/R}}}{3600} \tag{4-24}$$

where P_{Bld} is in kW, Q_{Bld} is in m^3/h, and $T_{\mathrm{S/R}}$ is the TES tank supply and return water temperature difference. Therefore, increases in Q_{Bld} can lead to decrease in $T_{\mathrm{S/R}}$ and vice versa. Large $T_{\mathrm{S/R}}$ can only occur when the top of the TES tank is at high temperatures (for example, right after when the boiler is OFF) and the building is calling for heat at the same time. Figure 4-18 shows the plot of equation (4-24) for building demand ranging from 5 kW to 85 kW. Low building flow rates can produce high $T_{\mathrm{S/R}}$ and therefore, a higher level of stratification.

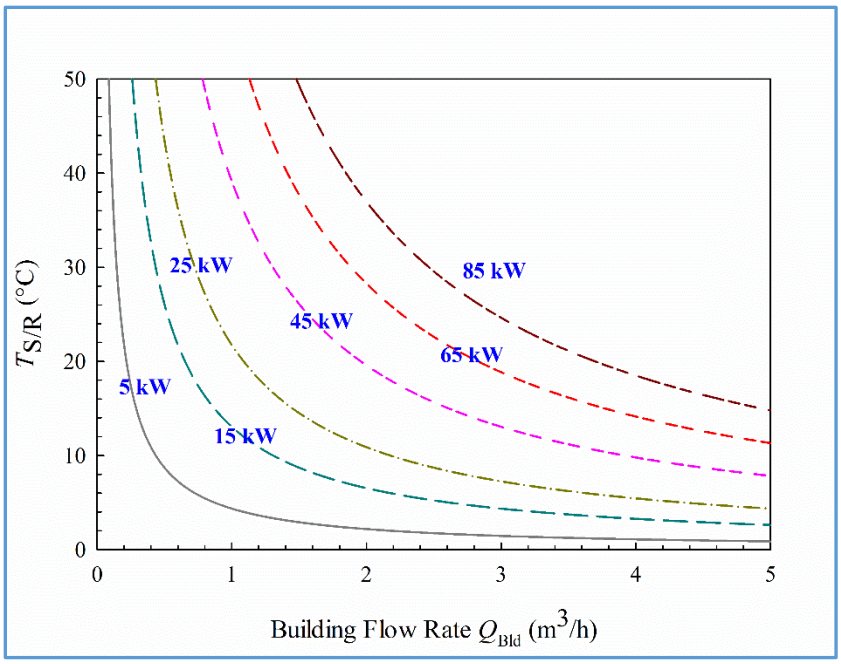

Figure 4-18. TES tank supply and return temperature difference as a function of building flow rate at different heat demands

4.4 TES Tank Sizing for Different Residential Systems

Residential scale wood pellet boilers are usually less than 50 kW. Table 4-2 lists all the different boiler systems being simulated.

Table 4-2. List of simulation details for TES tank sizing (assuming an average value of 78% thermal efficiency)

Nominal Capacity* (kW)	Renewable Heat NY Recommendation** (m^3)	Simulation Start Volume*** (m^3)
5	0.13	0.1
10	0.26	0.2
15	0.39	0.3
20	0.52	0.5
25	0.65	0.7
30	0.77	0.9
35	0.90	1.1
40	1.03	1.1
45	1.16	1.1
50	1.29	1.2

* In the simulation, nominal capacity is used to specify the fire-tube heat exchanger duty

** Renewable Heat NY recommended 2 gallons per kBtu/h capacity[179]

*** Simulation volume ranges from lower end to upper end until a continuous dropping in discharge efficiency is observed.

The simulation start volume for TES tanks are based on the recommended values from Renewable Heat NY[179] and expanded to larger volumes. Boiler ON/OFF temperature settings for all the simulations are 60/75 °C.

4.4.1 Building Flow Rate and Building Load Effect

A 5-kW boiler with a TES tank volume V = 0.1 m^3 is discussed for simplicity. From equation (4-16), boiler loop flow rate Q_B = 0.4 m^3/h. Building loop flow rate ranges from Q_{Bld} = 0.1 m^3/h to Q_{Bld} = 0.3 m^3/h with an interval of 0.05 m^3/h. Two categories of performance indicators are used. On the boiler side:

$$t_{ON} > 1 \text{ h} \tag{4-25}$$

$$\frac{t_{OFF}}{t_{ON}} > 1 \tag{4-26}$$

$$\text{Boiler Output Temperature} < 85\ ℃ \tag{4-27}$$

where t_{ON} is boiler cycle ON time (or t_c) and t_{OFF} is boiler cycle OFF time. (4-25) and (4-26) prevent boiler short-cycling and (4-27) is a safety measure for the boiler to prevent boiler over heating. On the TES tank side, the goal is to achieve maximum possible discharge efficiency.

Figure 4-19 shows a full examination of the boiler when fixing the TES tank volume at V = 0.1 m^3. Figure 4-19 (a) shows that boiler OFF/ON time ratio increases with decreasing building heat demand, but the building flow rate change has almost no effect. This result is because at high building heat demand (e.g. 80% of boiler output capacity), the boiler takes a longer time to heat the TES tank (long ON time) and the TES tank can only supply the heat demand for a short period (short OFF time). Therefore, the building heat demand should neither be too high nor too low compared to the boiler's nominal capacity. From Figure 4-19 (a) and (b), the appropriate building heat demand is between 20 – 50% of boiler's output capacity to satisfy equations (4-25) and (4-26). The

preferable building heat demand is 40% of boiler nominal capacity of 2 kW such that the boiler ON time is ≥ 1 hour and OFF/ON time ratio is around 1.5.

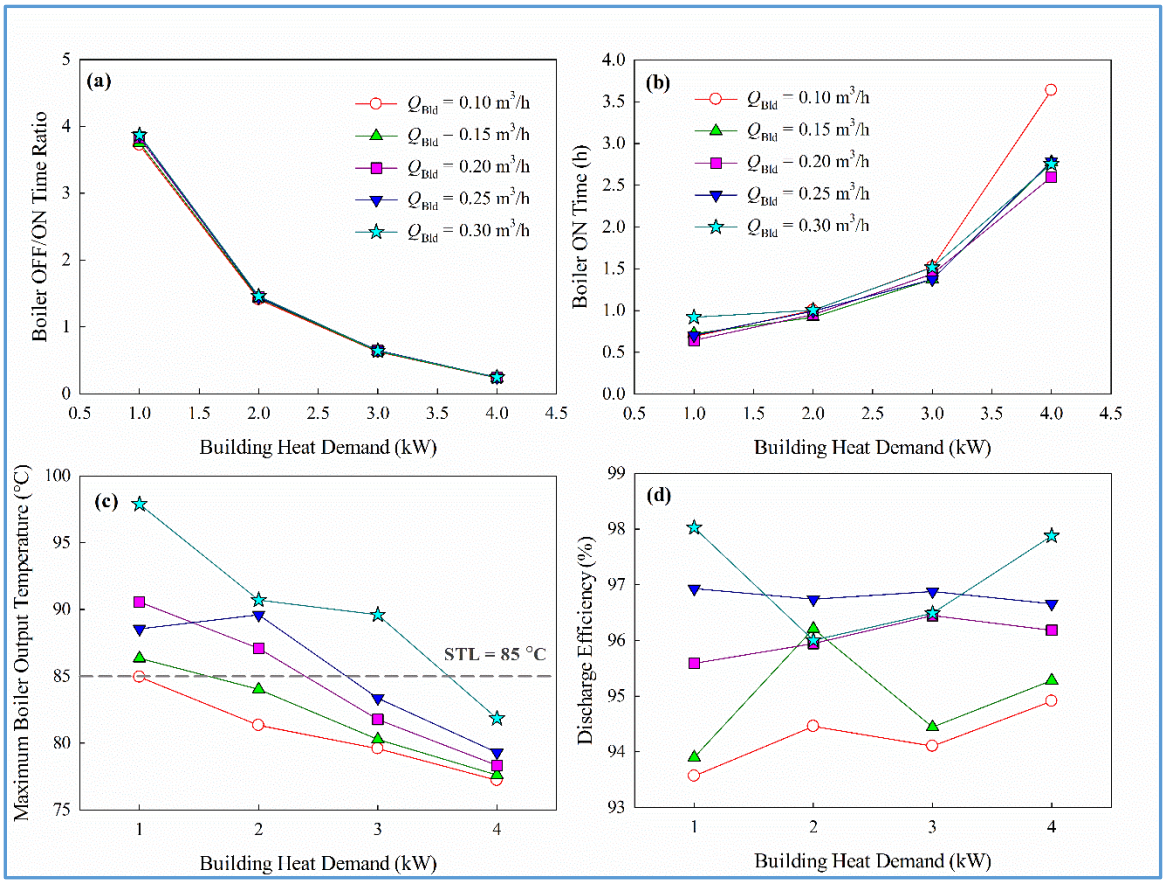

Figure 4-19. The effect of building heat demand and building flow rate on (a) boiler OFF/ON time ratio, (b) boiler ON time, (c) maximum boiler output temperature, and (d) TES tank discharge efficiency

However, the boiler has a safety temperature limit (STL) of 85°C, which means the boiler output temperature cannot exceed 85°C. Figure 4-19 © shows that building heat demand is the key factor determining boiler output temperature. Low heat demand means a small TES tank supply and return water temperature difference, which increases boiler supply water temperature dramatically. This phenomenon has been seen in WPB where the low demand from DHW tank often triggers the STL of the boiler. Figure 4-19

© also shows that boiler output temperature increase is magnified by building flow rate such that high building flow rates in combination with low building demand is disastrous for boiler operation. Therefore, the building flow rate Q_{Bld} = 0.1 m^3/h (or ¼ of boiler flow rate) is the best option.

Figure 4-19 (d) shows the need of TES tank sizing to maximize discharge efficiency since building demand at 2 kW and building flow rate at 0.1 m^3/h does not produce the highest discharge efficiency.

In conclusion, the TES tank size must be based on both the boiler operation and building heat demand. The optimum operating conditions are:

(1) Boiler flow rate $Q_B = 0.08N$;

(2) Building flow rate $Q_{Bld} = 0.25Q_B = 0.02\ N$;

(3) Building heat demand $P_{Bld} = 0.4\ N$;

(4) TES tank aspect ratio AR = 3.0.

Based on those optimum operating conditions, the next step is to size the TES tank to obtain highest discharge efficiency.

4.4.2 TES Tank Sizing

To minimize simulation error and reduce simulation time, the original system was simplified for TES tank sizing. The conversion reactor and fire-tube heat exchanger were replaced with a heater. Boiler capacities were determined by specifying the output of the heater. The simplified simulation flow sheet is shown below. Each simulation must be fine-tuned to avoid any flow control issue.

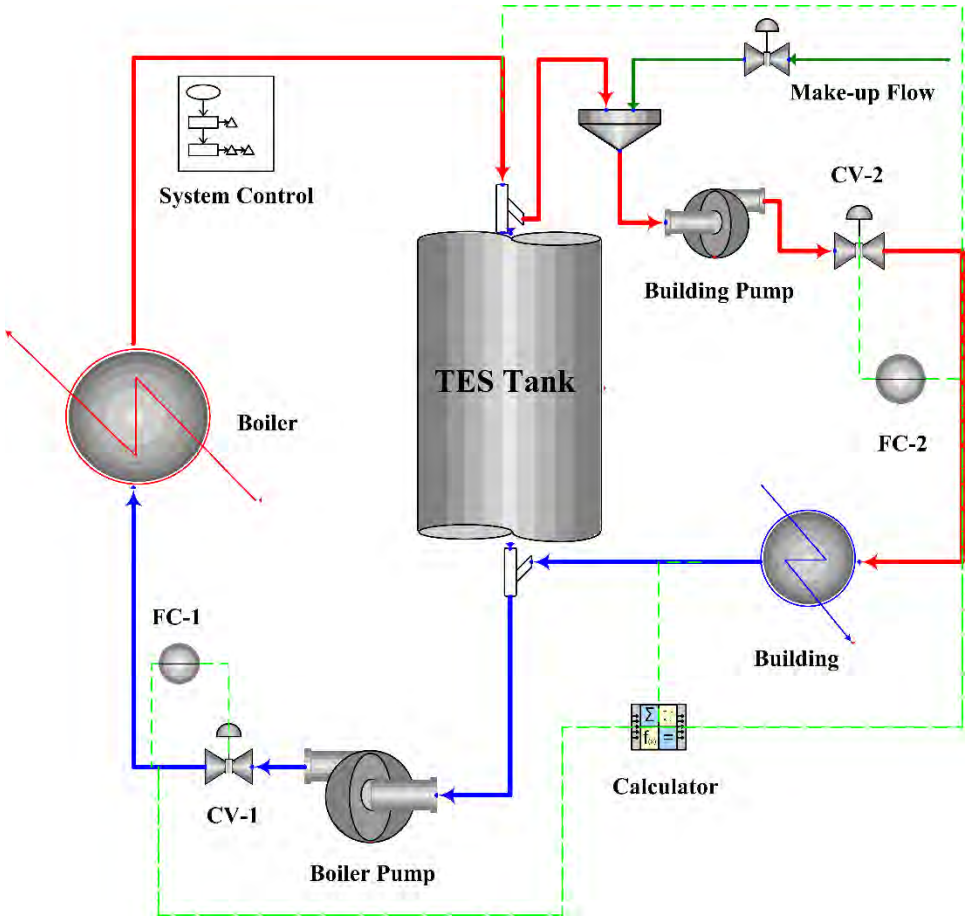

Figure 4-20. Simplified simulation flow sheet for TES tank sizing (FC and CV are short for flow controller and control valve)

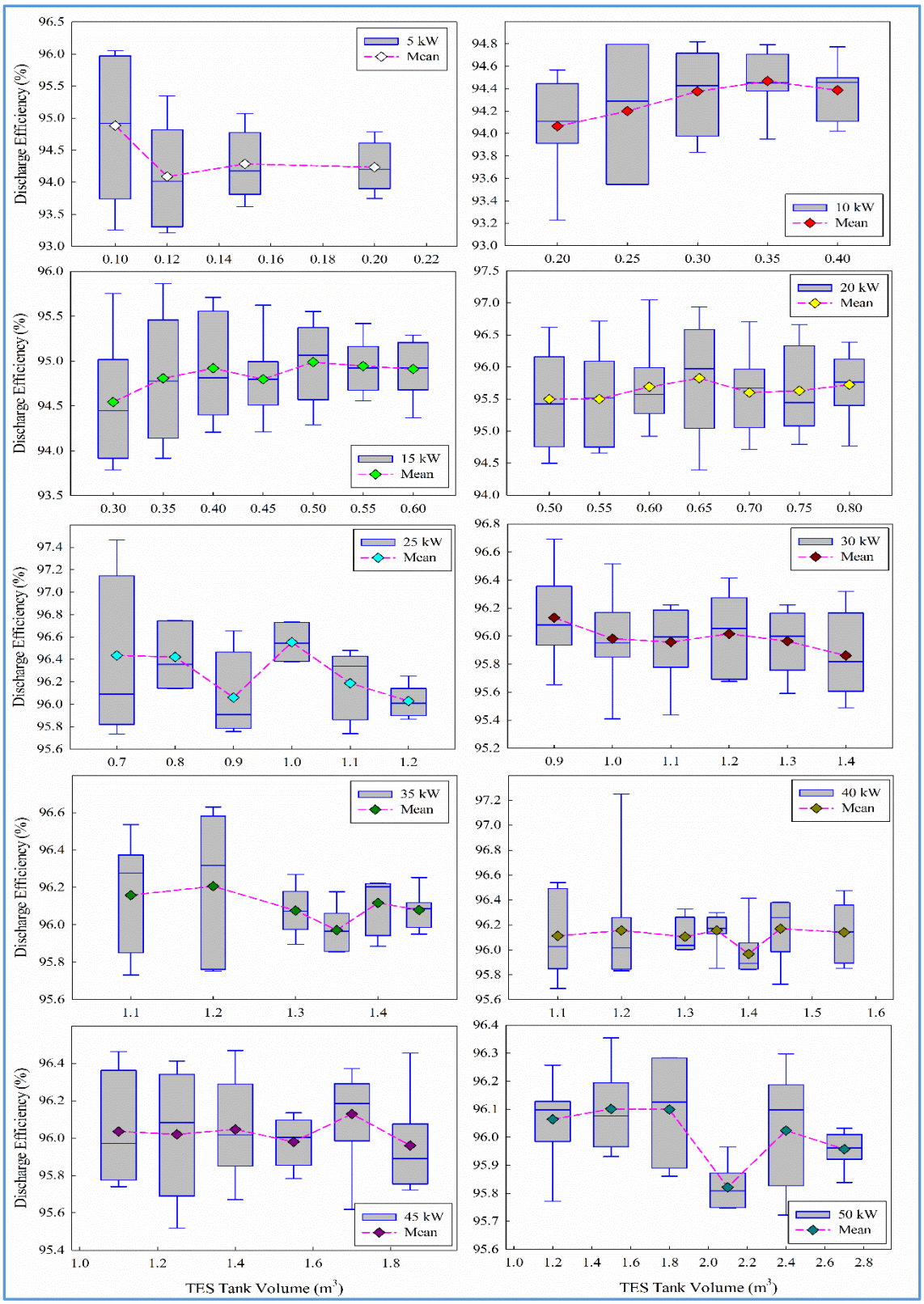

Figure 4-21. TES tank volume optimization based on discharge efficiency

Figure 4-21 shows the optimization process for boilers with nominal capacity from 5 kW to 50 kW. The simulation settings for boiler, boiler flow rate, building flow rate, and building demand are determined by the optimum operational conditions discussed previously. For each boiler, different volumes of TES tanks were tried and compared. With each specified TES tank volume, the simulation ran the system for 8 boiler cycles. In order to minimize the accumulative error induced by dynamic flow and controller adjusting, the step time was set at 1 second.

From Figure 4-21, the optimum TES tank volume was selected. The correlation between optimum TES tank volume and boiler nominal capacity is shown in Figure 4-22.

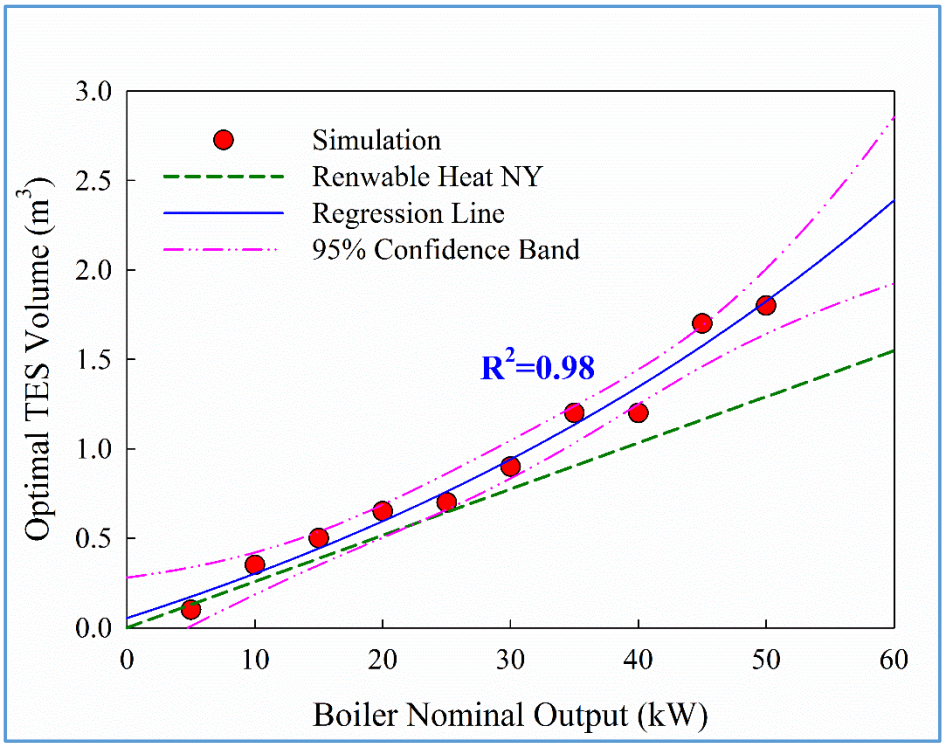

Figure 4-22. Optimum TES tank volume as a function of boiler nominal capacity compared with Renewable Heat NY recommendation line

A very high correlation was observed with $R^2 = 0.98$. The correlation equation is

$$V_{\text{opt}} = -1.342 + 1.396 \exp(0.01638N) \quad (4\text{-}28)$$

where V_{opt} is the optimum TES tank volume (m^3) and N_{opt} is boiler nominal output capacity (kW).

Figure 4-22 also shows that when boiler output capacity is less than 20 kW, the Renewable Heat NY recommendation values are very close to optimum values. However, when the boiler nominal output exceeds 20 kW, the difference becomes larger. It should also be noted the optimum TES tank has an aspect ratio of 3, which means the height of the tank would reach 2.0 m when the volume is 0.7 m^3. For many installations, there will not be enough space to install the tank since basement ceiling heights are often lower than 2 m. Therefore, multiple lower volume TES tanks connected in parallel could be used to provide the recommended volume. The above simulation is based on optimum heat demand and therefore can cover both high temperature and low temperature distribution system.

4.5 Wood Pellet Heating System Sizing

The PB and WPB systems represent low temperature and high temperature heating systems, respectively. The average heat load per unit area are calculated according to the original design is:

$$P_{\text{low}} = \frac{91969\ \text{Btuh}}{4376\ \text{ft}^2} = 0.00524\,\frac{\text{Btuh}}{\text{ft}^2} = 0.0663\ \text{kW/m}^2 \tag{4-29}$$

$$P_{\text{high}} = \frac{78264\ \text{Btuh}}{1532\ \text{ft}^2} = 51.09\,\frac{\text{Btuh}}{\text{ft}^2} = 0.1612\ \text{kW/m}^2 \tag{4-30}$$

The use of DHW depends on the number of occupants per family house, the number of appliance, and personal habits. Hendron and Engebrecht[187] provided a method to estimate DHW use as

$$Q_{\text{DHW}} = Q_{\text{Fix}} + Q_{\text{ClothesW}} + Q_{\text{DishW}} \tag{4-31}$$

where Q_{DHW} is the total daily DHW use, Q_{Fix} is the fixture hot water use, Q_{ClothesW} is the clothes washer hot water use, and Q_{DishW} is the dish washer hot water use. All units are in gallons per day (gpd). According to the manuscript,[187] Q_{ClothesW} and Q_{DishW} can be estimated based on the number of occupants, n_{occ}, as

$$Q_{\text{ClothesW}} = 4.0 \times \left(\frac{123 + 61n_{\text{occ}}}{365}\right) \tag{4-32}$$

$$Q_{\text{DishW}} = 8.0 \times \left(\frac{91 + 30n_{\text{occ}}}{365}\right) \tag{4-33}$$

Parker and Fairey[188] developed an improved model to estimate the fixture hot water use based on the number of occupants, as

$$Q_{\mathrm{Fix}} = 18.629 n_{\mathrm{occ}} - 4.8432 \tag{4-34}$$

Thus, the total daily use of DHW can be estimated using the number of occupants in the family. The average winter tap water temperature in Potsdam, NY is 9.2 °C (48.5 °F).[189] Assuming an average DHW temperature of 54.4 °C (130 °F), the energy consumption for DHW can be calculated as

$$P_{\mathrm{DHW}} = 1.98 \times 10^{-6} Q_{\mathrm{DHW}} \rho_{\mathrm{w}} c_{\mathrm{p,w}} \tag{4-35}$$

where P_{DHW} is in kW, Q_{DHW} is in gpd, ρ_{w} is water density in kg/m^3, and $c_{\mathrm{p,w}}$ is water heat capacity in kJ/kg/K. The sizing of the heating system can therefore be 183stimated with only two required parameters: the total area of space heating A_{T} and number of occupants in the house n_{cc}. Figure 4-23 shows the performance based wood pellet heating system sizing algorithm.

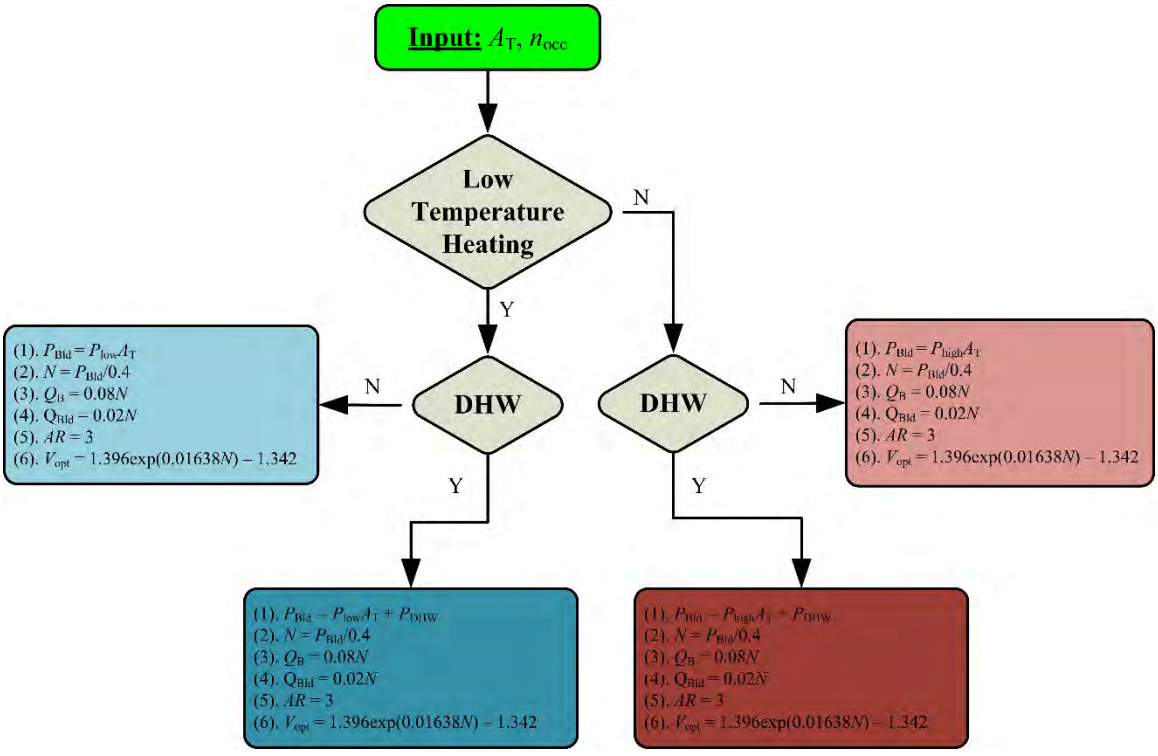

Figure 4-23. Performance based wood pellet heating system sizing algorithm

Chapter 5. Conclusions and Future Work

5.1 Conclusions

Biomass is an important part of renewable energy. Biomass energy utilization has been significantly increased over the past decade in areas such as space heating, electricity generation, and biofuel production. Biomass feedstock can provide high energy density and uniform quality through pelletizing, which also makes the design and automation of modern biomass pellet burners easier to achieve.

The use of wood pellets and wood pellet heating systems has dramatically increased. A typical wood pellet heating system includes a wood pellet boiler for heat generation, a thermal energy storage (TES) tank for heat storage, and the building for heat consumption.

Three modern wood pellet heating systems (PB, WPB, and LGB) were installed and monitored since spring 2015 to evaluate the system performance in terms of boiler operational characteristics, boiler efficiency (thermal efficiency, combustion efficiency, and heat transfer efficiency), boiler emissions, TES tank efficiency, and overall system efficiency.

The boiler performance was evaluated based on cycles. A complete boiler cycle included seven stages: flush, fill, ignition, stabilization, automatic combustion, burnout, and post-ventilation stage. Each stage had its own time range and was a part of a complete boiler cycle. The automatic combustion stage was the longest stage in each boiler cycle, where boiler flue gas was in 160°C and 10% O_2 content. An ideal boiler

design should be able to maximize the ratio of boiler OFF/ON time (zone II of boiler OFF vs ON time chart)

The boiler's thermal efficiency showed a high correlation with boiler output load. Therefore, it is essential to fire the boiler at maximum output load to obtain the highest possible thermal efficiency. This correlation was found to be caused by the change in boiler stoker feed rate. A constant stoker feed rate will lead to a linear correlation between boiler thermal efficiency and boiler output load, and a variable stoker feed rate will produce a logarithmic correlation. High thermal efficiencies were observed at PB. Lower thermal efficiencies at WPB and LGB were caused by boiler modulation and insufficient cleaning, respectively.

The boiler's combustion efficiency was linearly correlated with excess air. The three boilers had excess air ratios around 1.8 resulting in combustion efficiency between 90 – 95%. Outdoor temperature also affected boiler combustion efficiency.

The boiler's heat transfer efficiency is an indicator of the fouling rate of boiler fire tube heat exchanger. PB boiler was found to have a heat transfer efficiency drop of 0.026% per boiler cycle. It was found that boiler needed to be manually cleaned after 55 days of continuous operation before the heat transfer efficiency dropped by over 10%.

The measured emissions included gaseous (CO, NO_x, and SO_2) and particulate matter (PM) emissions. CO emission is an indicator of combustion quality. PB boiler operational parameters were optimized for minimum CO emissions with excess air at 2.35 and stoker feed fraction at 0.44. PM emission was dominated by particle size less

than 2.5 μm ($PM_{2.5}$) with two distinctive modes at 50 – 60 nm and 120 – 150 nm, respectively.

The TES operation has two phases: charge and discharge. During charge, the boiler heats the tank to a uniform temperature. During discharge, the TES tank supplies heat to the building and creates stratification inside the tank. The existence of stratification improves the TES tank performance. The TES tank discharge efficiency was found to be correlated with a dimensionless flow factor that is a function of the temperature difference inside the TES tank and the temperature difference between the TES tank supply and the return water temperature.

A process dynamic simulation was constructed using the field data. The model could represent the boiler heating system within acceptable error. A system size estimation was performed for boilers with nominal capacity ranging from 5 kW to 50 kW. The optimum TES tank aspect ratio was found to be 3 and the optimum TES tank volume was found to be exponentially correlated with boiler nominal output load. A systematic sizing algorithm was developed.

The results in this study provide valuable insights for future hydraulic based wood pellet heating system design and optimization.

5.2 Future Work

There is related work to this study that needs be done in the future.

(1) *Kinetic Simulation of Wood Pellet Boiler*: The wood pellet boiler simulation in this study was constructed using a conversion reactor. The conversion reactor restricted the possibility of further investigation of the boiler and cannot represent the real case reaction kinetics. A kinetic simulation of the boiler can provide detailed wood pellet boiler combustion optimization.

(2) *Field Validation of Optimized System*: The system optimization will need to be validated from field monitoring. The current system can be modified based on the optimized parameters in this study and the system performance can be evaluated and compared.

(3) *Further System Optimization*: The current system optimization is a performance based optimization, which could lead to very high capital cost for customers. Therefore, further system optimization should balance cost and performance.

(4) *System Scale Up*: The current system optimization is only suitable for residential heating systems. It could be scaled up into larger systems, providing sufficient field data monitoring.

Refereneces

1 Ellabban, O., Abu-Rub, H., and Blaabjerg, F. 2014. Renewable energy resources: Current status, future prospects and their enabling technology. *Renewable and Sustainable Energy Reviews*, **39**, 748-764.

2 Jacobson, M. Z., Delucchi, M. A. 2011. Providing all global energy with wind, water, and solar power, Part I: Technologies, energy resources, quantities and areas of infrastructure, and materials. *Energy Policy*, **39**(3), 1154-1169.

3 Delucchi, M. A., Jacobson, M. Z. 2011. Providing all global energy with wind, water, and solar power, Part II: Reliability, system and transmission costs, and policies. *Energy Policy*, **39**(3), 1170-1190.

4 Goetzberger, A., Hoffmann, V. U. 2005. Photovoltaic solar energy generation (Vol. 112). Springer Science & Business Media, p1-2.

5 Weiss, W. W. 2003. Solar heating systems for houses: a design handbook for solar combisystems. Earthscan.

6 Fthenakis, V., Kim, H. C. 2009. Land use and electricity generation: A life-cycle analysis. *Renewable and Sustainable Energy Reviews*, **13**(6), 1465-1474.

7 U.S. Department of Energy, 2015. Top 10 things you didn't know about hydropower. <http://breakingenergy.com/2015/08/18/top-10-things-you-didnt-know-about-hydropower-3/>. [accessed January 3, 2017]

8 Bureau of Reclamation, Frequently Asked Questions, <https://www.usbr.gov/lc/hooverdam/faqs/powerfaq.html>. [accessed January 3, 2017]

9 Dickson, M. H., Fanelli, M. 2013. Geothermal energy: utilization and technology. Routledge, p2-6, ISBN 978-1-84407-184-5.

10 Field, C. B., Campbell, J. E., & Lobell, D. B. (2008). Biomass energy: the scale of the potential resource. *Trends in Ecology & Evolution*, **23**(2), 65-72.

11 Haq, Z. 2002. Biomass for electricity generation. Washington, DC: Energy Information Administration.

12 Parikka, M. 2004. Global biomass fuel resources. *Biomass and Bioenergy*, **27**(6), 613-620.

13 Verma, V. K., Bram, S., De Ruyck, J. 2009. Small scale biomass heating systems: standards, quality labelling and market driving factors–an EU outlook. *Biomass and bioenergy*, **33**(10), 1393-1402.

14 Vallios, I., Tsoutsos, T., Papadakis, G. 2009. Design of biomass district heating systems. *Biomass and Bioenergy*, **33**(4), 659-678.

15 REN21.2016. *Renewables 2016 Global Status Report*, ISBN 978-3-9818107-0-7, pp.17-18.

16 IEA World Energy Outlook, 2001 – 2016, < http://www.iea.org/publications/>

17 IEA Key World Energy Statistics, 2001 – 2006, < https://www.iea.org/publications/>

18 International Energy Agency, 2001, World Energy Outlook 2001 Insights, p312.

19 Panwar, N. L., Kaushik, S. C., and Kothari, S. 2011. Role of renewable energy sources in environmental protection: a review. *Renewable and Sustainable Energy Reviews*, **15**(3), 1513-1524.

20 Sims, R. E. H. 2004. Renewable energy: a response to climate change. *Solar Energy*, **76**(1), 9-17.

21 Mann, M., Spath, P. 2001. A life cycle assessment of biomass cofiring in a coal-fired power plant. *Clean Products and Processes*, **3**(2), 81-91.

22 Burkhardt III, J. J., Heath, G. A., Turchi, C. S. 2011. Life cycle assessment of a parabolic trough concentrating solar power plant and the impacts of key design alternatives. *Environmental science & technology*, **45**(6), 2457-2464.

23 Dincer, I. 2000. Renewable energy and sustainable development: a crucial review. *Renewable and Sustainable Energy Reviews*, **4**(2), 157-175.

24 IPCC, 2011, IPCC Special Report on Renewable Energy Sources and Climate Change Mitigation, p19, ISBN 978-92-9169-131-9. <https://www.ipcc.ch/pdf/special-reports/srren/SRREN_FD_SPM_final.pdf >. [accessed January 3, 2017]

25 Patel, M. R. 2005. Wind and solar power systems: design, analysis, and operation. CRC press, p3.

26 Brunekreef, B., Holgate, S. T. 2002. Air pollution and health. *The Lancet*, **360**(9341), 1233-1242.

27 Machol, B., Rizk, S. 2013. Economic value of US fossil fuel electricity health impacts. *Environment International*, **52**, 75-80.

28 Frondel, M., Ritter, N., Schmidt, C. M., Vance, C. 2010. Economic impacts from the promotion of renewable energy technologies: The German experience. *Energy Policy*, **38**(8), 4048-4056.

29 O'Sullivan, M., Edler, D., Ottmuller, M., Lehr, U., 2009. Gross Employment from Renewable Energy in Germany in the Year 2008 – A First Estimate, March 2009, Berlin.

30 Wei, M., Patadia, S., Kammen, D. M. 2010. Putting renewables and energy efficiency to work: How many jobs can the clean energy industry generate in the US? *Energy Policy*, **38**(2), 919-931.

31 McKendry, P. 2002. Energy production from biomass (part 1): overview of biomass. *Bioresource Technology*, **83**(1), 37-46.

32 Dong, L., Liu, H., Riffat, S. 2009. Development of small-scale and micro-scale biomass-fuelled CHP systems–A literature review. *Applied Thermal Engineering*, **29**(11), 2119-2126.

33 Regalbuto, J. R. 2009. Cellulosic biofuels—got gasoline? *Science*, **325**(5942), 822-824.

34 MacCarty, N., Ogle, D., Still, D., Bond, T., Roden, C. 2008. A laboratory comparison of the global warming impact of five major types of biomass cooking stoves. *Energy for Sustainable Development*, **12**(2), 56-65.

35 Gunaseelan, V. N. 1997. Anaerobic digestion of biomass for methane production: a review. *Biomass and Bioenergy*, **13**(1), 83-114.

36 Lehmann, J., Gaunt, J., Rondon, M. 2006. Bio-char sequestration in terrestrial ecosystems–a review. *Mitigation and Adaptation Strategies for Global Change*, **11**(2), 395-419.

37 Alila, S., Besbes, I., Vilar, M. R., Mutjé, P., Boufi, S. 2013. Non-woody plants as raw materials for production of microfibrillated cellulose (MFC): a comparative study. *Industrial Crops and Products*, **41**, 250-259.

38 A. Milbrandt, 2005. A Geographic Perspective on the Current Biomass Resource Availability in the United States, National Renewable Energy Laboratory. <http://www.afdc.energy.gov/pdfs/39181.pdf> [accessed January 13, 2017].

39 Brethauer, S., Wyman, C. E. 2010. Review: continuous hydrolysis and fermentation for cellulosic ethanol production. *Bioresource Technology*, **101**(13), 4862-4874.

40 Solomon, B. D., Barnes, J. R., Halvorsen, K. E. 2007. Grain and cellulosic ethanol: History, economics, and energy policy. *Biomass and Bioenergy*, **31**(6), 416-425.

41 Chandrasekaran, S. R., Hopke, P. K., Hurlbut, A., Newtown, M. 2013. Characterization of emissions from grass pellet combustion. *Energy & Fuels*, **27**(9), 5298-5306.

42 Abbasi, T., Abbasi, S. A. 2010. Biomass energy and the environmental impacts associated with its production and utilization. *Renewable and Sustainable Energy Reviews*, **14**(3), 919-937.

43 IPCC Climate Change 2014: Mitigation of Climate Change. <http://www.ipcc.ch/report/ar5/wg3/>. [accessed January 17, 2017]

44 International Energy Agency, Bioenergy Statistics. <https://www.iea.org/topics/renewables/subtopics/bioenergy/>. [accessed January 17, 2017]

45 Farrell, A. E., Plevin, R. J., Turner, B. T., Jones, A. D., O'hare, M., Kammen, D. M., 2006. Ethanol can contribute to energy and environmental goals. *Science*, **311**(5760), 506-508.

46 Henderson, S. B., Brauer, M., MacNab, Y. C., Kennedy, S. M. 2015. Three measures of forest fire smoke exposure and their associations with respiratory and cardiovascular health outcomes in a population-based cohort (Doctoral dissertation, University of British Columbia).

47 Lewtas, J. 2007. Air pollution combustion emissions: characterization of causative agents and mechanisms associated with cancer, reproductive, and cardiovascular effects. *Mutation Research/Reviews in Mutation Research*, **636**(1), 95-133.

48 Künzli, N., Kaiser, R., Medina, S., et al. 2000. Public-health impact of outdoor and traffic-related air pollution: a European assessment. *The Lancet*, **356**(9232), 795-801.

49 Guo, H., Lee, S., Chan, L. Y., Li, W. M. 2004. Risk assessment of exposure to volatile organic compounds in different indoor environments. *Environmental Research*, **94**(1), 57-66.

50 Ross, A. B., Jones, J. M., Chaiklangmuang, S., Pourkashanian, M., Williams, A., Kubica, K., et al. 2002. Measurement and prediction of the emission of pollutants from the combustion of coal and biomass in a fixed bed furnace. *Fuel*, **81**(5), 571-582.

51 Baxter, L. 2005. Biomass-coal co-combustion: opportunity for affordable renewable energy. *Fuel*, **84**(10), 1295-1302.

52 Fargione, J., Hill, J., Tilman, D., Polasky, S., Hawthorne, P. 2008. Land clearing and the biofuel carbon debt. *Science*, **319**(5867), 1235-1238.

53 Larson, E. D. 2006. A review of life-cycle analysis studies on liquid biofuel systems for the transport sector. *Energy for Sustainable Development*, **10**(2), 109-126.

54 ASTM D3172-13, Standard practice for proximate analysis of coal and coke. <https://www.astm.org/Standards/D3172.htm> [accessed January 23, 2017].

55 ASTM E 775-87 to ASTM E 778-87, Standard test method for sulfur, chlorine, carbon/hydrogen, and nitrogen.

56 Vassilev, S. V., Baxter, D., Andersen, L. K., Vassileva, C. G. 2010. An overview of the chemical composition of biomass. *Fuel*, **89**(5), 913-933.

57 Mohan, D., Pittman, C. U., Steele, P. H. 2006. Pyrolysis of wood/biomass for bio-oil: a critical review. *Energy & Fuels*, **20**(3), 848-889.

58 Obernberger, I., Brunner, T., Bärnthaler, G. 2006. Chemical properties of solid biofuels – significance and impact. *Biomass and Bioenergy*, **30**(11), 973-982.

59 Chandrasekaran, S. R., Hopke, P. K., Rector, L., Allen, G., Lin, L. 2012. Chemical composition of wood chips and wood pellets. *Energy & Fuels*, **26**(8), 4932-4937.

60 Van Loo, S., Koppejan, J., 2010, The Handbook of Biomass Combustion and Co-firing, pp.9, ISBN: 978-1-84971-104-3.

61 Gaur, S., Reed, T.B., 1995. An atlas of thermal data for biomass and other fuels. NREL/TB-433-7965, UC Category: 1310, DE95009212. eq.9.1, p9-2.

62 McKendry, P. 2002. Energy production from biomass (part 2): conversion technologies. *Bioresource Technology*, **83**(1), 47-54.

63 Angrisani, G., Bizon, K., Chirone, R., Continillo, G., Fusco, G., Lombardi, S., et al. 2013. Development of a new concept solar-biomass cogeneration system. *Energy Conversion and Management*, **75**, 552-560.

64 Yaman, S. 2004. Pyrolysis of biomass to produce fuels and chemical feedstocks. *Energy Conversion and Management*, **45**(5), 651-671.

65 Biomass gasifier for thermal and power applications. <http://www.teriin.org/technology/biomass-gasifier> [accessed January 26, 2017]

66 Dasappa, S., Paul, P. J., Mukunda, H. S., Rajan, N. K. S., Sridhar, G., Sridhar, H. V. 2004. Biomass gasification technology–a route to meet energy needs. *Current Science*, **87**(7), 908-916.

67 Kshirsagar, M. P., Kalamkar, V. R. 2014. A comprehensive review on biomass cookstoves and a systematic approach for modern cookstove design. *Renewable and Sustainable Energy Reviews*, **30**, 580-603.

68 Features and options of the best wood pellet stoves. <http://www.brighthub.com/environment/green-living/articles/73340.aspx > [accessed January 30, 2017].

69 Why catalytic combusters? <http://www.woodstove.com/pages/pdffiles/why_cats.pdf> [accessed January 30, 2017].

70 Eruheat: log biomass boilers, <http://www.euroheat.co.uk/Homes/149/Log-Biomass-Boilers.html>; Eco Heat & Power Ltd., Fröling T4 wood chip boilers, <http://www.ecoheat.co.uk/biomass_wood-chip-boilers.php>; TARM BiOMASS, Fröling P4 wood pellet boiler, <http://woodboilers.com/froling-p4-wood-pellet-boiler.html>. [accessed January 30, 2017]

71 Technical assessment of grass pellets as boiler fuel in Vermont. Vermont Grass Energy Partnership, January 2011, Final Report. <http://www.biomasscenter.org/images/stories/grasspelletrpt_0111.pdf>, [accessed January 30, 2017].

72 Gilbe, C., Ohman, M., Lindström, E., Boström, D., Backman, R., Samuelsson, R., et al. 2008. Slagging characteristics during residential combustion of biomass pellets. *Energy & Fuels*, **22**(5), 3536-3543.

73 United States Environmental Protection Agency, NAAQS Table. <https://www.epa.gov/criteria-air-pollutants/naaqs-table> [accessed January 30, 2017].

74 Fact sheet: summary of requirements for wood-fired hydronic heaters, EPA's air rules for residential wood heaters. <https://www.epa.gov/residential-wood-heaters/fact-sheet-summary-requirements-wood-fired-hydronic-heaters> [accessed January 30, 2017].

75 United States Environmental Protection Agency, Compliance requirements for residential wood heaters <https://www.epa.gov/residential-wood-

heaters/compliance-requirements-residential-wood-heaters> [accessed January 30, 2017]

76 Fiedler, F. 2004. The state of the art of small-scale pellet-based heating systems and relevant regulations in Sweden, Austria and Germany. *Renewable and Sustainable Energy Reviews*, **8**(3), 201-221.

77 Alessandro Guercio, La sostenibilità energetica nel processo di produzione del Pellet, Pellet Day, 2015. <http://www.forlener.it/docs/forlener%202015/Produzione%20sostenibile%20del%20pellet%20-%20Guercio.pdf> [accessed January 31, 2017]

78 Hansen, M. T., Jein, A. R., Hayes, S., Bateman, P. 2009. English handbook for wood pellet combustion. Europe: National Energy Foundation.

79 Kuokkanen, M. J., Vilppo, T., Kuokkanen, T., Stoor, T., Niinimäki, J. 2011. Additives in wood pellet production–a pilot-scale study of binding agent usage. *BioResources*, **6**(4), 4331-4355.

80 Pellet Fuels Institute Standard Specification for Residential/Commercial Densified Fuel, 2011. <http://www.weedcenter.org/cig/docs/PFI-Standard-Specification-November-2011.pdf>. [accessed January 31, 2017]

81 García-Maraver, A., Popov, V., Zamorano, M. 2011. A review of European standards for pellet quality. *Renewable Energy*, **36**(12), 3537-3540.

82 Published standard. CEN/TS 14588 CEN/TC 335. Solid biofuels. Terminology, definitions and descriptions; 2004.

83 Yang, H., Yan, R., Chen, H., Lee, D. H., Zheng, C. 2007. Characteristics of hemicellulose, cellulose and lignin pyrolysis. *Fuel*, **86**(12), 1781-1788.

84 Franco, C., Pinto, F., Gulyurtlu, I., Cabrita, I. 2003. The study of reactions influencing the biomass steam gasification process. *Fuel*, **82**(7), 835-842.

85 North Carolina State University, MAE 406, Course material. <https://www.mae.ncsu.edu/eckerlin/courses/mae406/chapter3.pdf> [accessed February 2, 2017].

86 Rika Pellet Stoves, <http://www.rika.at/en/B2C/>.

87 Pellergy Alpha Wood Pellet Boiler, <http://www.pellergy.com/pellergy-alpha-wood-pellet-boiler/>.

88 Nussbaumer, T. 2003. Combustion and co-combustion of biomass: fundamentals, technologies, and primary measures for emission reduction. *Energy & Fuels*, **17**(6), 1510-1521.

89 Lo¨fgren B, Windesta˚ l B. Prestandatest av Pelletsbra¨nnare. Konsumentverket/A¨ fab 2001; 43.

90 AFAB (UK) Ltd., Technology and function with pellet heat. <http://www.afabinfo.com/uk_ltd/pellets_technology_and_function.php> [accessed February 6, 2017].

91 Chandrasekaran, S. R., Laing, J. R., Holsen, T. M., Raja, S., Hopke, P. K. 2011. Emission characterization and efficiency measurements of high-efficiency wood boilers. *Energy & Fuels*, **25**(11), 5015-5021.

92 Carvalho, L., Wopienka, E., Pointner, C., Lundgren, J., Verma, V. K., Haslinger, W., et al. 2013. Performance of a pellet boiler fired with agricultural fuels. *Applied Energy*, **104**, 286-296.

93 Verma, V. K., Bram, S., Delattin, F., De Ruyck, J. 2013. Real life performance of domestic pellet boiler technologies as a function of operational loads: A case study of Belgium. *Applied Energy*, **101**, 357-362.

94 Verma, V. K., Bram, S., Delattin, F., Laha, P., Vandendael, I., Hubin, A., et al. 2012. Agro-pellets for domestic heating boilers: Standard laboratory and real life performance. *Applied Energy*, **90**(1), 17-23.

95 Lajili, M., Jeguirim, M., Kraiem, N., Limousy, L. 2015. Performance of a household boiler fed with agropellets blended from olive mill solid waste and pine sawdust. *Fuel*, **153**, 431-436.

96 Žandeckis, A., Timma, L., Blumberga, D., Rochas, C., Rošā, M. 2013. Solar and pellet combisystem for apartment buildings: Heat losses and efficiency improvements of the pellet boiler. *Applied Energy*, **101**, 244-252.

97 Carlon, E., Schwarz, M., Golicza, L., Verma, V. K., Prada, A., Baratieri, M., et al. 2015. Efficiency and operational behaviour of small-scale pellet boilers installed in residential buildings. *Applied Energy*, **155**, 854-865.

98 EN 303-5 heating boilers – Part 5: heating boilers for solid fuels, manually and automatically stoked, nominal heat output of up to 500 kW – terminology, requirements, testing and marking; 2012.

99 CSA B415.1, 2009. Performance testing of solid-fuel-burning heating appliances. Canadian Standards Association, Canada.

100 CleaverBrooks, The impact of excess air on efficiency. <https://imgv2-2-f.scribdassets.com/img/document/199568911/original/e3024aee60/1466546463> [accessed February 6, 2017].

101 Johansson, L. S., Leckner, B., Gustavsson, L., Cooper, D., Tullin, C., Potter, A. 2004. Emission characteristics of modern and old-type residential boilers fired with wood logs and wood pellets. *Atmospheric Environment*, **38**(25), 4183-4195.

102 Johansson, L. S., Tullin, C., Leckner, B., Sjövall, P. 2003. Particle emissions from biomass combustion in small combustors. *Biomass and Bioenergy*, **25**(4), 435-446.

103 Sippula, O., Hytönen, K., Tissari, J., Raunemaa, T., & Jokiniemi, J. 2007. Effect of wood fuel on the emissions from a top-feed pellet stove. *Energy & Fuels*, **21**(2), 1151-1160.

104 Olsson, M., Kjällstrand, J. 2004. Emissions from burning of softwood pellets. *Biomass and Bioenergy*, **27**(6), 607-611.

105 Dias, J., Costa, M., Azevedo, J. L. T. 2004. Test of a small domestic boiler using different pellets. *Biomass and Bioenergy*, **27**(6), 531-539.

106 Win, K. M., Persson, T., Bales, C. 2012. Particles and gaseous emissions from realistic operation of residential wood pellet heating systems. *Atmospheric Environment*, **59**, 320-327.

107 Lamberg, H., Sippula, O., Tissari, J., Jokiniemi, J. 2011. Effects of air staging and load on fine-particle and gaseous emissions from a small-scale pellet boiler. *Energy & Fuels*, **25**(11), 4952-4960.

108 Schmidl, C., Luisser, M., Padouvas, E., Lasselsberger, L., Rzaca, M., Ramirez-Santa Cruz, et al. 2011. Particulate and gaseous emissions from manually and automatically fired small scale combustion systems. *Atmospheric Environment*, **45**(39), 7443-7454.

109 Rabaçal, M., Fernandes, U., Costa, M. 2013. Combustion and emission characteristics of a domestic boiler fired with pellets of pine, industrial wood wastes and peach stones. *Renewable Energy*, **51**, 220-226.

110 Roy, M. M., Dutta, A., Corscadden, K. 2013. An experimental study of combustion and emissions of biomass pellets in a prototype pellet furnace. *Applied Energy*, **108**, 298-307.

111 Bignal, K. L., Langridge, S., Zhou, J. L. (2008). Release of polycyclic aromatic hydrocarbons, carbon monoxide and particulate matter from biomass combustion

in a wood-fired boiler under varying boiler conditions. *Atmospheric Environment*, **42**(39), 8863-8871.

112 Hedman, B., Näslund, M., Marklund, S. 2006. Emission of PCDD/F, PCB, and HCB from combustion of firewood and pellets in residential stoves and boilers. *Environmental Science & Technology*, **40**(16), 4968-4975.

113 Hollands, K. G. T., Lightstone, M. F. 1989. A review of low-flow, stratified-tank solar water heating systems. *Solar Energy*, **43**(2), 97-105.

114 Han, Y. M., Wang, R. Z., & Dai, Y. J. 2009. Thermal stratification within the water tank. *Renewable and Sustainable Energy Reviews*, **13**(5), 1014-1026.

115 Nelson, J. E. B., Balakrishnan, A. R., Murthy, S. S. 1999. Parametric studies on thermally stratified chilled water storage systems. *Applied Thermal Engineering*, **19**(1), 89-115.

116 Consul, R., Rodrıguez, I., Perez-Segarra, C. D., Soria, M. 2004. Virtual prototyping of storage tanks by means of three-dimensional CFD and heat transfer numerical simulations. *Solar Energy*, **77**(2), 179-191.

117 Johannes, K., Fraisse, G., Achard, G., Rusaouën, G. 2005. Comparison of solar water tank storage modelling solutions. *Solar Energy*, **79**(2), 216-218.

118 Lavan, Z., Thompson, J. 1977. Experimental study of thermally stratified hot water storage tanks. *Solar Energy*, **19**(5), 519-524.

119 Eames, P. C., Norton, B. 1998. The effect of tank geometry on thermally stratified sensible heat storage subject to low Reynolds number flows. *International Journal of Heat and Mass Transfer*, **41**(14), 2131-2142.

120 Haller, M. Y., Mojic, I., Frank, E., Kaufmann, M., Lötscher, L., Podhradsky, J., et al. 2014. Disturbance of stratification caused by direct horizontal inlets into a water storage tank. In *EuroSun 2014 Conference*, ISES Europe, Aix-les-Bains, France, Sept (pp. 16-19).

121 García-Marí, E., Gasque, M., Gutiérrez-Colomer, R. P., Ibáñez, F., González-Altozano, P. 2013. A new inlet device that enhances thermal stratification during charging in a hot water storage tank. *Applied Thermal Engineering*, **61**(2), 663-669.

122 Altuntop, N., Arslan, M., Ozceyhan, V., Kanoglu, M. 2005. Effect of obstacles on thermal stratification in hot water storage tanks. *Applied Thermal Engineering*, **25**(14), 2285-2298.

123 Erdemir, D., Altuntop, N. 2016. Improved thermal stratification with obstacles placed inside the vertical mantled hot water tanks. *Applied Thermal Engineering*, **100**, 20-29.

124 Zachar, A., Farkas, I., Szlivka, F. 2003. Numerical analyses of the impact of plates for thermal stratification inside a storage tank with upper and lower inlet flows. *Solar Energy*, **74**(4), 287-302.

125 Nelson, J. E. B., Balakrishnan, A. R., & Murthy, S. S. 1999. Parametric studies on thermally stratified chilled water storage systems. *Applied Thermal Engineering*, **19**(1), 89-115.

126 Shyu, R. J., Lin, J. Y., Fang, L. J. 1989. Thermal analysis of stratified storage tanks. *Journal of Solar Energy Engineering*, **111**(1), 54-61.

127 Armstrong, P., Ager, D., Thompson, I., McCulloch, M. 2014. Improving the energy storage capability of hot water tanks through wall material specification. *Energy*, **78**, 128-140.

128 Cristofari, C., Notton, G., Poggi, P., Louche, A. 2003. Influence of the flow rate and the tank stratification degree on the performances of a solar flat-plate collector. *International Journal of Thermal Sciences*, **42**(5), 455-469.

129 Wu, L., Bannerot, R. B. 1987. Experimental study of the effect of water extraction on thermal stratification in storage. In Solar Engineering, *Proc. of ASME-JSME-JSES Solar Energy Conf* (pp. 445-451).

130 Adams, D. A., Miller, J. A. 1994. A coefficient to characterize mixing in solar water storage tanks. *Transactions of the ASME Journal of Solar Energy Engineering*, **116**, 94–99.

131 Fernandez-Seara, J., Uhía, F. J., Sieres, J. 2007. Experimental analysis of a domestic electric hot water storage tank. Part I: Static mode of operation. *Applied Thermal Engineering*, **27**(1), 129-136.

132 Fernandez-Seara, J., Uhı, F. J., Sieres, J. 2007. Experimental analysis of a domestic electric hot water storage tank. Part II: dynamic mode of operation. *Applied Thermal Engineering*, **27**(1), 137-144.

133 Rosen, M. A., Dincer, I. 2003. Exergy methods for assessing and comparing thermal storage systems. *International Journal of Energy Research*, **27**(4), 415-430.

134 Siegenthaler, J., 2016. Hydronics for high efficiency biomass boilers. Renewable Heat NY Hydronics Training.

<https://www.google.com/url?sa=t&rct=j&q=&esrc=s&source=web&cd=1&cad=rja&uact=8&ved=0ahUKEwjt8p64lIPSAhVBSiYKHRT0DOwQFggaMAA&url=https%3A%2F%2Fwww.nyserda.ny.gov%2F-%2Fmedia%2FFiles%2FEERP%2FRenewables%2FBiomass%2Fbiomass-hydronics-training.pdf&usg=AFQjCNEnCDyP0v_-ujF3x7OUd7fyFHU-cA&bvm=bv.146496531,d.eWE > [accessed February 9, 2017].

135 VarioWIN, Windhager Danmark. <http://www.windhager.dk/wp-content/uploads/2015/09/variowin.pdf> [accessed February 9, 2017].

136 Weather Underground. https://www.wunderground.com/ [accessed March 28, 2017]

137 EPA Conditional Test Method-039. https://www3.epa.gov/ttnemc01/ctm/ctm-039.pdf [accessed March 28, 2017]

138 Telmo, C., Lousada, J. 2011. Heating values of wood pellets from different species. *Biomass and Bioenergy*, **35**(7), 2634-2639.

139 Sheng, C., Azevedo, J. L. T. 2005. Estimating the higher heating value of biomass fuels from basic analysis data. *Biomass and Bioenergy*, **28**(5), 499-507.

140 Huang, J., Hopke, P. K., Choi, H. D., Laing, J. R., Cui, H., Zananski, T. J., et al. 2011. Mercury (Hg) emissions from domestic biomass combustion for space heating. *Chemosphere*, **84**(11), 1694-1699.

141 McCutcheon, S.C., Martin, J.L, Barnwell, T.O. Jr., 1993. Handbook of Hydrology, McGraw-Hill, New York, NY, p11.3.

142 Mann, H.B., 1945. Nonparametric tests against trend, Econometrica, **13**, 245–259

143 Kendall, M.G., 1975. Rank Correlation Methods. Griffin, London, UK.

144 Tschamber, V., Trouvé, G., Leyssens, G., Le-Dreff-Lorimier, C., Jaffrezo, J. L., Genevray, P., et al. 2016. Domestic Wood Heating Appliances with Environmental High Performance: Chemical Composition of Emission and Correlations between Emission Factors and Operating Conditions. *Energy and Fuels*, **30**(9), 7241-7255.

145 Zhou, J., Masutani, S. M., Ishimura, D. M., Turn, S. Q., Kinoshita, C. M. 2000. Release of fuel-bound nitrogen during biomass gasification. *Industrial and Engineering Chemistry Research*, **39**(3), 626-634.

146 ASME Power Test. Steam Generating Units (ASME PTC 4.1). 1965; ASME, New York.

147 Olsson, M., Kjällstrand, J. 2006. Low emissions from wood burning in an ecolabelled residential boiler. *Atmospheric Environment*, **40**(6), 1148-1158.

148 Win, K. M., Persson, T., Bales, C. 2012. Particles and gaseous emissions from realistic operation of residential wood pellet heating systems. *Atmospheric Environment*, **59**, 320-327.

149 Boman, C., Pettersson, E., Westerholm, R., Boström, D., Nordin, A. 2011. Stove performance and emission characteristics in residential wood log and pellet combustion, part 1: pellet stoves. *Energy and Fuels*, **25**(1), 307-314.

150 Ragland, K. W., Aerts, D. J., Baker, A. J. 1991. Properties of wood for combustion analysis. *Bioresource Technology*, **37**(2), 161-168.

151 Obaidullah, M., Bram, S., Verma, V. K., De Ruyck, J. 2012. A review on particle emissions from small scale biomass combustion. *International Journal of Renewable Energy Research (IJRER)*, **2**(1), 147-159.

152 Tissari, J. Fine particle emissions from residential wood combustion. 2008, Doctoral Thesis, University of Kuopio, Kuopio

153 Qiu, G. 2013. Testing of flue gas emissions of a biomass pellet boiler and abatement of particle emissions. *Renewable Energy*, **50**, 94-102.

154 Fernandes, U., Costa, M. 2012. Particle emissions from a domestic pellets-fired boiler. *Fuel Processing Technology*, **103**, 51-56.

155 Wiinikka, H., Gebart, R. 2005. The influence of fuel type on particle emissions in combustion of biomass pellets. *Combustion Science and Technology*, **177**(4), 741-763.

156 Tissari, J., Lyyränen, J., Hytönen, K., Sippula, O., Tapper, U., Frey, A., et al. 2008. Fine particle and gaseous emissions from normal and smouldering wood combustion in a conventional masonry heater. *Atmospheric Environment*, **42**(34), 7862-7873.

157 Limousy, L., Jeguirim, M., Dutournié, P., Kraiem, N., Lajili, M., Said, R. 2013. Gaseous products and particulate matter emissions of biomass residential boiler fired with spent coffee grounds pellets. *Fuel*, **107**, 323-329.

158 Hedberg, E., Kristensson, A., Ohlsson, M., Johansson, C., Johansson, P. Å., Swietlicki, E., et al. 2002. Chemical and physical characterization of emissions from birch wood combustion in a wood stove. *Atmospheric Environment*, **36**(30), 4823-4837.

159 Mavrocordatos, D., Kaegi, R., Schmatloch, V. 2002. Fractal analysis of wood combustion aggregates by contact mode atomic force microscopy. *Atmospheric Environment*, **36**(36), 5653-5660.

160 Baernthaler, G., Zischka, M., Haraldsson, C., Obernberger, I. 2006. Determination of major and minor ash-forming elements in solid biofuels. *Biomass and Bioenergy*, **30**(11), 983-997.

161 Khalil, M. A. K., Rasmussen, R. A. 2003. Tracers of wood smoke. *Atmospheric Environment*, **37**(9), 1211-1222.

162 Schauer, J. J., Kleeman, M. J., Cass, G. R., Simoneit, B. R. 2001. Measurement of emissions from air pollution sources. 3. C1− C29 organic compounds from fireplace combustion of wood. *Environmental Science & Technology*, **35**(9), 1716-1728.

163 Fine, P. M., Cass, G. R., Simoneit, B. R. 2001. Chemical characterization of fine particle emissions from fireplace combustion of woods grown in the northeastern United States. *Environmental Science & Technology*, **35**(13), 2665-2675.

164 Tafur-Marinos, J. A., Ginepro, M., Pastero, L., Torazzo, A., Paschetta, E., Fabbri, D., et al. 2014. Comparison of inorganic constituents in bottom and fly residues from pelletised wood pyro-gasification. *Fuel*, **119**, 157-162.

165 Bølling, A. K., Pagels, J., Yttri, K. E., Barregard, L., Sallsten, G., Schwarze, P. E., et al. 2009. Health effects of residential wood smoke particles: the importance of combustion conditions and physicochemical particle properties. *Particle and Fibre Toxicology*, **6**(1), 29.

166 McDonald, J. D., Zielinska, B., Fujita, E. M., Sagebiel, J. C., Chow, J. C., Watson, J. G. 2000. Fine particle and gaseous emission rates from residential wood combustion. *Environmental Science & Technology*, **34**(11), 2080-2091.

167 Fine, P. M., Cass, G. R., Simoneit, B. R. 2004. Chemical characterization of fine particle emissions from the wood stove combustion of prevalent United States tree species. *Environmental Engineering Science*, **21**(6), 705-721.

168 Menzie, C. A., Potocki, B. B., Santodonato, J. 1992. Exposure to carcinogenic PAHs in the environment. *Environmental Science & Technology*, **26**(7), 1278-1284.

169 Bhargava, A., Khanna, R. N., Bhargava, S. K., Kumar, S. 2004. Exposure risk to carcinogenic PAHs in indoor-air during biomass combustion whilst cooking in rural India. *Atmospheric Environment*, **38**(28), 4761-4767.

170 Simoneit, B. R., Schauer, J. J., Nolte, C. G., Oros, D. R., Elias, V. O., Fraser, M. P., et al. 1999. Levoglucosan, a tracer for cellulose in biomass burning and atmospheric particles. *Atmospheric Environment*, **33**(2), 173-182.

171 Fraser, M. P., Lakshmanan, K. 2000. Using levoglucosan as a molecular marker for the long-range transport of biomass combustion aerosols. *Environmental Science & Technology*, **34**(21), 4560-4564.

172 Simoneit, B. R. 2002. Biomass burning—a review of organic tracers for smoke from incomplete combustion. *Applied Geochemistry*, **17**(3), 129-162.

173 Saha, M., Togo, A., Mizukawa, K., Murakami, M., Takada, H., Zakaria, M. P., et al. 2009. Sources of sedimentary PAHs in tropical Asian waters: differentiation between pyrogenic and petrogenic sources by alkyl homolog abundance. *Marine Pollution Bulletin*, **58**(2), 189-200.

174 Volkman, J.K., Revill, A.T., Murray, A.P. Applications of biomarkers for identifying sources of natural and pollutant hydrocarbons in aquatic environments. In ACS Symposium Series; Washington, DC, 671: 110-132.

175 Han, Y. M., Wang, R. Z., Dai, Y. J. 2009. Thermal stratification within the water tank. *Renewable and Sustainable Energy Reviews*, **13**(5), 1014-1026.

176 Hariharan, K., Badrinarayana, K., Murthy, S. S., Murthy, M. K. 1991. Temperature stratification in hot-water storage tanks. *Energy*, **16**(7), 977-982.

177 Ievers, S., Lin, W. 2009. Numerical simulation of three-dimensional flow dynamics in a hot water storage tank. *Applied Energy*, **86**(12), 2604-2614.

178 Thermal storage vessel sizing, Homemicro Co, UK. <http://www.homemicro.co.uk/download/lzc_buffer.pdf> [accessed April 9, 2017]

179 Renewable Heat New York, Biomass Boiler Program Manual. <https://www.google.com/url?sa=t&rct=j&q=&esrc=s&source=web&cd=1&cad=rja&uact=8&ved=0ahUKEwiRgbmVu5nTAhUM2oMKHV0fBcoQFggaMAA&url=https%3A%2F%2Fwww.nyserda.ny.gov%2F-%2Fmedia%2FFiles%2FFO%2FCurrent-Funding-Opportunities%2FPON-3010%2F3010attg.pdf&usg=AFQjCNHaUK5h2gtHk3qA376ldwpmi51NwQ> p21 [accessed April 9, 2017]

180 Chaney, J., Liu, H., Li, J. 2012. An overview of CFD modelling of small-scale fixed-bed biomass pellet boilers with preliminary results from a simplified approach. *Energy Conversion and Management*, **63**, 149-156.

181 Zhang, X., Chen, Q., Bradford, R., Sharifi, V., Swithenbank, J. 2010. Experimental investigation and mathematical modelling of wood combustion in a moving grate boiler. *Fuel Processing Technology*, **91**(11), 1491-1499.

182 Eskilsson, D., Rönnbäck, M., Samuelsson, J., Tullin, C. 2004. Optimisation of efficiency and emissions in pellet burners. *Biomass and Bioenergy*, **27**(6), 541-546.

183 Collazo, J., Porteiro, J., Patino, D., Granada, E. 2012. Numerical modeling of the combustion of densified wood under fixed-bed conditions. *Fuel*, **93**, 149-159.

184 Collazo, J., Porteiro, J., Míguez, J. L., Granada, E., Gómez, M. A. 2012. Numerical simulation of a small-scale biomass boiler. *Energy Conversion and Management*, **64**, 87-96.

185 Brink, A., Kilpinen, P., Hupa, M. 2001. A simplified kinetic rate expression for describing the oxidation of volatile fuel-N in biomass combustion. *Energy & Fuels*, **15**(5), 1094-1099.

186 Ievers, S., Lin, W. 2009. Numerical simulation of three-dimensional flow dynamics in a hot water storage tank. *Applied Energy*, **86**(12), 2604-2614.

187 Hendron, R., and C. Engebrecht, 2009. Building America research benchmark definition. NREL-TP-550/47246. Golden, CO: National Renewable Energy Laboratory

188 Parker, D. S., Fairey, P. 2015. Estimating Daily Domestic Hot-Water Use in North American Homes. *ASHRAE Transactions*, **121**, 258.

189 Residential heat pump water heaters FTA – Appendix D: cold water inlet temperatures for selected U.S. locations. <http://www.gfxtechnology.com/WaterTemp.pdf> [accessed April 21, 2017]

Appendix – Detailed Simulation Construction Steps

This chapter presents the detailed step-by-step construction of the wood pellet heating system. The final flow sheet is shown in Figure 4-1.

The first thing to do for the simulation is to select property package, as shown below.

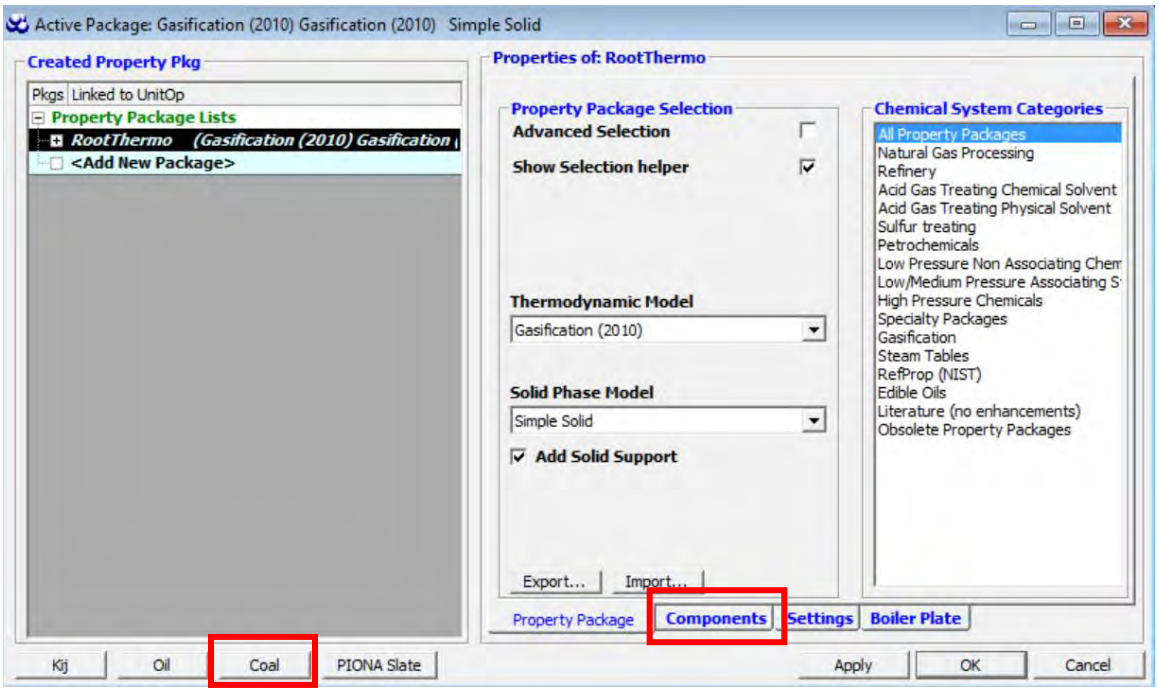

After selecting the property packages, the next step is to define the wood pellet fuel. Select “Coal” from the property selection panel to open the fuel characterization window, as shown below. Set the molecular weight at 10,000 and input the higher heating value of 19.1 MJ/kg based on our wood pellet fuel characterization results. The next step is to input the fuel compositions. The fractions of each component is shown in the table below. The total fractions will add to 100%. After input all the compounds, characterize the install the wood pellet fuel. The compound wood pellet will be available to use.

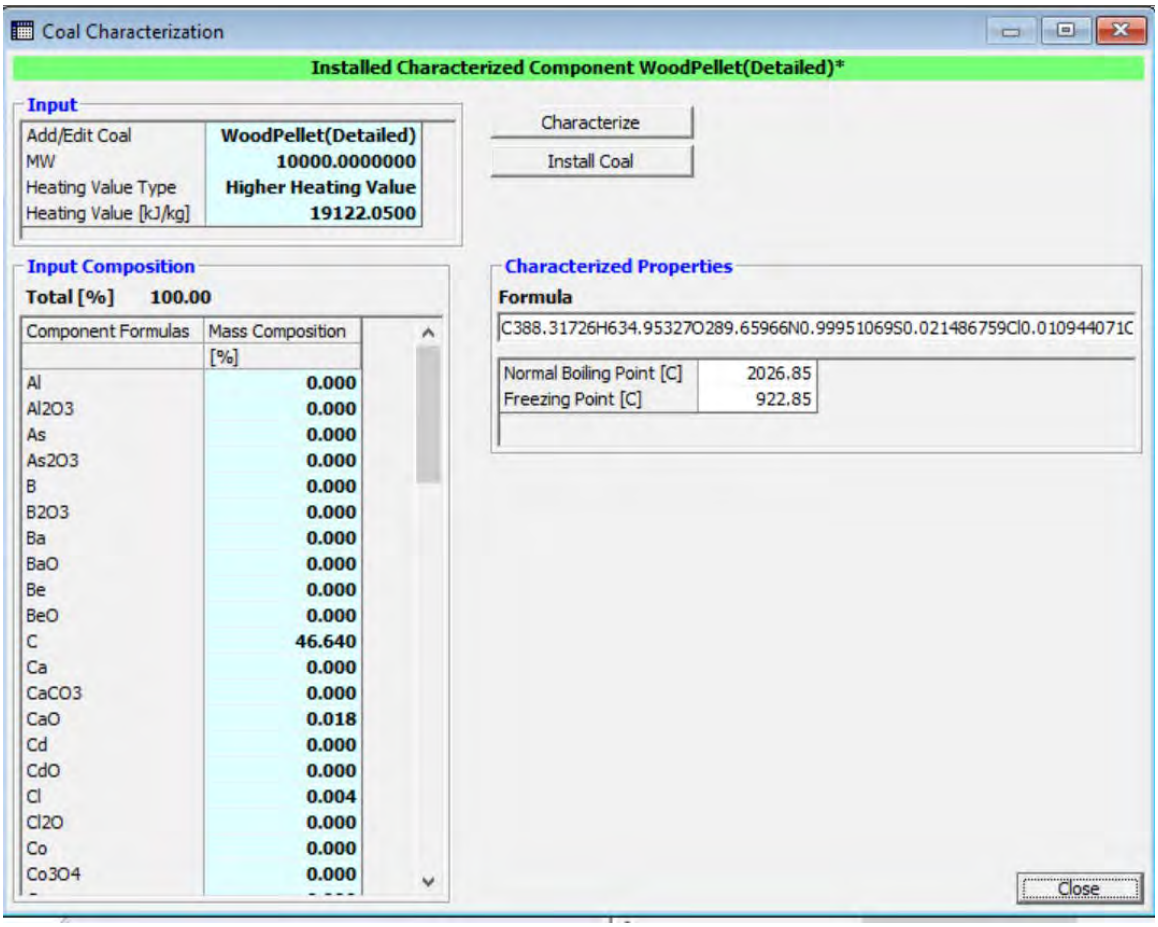

Compound	Percentage (%)
C	46.64
CaO	0.018
Cl	0.004
H	6.4
K_2O	0.464
N	0.14
Na_2O	0.08
O	46.23
S	0.007
SiO_2	0.018

After defining the wood pellet fuel, the next step is to add all the related components.

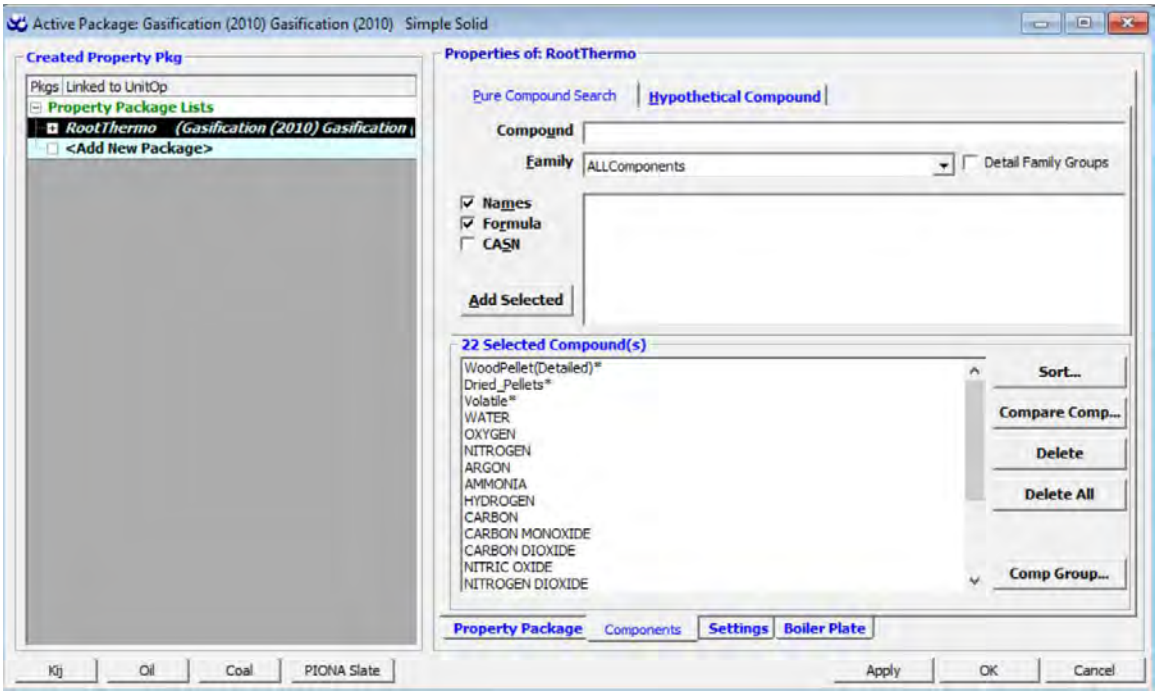

A total of 22 compounds were added: wood pellet, dried pellets, volatile, water, oxygen, nitrogen, argon, ammonia, hydrogen, carbon, carbon monoxide, carbon dioxide, nitric oxide, nitrogen dioxide, methane, benzene, calcium oxide, dipotassium oxide, magnesium oxide, disodium oxide, sulfur, and sulfur dioxide. The compound wood pellet has been defined previously and was added automatically after installation. Dried pellets and volatile are hypothetical compounds defined below.

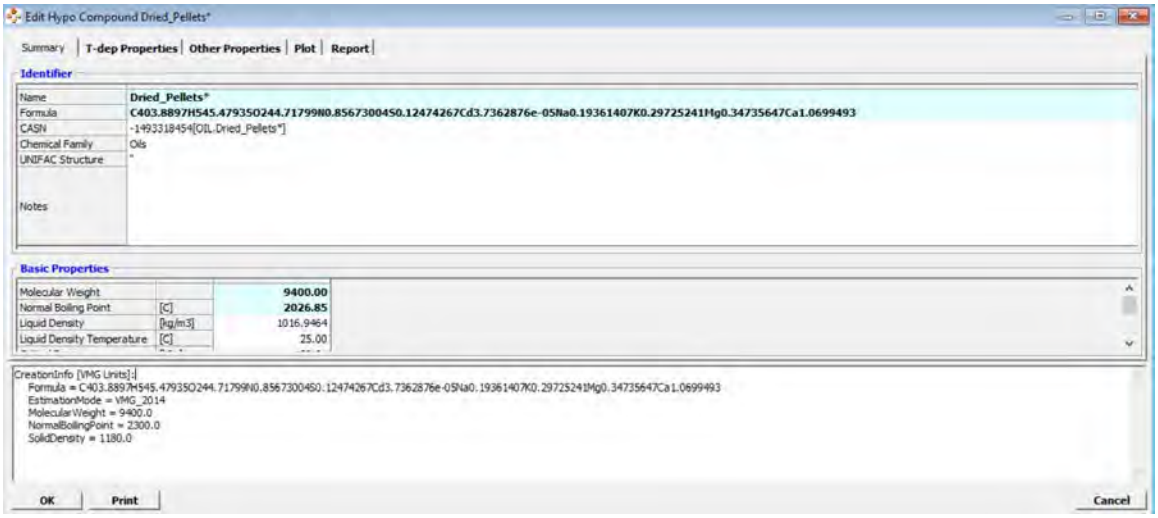

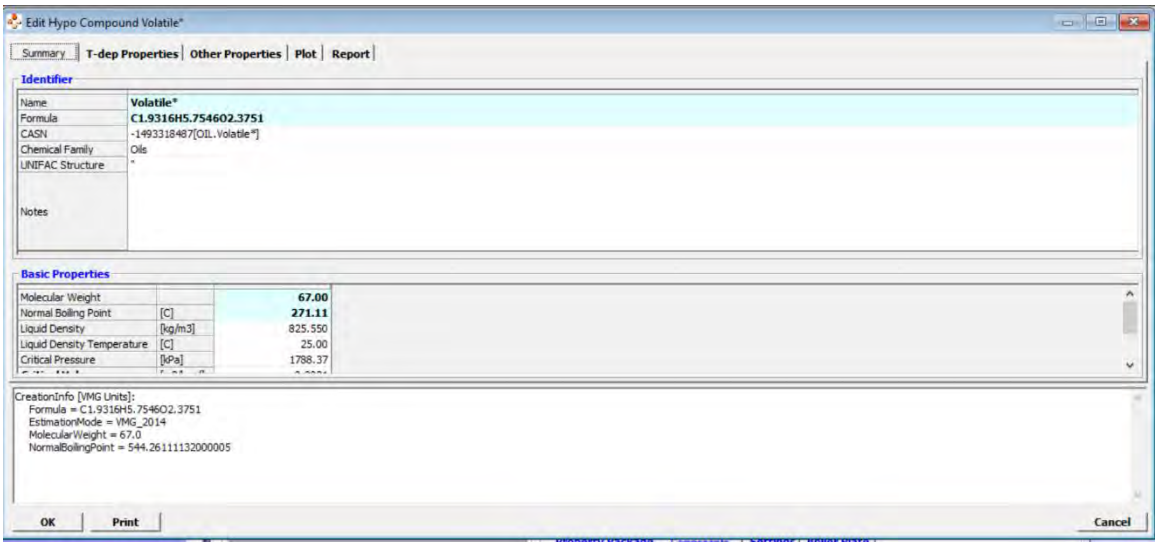

Now that all the compounds have been defined. The simulation flow sheet can be constructed. The feed stream wood pellet is defined as 100% wood pellet at 20 °C, and 1 atm pressure. The mass flow rate is set at 3.985 kg/h based on field data. The stream definition is shown below.

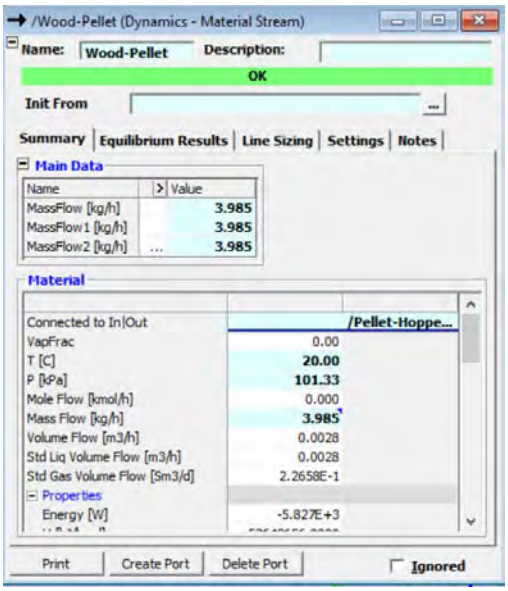

Another feed stream air is defined using the standard composition of air that it contains 20.947% oxygen, 78.084% nitrogen, 0.934% argon, and 0.033% carbon dioxide. The air supply is set at 25 °C and 1 atm. The volumetric flow rate is determined at 33.5885 m^3/h to produce a 10% oxygen content in the flue gas. The definition of the stream is shown below.

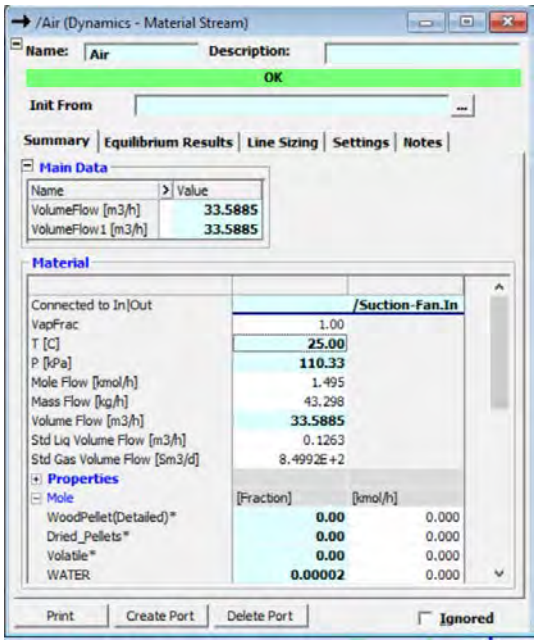

After both streams have been defined, the next step is to add the pump and valves to simulate the pellet hopper and auger. The settings for the pellet hopper, pellet auger, and the suction fan is shown below.

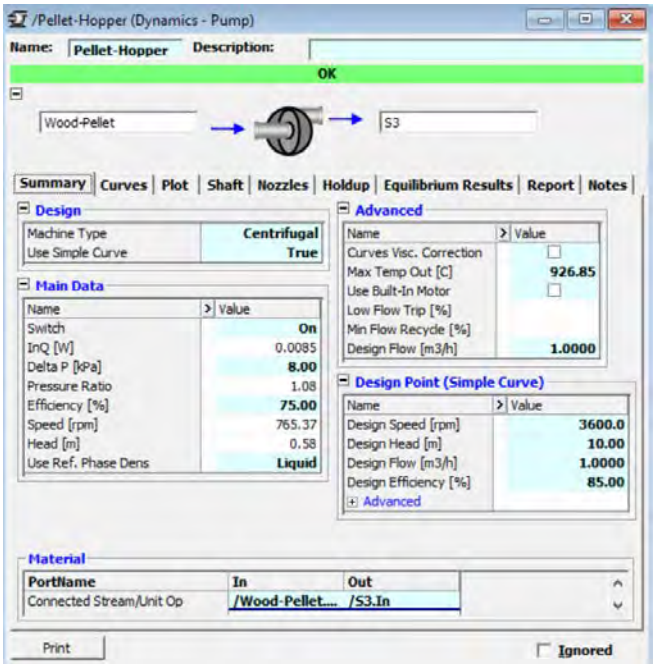

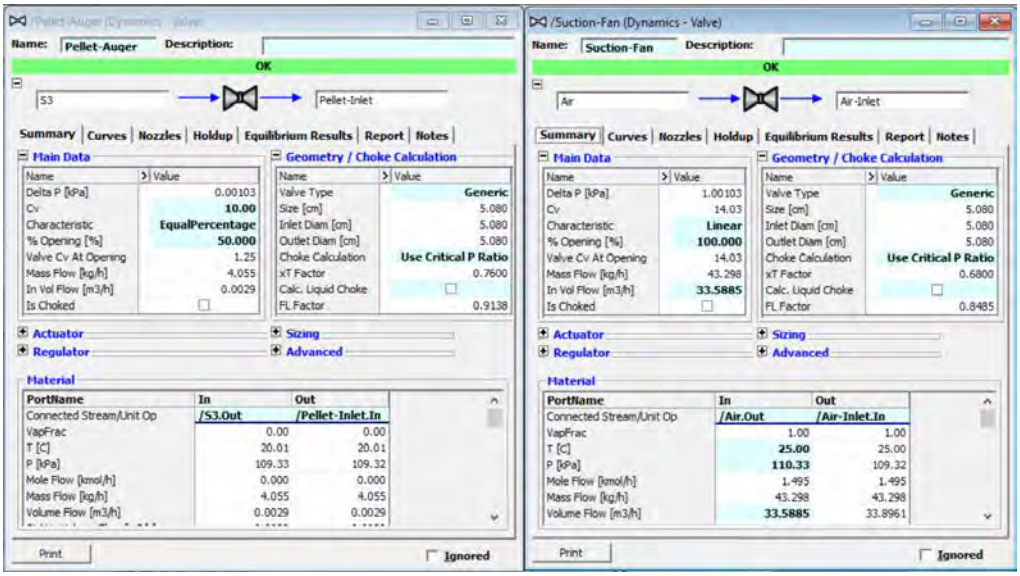

The next component is the air-fuel mixer. The mixer has 2 inlets and the branch angle is set to be 90 degree. The settings are shown in the figure below. The warning

message can be ignored because the mixer is an imaginary component that does not exist in real systems. The purpose of the mixer is to mix the wood pellet with supplied air into one stream before going into the reactor.

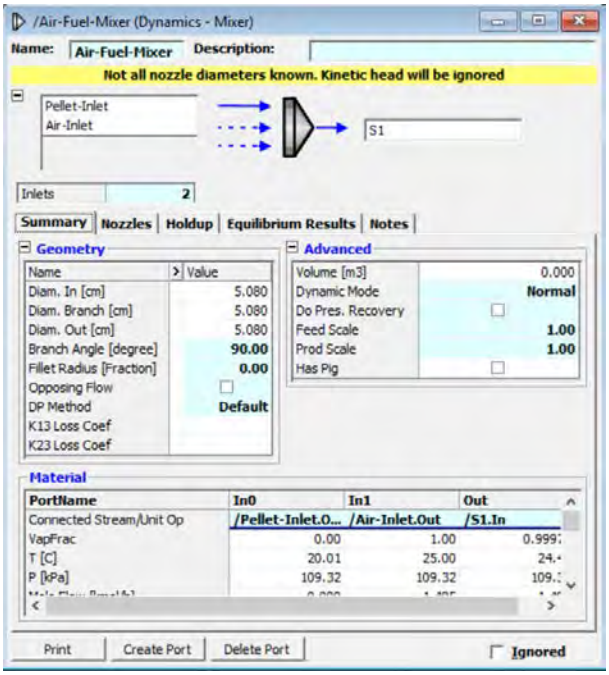

The next component is the conversion reactor, where a total of 14 reactions occurred. The details of the reactions and conversion factor for each reaction have been discussed from equations (4-1) to (4-15). Aside from that, the orientation of the reactor is set to be vertical with 90 degree inclination. The volume of the reactor is set to be 0.019 m^3 based on the estimation of the size of the combustion chamber of the wood pellet boiler used on site. The detailed information is shown below.

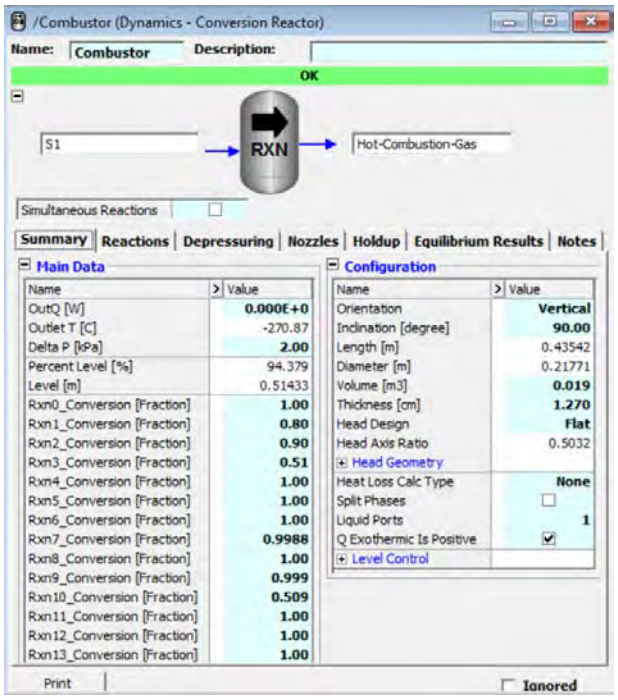

The next component is the fire tube heat exchanger. In the simulation, a shell and tube heat exchanger is selected. The combustion gas passes through the tube passage and water is flowing through the shell passage. There shell pressure drop is set to be 6 kPa and the heat transfer coefficient *UA* is set to be 38 W/K. Tube volume is estimated to be 0.019 m^3 and shell volume is 0.038 m^3 (provided by the manufacturer). The component is shown below. The warning message can be ignored when running the dynamic simulator.

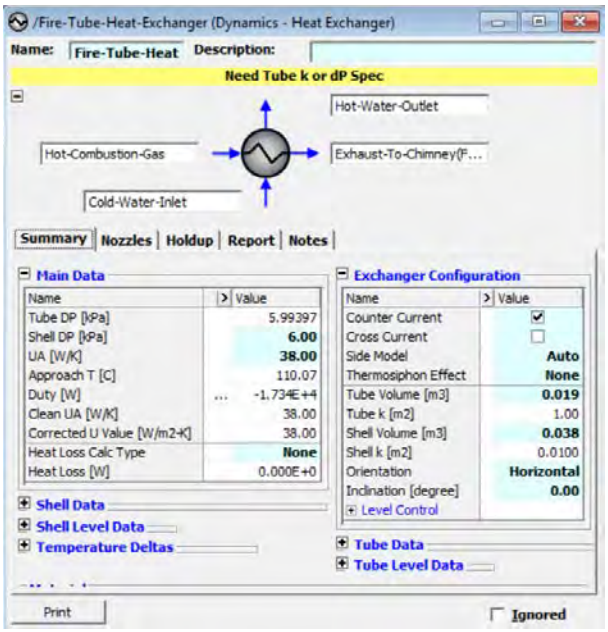

Therefore, the boiler simulation has been completed. The next component is the TES tank. The module selected is a pipe segment, as shown below. The heat loss from the tank surface is fixed at 4.5×10^{-5} W/cm^2/K. For the on-site system, there are two TES tanks connected in parallel given a total volume of 238 gallons. The simulation adopts the same aspect ratio as the on-site installation but using only one TES tank. The length of the pipe is set to be 1.37554 m, inner diameter is 91.7025 cm, outer diameter is 94.425 cm, and the roughness is set to be 0.0003 cm. The tank is vertical so the elevation of the top of the pipe is set to be equal to the length of pipe. The component is shown below.

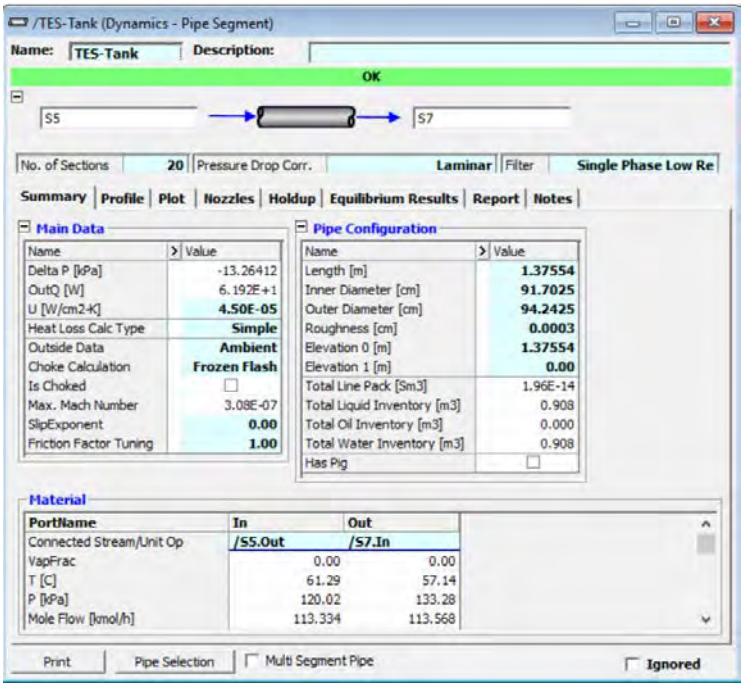

There is one mixer at the bottom of the pipe segment and one splitter at the top. The mixer and splitter provide extra connections for the pipe segment to act as a 4-pipe configuration in a wood pellet boiler heating system. Consider the difference in pipe diameter and the TES tank diameter, the mixer and splitter configurations are shown in the figure below.

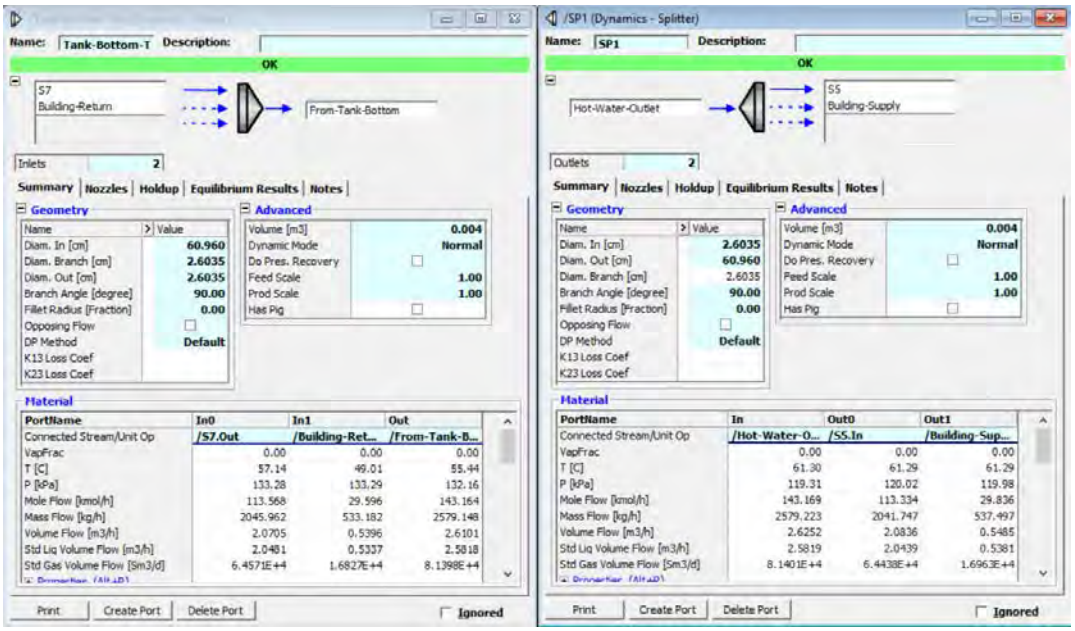

The boiler circulator is the pump that moves the water into the boiler for heating. It is a centrifugal pump with design speed of 2400 rpm, design heat of 10 m, design flow rate of 5 m^3/h, and design efficiency of 85%. The pump is set at 1800 rpm at 80% efficiency. The detailed information for the pump is shown below.

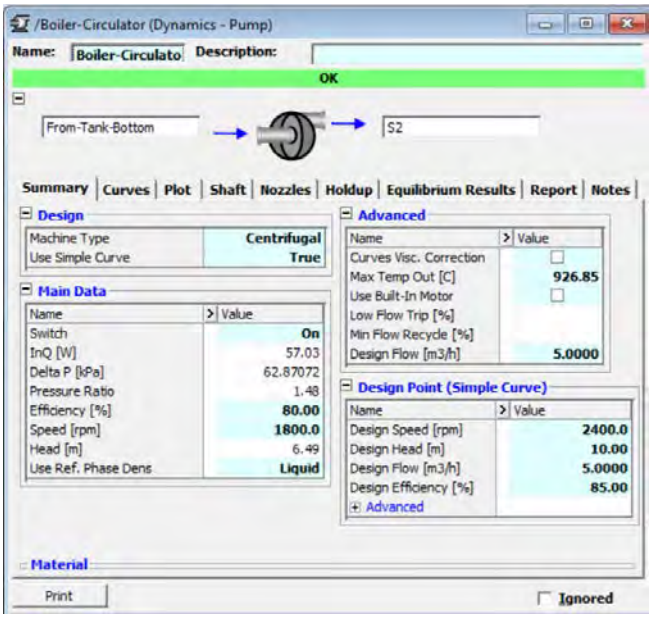

The control valve and the controller works together to achieve a set flow rate of 2.6119 m^3/h (or 11.5 gpm) based on field data. The control valve has a *C*v of 50 and the characteristic is selected with EqualPercentage. The control valve size is chosen based on the actual piping size. The details for the boiler loop flow control valve and the controller is shown below.

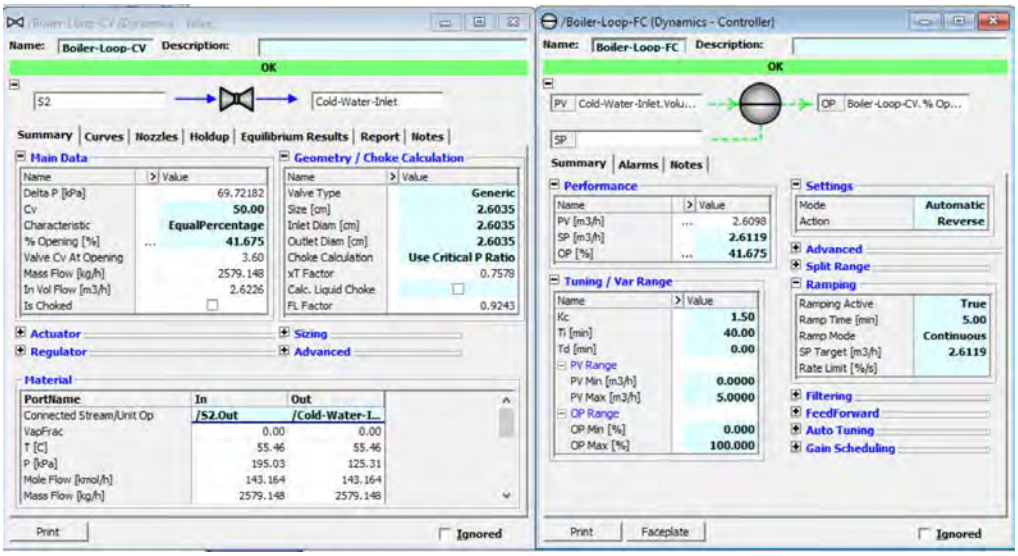

In the boiler loop, the building circulator provides the head loss in the building loop. The design flow rate is much smaller than boiler circulator. The pump is also a centrifugal pump with design speed of 2400 rpm, design head of 10 m, design flow 1 m^3/h, and design efficiency of 85%. The component is shown in the figure below.

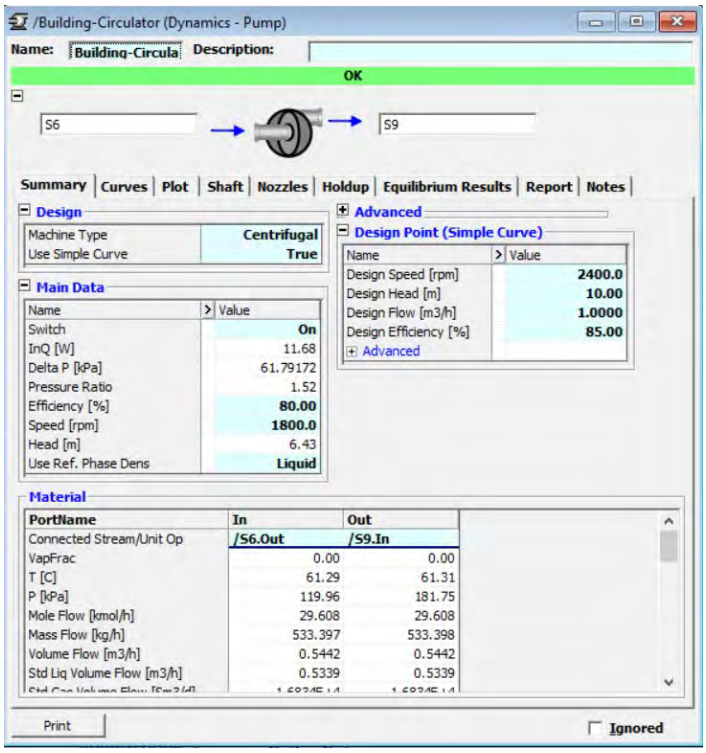

The building loop flow rate is controlled by the building loop control valve and the controller. The flow rate is controlled at 0.5428 m^3/h (or 2.39 gpm). The controller settings and the valve settings are shown in the figure below.

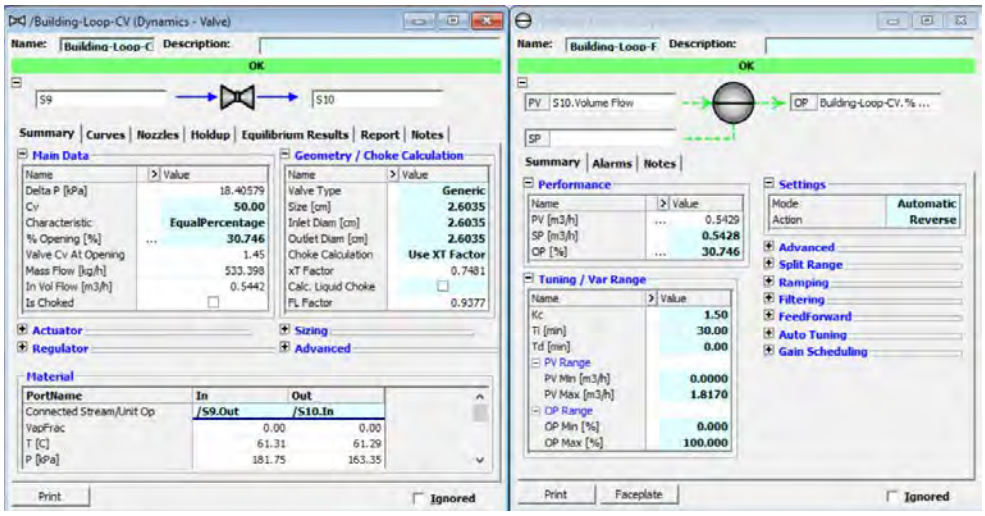

The building is represented by a cooler. The cooler has a constant heat demand set at 8.2 kW and pressure drop of 30 kPa. The cooler volume is set at 1 m^3. The detail information for the cooler is shown in the figure below.

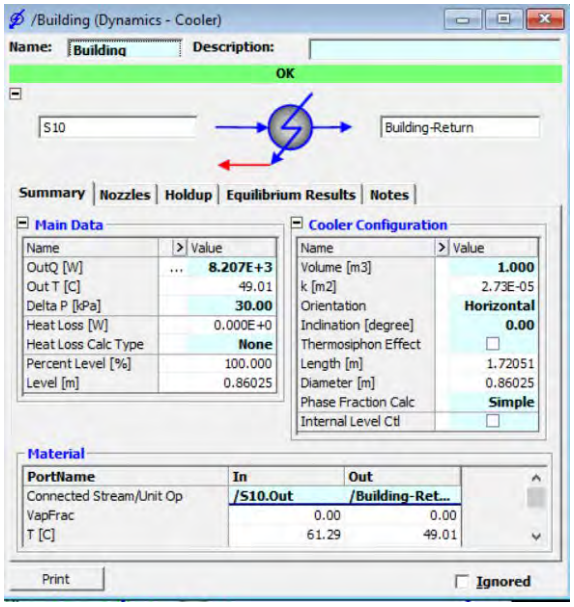

In the building loop, there is a makeup flow. It is important to have this flow to keep the system running stable without causing any pressure and temperature. The makeup flow is set at 120 kPa pressure. The flow temperature cannot be set but needs to be specified at an initial value. The temperature will change during simulation. The details of the makeup flow is shown in the figure below.

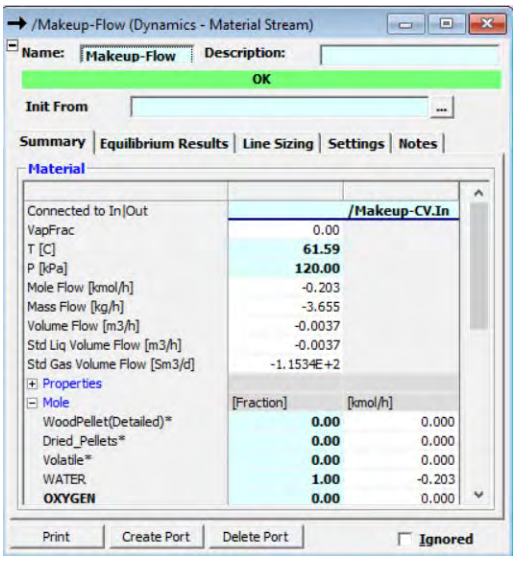

The makeup flow passes through the makeup control valve. The valve has a small C_v of 1 and is set to be a linear valve at 50% opening. The details are shown in the figure below.

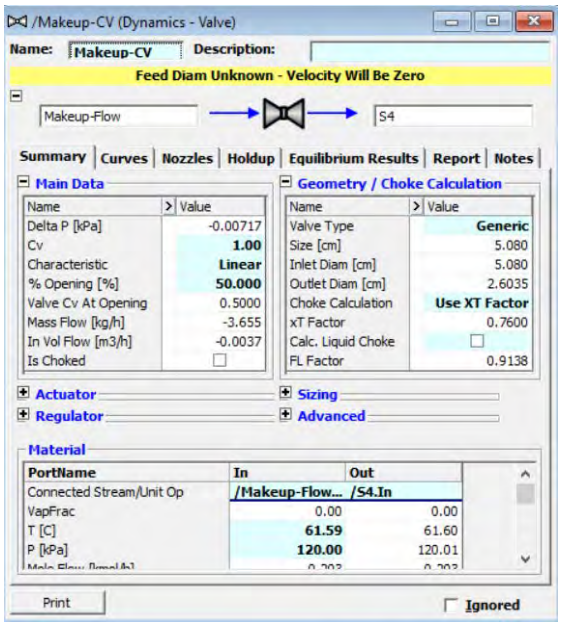

The makeup mixer mixes the makeup flow with the building loop flow. All the diameters are set to match the size of the on-site piping. The details of the makeup mixer is shown in the figure below.

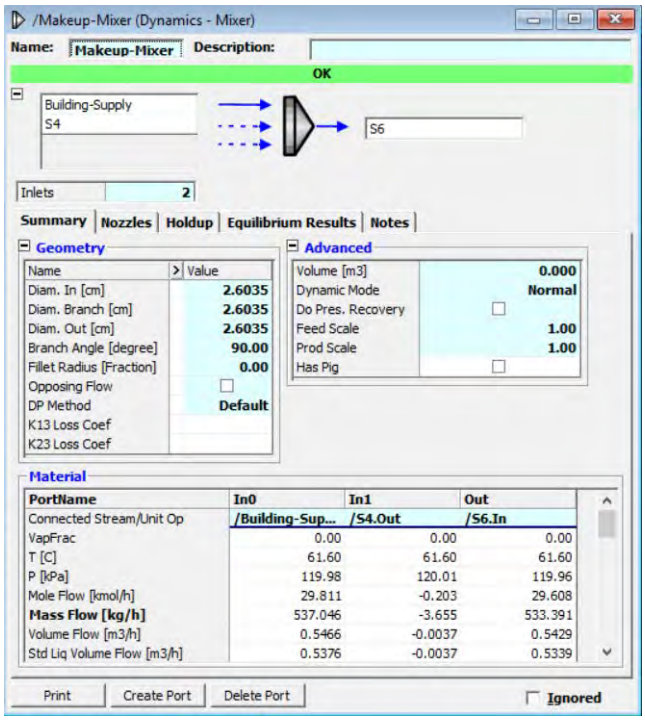

Until now, every component in the wood pellet heating system simulation has been defined and constructed. However, the system control logic is missing. An event scheduler is added to control the system operation. The system control logic has two parts: boiler OFF and boiler ON. The two parts are operated in cycle so that the system can run without stop. The details of the system control logic is shown in the three figures below. It is very important for the simulation to run based on the orders listed in the event scheduler.

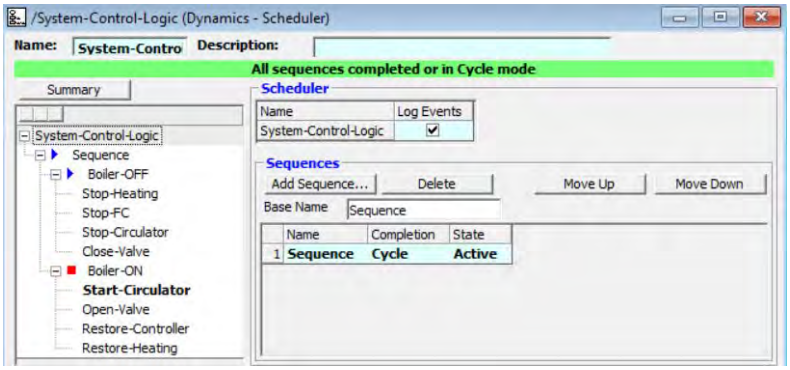

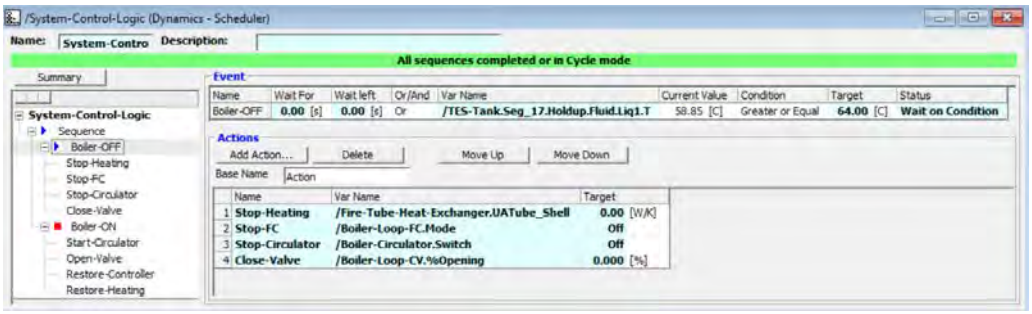

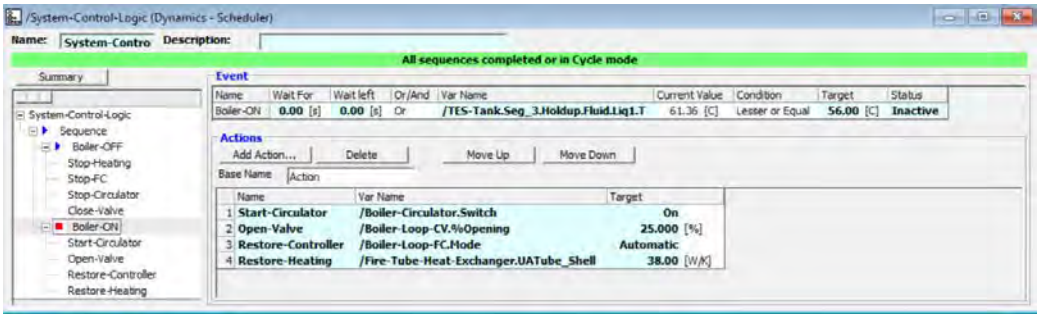

The variations in the wood pellet mass flow rate and variable building heat demand are achieved by adding noise to the specified value, as shown in the two figures below.

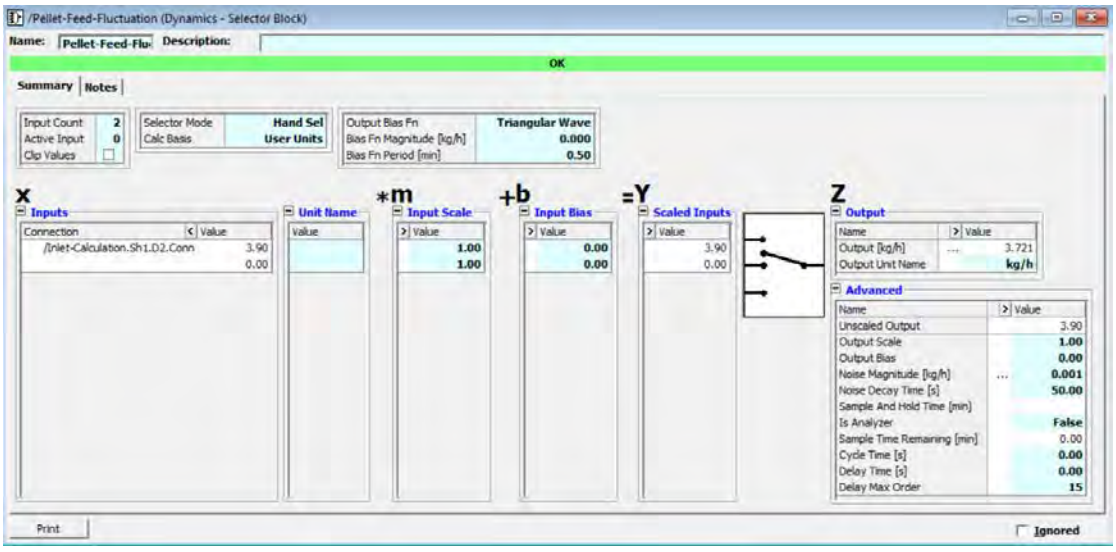

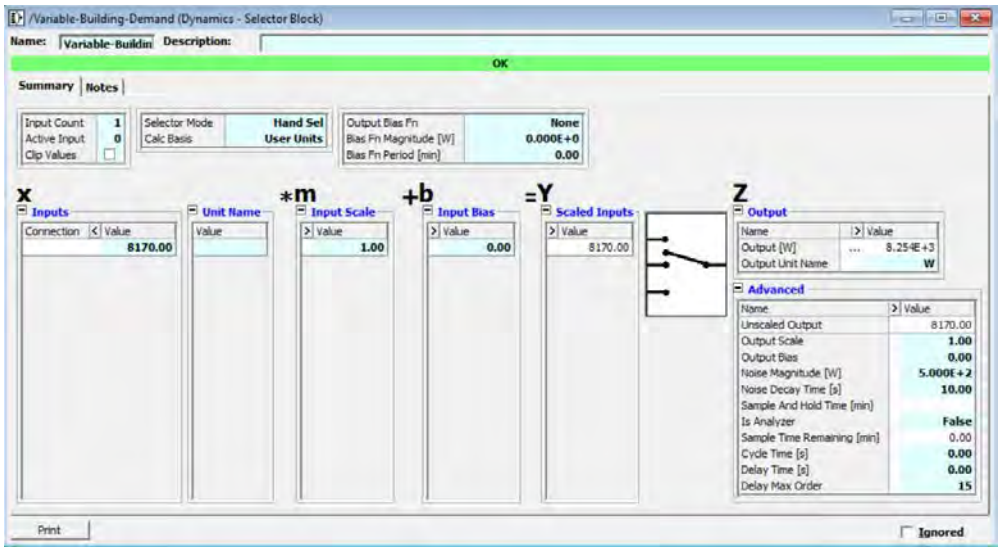

Until now, all the components in the system have been completely defined. The key to a successful construction of the simulation is to run the integrator every time you add a new component to keep the system stable. This is very important to have the overall system functioning.